



THE UNIVERSITY *of* EDINBURGH

This thesis has been submitted in fulfilment of the requirements for a postgraduate degree (e.g. PhD, MPhil, DClinPsychol) at the University of Edinburgh. Please note the following terms and conditions of use:

This work is protected by copyright and other intellectual property rights, which are retained by the thesis author, unless otherwise stated.

A copy can be downloaded for personal non-commercial research or study, without prior permission or charge.

This thesis cannot be reproduced or quoted extensively from without first obtaining permission in writing from the author.

The content must not be changed in any way or sold commercially in any format or medium without the formal permission of the author.

When referring to this work, full bibliographic details including the author, title, awarding institution and date of the thesis must be given.

Imaging cerebrovascular alterations in experimental models of ageing and vascular cognitive impairment

Jessica Duncombe BSc (Hons) MSc

Doctor of Philosophy
University of Edinburgh
2017



THE UNIVERSITY
of EDINBURGH

Table of Contents

Acknowledgements	9
Declaration	10
List of Figures	11
List of Tables	14
Abstract	15
List of Abbreviations	19
 1. Introduction	 23
1.1 The cerebrovascular system	26
1.1.1 Cells of the neurovascular unit	26
1.1.2 Neurovascular coupling	30
1.1.3 Autoregulation	33
1.1.4 Blood-brain barrier	33
1.1.5 Perivascular and glymphatic clearance	34
1.2 Dysfunction of the cerebrovascular system	36
1.2.1 Chronic cerebral hypoperfusion	38
1.2.2 Disruption of neurovascular coupling	41
1.2.3 Inflammation	43
1.2.4 Blood-brain barrier breakdown	44
1.2.5 Cerebral amyloid angiopathy	46
1.2.6 Interactions between amyloid and vascular disease	47
1.2.7 Oxidative stress	49
1.2.8 Current treatment options for prevention of VCI	55
1.3 Animal models of vascular cognitive impairment	59
1.3.1 Cerebral hypoperfusion	59
1.3.2 Amyloid deposition	62
1.3.3 Additional models of VCI	64
1.4 Imaging the cerebrovascular system	66
1.4.1 Resting cerebral blood flow	66
1.4.2 Vessel number	67
1.4.3 Inflammation	68
1.5 Summary	71

1.6 Hypothesis	71
1.7 Aims	71
2. Materials and Methods	73
2.1 Animals	74
2.2 Chronic cerebral hypoperfusion	76
2.3 Apocynin administration	76
2.4 Laser speckle imaging to assess baseline blood flow changes	76
2.5 Laser speckle imaging to assess neurovascular coupling	79
2.6 Mouse physiology during neurovascular coupling experiments	80
2.7 Barnes maze assessment of spatial learning and memory	80
2.7.1 Acclimatisation phase	81
2.7.2 Learning phase	81
2.7.3 Acquisition probe	82
2.7.4 72 hour probe	82
2.7.5 Reminder phase	82
2.7.6 Reversal learning phase	82
2.7.7 Reversal acquisition probe	83
2.7.8 72 hour reversal probe	83
2.7.9 Inclusion criteria	83
2.7.10 Performance measures	83
2.8 Unilateral ibotenic acid lesion	85
2.9 Magnetic resonance imaging	85
2.9.1 Arterial spin labelling	86
2.9.2 Q-map imaging	88
2.9.3 Contrast-enhanced T2* imaging	89
2.10 Transcardial perfusion	94
2.11 Tissue processing	94
2.11.1 Paraffin	94
2.11.2 Frozen	94
2.12 Histology	94
2.12.1 Haematoxylin and eosin staining	94
2.12.2 DAB enhanced Perls' Prussian Blue	95
2.13 Immunohistochemistry	95

2.13.1 Immunoperoxidase labelling	95
2.13.2 Immunofluorescent labelling	96
2.14 Analysis of immunohistochemistry	97
2.15 Tissue processing for biochemistry	99
2.16 Determination of protein concentration	99
2.17 Dot blot assay	100
2.18 Analysis of dot blot assay	100
2.19 Enzyme-linked immunosorbent assay (ELISA)	101
2.20 Statistical analysis	101

3. Development and validation of MRI approaches to assess vascular

parameters in vivo	104
3.1 Introduction	105
3.1.1 Aims	107
3.2 Methods	108
3.2.1 Animals	108
3.2.2 Ibotenic acid lesion	108
3.2.3 Cerebral hypoperfusion surgery	109
3.2.4 Magnetic resonance imaging	109
3.2.5 Optimisation of ASL parameters	109
3.2.6 Validation of ASL using laser speckle imaging	109
3.2.7 Validation of Q-map derived vessel number using collagen IV immunohistochemistry	110
3.2.8 Validation of ce-T2* using Iba1 immunohistochemistry and enhanced Perl's stain	110
3.2.9 Statistical analysis	110
3.3 Results	112
3.3.1 Arterial spin labelling can be used to assess resting cerebral blood flow in vivo	112
3.3.2 Q-map imaging can be used to measure vessel number in vivo	121
3.3.3 T2 imaging can be used for the detection of vascular lesions in vivo ..	125
3.3.4 Contrast-enhanced T2* imaging can detect areas of inflammation in vivo	127
3.4 Discussion	131
3.4.1 Arterial spin labelling as a tool to assess resting cerebral blood flow ..	131

3.4.2 Q-map imaging assessment of vessel number in vivo	133
3.4.3 Detection of vascular lesions using structural T2 imaging	137
3.4.4 In vivo assessment of neuroinflammation using contrast-enhanced T2*	138
3.4.5 Conclusions	141
4. Imaging cerebrovascular alterations in experimental models of ageing and cerebral amyloid angiopathy	142
4.1 Introduction	143
4.1.1 Hypothesis	144
4.1.2 Aims	144
4.2 Methods	145
4.2.1 Animals	145
4.2.2 Magnetic resonance imaging to assess structural alterations, resting blood flow and vascular density	145
4.2.3 Magnetic resonance imaging analysis	145
4.2.4 Laser speckle imaging to assess neurovascular coupling	146
4.2.5 Tissue processing	146
4.2.6 Immunohistochemistry to assess neurovascular unit structure	146
4.2.7 Statistical analysis	147
4.3 Results	148
4.3.1 TgSwDI mice exhibit parenchymal and vascular amyloid deposition which is absent in wild-type mice	148
4.3.2 Alterations in resting cerebral blood flow in wild-type and TgSwDI mice	149
4.3.3 Alterations in vascular density in wild-type and TgSwDI mice	156
4.3.4 CBF increases to whisker stimulation are significantly attenuated in aged wild-type and TgSwDI mice	156
4.3.5 Reduced pericyte coverage of blood vessels in aged mice	162
4.3.6 Reduced coverage of blood vessels by astrocytic endfeet AQP4 in aged mice	166
4.3.7 Microglial activation/number is increased with ageing and exacerbated in TgSwDI mice	172
4.3.8 Alterations in expression of p47 subunit of NADPH oxidase 2	175
4.4 Discussion	178
4.4.1 Neurovascular coupling is impaired with age	178

4.4.2 Neurovascular coupling was not further impaired in the presence of cortical amyloid	179
4.4.3 Contribution of pericytes to neurovascular coupling	181
4.4.4 Contact between astrocytes and blood vessels may be critical for normal neurovascular coupling	182
4.4.5 Microglial activation is associated with reduced neurovascular coupling	184
4.4.6 Conclusions	185

5. The impact of chronic cerebral hypoperfusion and amyloid deposition

on vascular function and cognitive decline 186

5.1 Introduction	187
5.1.1 Hypothesis	189
5.1.2 Aims	189
5.2 Methods	190
5.2.1 Animals	190
5.2.2 Chronic cerebral hypoperfusion surgery	190
5.2.3 In vivo vascular imaging	191
5.2.4 Analysis of in vivo MRI	191
5.2.5 Laser speckle imaging of baseline blood flow	191
5.2.6 Barnes Maze	192
5.2.7 Laser speckle imaging of neurovascular coupling	192
5.2.8 Tissue collection and processing	192
5.2.9 Amyloid quantification	193
5.2.10 Quantification of ischaemic and haemorrhagic lesion burden	193
5.2.11 Dot blot assay	193
5.2.12 Statistical analysis	194
5.3 Results	195
5.3.1 Blood flow is reduced following cerebral hypoperfusion	195
5.3.2 TgSwDI mice develop amyloid deposition that is absent in wild type mice	200
5.3.3 Neurovascular coupling is significantly impaired following cerebral hypoperfusion	200
5.3.4 Hypoperfusion induces development of vascular lesions	203
5.3.5 Contrast enhanced T2* signal is altered in hypoperfused mice	210

5.3.6 Spatial learning, but not spatial memory, is impaired following hypoperfusion	213
5.3.7 Reversal learning and memory are impaired in hypoperfused and TgSwDI mice	214
5.3.8 Markers of oxidative stress are increased following hypoperfusion ...	220
5.4 Discussion	224
5.4.1 Cerebral hypoperfusion surgery induces sustained reduction in cerebral blood flow	224
5.4.2 Hypoperfusion impairs neurovascular coupling	225
5.4.3 Hypoperfusion induces vascular lesions and increased inflammation ..	227
5.4.4 Behavioural deficits are induced following cerebral hypoperfusion	229
5.4.5 Amyloid did not exacerbate vascular disruption, inflammation or cognitive abilities following cerebral hypoperfusion	231
5.4.6 Vascular dysfunction following cerebral hypoperfusion may be mediated by increased oxidative stress	235
5.4.7 Conclusions	240
6. The effect of apocynin, a NOX inhibitor, on vascular function and cognition following cerebral hypoperfusion in TgSwDI mice	242
6.1 Introduction	243
6.1.1 Hypothesis	245
6.1.2 Aims	245
6.2 Methods	246
6.2.1 Animals	246
6.2.2 Chronic cerebral hypoperfusion surgery	246
6.2.3 Apocynin administration	247
6.2.4 In vivo vascular imaging	247
6.2.5 Laser speckle imaging of baseline blood flow	247
6.2.6 Barnes Maze	248
6.2.7 Laser speckle imaging of neurovascular coupling	248
6.2.8 Tissue collection and processing	248
6.2.9 Quantification of ischaemic and haemorrhagic lesion burden	249
6.2.10 Amyloid quantification	249
6.2.11 Analysis of vascular NOX2 in vessel-enriched tissue fractions	249
6.2.12 Statistical analysis	250

6.3 Results	251
6.3.1 Water consumption is similar between non-treated and apocynin-treated mice	251
6.3.2 Apocynin does not protect against cortical blood flow reductions following cerebral hypoperfusion	251
6.3.3 Baseline regional cerebral blood flow is not altered by apocynin after 3 months of treatment	255
6.3.4 Apocynin rescues the impairment in neurovascular coupling following cerebral hypoperfusion	259
6.3.5 Apocynin does not reduce the development of vascular lesions but may selectively reduce cortical ischaemic pathology	259
6.3.6 Vascular NOX2 expression is not reduced in apocynin-treated mice ..	253
6.3.7 Inflammation is not reduced following treatment with apocynin	267
6.3.8 Apocynin administration does not reduce amyloid deposition	267
6.3.9 Spatial learning and memory deficits are not rescued by treatment with apocynin	267
6.4 Discussion	277
6.4.1 Apocynin treatment does not protect against blood flow reductions following cerebral hypoperfusion but may improve recovery of cortical blood flow	277
6.4.2 Neurovascular coupling is improved following treatment with apocynin	278
6.4.3 Apocynin treatment does not protect against overall vascular lesion development or inflammation	279
6.4.4 Vascular NOX2 expression is not reduced following apocynin treatment	282
6.4.5 Apocynin treatment did not reduce amyloid burden	283
6.4.6 Behavioural impairments are not rescued by apocynin treatment	283
6.4.7 Conclusions	286
7. Discussion	288
7.1 Summary	289
7.2 Future directions	289
7.3 Future implications for treatment of vascular cognitive impairment	290
8. References	292
9. Appendix	337
9.1 Appendix 1: List of publications	338

Acknowledgements

Firstly, I would like to acknowledge the tremendous guidance and support from my supervisor, Professor Karen Horsburgh. Her mentorship and encouragement have allowed me to successfully complete this work, without which this would not have been possible.

I would also like to thank all members of the Horsburgh lab, both past and present, for always making our lab a great place to work, be it through cake, coffee or just drawings of a dog. I would like to especially thank Dr. Yasmina Manso Sanz, whose passion for science sparked my own early on, Dr. Natalia Salvadores, who could always make me laugh even if things weren't going as we planned, and Dr. Luke Searcy, whose friendship, humour and advice helped me to really flourish. I would also like to acknowledge the tireless support of the LF2 animal unit staff, who would always have time to help, and particularly Duncan McNeil, who could find literally anything. Lastly, I would like to thank Emma Sigfridsson, her positivity and encouragement over a shared bottle of wine kept me going through the final months.

Thanks to my brother, Ollie, and to my Dad and Jules for our Friday parties and for always looking after me. Thanks as well to Robbie and Tricia, my Scottish family, your support throughout has meant a lot to me. My determination in completing this work has been shaped, in part, by the loss of a good friend. Harry, I remember you every day, and I think about how we would have celebrated this together.

Finally, I would like to thank, and probably apologise to, Scottish. Sorry for being grumpy, sorry for not cleaning the house in three months while I was writing. But thank you for sticking with me, for understanding, for all the fajitas, and for making me laugh every day.

Declaration

I declare that this thesis has been composed solely by myself, that it has not been submitted for any previous degree or qualification, and that the work described within this thesis comprises my own original work except where stated otherwise in the text.

Signed: _____

Date: _____

List of Figures

1.1 Cerebral blood supply	27
1.2 The neurovascular unit	28
1.3 Mechanisms of neurovascular coupling	31
1.4 Neuroimaging features of cerebral small vessel disease	37
1.5 Schematic representation of putative mechanisms leading to vascular cognitive impairment	56
2.1 Schematic of the TgSwDI mouse mutant human APP construct	75
2.2 Schematic representation of bilateral common carotid artery stenosis	77
2.3 Laser speckle imaging	78
2.4 Barnes Maze	84
2.5 T2 and ASL-MRI	87
2.6 Q-map imaging	91
2.7 Contrast-enhanced T2* imaging	93
2.8 Cortical and thalamic ROIs used for analysis	98
3.1 Arterial spin labelling can detect regional variations in resting cerebral blood flow	113
3.2 Reduction of CBF values obtained with slice thickness of 1mm	114
3.3 CBF values are reduced when measured using a slice thickness multiplier above 1.5 ..	115
3.4 Arterial spin labelling can detect reductions in cerebral blood flow following cerebral hypoperfusion surgery	118
3.5 Significant correlation between arterial spin labelling and laser speckle imaging derived measures of cortical blood flow	120
3.6 Q-map imaging can be used to measure vessel number in vivo	122
3.7 Q-map imaging can sensitively detect reductions in vessel number	123
3.8 Q-map derived measures of vessel number correlate with immunohistochemical measures of vessel density	124
3.9 Detection of ischaemic and haemorrhagic lesions by structural T2 magnetic resonance imaging	126
3.10 Use of contrast-enhanced T2* imaging to detect inflammation in vivo	128
3.11 Detection of iron following contrast-enhanced T2* imaging	130
4.1 Aged TgSwDI mice develop extensive cortical amyloid deposition	150
4.2 Pattern of cortical amyloid deposition in TgSwDI mice	151

4.3 Aged TgSwDI mice develop extensive thalamic amyloid deposition	152
4.4 Pattern of thalamic amyloid deposition in TgSwDI mice	153
4.5 Cortical blood flow is unchanged with ageing or in TgSwDI mice	154
4.6 Alterations in thalamic resting blood flow	155
4.7 Cortical vessel density is unchanged with ageing or between wild type and TgSwDI mice	157
4.8 Cortical vessel density is unchanged with ageing or between wild type and TgSwDI mice	158
4.9 Thalamic vessel density is increased with age and in TgSwDI mice	159
4.10 Thalamic vessel density is increased with age and in TgSwDI mice	160
4.11 Vascular response to whisker stimulation is significantly impaired in aged mice	161
4.12 Coverage of cortical vessels by PDGFR- β is significantly reduced in aged mice compared to young	163
4.13 Vascular pericyte coverage in the thalamus is significantly reduced in aged mice	165
4.14 AQP4 expression on cortical blood vessels is significantly reduced in aged mice compared to young	168
4.15 GFAP+ve astrocytes are increased in cortex of aged mice and exacerbated in TgSwDI mice	169
4.16 AQP4 expression on thalamic blood vessels is significantly reduced in aged mice compared to young	170
4.17 GFAP+ve astrocytes are increased in thalamus of aged mice and exacerbated in TgSwDI mice	171
4.18 Cortical microglial activation is enhanced in aged mice and exacerbated in TgSwDI ..	173
4.19 Thalamic microglial activation is enhanced in aged mice and exacerbated in TgSwDI ..	174
4.20 Cortical p47 expression is increased in aged mice compared to young	176
4.21 Thalamic p47 expression is increased in aged mice and exacerbated in TgSwDI	177
5.1 Cortical blood flow is persistently reduced following cerebral hypoperfusion	196
5.2 Cortical blood flow is persistently reduced following cerebral hypoperfusion	197
5.3 Arterial spin labelling was used to detect blood flow alterations at 3 months following cerebral hypoperfusion	198
5.4 Thalamic and hippocampal blood flow remains reduced 3 months following cerebral hypoperfusion	199
5.5 TgSwDI mice exhibit amyloid deposition that is not detectable in wild type mice	201

5.6 Neurovascular coupling is significantly impaired following cerebral hypoperfusion	202
5.7 Hypoperfusion induces development of vascular lesions	205
5.8 Hypoperfusion induces development of vascular lesions	207
5.9 Distribution of vascular lesions following cerebral hypoperfusion	209
5.10 The effect of hypoperfusion on contrast-enhanced T2* imaging	211
5.11 Hypoperfusion causes deficits on spatial learning	215
5.12 Hypoperfusion does not impair spatial memory	217
5.13 Reversal learning is impaired in TgSwDI mice	218
5.14 Reversal memory is impaired in hypoperfused and TgSwDI mice	219
5.15 Hypoperfusion increases NOX2 expression	221
5.16 Hypoperfusion increases NOX4 expression in wild type mice	222
5.17 Hypoperfusion increases brain 3-nitrotyrosine content	223
5.18 Proposed pathway of pathological events following chronic cerebral hypoperfusion ..	241
6.1 Apocynin administration does not affect water consumption	252
6.2 Apocynin treatment does not protect against cortical blood flow reductions following hypoperfusion surgery	253
6.3 Apocynin treatment does not protect against cortical blood flow reductions following hypoperfusion surgery	254
6.4 Arterial spin labelling was used to detect blood flow alterations at 3 months following hypoperfusion	256
6.5 Effect of apocynin on recovery of resting cerebral blood flow	257
6.6 Effect of apocynin on recovery of resting cerebral blood flow	258
6.7 Apocynin rescues the impairment on neurovascular coupling following cerebral hypoperfusion	261
6.8 Apocynin does not protect against the development of vascular lesions	262
6.9 Apocynin does not protect against the development of vascular lesions	264
6.10 Apocynin treatment may selectively protect against cortical ischaemic lesions	266
6.11 Apocynin treatment does not reduce vascular expression of NOX2	268
6.12 The effect of apocynin on contrast-enhanced T2* imaging	269
6.13 Apocynin administration does not affect amyloid deposition	271
6.14 Apocynin does not rescue deficits on spatial learning	273

6.15 Apocynin does not improve performance on spatial memory	274
6.16 Apocynin does not improve performance on reversal learning	275
6.17 Apocynin does not improve performance on reversal memory	276

List of Tables

Table 1.1 Drugs and drug classes in stroke that may be worth testing for the prevention or treatment of small vessel disease	58
Table 1.2 Experimental models of chronic cerebral hypoperfusion	62
Table 2.1 Blood gas analysis following neurovascular coupling experiments	80
Table 2.2 Primary and secondary antibodies used for immunohistochemistry	102
Table 2.3 Primary and secondary antibodies used for dot blot assays	113

Abstract

Vascular cognitive impairment describes a heterogeneous condition in which cognitive decline is precipitated by underlying cerebrovascular dysfunction. Ageing, as well as vascular diseases such as hypertension, stroke, cerebral small vessel disease and cerebral amyloid angiopathy, are risk factors for vascular cognitive impairment. The precise mechanisms by which these conditions impact the cerebral vasculature to drive cognitive decline, however, are unknown. Previous research has indicated that vascular risk factors can lead to microvascular oxidative stress, inflammation and endothelial dysfunction that can lead to tissue hypoperfusion, the development of white and grey matter vascular lesions (microinfarcts and microbleeds) and cognitive impairment. It was hypothesised that ageing, a prominent risk factor for cognitive decline, would induce impairments on neurovascular coupling resulting from neurovascular unit disruption. It was further hypothesised that induction of chronic cerebral hypoperfusion would mediate neurovascular dysfunction and vascular lesion development through increased oxidative stress, resulting in cognitive decline. Finally, it was also hypothesised that neurovascular impairments resulting from ageing and chronic cerebral hypoperfusion would be exacerbated in the presence of amyloid deposition. Four studies were performed in order to test these hypotheses.

Vascular risk factors can be reproduced using experimental mouse models and provide a valuable basis in which to test hypotheses and therapeutic interventions. As such, a primary aim of this thesis was to develop and validate sensitive MRI approaches that would allow the detection of vascular alterations in vivo. In the first series of studies, MRI techniques to assess resting cerebral blood flow, vessel number, vascular lesions and inflammation in experimental mice were validated using established in vivo and ex vivo techniques, so that these techniques

could be used in subsequent studies for vascular assessments in vivo. Arterial spin labelling was developed to assess resting cerebral blood flow, and was able to detect reductions in blood flow following cerebral hypoperfusion that correlated well with those obtained from laser speckle imaging. Q-map imaging was able to detect reductions in vessel number in acute lesions, and in non-lesioned mice measures of vessel number correlated well with histopathological measures. Structural T2 imaging was performed in order to detect ischaemic and haemorrhagic lesions in chronically hypoperfused mice, and was validated using H&E and Perls' staining. Finally, contrast-enhanced T2* imaging was used to detect iron oxide uptake by macrophages in the brains of hypoperfused mice, which was further validated by the identification of iron-containing macrophages in immunostained brain sections.

The second study was conducted to test the hypothesis that ageing would impair neurovascular unit function and structure, and that these impairments would be exacerbated in the presence of amyloid pathology. The aim of the study was to incorporate previously developed in vivo imaging approaches in the assessment of vascular function and alterations in neurovascular unit structure in both wild type and TgSwDI mice. As predicted, ageing caused a pronounced deficit on measures of neurovascular coupling, however this was not exacerbated by accumulation of amyloid in TgSwDI mice and was not associated with alterations in baseline blood flow measured by arterial spin labelling. Structural assessment of the neurovascular unit revealed a loss of contact between astrocytic endfeet and vasculature, which was significantly associated with the impairment on neurovascular coupling, in addition to other markers of breakdown of the neurovascular unit such as loss of pericyte coverage and microglial activation. Age and thalamic vascular amyloid accumulation were also associated with an increase in the NADPH oxidase (NOX) subunit p47, indicative of increased oxidative stress.

Data from this experiment indicate that ageing can profoundly impair neurovascular coupling, mediated by gliosis and loss of astrocytic contacts with vasculature.

The third study aimed to test the hypothesis that chronic cerebral hypoperfusion (a prominent early feature of vascular cognitive impairment) would impair vascular function and induce the development of vascular lesions and cognitive decline. The impact of hypoperfusion on neurovascular coupling, ischaemic and haemorrhagic lesion burden and cognition was investigated in wild type and TgSwDI mice. Hypoperfusion induced deficits on neurovascular coupling, increased lesion burden and inflammation assessed with T2 and contrast-enhanced T2* imaging, and caused impairment on measures of learning and memory. Hypoperfusion was also associated with an increase in the levels of NOX2, NOX4 and 3-NT at 3 months following surgery, indicating persistent reactive oxygen species production and oxidative damage in hypoperfused mice. The findings from this study indicate that vascular dysfunction and cognitive impairment following hypoperfusion may be mediated by increased NADPH oxidase activity and resulting oxidative stress.

The previous studies indicated that markers of oxidative stress were induced in response to ageing, vascular amyloid accumulation and cerebral hypoperfusion. The final study sought to determine whether increased NOX activity mediates downstream pathological effects on vascular function, vascular lesion development and cognitive decline following hypoperfusion. NOX activity was inhibited pharmacologically by administration of apocynin to hypoperfused TgSwDI mice for 3 months following surgery. Treatment with apocynin significantly restored neurovascular coupling to a level similar to sham-operated mice, and there was a trend toward reduction of ischaemic vascular lesions. However, it was unable to rescue the prominent

inflammatory response or decline in cognitive ability, as apocynin-treated mice were no different on these measures to non-treated hypoperfused mice. The data indicate that whilst inhibiting NOX may have potential therapeutic value in improving vascular function, additional interventions, for example to reduce inflammation, may also be required in order to prevent cognitive decline.

Overall, the work outlined within the thesis indicate that vascular risk factors of ageing, cerebral amyloid angiopathy and cerebral hypoperfusion may converge on common pathways involving oxidative stress and increased inflammation in order to drive vascular dysfunction and lead to cognitive decline. Inhibition of NOX activity was able to rescue vascular function, however the results indicate that this was not sufficient to protect against cognitive impairment, suggesting additional therapeutic targets may need to be sought in order to fully preserve vascular health and prevent cognitive decline.

List of Abbreviations

20-HETE	20-hydroxyeicosatetraenoic acid
2VO	Two-vessel occlusion
3NT	3-nitrotyrosine
A β	Amyloid beta
ABC	ATP-binding cassette
AD	Alzheimer's disease
ANOVA	Analysis of variance
APP	Amyloid precursor protein
AQP4	Aquaporin-4
ARIA	Amyloid-related imaging abnormalities
ASL	Arterial spin labelling
ATP	Adenosine triphosphate
BACE1	Beta-secretase 1
BBB	Blood-brain barrier
BCAS	Bilateral common carotid artery stenosis
BCCAO	Bilateral common carotid artery occlusion
BOLD	Blood-oxygenation level dependent
CAA	Cerebral amyloid angiopathy
(r)CBF	(resting) Cerebral blood flow
CADASIL	Cerebral autosomal dominant arteriopathy with subcortical infarcts and leukoencephalopathy
CCH	Chronic cerebral hypoperfusion
CE-T2*	Contrast-enhanced T2*
CNS	Central nervous system
COX-2	Cyclooxygenase-2
CSF	Cerebrospinal fluid
DAB	Diaminobenzidine
EET	Epoxyeicosatrienoic acid
EP4	E-type prostanoid receptor 4
GAPDH	Glyceraldehyde 3-phosphate dehydrogenase
GFAP	Glial fibrillary acidic protein
H&E	Haematoxylin and eosin

HHcy	Hyperhomocysteinemia
HIF	Hypoxia inducible factor
Iba1	Ionised calcium binding adaptor molecule 1
ICAM	Intercellular adhesion molecule
IL	Interleukin
ISF	Interstitial fluid
LRP-1	Low density lipoprotein receptor related protein
MAPK	Mitogen activated protein kinases
MCAO	Middle cerebral artery occlusion
MCI	Mild cognitive impairment
MCP-1	Monocyte chemoattractant protein 1
MMP	Matrix metalloproteinase
MRI	Magnetic resonance imaging
NFKB	Nuclear factor kappa-light-chain-enhancer of activated B cells
NMDA	N-methyl-D-aspartate receptor
NO	Nitric oxide
NOS	Nitric oxide synthase
NOX	Nicotinamide adenine dinucleotide phosphate (NADPH) oxidase
NRF2	Nuclear factor (erythroid-derived 2)-like 2
PB	Phosphate buffer
PBS	Phosphate buffered saline
PDGFR- β	Platelet derived growth factor receptor-beta
PET	Positron emission tomography
PI3K	Phosphoinositide 3-kinase
RNS	Reactive nitrogen species
ROS	Reactive oxygen species
SHR	Spontaneously hypertensive rat
SPIO	Superparamagnetic iron oxide
TB	Tris buffer
TGF- β	Transforming growth factor beta
TNF- α	Tumour necrosis factor alpha
TOF-MRA	Time of flight magnetic resonance angiography
TRPA1	Transient receptor potential cation channel A1

TRPV4	Transient receptor potential cation channel V4
UCCAO	Unilateral common carotid artery occlusion
USPIO	Ultrasmall superparamagnetic iron oxide
VCAM	Vascular cell adhesion molecule
VCI	Vascular cognitive impairment
VSMC	Vascular smooth muscle cell

Chapter 1.

Introduction

Introduction

1.1 Overview

The brain is critically dependent on continuous, uninterrupted blood supply in order to support neuronal activity. Delivery of blood is mediated by the neurovascular unit, comprising endothelial cells, pericytes, astrocytes, microglia and neurons (Lok et al. 2007). Together, the neurovascular unit mediates essential functions of the cerebrovascular system, such as neurovascular coupling, formation of the blood-brain barrier, and clearance of waste products from brain interstitium (Phillips et al. 2016; Zlokovic, 2008; Engelhardt et al. 2016). A functional cerebrovascular system is therefore critical for the effective delivery of oxygen and glucose to brain cells, and disruption of the vascular system may result in loss of ATP-dependent processes, alterations in protein synthesis, cell ischaemia and ultimately cell death (Zlokovic, 2011). The increasing burden of neuronal loss may eventually lead to impairments on cognition. Cognitive decline that arises through disruption of the cerebral vasculature has been termed vascular cognitive impairment, and may be characterised by a spectrum of vascular pathology, including white matter lesions, microinfarcts, microhaemorrhages, lacunar infarcts, and cerebral amyloid angiopathy. Conditions that affect the vascular system increase the risk of cognitive impairment, and have been identified as vascular risk factors (Abraham et al. 2016). Among these, ageing is the strongest risk factor for development of cognitive decline (Akinyemi et al. 2013), and cerebral hypoperfusion – a reduction in blood flow to the brain – has also been identified as an important early risk factor that precedes cognitive impairment (Ruitenberg et al. 2005) and correlates with cognition (Alosco et al. 2013). Vascular risk factors such as ageing, cerebral hypoperfusion and cerebral amyloid angiopathy may disrupt the cerebral vasculature through increased oxidative stress and inflammation, resulting in impaired neurovascular function and insufficient delivery of blood to brain tissue, culminating in tissue

degeneration and cognitive impairment. In order to understand the pathological progression induced by vascular risk factors, animal models of vascular cognitive impairment have been established (Jiwa, Garrard and Hainsworth, 2010). In particular, animal models of hypoperfusion and cerebral amyloid angiopathy recapitulate key features of vascular cognitive impairment, and are used in the work described in this thesis to test hypotheses related to the development of cognitive decline. This is facilitated by the use of magnetic resonance imaging approaches to sensitively detect vascular alterations in vivo. The use of imaging approaches in experimental models therefore provides a basis to explore the mechanisms by which ageing, cerebral hypoperfusion and cerebral amyloid angiopathy contribute to cerebrovascular pathology and drive vascular cognitive impairment. Investigation of these mechanisms will form the central theme of the work in this thesis.

1.1 The cerebrovascular system

The dynamic network of blood vessels that make up the cerebral vascular system performs numerous essential roles to support brain homeostasis and coordinate complex aspects of brain function. The vascular system enables clearance of toxic molecules from brain parenchyma into the bloodstream, prevents entry of circulating cells and noxious stimuli into brain parenchyma, and also delivers vital metabolites required for cell function, such as glucose and oxygen, to cells within the central nervous system (Zlokovic, 2011; Engelhardt et al. 2016). Unlike peripheral tissues, such as muscle and liver, the brain contains minimal endogenous energy reserves and thus is critically dependent on a continuous supply of blood to maintain normal function (Girouard and Iadecola, 2006). Reflective of this, blood flow to the brain is ~50ml/100g/min (Cipolla, 2009), which comprises approximately 20% of the total blood supply (Zlokovic, 2008). This is delivered via a network of vessels that originate from the carotid and vertebral arteries in the neck to form the Circle of Willis at the base of the brain. This structure gives rise to multiples arteries that feed deep brain structures as well as those that extend to the cortical surface, where they travel along the surface before entering the cortex as penetrating arterioles (Figure 1.1). As the blood vessels extend deeper into the cortex, extensive branching gives rise to smaller arterioles and capillaries, eventually reaching the periventricular white matter. This organisation of the cerebral vessels results in regional variations in blood supply: deeper structures such as the periventricular white matter lack collateral supply, whilst the cortex is relatively well perfused, being supplied by large surface arteries and multiple arterioles.

1.1.1 The neurovascular unit

Blood vessels within the brain are integrated with pericytes, astrocytes, microglia and neurons to form the neurovascular unit (Lok et al. 2007) (Figure 1.2). The neurovascular unit

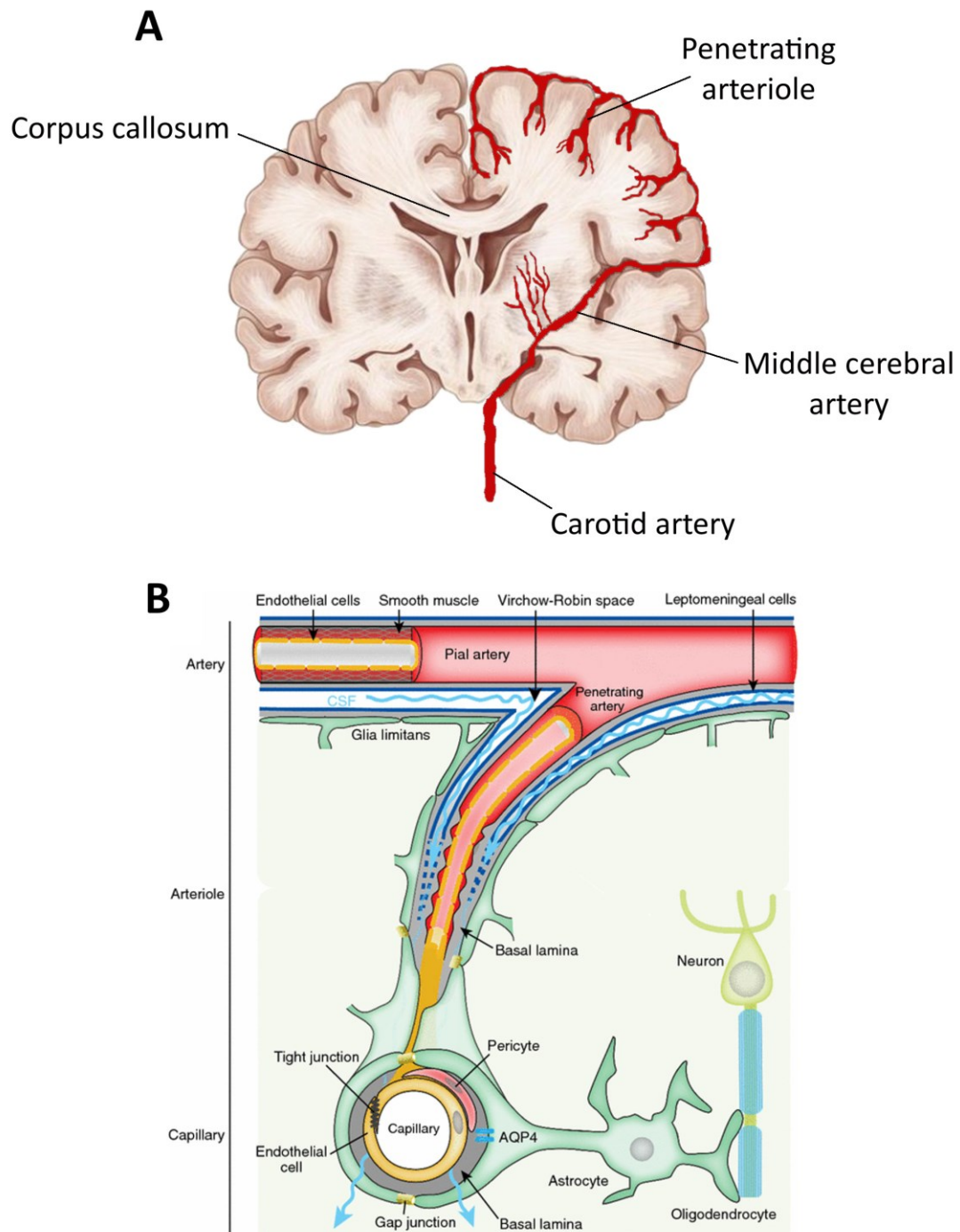


Figure 1.1 Cerebral blood supply. (A) Representation of cerebral blood supply and vulnerability of white matter tracts due to their location at vessel end terminals. (B) Cortical surface arterioles arising from cerebral arteries penetrate the brain perpendicular to the cortical surface, becoming penetrating arterioles. These vessels then branch to form cerebral capillaries. Adapted from Jessen et al. (2015).

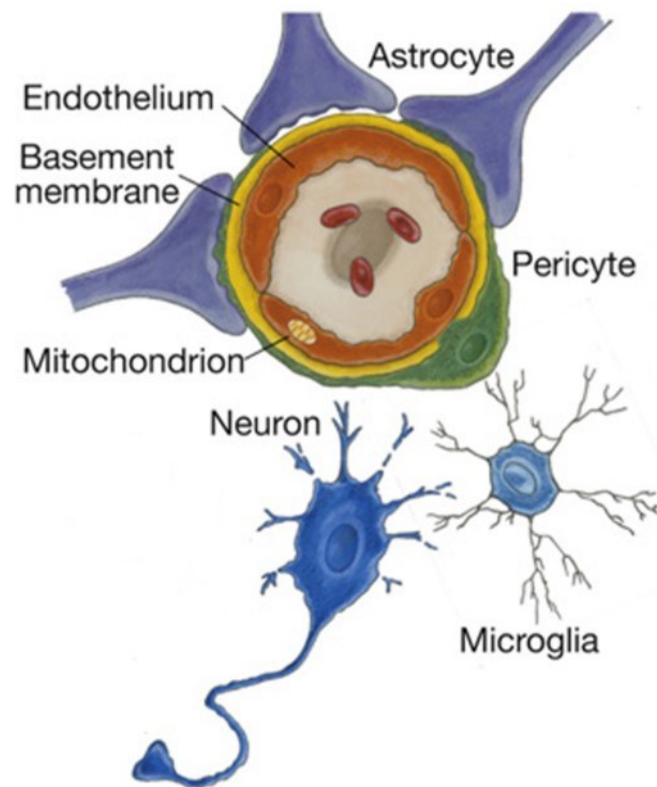


Figure 1.2 The neurovascular unit. Adapted from Zlokovic (2008).

is responsible for mediating blood vessel diameter in response to neuronal activity (neurovascular coupling) or blood pressure fluctuations (autoregulation), controlling the exchange of substances between blood and brain parenchyma via the formation of the blood brain barrier, and for the clearance of solutes from brain interstitium (Phillips et al. 2016; Zlokovic, 2008; Engelhardt et al. 2016). Endothelial cells form the basis of blood vessel structures and are arranged in continuous tubular formations connected by tight junctions, providing a physical barrier that restricts the movement of substances into the brain (Hasseloff et al. 2015). The endothelium is ensheathed on the abluminal side by mural cells. At the capillary level these are pericytes, characterised by the expression of platelet-derived growth factor receptor- β (PDGFR- β) (Hutter-Schmid and Humpel, 2016), whilst on larger arterioles and arteries the endothelium is covered by vascular smooth muscle cells (VSMCs), which express contractile proteins such as actin and myosin to provide regulation of vessel diameter (Hill et al. 2015). A basement membrane comprised of structural proteins (such as collagens, nidogens, laminins and heparan sulphate proteoglycan) also covers the abluminal side and provides an anchoring structure for cell binding as well as an additional layer of the blood brain barrier (Zlokovic, 2008). The endothelium is extensively contacted by astrocytic projections that terminate on the endothelium as astrocytic endfeet. Astrocytes also extend processes to contact neuronal synapses and nodes of Ranvier, and are thought to be critically important for transducing neuronal activity into increases in blood flow, in a process termed neurovascular coupling (Gordon, Howarth and MacVicar, 2016). Neurons are also able to extend processes to contact vessels directly on the basement membrane, allowing further neuronal regulation of vascular tone (Hamel, 2006). Microglia, the resident immune cells of the brain, also modulate function of the neurovascular unit through the production of cytokines and chemokines, which act on the vasculature to alter the expression of tight junction proteins and mediate changes in

blood-brain barrier function (Hudson et al. 2005). Perivascular macrophages are also embedded in the basement membrane to engulf cellular debris and modulate the immune response to circulating cytokines (Serrats et al. 2010).

1.1.2 Neurovascular coupling

Cerebral blood flow is regulated by the neurovascular unit, whereby regional blood flow can be rapidly adjusted according to changes in neuronal activity. This process is termed neurovascular coupling, and ensures that firing neurons are supplied with the oxygen and glucose required to drive ATP-dependent ion channel transporters and repolarise, allowing them to fire again. The process of neurovascular coupling is widely described and forms the basis of the blood oxygenation level dependent (BOLD) signal used in functional magnetic resonance imaging, allowing areas of brain activation to be mapped in response to a stimulus or cognitive task (Sokunbi et al. 2016). However, the precise signalling pathways by which it occurs are not fully understood, and several mechanisms may be utilised in order to provide control of blood flow at all levels of the vascular bed (Figure 1.3). Subcortical neurons project to cortical microvessels and release neurotransmitters such as acetylcholine, serotonin or norepinephrine. Receptors for these vasoactive transmitters are expressed on vascular smooth muscle and endothelial cells, where they induce either vasodilation or vasoconstriction to allow direct neuronal modulation of vascular tone (Hamel, 2006). Neuronal activity can also regulate blood flow through astrocytes, being ideally situated between neurons and blood vessels. Neuronal activity elicits intracellular calcium increases in the fine processes of astrocytes located at synapses (Otsu et al. 2015). This intracellular calcium increase is thought to be mediated by several distinct pathways: (1) glutamate released into the synaptic cleft binds to astrocytic glutamate receptors; (2) direct calcium entry via spontaneously-opening astrocytic TRPA1 channels; and (3) neurotransmitter-mediated effects on astrocytic sodium/calcium

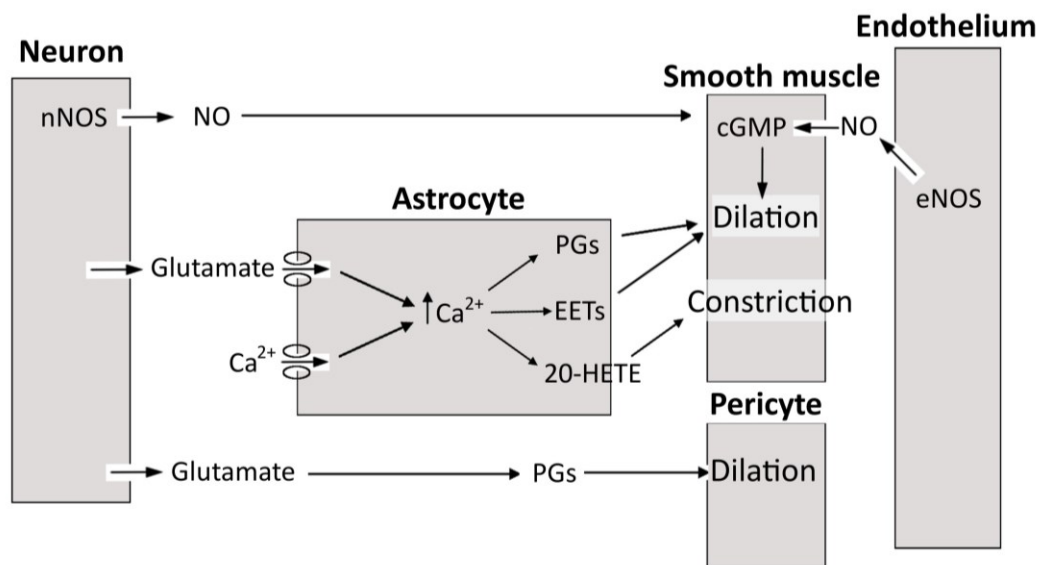


Figure 1.3 Mechanisms of neurovascular coupling. Adapted from Koehler, Gebremedhin and Harder et al (2006)

exchange pumps (for review see Bazargani and Attwell, 2016). This increase in intracellular calcium in turn leads to the release of arachidonic acid-derived vasoactive substances such as prostaglandins, epoxyeicosatrienoic acids (EETs) and 20-hydroxyeicosatetraenoic acid (20-HETE) from the astrocyte endfoot, which bind to their respective receptors on endothelium or smooth muscle to induce vasodilation or constriction (Gordon, Howarth and MacVicar, 2016). Astrocytes have also been shown to respond to metabolic signals related to brain tissue oxygenation, and that the availability of oxygen determines downstream effects on vessel diameter (Gordon et al. 2008). The red blood cells themselves have also been highlighted as mediators of neurovascular coupling (Wei et al. 2016; Ellsworth et al. 2009). Recent work in particular suggests that the initial decrease in tissue oxygen tension (PO_2) caused by neuronal activity is detected by capillary erythrocytes, which are then able to increase flow velocity through modulation of their cytoskeleton to reduce shear (Wei et al. 2016). This increase in red blood cell velocity through capillaries was shown to occur prior to arteriole dilation and may represent an initial phase of neurovascular coupling, subsequently followed by dilation of larger upstream vessels which may be mediated by astrocytic signalling as described above, or additionally through retrograde propagation of vasodilatory signals by the endothelium itself (Chen et al. 2014). In addition to modulation of capillary blood flow by erythrocytes, pericytes have also been suggested to control capillary diameter through activation of their EP4 receptor by prostaglandins in response to glutamate release from active neurons (Hall et al. 2014). Pericytes were also suggested to irreversibly constrict following cerebral ischaemia in vivo, contributing to the observed reperfusion deficit following middle cerebral artery occlusion in experimental mouse models (Hall et al. 2014). However, other studies have not supported a role for pericytes in control of neurovascular coupling- Hill et al. (2015) demonstrate that pericytes lack the contractile fibres required for modulation of capillary diameter and suggest

that smooth muscle cells, rather than pericytes are responsible for the ‘no-reflow’ phenomenon following cerebral ischaemia. Differing criteria for classification of a pericyte versus smooth muscle may explain some of the discrepancies between these two studies. However, Wei et al. (2016) also observed very few pericytes that possessed the contractile machinery necessary for control of blood flow (30% were smooth muscle actin positive). Wei et al. (2016) also found no effect of pericyte cell body proximity on capillary diameter, suggesting they do not play a prominent role (although the influence of pericyte processes was not investigated).

1.1.3 Autoregulation

In addition to coordinating blood flow with neuronal activity, the cerebral vasculature is also able to protect itself against fluctuations in blood pressure through a process termed autoregulation, mediated by the relaxation or constriction of vascular smooth muscle in response to low or high blood pressure (Fog, 1938; Cipolla, 2009). Vasodilatory mediators are also released in conditions of low blood flow as a result of hypoxia and activation of metabolic factors (Cipolla, 2009). This ensures that cerebral blood flow remains fairly constant, at approximately 50ml per 100g of brain tissue per minute, and prevents reductions in blood supply caused by peripheral blood pressure alterations. If blood supply does fall, the percent of oxygen extracted from the blood, known as the oxygen extraction fraction, can be increased in order to compensate for fluctuations in blood flow (Jespersen and Ostergaard, 2012).

1.1.4 Blood-brain barrier

Another important function of the neurovascular unit is the formation and maintenance of the blood brain barrier (BBB) in order to control the exchange of substances between brain parenchyma and blood. The BBB is formed by the tight junctions between endothelial cells of the cerebral vessels, these express tight junction proteins including occludin, claudin and zona

occludens, and are able to limit the entry of substances based on size and charge (for review see Anderson and Van Itallie, 2009). This restricts the paracellular exchange of cells and molecules between the bloodstream and the parenchyma and protects the brain from peripheral infection. Brain endothelial cells are also adapted to restrict transcellular movement (movement of molecules through cells), and express transporters that either facilitate or prevent diffusion into the parenchyma. Expression of the Glut1 transporter enables glucose to cross the blood-brain barrier and enter the brain, whilst expression of ATP-binding cassette (ABC) transporters such as P-glycoprotein prevents the entry of substances into the brain and presents a challenge for drug delivery to brain parenchyma (Cho et al. 2016). Additionally, BBB function is regulated by cell types other than the endothelium. Pericytes play a critical role in the formation of the BBB and vascular maturation via bidirectional transforming growth factor (TGF- β) signalling between pericytes and endothelial cells. Genetic deletion of either TGF- β or its receptor, Alk5, is embryonic lethal due to improper vascular development (Dickson et al. 1995; Larsson et al. 2001); depletion of pericytes by homozygous PDGFR- β knockout also results in non-viable embryos (Soriano, 1994). BBB maintenance has also been shown to be critically dependent on pericytes, as mice deficient in PDGFR β develop a progressive increase in permeability resulting in substantial extravasation of intravascular proteins into the parenchyma (Bell et al. 2010). Astrocytes have also been shown to promote the formation and maintenance of the BBB in development and in adulthood. They have been shown to exert barrier-promoting effects through multiple pathways that act on the endothelium, including secretion of Sonic hedgehog and angiotensinogen (Alvarez et al. 2011; Wosik et al. 2007).

1.1.5 Perivascular and glymphatic clearance of waste substances from brain

The clearance of extracellular solutes from brain tissue has been demonstrated to occur via two main pathways- perivascular drainage of interstitial fluid (ISF) and glymphatic drainage of

cerebrospinal fluid (CSF). The perivascular drainage pathway describes the removal of waste through drainage of ISF from the extracellular space. This occurs along the basement membrane of capillaries, arterioles and arteries to eventually leave the brain via the cervical lymph nodes, and has been demonstrated in vivo by the intraparenchymal injection of fluorescent tracers (Carare et al. 2008). The perivascular drainage of ISF is thought to be driven by arterial pulsations, specifically the reflection wave that follows an arterial wall pulse. The reflection wave moves in the opposite direction to blood flow, so ISF is drained out of the brain via arterioles and arteries (Schley et al. 2006). On the other hand, the glymphatic drainage pathway is also driven by arterial pulsations but drainage occurs via a paravenous route and is dependent on the expression of the water channel aquaporin-4 on astrocytic endfeet (Iliff et al. 2012). This pathway has been demonstrated in vivo by the injection of fluorescent tracers into the CSF of the cisterna magna, which then enters brain parenchyma along para-arterial routes and mixes with ISF in the interstitium before being drained along paravenous routes to the cervical lymph nodes. CSF and ISF movement along arteries occurs in spatially distinct compartments and the relationship between the two systems is currently unclear. Both systems are reported to be involved in the clearance of soluble amyloid protein (Iliff et al. 2012; Hawkes et al. 2014), and failure of these drainage pathways has been reported in ageing (Hawkes et al. 2011) and may underlie the accumulation of amyloid along vascular basement membranes in cerebral amyloid angiopathy (Carare et al. 2013).

The neurovascular unit is therefore able to ensure that metabolic demands of brain tissue are met, it protects the brain from invading pathogens and from inflammatory mediators in the bloodstream; and is also able to clear unwanted substances from the brain parenchyma via the bloodstream or ISF/CSF drainage.

1.2 Vascular cognitive impairment

The human brain is critically reliant on uninterrupted and finely tuned metabolic control in order to maintain synaptic transmission (Harris, Jolivet and Attwell, 2012). As such, dysfunction of the cerebral vasculature leaves brain cells vulnerable to deficits in oxygen and glucose. Neurons are particularly vulnerable, they have minimal endogenous energy reserves yet synaptic transmission is estimated to use 41% of the total ATP generated in the cortex (Attwell and Laughlin, 2001). Reductions in the availability of oxygen and glucose affect the generation of ATP by neuronal mitochondria and impairs ATP-dependent neuronal functions. Ultimately, if energy deficits are sustained neuronal apoptosis may occur, and the increasing burden of synaptic loss may eventually lead to a state of cognitive impairment (Zlokovic, 2011). Cognitive impairment caused by underlying cerebrovascular disruption has been termed vascular cognitive impairment (VCI). In neuropathological studies, VCI can manifest as myelin loss and rarefaction, microinfarcts, lacunar infarcts, cerebral amyloid angiopathy and microhaemorrhages, which together make up a spectrum of pathology described as cerebral small vessel disease (Skrobot et al. 2016). In addition, other vascular pathologies including large infarcts, arteriolosclerosis and atherosclerosis may also be present in VCI (Skrobot et al. 2016). In one individual, multiple vascular pathologies may be present, and the increasing burden of vascular pathology is associated with increasing risk of VCI (Skrobot et al. 2016). In neuroimaging studies, small vessel disease is identified by lacunes, white matter hyperintensities, subcortical infarcts, microbleeds, perivascular spaces and brain atrophy (Wardlaw et al. 2013) (Figure 1.4). Due to the heterogeneous nature of underlying vascular disturbance, the cognitive changes associated with vascular cognitive impairment may be variable and dependent on lesion location, particularly for VCI caused by large vessel pathology such as ischaemic stroke. However, individuals with subcortical vascular disease

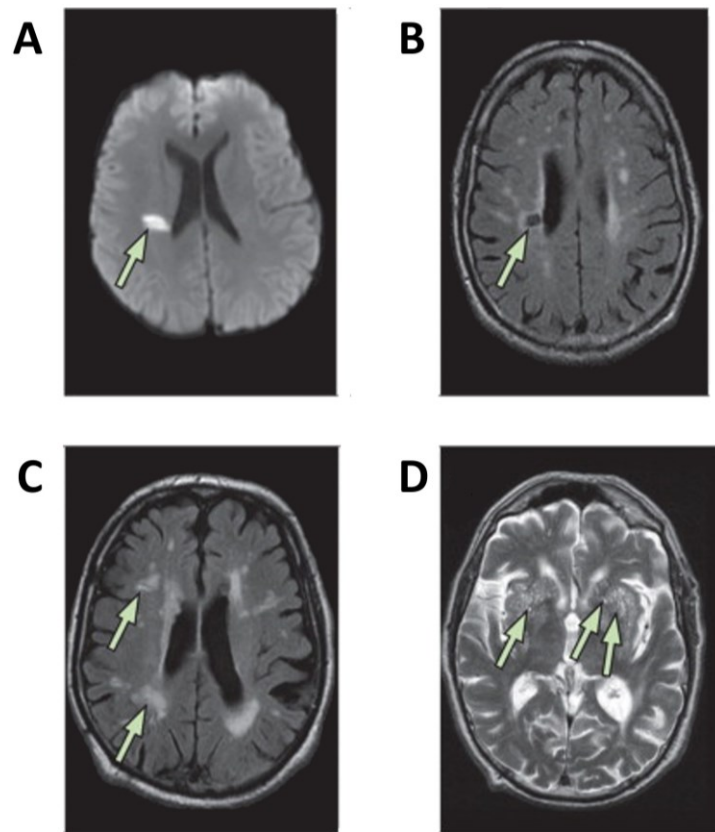


Figure 1.4 Neuroimaging features of cerebral small vessel disease. (A) Diffusion-weighted image of an acute small deep lacunar infarct. (B) Lacune on FLAIR imaging. (C) White matter hyperintensities on FLAIR imaging. (D) Perivascular spaces on T2-weighted imaging. Taken from Wardlaw et al (2013).

(i.e. those with lacunar infarcts and white matter lesions) typically develop impairments on tasks dependent on frontostriatal-thalamic circuits, such as speed of information processing, attention and executive function (O'Brien, 2006). In this respect, vascular cognitive impairment differs from that of Alzheimer's disease, in which individuals typically present with impairments on measures of episodic and semantic memory (Jahn, 2013). Vascular disruption is suspected to be responsible for 15% of dementia cases whilst Alzheimer's disease causes approximately 70% of cases (O'Brien and Thomas, 2015; Castellani, Rolston and Smith, 2011); however a considerable proportion of individuals with Alzheimer's disease also have some degree of cerebrovascular pathology (Attems and Jellinger, 2014). Despite clear evidence for the contribution of cerebral small vessel disease to the pathogenesis of vascular cognitive impairment (Banerjee et al. 2016; Wardlaw, Smith and Dichgans 2013), little is known about how cerebral small vessel disease and other vascular pathologies may occur. The incidence of VCI is significantly influenced by conditions that affect the vascular system, such as ageing, chronic cerebral hypoperfusion, stroke, hypertension and diabetes. These vascular risk factors may precipitate vascular disruption through endothelial dysfunction, inflammation and blood-brain barrier breakdown, to eventually lead to the development of vascular lesions observed in VCI.

1.2.1 Chronic cerebral hypoperfusion

Chronic cerebral hypoperfusion – a reduction in blood flow to the brain – is prominently associated with declining cognitive ability. Measurements of cerebral blood flow are able to identify and predict which individuals may progress from healthy cognition to a state of cognitive impairment (Ruitenberg et al. 2005), and those at increased genetic risk for developing dementia (Thambisetty et al. 2010). Individuals with stenosis of cerebral arteries exhibit greater cognitive deterioration relative to those without stenosis (Buratti et al. 2014;

Zhu et al. 2014). On neuroimaging studies, individuals with vascular dementia exhibit reduced perfusion of the frontal cortices, and perfusion deficits were correlated with the burden of white matter lesions (Schuff et al. 2009). As discussed above, white matter may be vulnerable to blood flow changes as it lies at the border of vascular supply territories, both from large arteries supplying deep brain structures and from penetrating arterioles entering the brain from the cortical surface (Figure 1.1). Blood supply to the white matter is therefore likely to be compromised to a greater extent relative to other brain regions (e.g. cortex) and may even be diverted away from white matter to maintain blood flow in regions higher in the vascular tree (Mandell et al. 2008). Impairments in blood flow regulation have been suggested to underlie the development of white matter lesions, a term that incorporates a spectrum of pathological and neuroimaging features such as demyelination, lacunar infarcts and arteriosclerosis, as well as white matter hyperintensities seen on magnetic resonance imaging. White matter lesions are a prominent feature of VCI (Moorhouse and Rockwood, 2008) and correlate with cognition (Ai et al. 2014). Several imaging studies have suggested that reductions in cerebral blood flow precede the development or expansion of white matter lesions (Promjunyakul et al. 2015; Bernbaum et al. 2015). However, a recent meta-analysis suggested that overall, data from longitudinal studies was insufficient to support the idea that hypoperfusion occurs first in white matter and leads to white matter lesions, although perfusion was often measured globally rather than in white matter specifically (Shi et al. 2016; van der Veen et al. 2015; ten Dam et al. 2007). In another longitudinal imaging study, Sam et al. (2016) showed that cerebrovascular reactivity (rather than resting flow) was reduced in normally appearing white matter that progressed to white matter hyperintensities, relative to white matter that remained healthy over the following year, suggesting that other vascular parameters may be important when considering white matter viability. Neuropathological evidence also suggests an ischaemic

environment in white matter lesions suggestive of hypoperfusion, with upregulation of hypoxia-regulated genes and proteins such as hypoxia-inducible factors (HIFs) 1 and 2, and matrix metalloproteinase-7 (MMP-7) (Fernando et al. 2006). Further evidence for the involvement of hypoperfusion in development of cognitive impairment comes from studies that have shown an increase in the risk for dementia in individuals that have previously suffered a stroke (Pendlebury and Rothwell, 2009). Post-stroke dementia occurs in 10-30% of stroke survivors (Pendlebury and Rothwell, 2009), whilst impairment on at least one cognitive domain has been shown to occur in more than 80% of individuals at 3 months post-stroke (Jokinen et al. 2015). Although stroke pathology is fundamentally associated with an acute period of hypoperfusion, it also is likely to induce a spectrum of other pathological changes that induce vascular disruption and neurodegeneration, such as neuroinflammation and blood-brain barrier disruption. Ageing, the strongest risk factor for the development of cognitive decline, has been consistently associated with reduced cerebral blood flow (Tarumi et al. 2014; Aanerud et al. 2012), with blood flow suggested to decrease by 27% over 70 years of life (Chen, Rosas and Salat, 2011). Increasing age is associated with a decrease in capillary density (Brown and Thore, 2011), this loss of the vascular bed may contribute to the reduced perfusion seen in ageing. Cerebral hypoperfusion may be precipitated in a range of vascular diseases. Hypertension is strongly associated with development of white matter lesions (Godin et al. 2011; Gottesman et al. 2010), has been identified as a risk factor for vascular cognitive impairment (Gorelick et al. 2011) and cognitive performance has been shown to be reduced in both hypertensive animal models (Obari et al. 2016) and hypertensive individuals (Gasecki et al. 2013). Increased blood pressure in hypertensive individuals can lead to vascular remodelling, in which the inward growth of vascular smooth muscle cells reduces the vessel lumen (Perrotta, Lembo and Carnevale, 2016). This occurs in conjunction with deposition of

atherosclerotic plaques in peripheral vessel walls (Li and Chen, 2005), which further narrows the vessels and impedes the flow of blood to the brain. In agreement with this data, longitudinal studies have shown greater decline in cerebral blood flow over time in hypertensive individuals compared to normotensive controls (Beason-Held et al. 2007), which may precipitate the development of white matter lesions. Diminished vascular capacity for autoregulation has been identified in hypotension (Duschek and Schandry, 2006) leaving the brain vulnerable to fluctuations in blood pressure and reduced overall flow. The resulting reduction in perfusion has also been shown to associate with impaired cognitive performance (Duschek and Schandry, 2007). Reduced cerebral blood flow velocity and regional perfusion has also been reported for diabetic individuals (Novak et al. 2006; Last et al. 2007), and cognitive function is synergistically impaired in combined rat models of diabetes and cerebral hypoperfusion when compared to either condition alone (Kwon et al. 2015).

1.2.2 Disruption of neurovascular coupling

As well as changes in baseline perfusion that may contribute to VCI, disruption of the vasculature may impair dynamic modulation of blood flow in response to changing metabolic demands of brain tissue, such as in neurovascular coupling or the vasodilatory response to hypercapnia. In normal ageing, a number of structural alterations in the vascular bed have been documented that may impair vasomotor reactivity, for example vessel wall thickening due to deposition of collagen in the basement membrane, and degeneration of vascular smooth muscle cells on arterioles (Kalaria, 2011). These alterations reduce the elasticity of the vessels and the ability to dilate and constrict in response to vasoactive mediators. In line with this, studies of cerebrovascular reactivity find an age-related decline in vascular function (Blair et al. 2016). Studies of cerebrovascular reactivity in small vessel disease are limited. Yezhuvath et al. (2012)

found impaired cerebrovascular reactivity in the forebrain was associated with burden of white matter hyperintensities, whilst Conijn et al. (2012) found cerebrovascular reactivity was impaired in individuals with microbleeds, but was not associated with burden of white matter pathology, and other studies have found no associations at all (Richiardi et al. 2015). A recent meta-analysis concluded that due to the small total number of individuals assessed and the significant variations in methodology used, there is currently insufficient evidence to determine a role for cerebrovascular reactivity in the pathophysiology of small vessel disease (Blair et al. 2016). However, vascular reactivity and autoregulation have been shown to be impaired in other risk factors for VCI, such as hypertension and stroke (Blair et al. 2016; Daulatzai, 2016; Stevenson et al. 2010); and also correlate with cognitive performance (Richiardi et al. 2015). Deficits on vascular reactivity are likely to be further compounded by disruption of the neurovascular unit and the cells that mediate neurovascular coupling. Ageing is associated with a reduction in astrocytes in frontal white matter (Chen et al. 2016) and with increased astrocytic reactivity (Primiani et al. 2014; Cerbai et al. 2012). Loss of the contact between astrocytes and endothelium was also observed in aged mice (Kress et al. 2014) and in the brains of individuals with post-stroke dementia (Chen et al. 2016). Pericyte degeneration has also been reported in aged mice (Tucsek et al. 2014) and pericyte injury using CSF levels of PDGFR- β as a biomarker is also reported to increase with age (Montagne et al. 2012). Collectively, degeneration of the endothelium, astrocytes and pericytes of the neurovascular unit may diminish the ability to effectively coordinate changes in vessel diameter. Although the contribution of impaired vascular reactivity to cerebral small vessel disease is currently unclear, sustained impairments on dynamic regulation of flow are likely to lead to a state of chronic hypoxia within tissue, and may initiate downstream signalling events leading to inflammation and potentially ischaemia. The impact of reduced vascular reactivity on development of white

matter lesions and other pathology associated with small vessel disease and cognitive impairment therefore remains an important area of investigation.

1.2.3 Inflammation

Neuroinflammation describes the physiological response of immune cells in the brain to invading pathogens or cell debris. Microglia and astrocytes, the immune mediators of the brain, are able to recognise foreign pathogens or endogenous markers of host cell degeneration or stress through specific receptors, initiating morphological changes (gliosis) and secretion of pro-inflammatory signalling molecules, such as cytokines and chemokines (Ransohoff et al. 2015). This state of ‘activation’ enables glia to phagocytose pathogens or cell debris and defend the brain against infection. Release of pro-inflammatory mediators can also recruit immune cells from the periphery and facilitate their movement across the blood-brain barrier, in order to help fight the invading pathogen (Ransohoff et al. 2015). However, the physiological benefits of neuroinflammation rely critically on the resolution of the inflammatory response, as many pro-inflammatory signalling molecules also exert deleterious effects on normal cell function (Minter, Taylor and Crack; 2016). Prolonged, unresolved neuroinflammation may therefore impair the function of the cerebral vasculature to induce vascular cognitive impairment. Microarray analysis of gene expression throughout ageing revealed that increasing age was significantly associated with increased expression of pro-inflammatory genes, such as NFkB, IL1R1, and genes related to TNF- α signalling pathways (Primiani et al. 2014). Chronic inflammation is also implicated in hypertension, atherosclerosis and diabetes, and genetic mutations encoding inflammasomes – protein complexes that process inactive IL-1 β and IL18 to their active forms – are associated with increased risk of hypertension and increased risk of vascular pathology arising from type 2 diabetes (Omi et al. 2006; Klen et al. 2015). Both hypertensive and diabetic individuals also exhibit higher circulating levels of pro-inflammatory

cytokines such as IL-1 β (Krishnan et al. 2014; Lee et al. 2013). The downstream effects of these pro-inflammatory mediators are thought to be deleterious to the vasculature, and contribute to the development of small vessel disease and white matter lesions leading to vascular cognitive impairment. Interleukins such as IL-1 β induce the expression of matrix metalloproteinases (MMPs), which are able to degrade the basement membrane (Vecil et al. 2000; Yang et al. 2015). The basement membrane contains vital scaffolding proteins that anchor astrocyte endfeet to the vessels, and mediate endfoot polarisation of aquaporin-4 (Yan et al. 2016). Binding of aquaporin-4 to the agrin-dystroglycan complex within the basement membrane is therefore essential to maintaining functional contact between astrocytes and vessels, which may be lost where the basement membrane is disrupted (Yan et al. 2016; Wilcock, Vitek and Colton, 2009). Reactive astrogliosis caused by pro-inflammatory cytokines may also disturb astrocytic regulation of blood flow through changes in the expression of astrocyte calcium and sodium channels (Verkhratsky et al. 2016; Boscia et al. 2016). Consistent with this, white matter lesions in VCI have been shown to occur around vessels with inflammatory features, such as reactive astrogliosis and microgliosis, increased expression of MMPs and blood-brain barrier breakdown (Rosenberg, 2009). MMP-9 was also found to be elevated in the CSF of individuals with VCI relative to controls (Adair et al. 2004).

1.2.4 Blood-brain barrier breakdown

Increases in blood-brain barrier permeability have been identified in ageing, small vessel disease and vascular dementia (Bridges et al. 2014; Farrall and Wardlaw, 2009; Wardlaw et al. 2016). Animal models have also shown blood-brain barrier breakdown following hypoperfusion (Holland et al. 2015) and in hypertension (Bailey et al. 2009). Increases in blood-brain barrier permeability may be an early feature contributing to the pathogenesis of small vessel disease (Wardlaw, 2010), through leakage of harmful blood products into brain

parenchyma, leukocyte infiltration and disruption of the neurovascular unit (Bridges et al. 2014; Amantea et al. 2009). Hypoxia has been shown to induce the stabilisation of hypoxia inducible factor 1, resulting in phosphorylation of tight junction proteins and their mislocalisation, leading to BBB disruption (Engelhardt et al. 2014). Induction of hypoxic signalling is also associated with increased angiogenesis in order to increase tissue perfusion (Li et al. 2010), however, induction of angiogenic factors such as VEGF can also increase blood-brain barrier permeability, allowing entry of blood-products into the brain (Rigau et al. 2007; Zhang et al. 2000). The entry of blood products such as fibrinogen can induce microglial activation and production of pro-inflammatory cytokines such as interleukins and TNF- α , which modulate blood-brain barrier permeability through decreased tight junction protein expression and activation of matrix metalloproteinases that digest the basement membrane (Davalos et al. 2012; Turner and Sharp, 2016; Wang et al. 2014). Inflammatory chemokines also drive recruitment of circulating leukocytes from the bloodstream (Mildner et al. 2007). This process involves the increased expression of adhesion molecules, such as ICAM-1 and VCAM-1, on the luminal surface of endothelial cells in conjunction with the downregulation of tight junction proteins such as VE-cadherin (Rossi et al. 2011), in order to destabilise the blood-brain barrier and facilitate entry of peripheral immune cells to the brain. The increases in blood-brain barrier permeability resulting from hypoxia and inflammation may therefore contribute to blood-brain barrier 'leakiness' as evidenced in MRI studies of small vessel disease and vascular dementia (Farrall and Wardlaw, 2009), and severe blood-brain barrier disruption may progress to development of microhaemorrhages in some cases (Wardlaw, 2010). Disruption of the blood brain barrier is likely to drive further tissue hypoperfusion and inflammation, and the subsequent development of vascular and white matter lesions as a result of insufficient blood supply.

1.2.5 Cerebral amyloid angiopathy

Deposition of amyloid protein within brain parenchyma is a pathological hallmark of Alzheimer's disease, but in addition to parenchymal amyloid deposition, at least 90% of Alzheimer's disease patients also develop accumulation of amyloid within the vascular basement membrane of leptomeningeal medium and small-sized arteries and cortical arterioles (Love and Miners, 2016), a condition known as cerebral amyloid angiopathy. Cerebral amyloid angiopathy (CAA) is highly associated with cerebral small vessel disease. Individuals with pathologically confirmed CAA have a greater burden of small vessel disease (Charidimou et al. 2016), CAA is associated with white matter hyperintensities (Gurol et al. 2006; Holland et al. 2008); dilated perivascular spaces (van Veluw et al. 2015; Roher et al. 2003); arteriolosclerosis (Thal et al. 2003) and myelin loss (Tian et al. 2004). Amyloid has been shown to exert profound pathological effects on the vasculature, inducing degeneration of smooth muscle cells, vessel wall thickening and blood-brain barrier breakdown (Brown and Thore, 2011, Reijmer, van Veluw and Greenberg, 2016). The induction of vascular degeneration by CAA is associated with development of microbleeds (Dierksen et al. 2010; Gurol et al. 2012; Reuter et al. 2016; Fisher et al. 2011), another prominent feature of small vessel disease. Amyloid species have been shown to strongly activate microglia and astrocytes to induce proinflammatory cytokine production (Salminen et al. 2009), pericyte degeneration has also been observed in CAA (Giannoni et al. 2016); and both inflammation and loss of pericytes may contribute to blood-brain barrier breakdown observed in CAA and small vessel disease (Minter, Taylor and Crack, 2016; Sengillo et al. 2013). The presence of vascular amyloid has been shown in mouse models to induce cerebral hypoperfusion (Dorr et al. 2012; Massaad et al. 2010), hypoperfusion is also a prominent early feature of Alzheimer's disease (Chao et al. 2010). Vascular amyloid impairs the vasomotor responses to vasoactive stimuli or neuronal

activation (Kimbrough et al. 2015; Han et al. 2015; Dumas et al. 2012). Increased levels of soluble amyloid as well as the application of exogenous amyloid have also been shown to impair vascular function (Han et al. 2008; Park et al. 2005). Vascular amyloid is proposed to form a rigid cast around the vessels, restricting their dilation or constriction (Kimbrough et al. 2015). Degeneration of the vasculature, for example loss of vascular smooth muscle as described above, is likely to exacerbate this loss of contractility. Vascular amyloid is also proposed to mediate vascular dysfunction through disruption of endothelial signalling pathways induced by reactive oxygen species production (Han et al. 2015). Drainage of interstitial fluid is also reported to be impaired in mouse models of vascular amyloid deposition (Abel-Ornath et al. 2013; Hawkes et al. 2011) and is suggested to underlie the accumulation of vascular amyloid in CAA through impaired clearance of soluble amyloid (Hawkes et al. 2014). Furthermore, amyloid may reduce the levels of low density lipoprotein receptor-related protein 1 (LRP1) expression on endothelial cells (Deane et al. 2004; Bell et al. 2009) which mediates removal of amyloid across the blood brain barrier into the bloodstream (Storck et al. 2016). Two methods of amyloid clearance are therefore impaired in CAA, and may exacerbate the accumulation of amyloid at the vasculature. Collectively, amyloid drives substantial alterations in the vasculature that contribute to the development of small vessel disease and cognitive impairment.

1.2.6 Interactions between amyloid and vascular disease

Cerebrovascular pathology is frequently observed in Alzheimer's disease brain (Attems and Jellinger, 2014). Although, Alzheimer's disease is neuropathologically characterised by the deposition of amyloid plaques in brain parenchyma and the inclusion of hyperphosphorylated tau in neurons, neuropathological and neuroimaging studies indicate a spectrum of pathology between purely Alzheimer's disease or vascular dementia, where the majority of individuals

present with mixed pathology (Schneider et al. 2007). A body of evidence suggests that there may be significant interaction between cerebrovascular disease and Alzheimer's pathology. Hypoperfusion is an early feature of Alzheimer's disease that follows a stereotyped pattern which mirrors the accumulation of amyloid in early stages of the disease (Love and Miners, 2016). As noted above, amyloid exerts potent vasoconstrictive effects on the vasculature, soluble amyloid in brain parenchyma may therefore constrict vessels leading to hypoperfusion. Hypoperfusion in turn has been shown to increase the expression of amyloid precursor protein (Bennett et al. 2000; Salvadores et al, unpublished), and subsequently to favour processing by the amyloidogenic pathway mediated by increases in BACE1 (Zhang et al. 2016) resulting in enhanced vascular and parenchymal deposition (Okamoto et al. 2012; Zhiyou et al. 2009; Kitaguchi et al. 2009). Individuals with Alzheimer's disease have impaired vascular function (den Abeelen et al. 2014; Nation et al. 2013) and exhibit vascular degeneration (Baloyannis and Baloyannis, 2012; Challa et al. 2004). Findings from the Nun Study indicated that individuals with Alzheimer's disease pathology (senile plaques and neurofibrillary tangles) were more likely to be demented and have poorer cognitive function if lacunar infarcts were also present (Snowdon et al. 1997), indicating that vascular disease may enhance the severity of Alzheimer's disease and lower the threshold for cognitive impairment. There is evidence that the enlarged perivascular spaces characteristic of small vessel disease may reflect underlying disruption of ISF flow, and that this impedes the clearance of soluble proteins leading to a build-up of CAA (Weller et al. 2015). However, not all post-mortem studies have observed an interaction between vascular disease and Alzheimer's pathology (Esiri et al. 2014; Schneider et al. 2004), with reports that the effect of concomitant vascular disease is additive, rather than synergistic (Schneider et al. 2004; Park et al. 2014). Preclinical research, which avoids the confounds of studying end-stage disease associated with post-mortem experiments,

has examined potential interactions between vascular disease and Alzheimer's pathology using experimental models that aim to recapitulate aspects of small vessel disease, in addition to the use of APP-transgenic mice. In amyloid-expressing mice, induction of cerebral hypoperfusion was associated with enhanced vascular amyloid deposition (Okamoto et al, 2012) and a synergistic impairment on measures of learning and memory (Pimentel-Coehlo, Michaud and Rivest 2013; Yamada et al. 2011). Similarly, hypertension has also been shown to increase vascular amyloid accumulation, neuronal degeneration and accelerate learning and memory impairments in amyloid transgenic lines, relative to either hypertension or amyloid expression alone (Kruger et al. 2015; Faraco et al. 2016). Application of exogenous amyloid- β also exacerbated the neurovascular dysfunction induced by hypertension (Faraco et al. 2016). Dietary-induced hyperhomocysteinemia was also associated with redistribution of amyloid from parenchyma to the vasculature, and worsening of cognitive outcomes (Sudduth et al. 2014). Preclinical data therefore indicates that vascular pathology enhances the formation of CAA, which in turn exerts deleterious effects on the vasculature to disrupt vessel structure and function.

1.2.7 Oxidative stress

Reactive oxygen species (ROS) and reactive nitrogen species (RNS) are highly reactive molecules derived from oxygen or nitric oxide metabolism, including superoxide anions ($\bullet\text{O}_2^-$), hydroxyl radicals ($\bullet\text{OH}$), hydrogen peroxide (H_2O_2), nitric oxide ($\bullet\text{NO}$) and peroxynitrite (ONOO^-). In healthy tissue, ROS and RNS play a physiological role in regulating vascular homeostasis and various signalling pathways related to cell proliferation and survival (Zuo et al. 2015), however, increases in ROS/RNS are also associated with damage to proteins and lipids and deleterious effects on cellular homeostasis (Valko et al. 2007). Because of this, the production of ROS/RNS is balanced by the activity of antioxidant molecules that prevent

pathological build-up of ROS/RNS. These include free radical scavengers such as glutathione, vitamins C and E, and antioxidant enzymes such as superoxide dismutase, which are able to convert superoxide to hydrogen peroxide which is then further metabolised to oxygen and water by glutathione peroxidase (Trachootham et al. 2008). However, in many disease states this balance becomes disrupted, either through increased ROS/RNS production or through reduced antioxidant activity, leading to a state of oxidative or nitrosative stress (Drummond et al. 2011). This has also been proposed to occur as an early event in vascular dysfunction that may contribute to vascular cognitive impairment (Iadecola, 2013). Within the brain, the major sources of ROS/RNS are enzymatic systems including NADPH oxidase (NOX), xanthine oxidase, nitric oxide synthase (NOS) and mitochondria. The expression and activity of different ROS/RNS sources is heterogeneous and cell-dependent, and the pathological contribution of each source likely depends on the disease state.

1.2.7.1 NADPH oxidases

NADPH oxidases (NOX) are membrane-bound enzymes that generate superoxide species through oxidation of NADPH. A total of 7 NOX isoforms have been described (NOX1, NOX2, NOX3, NOX4, NOX5, DUOX1, DUOX2), each differs in their subunit composition, cellular expression and method of activation. Within the brain, NOX1, NOX2 and NOX4 are the best described, although expression of NOX3 is also reported in neurons. NOX5 is absent from mouse and rat models so has not been extensively studied, also very little is known about DUOX1 and DUOX2 isoforms of NOX within the CNS. NOX1 expression has been described in neurons, astrocytes, microglia, endothelial cells and vascular smooth muscle cells. NOX1 activation depends on the translocation of cytosolic subunits p47phox and p67phox to the membrane, following which NOX1 is able to generate superoxide. NOX2 is activated in a similar manner, through translocation of the cytosolic organiser subunit p47phox (with

associated p67 and p40 subunits) to the membrane bound subunits, followed by interaction with GTPase Rac. NOX2 also produces superoxide, and is thought to be expressed in microglia, neurons, astrocytes and endothelial cells. NOX4 differs from other NOX isoforms in that its membrane bound subunits do not require interaction with cytosolic subunits, and as such NOX4 is constitutively active. In addition, NOX4 is also reported to produce hydrogen peroxide rather than superoxide anions. NOX4 is predominantly expressed in endothelial cells and vascular smooth muscle cells, but is also expressed in microglia, neurons and astrocytes.

1.2.7.2 Other sources of ROS/RNS

Mitochondria produce superoxide anions as a by-product of oxidative metabolism and the electron transport chain during the generation of ATP. Mitochondria have also been demonstrated to generate hydrogen peroxide. The enzyme xanthine oxidase is also reported to produce superoxide species as a by-product of purine metabolism. Nitric oxide synthase (NOS) is an enzyme responsible for the production of nitric oxide. Three isoforms exist: inducible NOS (iNOS), neuronal NOS (nNOS) and endothelial NOS (eNOS). nNOS and eNOS are constitutively active and predominantly expressed in neurons and endothelium respectively, although both isoforms are also expressed in other cell types. Once nitric oxide is generated, it can undergo a reaction with superoxide anions, to produce the highly reactive species peroxynitrite. Cyclooxygenase-2 (COX2), an enzyme that typically exerts vasoprotective effects through the activity of prostaglandins, is also able to generate superoxide species.

1.2.7.3 Physiological role of ROS signalling

The interaction of ROS/RNS with redox reactive residues on proteins causes the structure and function of those proteins to be altered, allowing ROS/RNS to regulate key signalling pathways involved in cellular homeostasis. These include MAPK signalling, PI3K signalling and Nrf2

antioxidant signalling (Trachootham et al. 2008). In addition, NOX2-mediated release of superoxide from phagocytic immune cells is critical for microbial defence, as individuals that lack this response are vulnerable to severe microbial infection in a condition known as chronic granulomatous disease (CGD) (Stasia and Li, 2008). ROS/RNS signalling is also critical for normal vascular function. Nitric oxide is a major mediator of vasodilation, it is generated and released by endothelial cells to decrease intracellular calcium in vascular smooth muscle cells and induce their relaxation and subsequent vasodilation (Vara and Pula, 2014). NOX4 signalling is also thought to promote the survival and proliferation of endothelial cells and vascular smooth muscle cells (Drummond et al. 2011).

1.2.7.4 Pathological ROS/RNS signalling

Due to the highly reactive nature of ROS/RNS and their propensity to affect protein structure and function, their activity is modulated by antioxidant defence mechanisms. When ROS/RNS signalling outweighs the antioxidant capacity of a cell, a state of oxidative stress is induced with numerous pathological consequences for cell function. In the vasculature, oxidative stress reduces the availability of nitric oxide, leading to the loss of vascular tone and inducing endothelial dysfunction. Endothelial dysfunction and increased production of free radicals is implicated in vascular cognitive impairment. Ageing, a prominent risk factor for small vessel disease and vascular cognitive impairment, is associated with increased oxidative stress. Cerebral arterioles of aged rats and mice demonstrate blunted responses to vasodilators that are reversed following treatment with apocynin, a NOX inhibitor, or tempol, a free radical scavenger (Mayhan et al. 2008; Modrick et al. 2009). Markers of oxidative stress are also increased in human ageing and in mouse models (Lucas et al. 2016; Park et al. 2007). Cerebral amyloid angiopathy has been shown to impair vascular function through increased activity of NOX2, resulting in increased levels of vascular 3-nitrotyrosine, a marker of nitrosative damage

caused by peroxynitrite formation (Han et al. 2015). Endothelial dysfunction is widely described in animal models of hypertension and also in clinical studies, with vessels isolated from animal models or hypertensive individuals showing diminished responses to vasodilators (Viridis et al. 2009; Viridis et al. 2013). This has been attributed both to enhanced NOX and COX activity, as inhibitors of each of these enzymes restores endothelial function and decreases the production of ROS/RNS in the vessel wall (Viridis et al. 2015; Viridis et al. 2013). Several hypertensive animal models are also generated by intravenous administration of angiotensin II, which acts to increase oxidative stress and diminish nitric oxide availability (Reckelhoff and Romero, 2003). The administration of apocynin also restores blood pressure and endothelial function in a genetic rat model of hypertension (Perassa et al. 2016). The impact of hypertension on the vascular system and the increases in ROS/RNS production in the vasculature may drive hypertrophy and endothelial dysfunction of the cerebral arterioles, leading to cerebral small vessel disease. Ischaemic stroke is associated with a rapid burst of ROS/RNS production upon cessation of blood flow, which is then followed by a second burst upon reperfusion, contributing to reperfusion injury (Rodrigo et al. 2013). This is associated with increased activity of NOX2, as genetic deletion of this isoform can reduce infarct progression (Jackman et al. 2009; Walder et al. 1997). Cellular damage and inflammatory processes that remain following ischaemic stroke may also drive sustained increases in oxidative stress after the initial insult. In addition, NOX4 signalling is strongly upregulated following stroke, and inhibition of NOX4 several hours after stroke onset was able to rescue neurological deficits and reduce mortality (Kleinschnitz et al. 2010). Studies of mild hypoperfusion also suggest that oxidative stress may play a pathogenic role in the development of cognitive impairment. Dong et al. (2011) show increased 3-nitrotyrosine in brains of hypoperfused mice, and showed that treatment with the superoxide scavenger tempol reduced

inflammation, reduced white matter lesions and improved performance on spontaneous alternation tests of behaviour, suggesting oxidative stress may result in the downstream pathologies that drive vascular cognitive impairment. Washida et al. (2010) also showed an increase in the number of endothelial cells positive for 8-hydroxy-deoxyguanosine (8-OHdG), a marker of oxidative stress in hypoperfused mice. In rat models of hypoperfusion, oxidative stress markers are also increased (Zhang et al. 2011; Ueno et al. 2009; Kim et al. 2008). Interestingly, increased oxidative stress has also been demonstrated in white matter lesions from individuals with vascular cognitive impairment (Back et al. 2011) and plasma markers of oxidative stress correlate with the extent of white matter damage (Shibata et al. 2004b). However, the source of ROS/RNS production has not been extensively studied in hypoperfusion models or in vascular cognitive impairment. Choi et al. (2014) demonstrated that an increase in NOX1 activity may be critical for ROS/RNS production in hippocampal neurons, and subsequently result in neuronal loss in hypoperfused rats. However, the impact of hypoperfusion on NOX isoform expression within the white matter or within the vasculature was not investigated, nor was the contribution of other ROS/RNS sources. Identification of the source of pathogenic ROS/RNS may be critical for the development of therapeutic interventions. Antioxidant scavengers such as vitamins C and E have failed or had limited success in clinical trials, the reasons for which are manifold. Typically they have been trialled in end-stage vascular disease (Schiffrin, 2010), antioxidants are also challenging to deliver in sufficiently high concentrations to neutralise superoxide, and the oxidation of treatment compounds may in some cases generate further oxidative species (Thomas and Stocker, 2000). Therefore, identifying the specific source of pathogenic ROS/RNS would enable greater targeting and delivery of therapeutic interventions to reduce oxidative stress. Vascular risk factors and small vessel disease pathology are associated with an increase in ROS/RNS

production, resulting in increased oxidative stress. Ultimately, this may result in oxidative damage to key proteins related to cellular homeostasis and vascular tone, driving endothelial dysfunction, hypoperfusion and degeneration of brain tissue, leading to vascular cognitive impairment (Figure 1.5).

1.2.8 Current treatment options for the prevention of VCI

To date there is a lack of approved, effective therapies for vascular cognitive impairment. Improving vascular health has been identified as a strategy for prevention of VCI (Gorelick et al. 2011), as such, drugs that target the cerebral vasculature and prevent the onset of cerebral small vessel disease (or halt its progression) may reduce the incidence of VCI. A list of drugs that may be effective in preventing small vessel disease can be found in Table 1.1 (Bath and Wardlaw, 2015). These include anti-platelet agents, blood-pressure lowering drugs, and vasodilators such as nitric oxide donors and phosphodiesterase inhibitors. Clinical trials with small vessel disease as a primary outcome are limited. However, some studies have indicated that blood-pressure lowering drugs may be successful in preventing vascular cognitive impairment (Valenzuela et al. 2012; Rouch et al. 2015). Clinical trials are currently ongoing to investigate effects of L-arginine, a NO donor, on white matter progression and cognition (Calabro et al. 2013) and cilostazol, a phosphodiesterase inhibitor and anti-platelet agent, on white matter lesion development (Bath and Wardlaw, 2015). Drugs licensed for the treatment of Alzheimer's disease, such as acetylcholinesterase inhibitors and the NMDA receptor antagonist memantine, have shown mild cognitive benefits in vascular dementia (Malouf and Birks, 2004; Ritter and Pilai, 2015); however these treatments are not disease-modifying. Administration of amyloid immunotherapy has been trialled in order to reduce cerebral

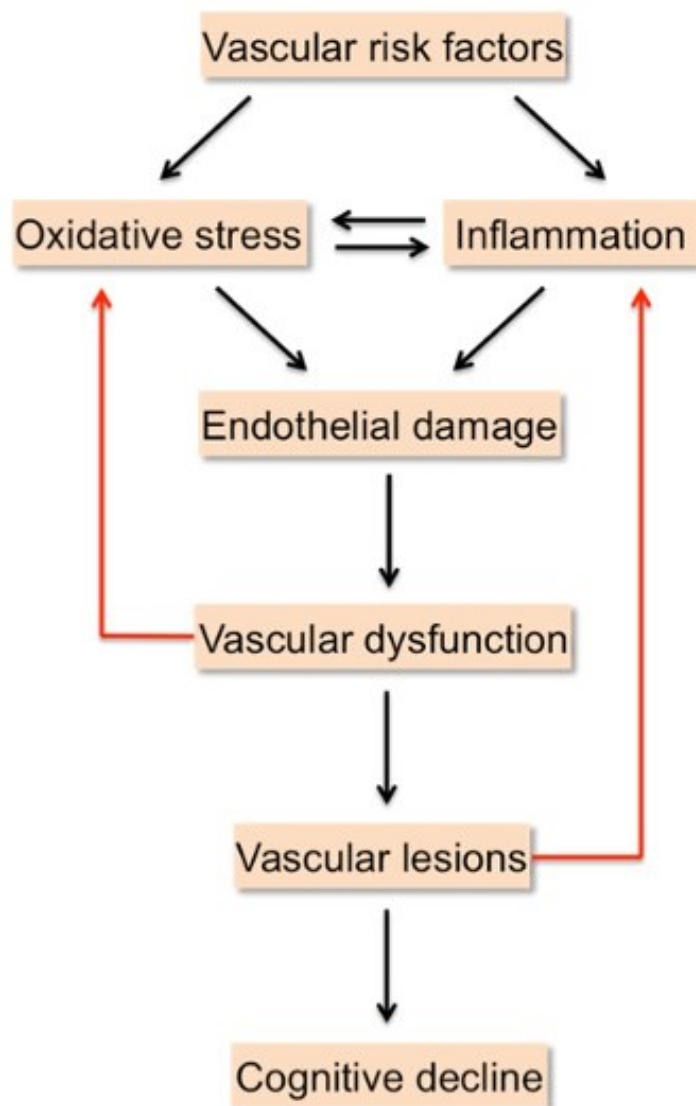


Figure 1.5 Schematic representation of putative mechanisms leading to vascular cognitive impairment. Oxidative stress and inflammation caused by vascular risk factors lead to vascular dysfunction and development of vascular lesions. This in turn further increases the production of reactive oxygen species and inflammatory cell activation, initiating a vicious cycle which ultimately results in cognitive impairment.

amyloid burden (Lannfelt, Relkin and Siemers, 2014). Although administration of bapineuzumab was shown to reduce cerebral vascular amyloid (Zago et al. 2013), it was associated with development of microhaemorrhages and visible haemosiderin deposits on T2* weighted imaging, known as amyloid-related imaging abnormalities (ARIA) (Zago et al. 2013; Arrighi et al. 2015). Although the incidence of ARIA reduces with increasing exposure to the drug (Arrighi et al. 2015), the effects of this initial insult on individuals with pre-existing vascular pathology is not known, and as such amyloid immunotherapy may not be a suitable strategy for treatment of small vessel disease in vascular cognitive impairment.

To date there is a lack of randomised, double blind, controlled clinical trials investigating the impact of therapeutic approaches to prevent or treat vascular cognitive impairment, and as such there are currently no approved intervention strategies. Experimental animal models provide a basis in which to study the underlying mechanisms that lead to vascular cognitive impairment. This may generate further insight as to existing drugs which may be effective if trialled in VCI, and also may reveal new targets for pharmacological intervention.

Table 1.1 Drugs and drug classes in stroke that may be worth testing for the prevention or treatment of small vessel disease. Taken from Bath and Wardlaw, 2015.

Activity	Drug	Indication	Notes
Acetylcholinesterase inhibitors	Donepezil	Dementia treatment	
	Galantamine	Dementia treatment	
	Memantine	Dementia treatment	
	Rivastigmine	Dementia treatment	
Anticoagulation	Warfarin	Secondary stroke prevention in AF	
Antiplatelet	Aspirin	Acute ischaemic stroke/TIA	Strong antiplatelet
		Secondary stroke prevention	
	Clopidogrel	Acute ischaemic stroke	Strong antiplatelet
		Secondary stroke prevention	
Blood pressure lowering		Secondary stroke prevention	
Lifestyle changes			
Lipid lowering	Statins	Primary/secondary stroke prevention	
Endothelin antagonists	Clazosentan, TAK-044	Subarachnoid haemorrhage	
Neurotrophin	Cerebrolysin	Vascular dementia	
Nitric oxide		Experimental acute stroke	Strong antiplatelet †
		Acute/subacute stroke	
Phosphodiesterase inhibitors	Cilostazol	Experimental acute stroke	
		Secondary stroke prevention	Weak antiplatelet
	Dipyridamole	Acute ischaemic stroke/TIA	Weak antiplatelet
		Secondary stroke prevention	
	Pentoxifylline	Acute ischaemic stroke	Weak antiplatelet
		Dementia prevention	
	Triflusal	Secondary stroke prevention	Weak antiplatelet
Prostacyclin	Prostacyclin	Acute ischaemic stroke	Strong antiplatelet
Stimulants	Amphetamine	Recovery from ischaemic stroke	
Vitamins	B6, B9, B12	Secondary stroke prevention	
Xanthine oxidase inhibitors	Allopurinol, febuxostat	Prevention of gout	
Other approaches	Nicotiflorin (flavonoid), minocycline and relaxin		

1.3 Animal models of vascular cognitive impairment

In order to more fully understand the contribution of vascular risk factors to the development of cognitive decline in VCI, experimental animal models have been established to allow the manipulation of vascular parameters such as cerebral blood flow and amyloid angiopathy. These models provide mechanistic insight into disease progression and an opportunity to test new therapeutic interventions.

1.3.1 Models of cerebral hypoperfusion

Hypoperfusion has been identified as an early clinical symptom of vascular cognitive impairment and is considered a biomarker for cognitive decline (Iturria-Medina et al. 2016). As such, animal models of cerebral hypoperfusion have been established to determine the pathological events that occur downstream to affect cognition. In clinical studies, reductions in blood flow between 20%-40% are typically observed (Nagata et al. 2016; Asllani et al. 2008), and a good experimental model should aim to replicate such a reduction. In rats and mice, experimental models of hypoperfusion have been developed by occluding or stenosing the cerebral arteries, typically the common carotid arteries. The most commonly used models of hypoperfusion and respective reductions in blood flow are outlined in Table 1.2. Reductions in blood flow vary considerably across models and species, and it is important to distinguish between models of hypoperfusion and ischaemia. In order to develop a model of mild cerebral hypoperfusion that recapitulates the subtle reductions in flow seen clinically, Shibata et al. (2004a) used microcoils to reduce the lumen size of the common carotid arteries in mice, known as bilateral common carotid artery stenosis (BCAS). This reduces blood flow to the forebrain, reproducing the reductions in flow observed in vascular cognitive impairment (Schuff et al. 2009). In the BCAS model, microarray analysis of white matter indicates that at

just 3 days following hypoperfusion there are alterations in multiple biological processes, with inflammatory pathways and angiogenesis being prominently altered (Reimer et al. 2011). At 1 month following BCAS there is reliable induction of white matter disruption (Shibata et al. 2004a; Holland et al. 2011), both when assessed using in vivo MRI approaches and also through histology. Other features that have been observed after 1 month include activation of astrocytes and microglia (Shibata et al. 2004a; Saggiu et al. 2016), disruption of axon-glia integrity (Reimer et al. 2011) and blood-brain barrier disruption (Nakaji et al. 2006). Several studies have also examined the effects of longer, sustained reductions in blood flow and demonstrate that in addition to white matter pathology, hypoperfused mice also develop profound vascular alterations. At 6 months following BCAS, hypoperfused mice develop microinfarcts and microbleeds, alterations in tight junction proteins and disruption of gliovascular interactions (Holland et al. 2015). At 8 months following BCAS, hippocampal neuronal loss was also observed, as well as further impairments on spatial reference memory (Nishio et al. 2010). Thus, the BCAS model is able to recapitulate key aspects of vascular cognitive impairment, particularly the pathological features of small vessel disease such as white matter lesions, microinfarcts and microbleeds, and progressive memory impairments related to forebrain circuitry. The BCAS model therefore offers an opportunity to test hypotheses related to vascular cognitive impairment and to trial potentially disease-modifying therapeutic interventions. One potential drawback of the BCAS model is that blood flow has been shown to recover in the month following surgery (Shibata et al. 2004). In an attempt to model the sustained reductions in flow observed in vascular cognitive impairment, Hattori et al. (2014) developed the ameroid constrictor model, in which constrictor devices are applied to the common carotid arteries and gradually reduce flow over 28 days (gradual common carotid

artery stenosis/GCAS). This model also avoids the acute reduction in flow immediately following surgery in BCAS or UCCAO models.

In addition to neuropathological features of VCI such as white matter disruption and inflammation, hypoperfusion models have also been shown to replicate aspects of cognitive dysfunction observed in VCI. In the BCAS model, impairments on spatial working memory are consistently found following 1 month hypoperfusion in the absence of other behavioural impairments (Shibata et al. 2007; Coltman et al. 2011; Saggu et al. 2016). Impaired spatial working memory has also been consistently reported in other models of hypoperfusion, including the ACAS model (Hattori et al. 2015), GCAS model (Hattori et al. 2014) and the rat 2V gradual occlusion model (Kitamura et al. 2012). At longer durations of hypoperfusion in the BCAS model (i.e. 8 months), spatial reference memory is also impaired, in line with hippocampal neuronal loss observed at this time (Nishio et al. 2010). In the ACAS model, impairments on spatial reference learning and memory are also observed after only 1 month, attributable to the greater blood flow reductions and evident white and grey matter pathology in this model (Hattori et al. 2015). Together, these behavioural findings highlight the relevance of hypoperfusion models to human VCI in which frontal-subcortical circuitry is disrupted.

Table 1.2 Experimental models of chronic cerebral hypoperfusion

Model Name	Species	Method	rCBF procedure baseline)	following (% of	Reference
One vessel occlusion (1VO)	Mouse	Unilateral occlusion of common carotid artery	60%		Yoshizaki et al. (2008)
	Rat	Unilateral occlusion of common carotid artery	75%		De Ley, Nshimyumuremyi and Leusen (1985)
Two vessel occlusion (2VO)	Rat	Bilateral occlusion of common carotid arteries	30% at 1 week, 60% at 4 weeks		Otori et al. (2003)
2VO or global ischaemia	Mouse	Bilateral occlusion of common carotid arteries	<5% immediately following procedure		Wellons et al. (2000) (C57Bl/6J)
BCAS	Mouse	Bilateral stenosis of the common carotid arteries using microcoils	70% at 2hrs, 85% at 28 days		Shibata et al. (2004a) (C57Bl/6J)
GCAS	Mouse	Gradual bilateral narrowing of the common carotid arteries using an ameroid constrictor	>95% at 2hrs, 75% at 28 days		Hattori et al. (2014)
ACAS	Mouse	Asymetric carotid artery stenosis by application of a microcoil to the left and ameroid constrictor to the right carotid	64% ameroid constrictor, 74% microcoil side		Hattori et al. (2015)
3VO	Rat	Bilateral occlusion of common carotid arteries, unilateral vertebral artery occlusion	50%		Busch et al. (2003)
4VO	Rat	Bilateral occlusion of common carotid arteries and vertebral arteries	~15%		Busch et al. (2003)

1.3.2 Models of amyloid deposition

In order to model the impact of amyloid deposition on vascular function, transgenic mice have been engineered to express the human amyloid precursor protein gene containing mutations known to cause familial Alzheimer's disease. The resulting pattern of amyloid deposition is therefore determined by the mutations expressed, and can vary substantially between different transgenic models. Specific mutations can be expressed to encourage vascular amyloid deposition, such as the Dutch and Iowa mutations discovered in families with inherited cerebral amyloid angiopathy. The most commonly used mouse models of vascular amyloid deposition include the Tg2576, TgSwDI, ArcA β and APP23 (Hsiao et al. 1996; Davis et al. 2004; Klohs et al. 2011; Calhoun et al. 1999). Using these models, vascular amyloid has been shown to contribute to oxidative stress, impairments on neurovascular coupling, neurovascular unit disruption, glial activation and the development of microhaemorrhages (Han et al. 2015; Kimbrough et al. 2015; Reuter et al. 2016). However, it should be noted that the majority of these models also develop parenchymal amyloid deposition, and are also associated with overexpression of the APP gene that has been implicated in disturbed postnatal development (Rodgers et al. 2012), and does not reflect the natural expression pattern of the endogenous gene.

Owing to the high degree of overlap between vascular pathology and Alzheimer's pathology observed in individuals with cognitive impairment, increasing interest has been paid to combined models of both cerebral hypoperfusion and amyloid deposition. Hypoperfusion has been shown to enhance both parenchymal and vascular amyloid deposition (Kitaguchi et al. 2009; Okamoto et al. 2012); however another study found that parenchymal amyloid plaque number was reduced following hypoperfusion whilst soluble amyloid species were increased (Yamada et al. 2011). The combination of hypoperfusion and amyloid deposition was also

shown to increase white matter disruption, impair cognition and to increase the number of cortical microinfarcts in these studies relative to either hypoperfusion or amyloid deposition alone, suggesting a synergistic interaction between these two pathologies. The additive effects of amyloid deposition and hypoperfusion will be further investigated in the work described in this thesis.

1.3.3 Additional models of VCI

Although some features of cerebral small vessel disease can be replicated in rodent models of hypoperfusion such as the BCAS model, other features of small vessel disease may be better replicated in alternative models such as the spontaneously hypertensive stroke-prone rat (SHRSP). The SHRSP develops hypertension, cortical infarcts, enlarged perivascular spaces, white matter lesions and microinfarcts and as such has been described as a potentially appropriate model for human lacunar stroke (for review see Bailey et al. 2011). Endothelial dysfunction occurs in SHRSPs in the form of blood-brain barrier leakage (Sironi et al. 2004), impaired autoregulation (Smeda, VanVliet and King, 1999) and increased vascular resistance (Werber and Heistad, 1984). Although the basis for propensity to stroke is not fully understood, the elevated blood pressure and consequent pathology in this model make it a suitable choice to study several features of small vessel disease. Additional models, such as the hyperhomocysteinemia (HHcy) model, develop vascular degeneration and learning and memory deficits following a diet that disrupts methionine or folate metabolism (Troen et al. 2008; Dayal and Lentz, 2008). Cerebral autosomal dominant arteriopathy with subcortical infarcts and leukoencephalopathy (CADASIL) is a genetic form of cerebral small vessel disease caused by mutations in the Notch3 gene, and is associated in humans with an early onset and increased risk for stroke and vascular dementia (Joutel et al. 1996; Chabriat et al. 2009). CADASIL can be modelled in mice by targeting Notch 3, resulting in blood-brain

barrier failure, pericyte dysfunction, reduced cerebral blood flow, deficits on neurovascular coupling and white matter damage (Joutel et al. 2010; Ghosh et al. 2015). The complexity and heterogeneity within small vessel disease means that no experimental model can faithfully recapitulate the complete spectrum of small vessel disease and vascular cognitive impairment. Certain models can be used to study specific aspects of neuropathology, such as the use of APP mice to study cerebral amyloid angiopathy, or models can be used to investigate mechanisms related to vascular risk factors, such as in the study of hypertensive stroke-prone rats. Within this thesis, induction of BCAS in mice will be used to investigate mechanisms by which hypoperfusion, an established risk factor for VCI, impacts on cerebral vasculature.

1.4 Imaging the cerebrovascular system

Alterations of the cerebrovascular system and disruption of cerebral blood supply is implicated in the development of vascular dementia, post-stroke dementia and Alzheimer's disease (Iadecola, 2013; Zlokovic, 2011). Experimental animal models, such as the BCAS model of cerebral hypoperfusion or transgenic mouse lines that recapitulate aspects of cerebral amyloid angiopathy, have been established to investigate how vascular alterations may contribute to cognitive decline. In both preclinical animal models and clinical studies of individuals with vascular cognitive impairment, imaging approaches such as magnetic resonance imaging (MRI) and positron emission tomography (PET) have been used to provide non-invasive, in vivo measures of vascular structure and function. These in vivo measures provide a basis on which to test hypotheses and to measure outcomes following therapeutic intervention. In preclinical models, in vivo observations can often be validated ex vivo, with clear translational value to the interpretation of clinical imaging findings. In particular, imaging approaches have been developed that allow key features of SVD to be studied in rodents (e.g. reduced CBF, vascular alterations and inflammation).

1.4.1 Resting cerebral blood flow

Reductions in resting cerebral blood flow are highly associated with cognitive impairment and can be modelled in mice using bilateral common carotid artery stenosis (BCAS). Alterations in resting cerebral blood flow can be assessed by MRI using an arterial spin labelling (ASL) approach, in which blood within a portion of the brain is magnetised, and the rate at which this is exchanged with non-magnetised blood can be used to assess the rate of blood flow (Kober et al. 2008). ASL has been used clinically to detect the reduction in cerebral blood flow that occurs with ageing (Liu et al. 2012), and also to show that further regional reductions in flow are present in individuals that go on to develop Alzheimer's disease (Chao et al. 2010). Hattori

et al. (2016) used ASL to detect persistent reductions in hippocampal and cortical blood flow at 1 month following BCAS in mice. ASL has also been used to investigate links between amyloid deposition and hypoperfusion in transgenic mice. In TgSWIND (J20) mice cerebral blood flow was reduced in the hippocampus where amyloid deposits were present but was similar to controls in the thalamus, a region spared from amyloid deposition in this model (Lin et al. 2013). Alterations in blood flow can also be assessed non-invasively using laser Doppler or laser speckle contrast imaging (Shibata et al. 2004; McQueen et al. 2014). In animal models and clinical studies, these techniques are limited to measuring blood flow in the superficial cortical vasculature and cannot provide measures of flow in deeper brain regions. PET imaging can also be used to measure cerebral blood flow, but requires the synthesis and administration of a radiolabelled tracer. The use of blood as an endogenous tracer in ASL, and the ability to measure blood flow in regions throughout the brain means that ASL may be advantageous for assessing blood flow changes in both experimental models and in clinical studies.

1.4.2 Vessel number

Alterations in vessel number have previously been reported to occur with ageing, following cerebral hypoperfusion and in amyloid-expressing transgenic mice or Alzheimer's disease brains (Brown and Thore, 2011; Park et al. 2014; Miao et al. 2005). Cerebral vessels typically range in diameter from approximately 1mm in cerebral arteries and veins, to approximately 5-10µm in diameter at the capillary level. Large, cerebral arteries can be directly visualised using time of flight magnetic resonance angiography (TOF-MRA), whereby the high flow rate in these vessels generates contrast between the stationary tissue and flowing blood (Beckmann, Stirnimann and Bochelen, 1999). TOF-MRA has been used to demonstrate remodelling of cerebral arteries following bilateral common carotid artery occlusion in rats (Soria et al. 2013), and to detect flow voids in aged APP mice (El Tayara et al. 2010). In small calibre vessels,

where flow rates are lower, direct visualisation can be achieved using contrast-enhanced MRA, whereby the steady-state concentration of iron oxide within the blood generates contrast against the extravascular compartment. Klohs et al. (2012) were able to demonstrate a reduction in intracortical vessels in aged arcA β mice relative to wild type mice, and were able to detect vessels just 20 μ m in diameter. This approach, however, requires sophisticated hardware and it is unclear what volume of the brain could be assessed at this resolution. In addition, immunohistochemistry from the same study did not detect a reduction in blood vessels. In order to quantify small calibre vessels throughout the brain, the index 'Q' can be calculated from the shift in relaxation rate of R2 and R2* caused by the administration of an intravascular contrast agent, and is proposed to directly relate to vessel density (Jensen and Chandra, 2000). Wu, Tang and Chandra (2004) further developed this approach to generate a measure of vessel number 'N'. Q-map imaging, and the subsequent calculation of vessel number, has been shown to be in good agreement with histological observations (Wu, Tang and Chandra, 2004; Bosomtwi et al. 2008), and the technique has been used to highlight increases in vessel density in tumours (Ullrich et al. 2011) as well as to longitudinally track the changes in vessel number following ischaemic stroke produced by middle cerebral artery occlusion (Boehm-Sturm et al. 2013). Q-map imaging may therefore represent a useful tool to study dynamic changes in vessel number following hypoperfusion or in amyloid-expressing mouse models, and potentially in response to therapeutic intervention.

1.4.3 Inflammation

Vascular diseases, such as hypertension, ischaemic stroke and diabetes, as well as dementias such as Alzheimer's disease and vascular dementia are associated with increased inflammation and the pathological production of pro-inflammatory cytokines and chemokines (for reviews see Viridis, Dell'Agnello and Taddei (2014) and Heneka et al. (2015)). MRI provides an

opportunity to study the dynamic changes in inflammation that occur following cerebral hypoperfusion, as well as in experimental models of amyloid deposition. Assessing neuroinflammation with MRI also provides an alternative to histology that is less labour-intensive, whilst still retaining the spatial resolution that is lost when performing biochemical assays. Inflammatory events/processes may be visualised on MRI through the use of iron oxide contrast agents that have a high intrinsic transverse relaxivity, and therefore appear hypointense on T2*-weighted images (Klohs et al. 2015). Following intravenous administration, iron oxide particles are phagocytosed by inflammatory macrophages. Ongoing inflammation within the brain is associated with the accumulation of inflammatory cells, and therefore an increase in the local concentration of iron oxide particles within the inflamed region, detected as a hypointensity on T2*-weighted imaging. Klohs et al. (2015) used this approach to detect iron oxide uptake in aged arcA β mice concurrent with vascular amyloid build-up. In this study, iron-containing cells were suggested to be perivascular macrophages rather than microglia or circulating immune cells, however the mechanism of iron uptake may vary according to the disease model, and areas of blood-brain barrier breakdown may also lead to iron accumulation in the parenchyma in the absence of inflammatory cells. In clinical imaging studies, contrast-enhanced T2* has been used to detect carotid atherosclerotic plaques (Trivedi et al. 2006) and to measure reductions in atherosclerotic inflammation following treatment with statins (Tang et al. 2009). In the brain, contrast-enhanced T2* has also been used to demonstrate inflammatory changes following ischaemic stroke (Saleh et al. 2004). Other approaches to measure inflammation in vivo include PET imaging using radiotracers that target specific aspects of neuroinflammation such as adhesion molecules or microglial activation (Jacobs, Tavitian and the INMiND Consortium, 2012), and ultrasound approaches that utilise targeted microbubbles to detect inflammatory processes (Lindner et al. 2009). Iron oxide contrast agents

for MRI can also be targeted to particular proteins, for example vascular cell adhesion molecule 1 (VCAM1), in order to increase the specificity for one aspect of neuroinflammation. The good safety profile of iron oxide contrast agents for MRI (Doerfler et al. 2000) combined with the high spatial resolution of MRI approaches make contrast-enhanced T2* imaging an attractive choice for detecting inflammatory events in vivo.

Overall, MRI approaches have significant utility and translational value for the detection of vascular alterations. The application of MRI approaches to experimental models can generate in vivo data on vascular structure and function, and would provide highly valuable tools to assess vascular parameters in longitudinal studies, as well as providing a basis with which to test hypotheses and therapeutic interventions. Within this thesis, MRI approaches to assess resting cerebral blood flow, vessel number, vascular lesion burden and inflammation will be developed for use in experimental mouse models. These approaches will then be utilised to investigate the impact of vascular risk factors such as ageing and chronic cerebral hypoperfusion on cerebral vasculature.

1.5 Summary

Vascular risk factors such as age, hypertension, stroke and cerebral amyloid angiopathy are associated with dysfunction of the cerebrovascular system, resulting in loss of adequate blood supply and the development of vascular lesions and small vessel disease. The accumulation of vascular pathology and tissue hypoxia ultimately leads to neuronal loss, cognitive decline and a condition of vascular cognitive impairment. Oxidative stress may be a critical early feature in driving endothelial dysfunction, and ongoing inflammation as a result of vascular risk factors may perpetuate tissue damage through the release of pro-inflammatory cytokines and further disruption of the neurovascular unit (Figure 1.5).

The overall aim of this thesis was to investigate the mechanisms by which ageing, cerebral hypoperfusion and amyloid deposition impair the structure and function of the cerebrovascular system. In order to investigate vascular alterations in experimental models, an important additional aim of this thesis was to develop and validate sensitive MRI approaches that would allow the detection of vascular alterations in vivo.

1.6 Hypothesis

It was hypothesized that ageing and chronic cerebral hypoperfusion would induce cerebrovascular dysfunction, inflammation and cognitive decline, and that the additional presence of amyloid deposition would exacerbate these impairments. It was further hypothesized that both ageing and chronic cerebral hypoperfusion are associated with increases in NOX-derived oxidative stress, and that inhibition of NOX activity would prevent cerebrovascular dysfunction and the onset of cognitive decline.

1.7 Aims

In order to address the hypotheses, the thesis investigated the following specific aims:

1. To develop MRI techniques that allow the in vivo assessment of vessel number, resting cerebral blood flow and cerebral inflammation; and to assess the sensitivity of these techniques and validate MRI-derived measures using established in vivo and ex vivo methods.
2. To assess resting cerebral blood flow, neurovascular coupling and structural integrity of the neurovascular unit in young and aged wild type mice and compare these changes to TgSwDI mice (with amyloid).
3. To assess oxidative stress, neurovascular coupling, vascular lesion development and spatial learning and memory following cerebral hypoperfusion in wild-type mice, and to investigate whether these alterations are exacerbated in TgSwDI mice (with amyloid).
4. To compare TgSwDI mice (with amyloid) treated with apocynin and non-treated mice on measures of neurovascular coupling, vascular lesion development, inflammation and cognition following cerebral hypoperfusion.

Chapter 2.

Materials and Methods

Materials and Methods

2.1 Animals

Male, heterozygous TgSwDI mice and their wild-type C57BL/6J littermates were bred in-house for use in studies. TgSwDI mice express human amyloid precursor protein (APP) containing the Swedish (K670N/M671L), Dutch (E693Q) and Iowa (D694N) mutations; human APP is expressed under the control of the Thy1.2 promoter and is approximately 50% below that of endogenous mouse APP expression (Davis et al. 2004) (Figure 2.1). In humans, the Swedish mutation increases the production and deposition of A β -40 and A β -42 peptides (Kalaria et al. 1996), whilst the Dutch and Iowa mutations are found in individuals with hereditary cerebral amyloid angiopathy and result in an increase in A β -40 production with extensive vascular amyloid accumulation (Levy et al. 1990; Grabowski et al. 2001). Heterozygous TgSwDI mice develop amyloid deposits starting around 6-7 months of age; by 12 months they have been shown to exhibit fibrillar microvascular amyloid accumulation in the thalamus, whilst in the cortex amyloid deposition is in the form of non-fibrillar, diffuse parenchymal plaques (Miao et al. 2005). Cortical amyloid is predominantly composed of A β -40 whilst microvascular amyloid comprises mainly A β -40 but also A β -42 (Miao et al. 2005). Previous work undertaken by Natalia Salvadores in the group provided information on the characteristics of these TgSwDI mice.

Unless otherwise stated, animals were group housed on a 12:12hr light/dark cycle and had unrestricted access to food and water. All experiments were conducted in accordance with the Animals (Scientific Procedures) Act 1986 and local ethical approval at the University of Edinburgh and were performed under personal and project licenses granted by the Home Office. The 'n' numbers used for each study can be found in the relevant Methods section.

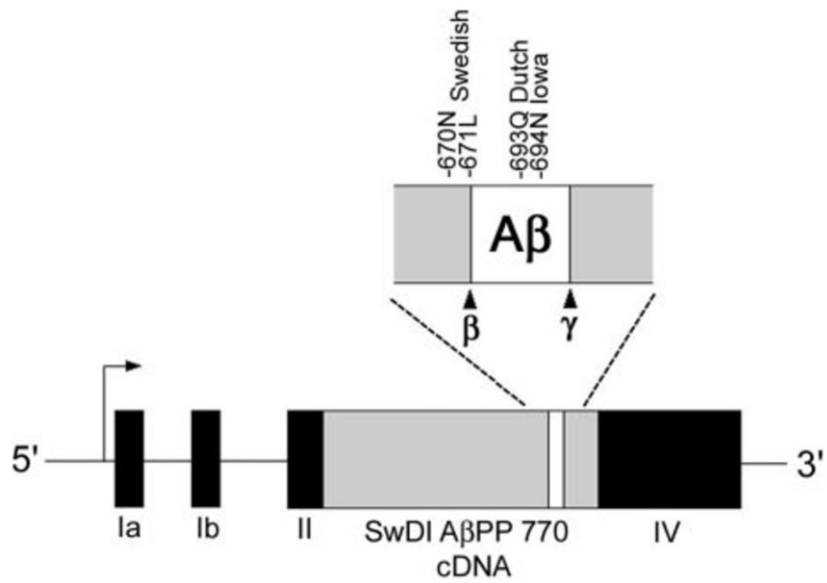


Figure 2.1 Schematic of the TgSwDI mouse mutant human APP construct. TgSwDI mice express human APP containing Swedish (K670N/M671L), Dutch (E693Q) and Iowa (D694N) mutations under the Thy1.2 promoter. Taken from Davis et al. 2004.

2.2 Chronic cerebral hypoperfusion

Chronic cerebral hypoperfusion surgery was performed according to previously published methods (Coltman et al. 2011) (Figure 2.2). Mice were first anaesthetised with 5% isoflurane, reduced to 1.5% for maintenance of anaesthesia during surgery. Via a small neck incision, the common carotid arteries were dissected and exposed. Microcoils with an inner diameter of 0.18mm (Sawane Spring Co. Japan) were applied to both common carotid arteries in order to reduce blood flow to the brain. There was a 30 minute recovery period before the application of the first and second microcoil. The wound was then sutured and the mice returned to an incubator to recover from anaesthesia. Sham mice underwent the exact same procedure except for the application of microcoils. All surgery was performed by Prof. Karen Horsburgh.

2.3 Apocynin administration

Apocynin was administered to mice via their drinking water at a dose of 30mg/kg/day. Apocynin stock solution was prepared by dissolving 1.25g apocynin (Sigma) in 1L drinking water heated to 60°C to aid dissolution. Aliquots of apocynin stock solution were then frozen at -20°C for storage. Working apocynin solution was then prepared using thawed stock solution diluted with drinking water to a final concentration of 30mg/kg based on average water consumption of a mouse at 4mls/day. Non-treated mice were given regular drinking water provided by the animal house. Apocynin and non-treated drinking water was replaced every 2-3 days and water consumption of each cage was recorded simultaneously.

2.4 Laser speckle imaging to assess baseline blood flow changes

Mice were anaesthetised with 5% isoflurane in 100% oxygen, reduced to 1.5% for maintenance of anaesthesia. Body temperature was monitored throughout the experiment using a rectal probe and modulated using a heat blanket. Mice were placed on a stereotaxic frame

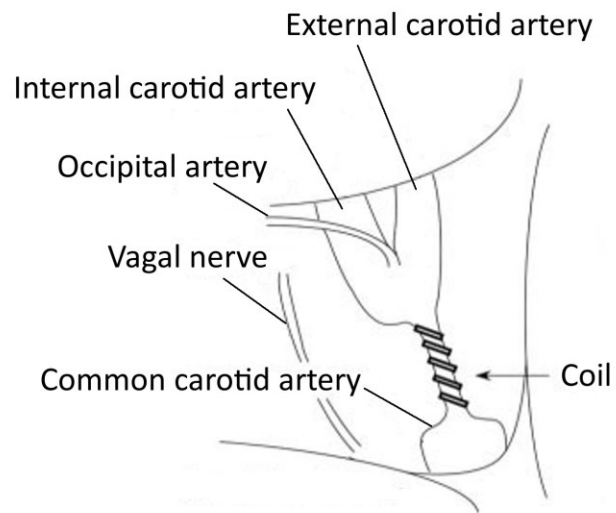


Figure 2.2 Schematic representation of bilateral common carotid artery stenosis. In order to induce cerebral hypoperfusion in mice, microcoils of 0.18mm internal diameter are applied to both common carotid arteries. Adapted from Shibata et al. (2004).

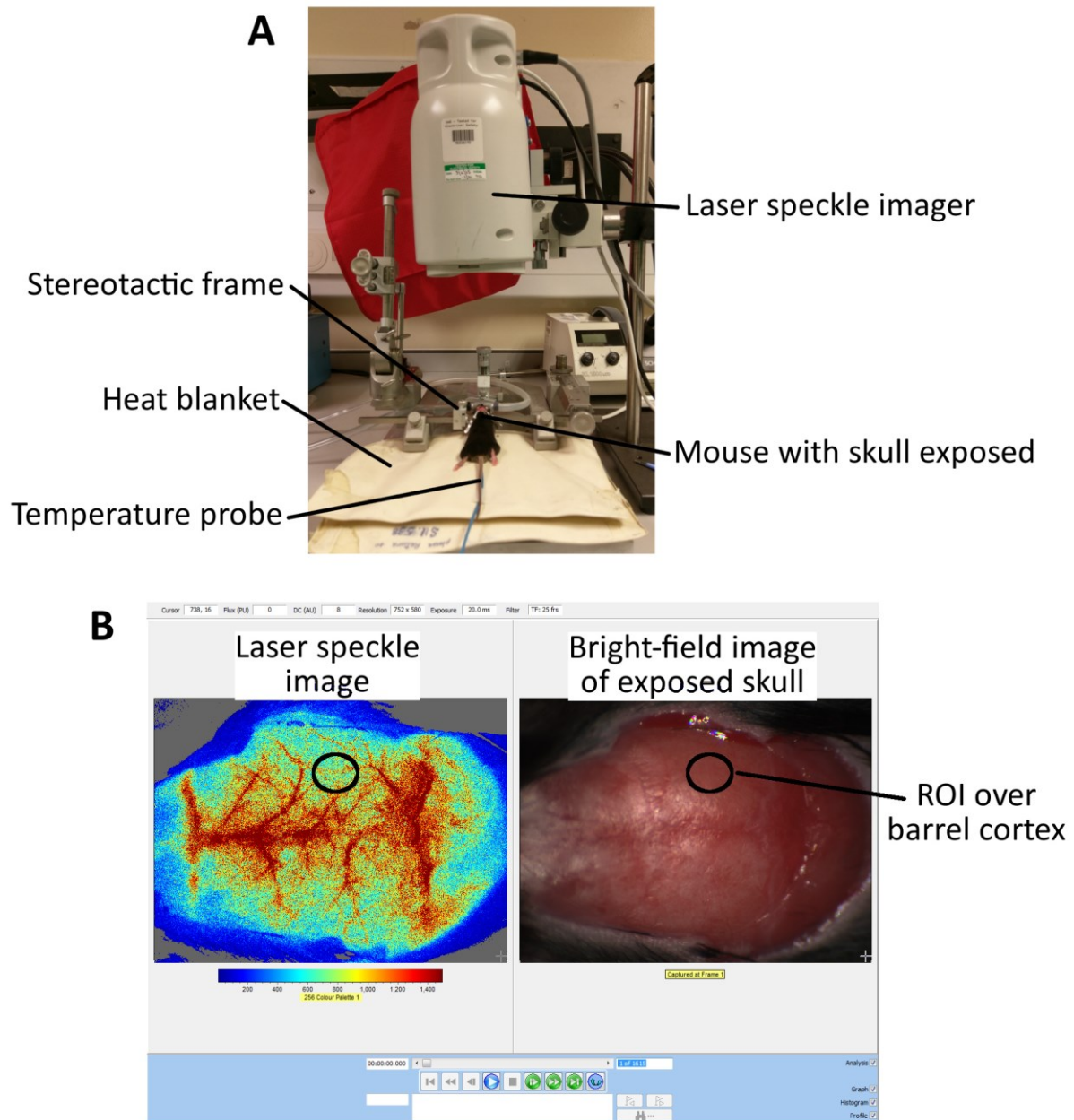


Figure 2.3 Laser speckle imaging. (A) Image showing setup for laser speckle imaging experiments. Images obtained from the laser speckle camera are viewed live on a computer as shown in (B). The bright-field image of the exposed skull can be used to place the region of interest (shown in black) over the barrel cortex, this region is then transferred to the laser speckle image in order to measure perfusion.

and ventilated via a nose cone with 100% oxygen at a rate of 150 breaths per minute. The head was fixed in place using ear and tooth bars and an incision was made over the midline. The scalp was retracted, the skull was cleaned of fur and a thin layer of ultrasound gel applied to prevent the skull drying. Stable baseline blood flow in the barrel cortex was recorded for 3 minutes using a laser speckle contrast imager (Moor FLPI2 Speckle Contrast Imager, Moor Instruments, UK) (Figure 2.3), after which the wound was sutured and the mouse was placed in an incubator to recover. Speckle contrast images were analysed using MoorFLPI-2 Review software (version 4.0).

2.5 Laser speckle imaging to assess neurovascular coupling

Mice were anaesthetised by intraperitoneal injection with α -chloralose (50mg/kg) and urethane (750mg/kg) in order to preserve physiological vascular responses. The left whiskers were cut and the right whiskers, to be stimulated, trimmed to 1cm. Preparation for laser speckle imaging was performed as described above in Methods section 2.4. Stable baseline blood flow in the barrel cortex was recorded for 2 minutes using a laser speckle contrast imager (Moor FLPI2 Speckle Contrast Imager, Moor Instruments, UK). The whiskers were then deflected back and forth for 30 seconds in order to stimulate blood flow to the contralateral barrel cortex. Blood flow was allowed to return to a stable baseline before beginning the next stimulation. Speckle contrast images were analysed using MoorFLPI-2 Review software (version 4.0). Peak response amplitude and mean response amplitude were recorded during stimulation, these were expressed as % increase from baseline to give a measure of vascular responsiveness. Results were averaged from 3 stimulations.

2.6 Mouse physiology during neurovascular coupling experiments

To ensure that measured neurovascular coupling responses were not due to abnormal physiology during recording, blood gas analysis was performed following a subset of neurovascular coupling experiments. The femoral artery was cannulated and ~95ul arterial blood was sampled for blood gas analysis using the Vetscan iSTAT1 with CG4 cartridges (Abaxis, UK). Results for pH, pO₂ and pCO₂ were within normal range (Iversen et al. 2012) and can be found in Table 2.1.

Table 2.1 Blood gas analysis following neurovascular coupling experiments		
pH	pO ₂ (mmHg)	pCO ₂ (mmHg)
7.35 ± 0.07	122 ± 42.32	33.31 ± 9.89

2.7 Barnes maze assessment of spatial learning and memory

The Barnes maze is a dry land maze designed to assess spatial learning and spatial memory (Barnes, 1979). The maze consists of a circular, white platform (115cm high x 91.5cm wide) with 20 “escape holes” located around the edge (Figure 2.4). Located under one of the escape holes is a small black box (the escape chamber) that the mouse may use to escape the maze, the other escape holes are unfilled. The maze is brightly lit and an aversive noise is played to encourage the mouse to escape. The mouse must navigate to this escape chamber by using spatial visual cues placed in the environment- large, high-contrast objects placed at the eye level of the mouse around the outside of the maze. Mice are trained over a period of time to locate the escape chamber using the spatial cues (learning task), then after a 3 day interval mice are returned to the maze to assess their memory of the chamber location (memory task). The location of the escape chamber is then moved 180° to the opposite side of the maze in order to assess executive function and cognitive flexibility (reversal task). ANY-maze tracking

software (v4.99, Stoelting Europe, Ireland) was used to record mouse behaviour via a camera fixed above the maze. Mice were run in groups of 10, each group was tested in the maze either in the morning (9am) or afternoon (2pm), the time of day of the test for each group was alternated to avoid any confounding effects of time e.g. to avoid one group always being tested in the afternoon and thus being more or less active compared to the morning group.

2.7.1 Acclimatisation phase

Mice were first gradually acclimatised to components of the Barnes maze in order to minimise stress caused by a novel environment and ensure authentic behavioural responses were observed in the maze. The first stage involved placing the mice in a 10.5cm diameter cylinder used to hold the mice for 10 seconds prior to the start of each trial. While in the cylinder, neither the maze nor any spatial cues can be seen by the mouse. This was performed once per day for two consecutive days. On the third day, mice were acclimatised to the maze itself. After being placed in the maze and held in the cylinder for 10 seconds, the cylinder was removed and the mice were allowed to freely explore the maze for 3 minutes. No aversive sound was played at this stage to enable the mice to explore in low-stress conditions. After 3 minutes, the mice were then gently guided to the escape hole to enter the escape chamber. Once in the chamber, they remained there for 2 minutes before being returned to the home cage.

2.7.2 Learning phase

The learning phase began one day after acclimatisation and was continued over 6 days with two trials per day performed 1 hour apart. After being placed in the maze, mice were held in the cylinder for 10 seconds. Upon removal of the cylinder, the mouse was then given 3 minutes to enter the escape chamber. During the learning phase, an aversive white noise (85db) was played for the duration of the trials, beginning when the cylinder was removed and ending once

the mouse entered the escape chamber. If after 3 minutes the mouse had not entered the escape chamber it was gently guided to it. For each mouse, the location of the escape chamber was kept the same for all acclimatisation and learning phase trials, however the location of the escape chamber was varied between different mice in order to minimise the contribution of olfactory cues. All maze equipment was also cleaned with 70% ethanol after each trial, apart from the escape chamber which was cleaned with 30% ethanol to prevent build-up of potentially aversive alcohol vapours.

2.7.3 Acquisition probe

In order to assess whether the mice had learnt the location of the escape hole, an acquisition probe was performed 1 hour after the final trial of the learning phase. Maze conditions were kept exactly the same as for the learning phase, with the exception that the escape chamber had been removed and the trial duration was reduced to 90 seconds.

2.7.4 72 hour probe

In order to assess the long-term spatial memory of the mice, a second probe trial was performed as above after an interval of 3 days.

2.7.5 Reminder phase

In order to account for any extinction of the escape chamber location memory due to the probe trials, mice then performed two additional trials in which the escape chamber was replaced in its original location. These trials were performed as for trials in the learning phase.

2.7.6 Reversal learning phase

In order to assess cognitive flexibility, the location of the escape chamber was then shifted 180° to the opposite side of the maze. All spatial cues remained the same. In this reversal learning

phase, mice were given two trials per day for 3 days. All aspects of the maze were the same as for the initial learning phase, with the exception of the escape chamber location.

2.7.7 Reversal acquisition probe

The reversal acquisition probe was performed 1 hour after the final reversal training trial, the escape chamber was removed and the probe duration was 90 seconds.

2.7.8 72 hour reversal probe

The 72 hour reversal probe was performed 3 days after the final reversal training day, the escape chamber was removed and the probe duration was 90 seconds.

2.7.9 Inclusion criteria

Performance in the Barnes maze is dependent on the mouse exploring the maze and being motivated to locate the escape chamber. Therefore, inclusion criteria were as follows: mice must enter a minimum of 3 quadrants in 2 of the learning phase trials. This highlighted 3 mice for exclusion, however 2 of these mice met the criteria because they learned the location of the escape chamber quickly and therefore did not explore further. The remaining 1 mouse was excluded from further analyses.

2.7.10 Performance measures

For learning and reversal learning phases, mice were assessed based on time taken to enter the escape chamber (escape latency). For each day of the learning and reversal phases, escape latency data was averaged over two trials. For probe trials, mice were assessed based on the proportion of time spent in the target quadrant i.e. the quadrant of the maze that had previously contained the escape chamber.

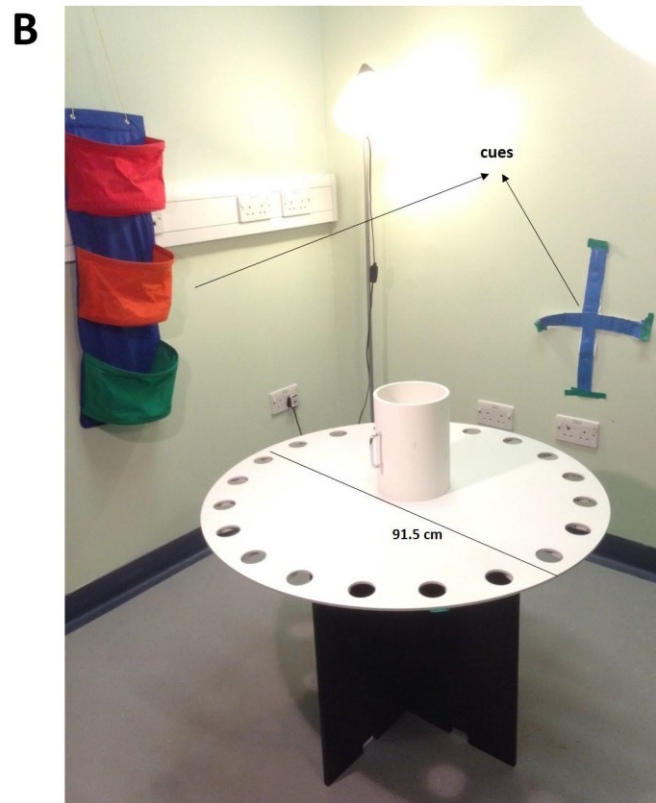
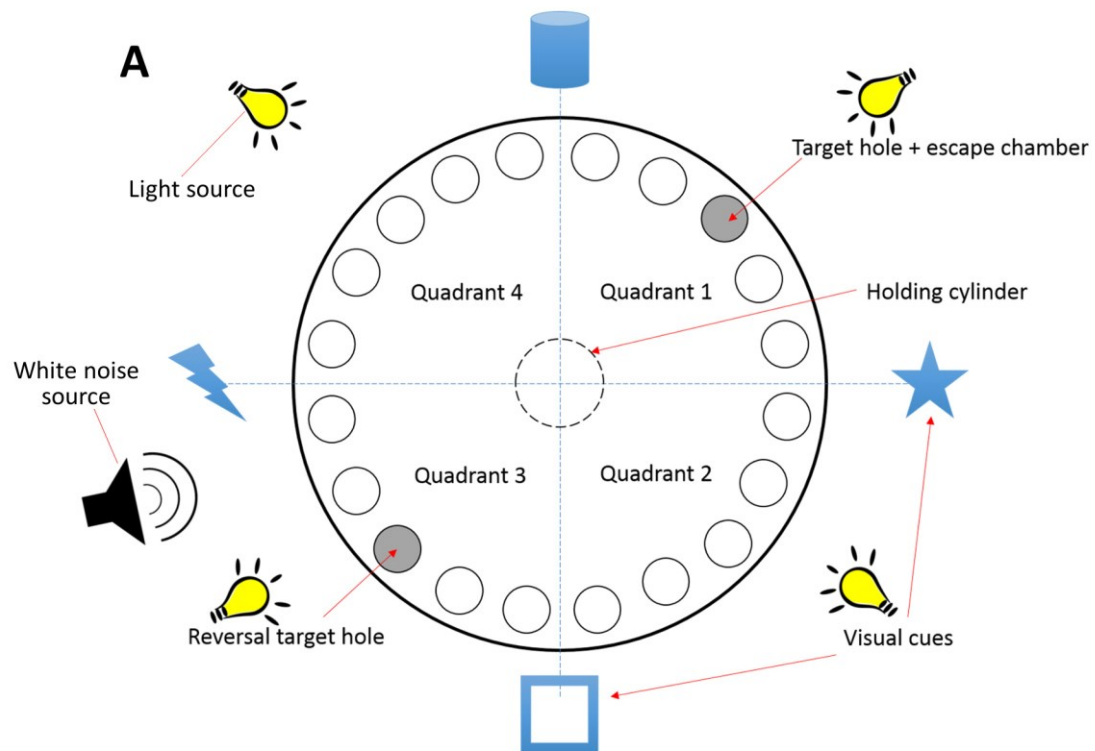


Figure 2.4 Barnes Maze. (A) Schematic drawing of the Barnes Maze apparatus used to test spatial learning and memory. (B) Photograph of Barnes Maze setup.

2.8 Unilateral ibotenic acid lesion

Mice were anaesthetised using 5% isoflurane in 100% oxygen. Isoflurane was reduced to 2% for maintenance of anaesthesia. Temperature was monitored with a rectal thermometer and controlled using a heat blanket. Mice were placed on a stereotactic frame, the scalp was retracted and a small area of the skull thinned using a dental drill. The skull was periodically cooled by washing with saline. A Hamilton syringe was used to inject 0.4 μ l of ibotenic acid (1mg/ml, Sigma) at the following stereotactic coordinates: B-1.94, 1.5mm, 3.5mm in order to lesion the thalamus of the right hemisphere. Following injection, the needle was left in place for 1 minute to prevent backflow of acid into the needle track. After removal of the needle, the wound was sutured and the mouse was returned to an incubator to recover from anaesthesia.

2.9 Magnetic resonance imaging

Mice were initially anaesthetised with 5% isoflurane in 100% oxygen and then anaesthesia was maintained with approximately 1.5% isoflurane. Mice were then placed in an MRI compatible holder (Rapid Biomedical, Wurzburg, Germany). Rectal temperature and respiration were monitored throughout (SA Instruments Inc., NY, US); temperature was maintained at 37.0°C through the use of a heated fan and respiration rate was kept between 70 and 100 breaths per minute by adjusting the concentration of isoflurane. All MRI data were collected using an Agilent 7T preclinical scanner (Agilent Technologies, Yarnton, UK); equipped with a high-performance gradient insert (120 mm inner diameter, maximum gradient strength 400 mT/m) and using a 72 mm quadrature volume coil and a phased array mouse brain coil (Rapid Biomedical GmbH, Rimpar, Germany). Unless otherwise stated, structural T2 imaging was performed at the outset to ensure that brain position and coronal slice location were consistent between mice (Figure 2.5 panel A). Sixteen contiguous slice locations were imaged using a T2-weighted structural sequence with a field-of-view (FOV) of 19.5 \times 19.5mm, an acquisition

matrix of 192×192 and slice thickness of 0.8mm, giving an acquisition voxel dimension of $0.1 \times 0.1 \times 0.8$ mm. The repetition (TR) and echo (TE) times were 3000 and 36ms respectively.

2.9.1 Arterial spin labelling

Resting cerebral blood flow can be calculated using arterial spin labelling (ASL), in which blood within a portion of the brain is magnetised, and the rate at which this is exchanged with non-magnetised blood can be used to assess the rate of resting blood flow (Kober et al. 2008). ASL was performed using a Look-Locker FAIR single gradient echo (LLFAIRGE) sequence (Kober et al. 2004; 2008) implemented in-house, covering a 1 or 1.5mm thick brain slice corresponding to Figure 46 in the Mouse Brain Atlas (Paxinos and Franklin, 2001) (Figure 2.5 panel B). Forty gradient echoes spaced 200ms apart were acquired after a slice-selective or global adiabatic inversion pulse for each phase-encoding, resulting in a total acquisition time of approximately 16 minutes for a 64×64 imaging matrix. The flip angle was 20° . The first 20° pulse occurred 3ms after the inversion pulse. The echo time was 1.42ms. Maps of cerebral blood flow were constructed from ASL data in Matlab using in-house scripts. Cerebral blood flow maps were analysed in ImageJ (v1.46, NIH, Bethesda, MD, USA) using regions of interest selected from T1 maps acquired with the ASL sequence.

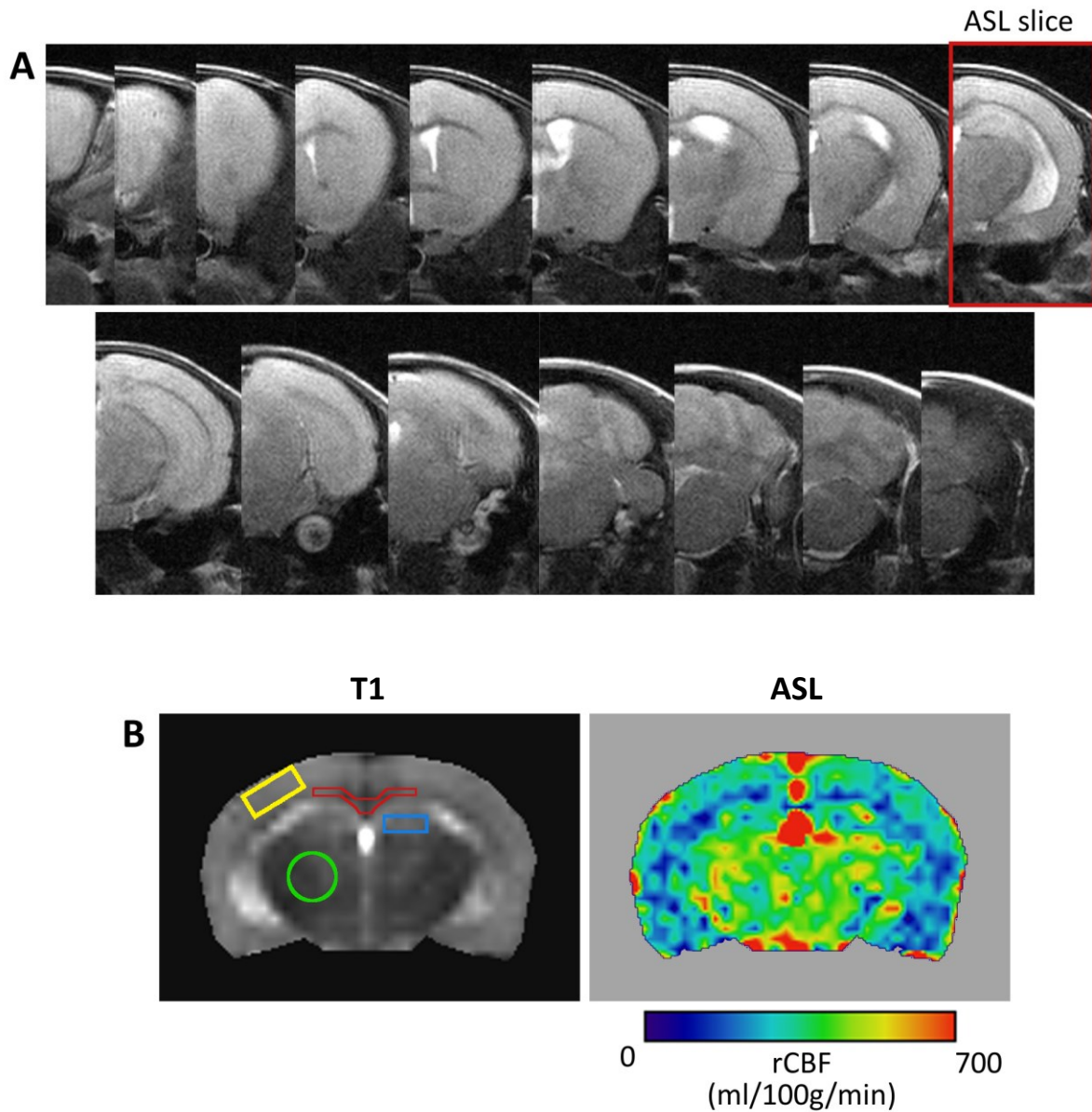


Figure 2.5 T2 and ASL-MRI. (A) Representative images depicting the 16 contiguous slices acquired throughout the brain by T2 imaging. Structural T2 imaging is performed at the outset of MRI experiments in order to determine the imaging slice location for subsequent ASL acquisition (highlighted in red). (B) T1 images acquired as part of the ASL sequence are used for unbiased region of interest selection (cortex: yellow, thalamus: green, corpus callosum: red, hippocampus: blue) and transferred to ASL images for analysis of cerebral blood flow.

2.9.2 Q-map imaging

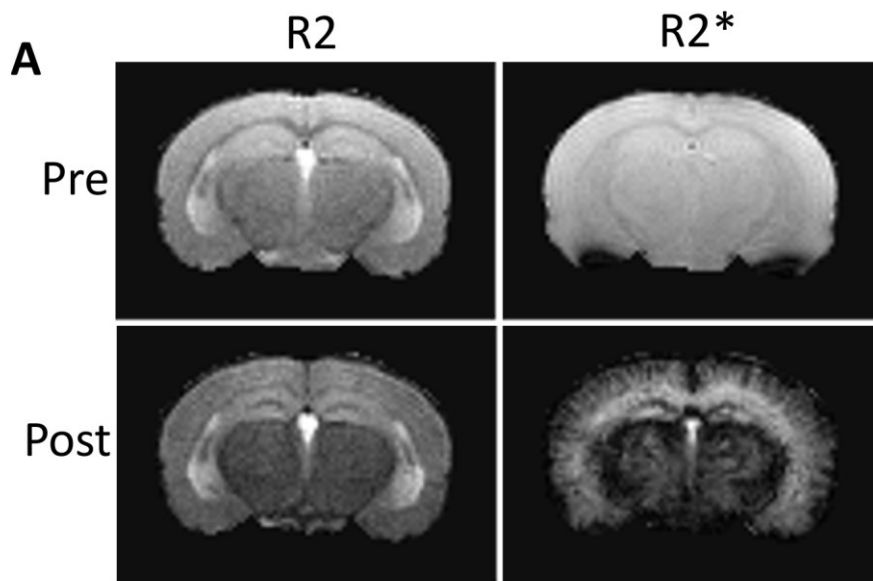
For mice undergoing Q-map imaging, the right femoral vein was cannulated prior to the mouse being placed in the scanner to allow for remote administration of the iron oxide contrast agent ferumoxytol. Q-map imaging was performed based on methods published by Boehm-Sturm et al (2013) (Figure 2.6). The technique allows the calculation of an index (“Q”) that is sensitive to microvessel density and can be used to provide in vivo measures of microvessel number. “Q” is calculated based on the shifts in gradient echo and spin echo relaxation rates following the administration of an intravascular contrast agent, in this case the ultrasmall superparamagnetic iron oxide ferumoxytol (Takeda Pharmaceutical Company Limited, Japan). The protocol consisted of R2 and R2* mapping scans performed before and 2 minutes after the intravenous injection of the iron oxide contrast agent ferumoxytol (30 μ l at 30mg Fe/kg). In order to avoid confounding effects of increased tissue diffusivity, as might be the case in ischaemic lesions, diffusion tensor (DT)-MRI was also performed to measure and account for water diffusion in the tissue. R2 was acquired with a multi echo multi slice (MEMS) spin echo sequence (repetition time 2700ms; 16 echoes; 16 slices of 0.8mm thickness; FOV 19.2x19.2mm; matrix size 128x128 and 4 signal averages) and R2* was acquired using a multi-echo multi slice gradient echo (MGEMS) sequence (repetition time 1000ms; 16 echoes; 16 slices at 0.8mm; FOV 19.2x19.2mm; matrix size 128x128; 4 signal averages; flip angle of 20°). The DTI protocol consisted of 10 T2-weighted volumes without the diffusion gradients applied and sets of diffusion-weighted ($b = 1000$ s/mm²) volumes acquired with diffusion gradients (amplitude 14.33 G/cm, duration 5 ms, separation 26 ms) applied in 60 non-collinear directions, giving a total of 70 volumes (Jones et al., 1999). Sixteen slice locations identical to those used in the T2-weighted scan were imaged with a FOV of 19.2x19.2mm and an acquisition matrix of 96x96, with a TR and TE of 2000ms and 36ms respectively. Total scan time was 1 hour 30

minutes. Once measures of 'Q' have been obtained, measures of vessel number 'N' can be calculated according to Boehm-Sturm et al. (2013), taking into account tissue water diffusivity. N-maps of vessel density were generated using Matlab and Image Calculator functions of Statistical Parametric Mapping 8 software (SPM8, <http://www.fil.ion.ucl.ac.uk/spm/software/spm8/>, Wellcome Trust Centre for Neuroimaging) and were analysed in ImageJ. Regions of interest were selected from T2-weighted structural scans.

2.9.3 Contrast-enhanced T2* imaging:

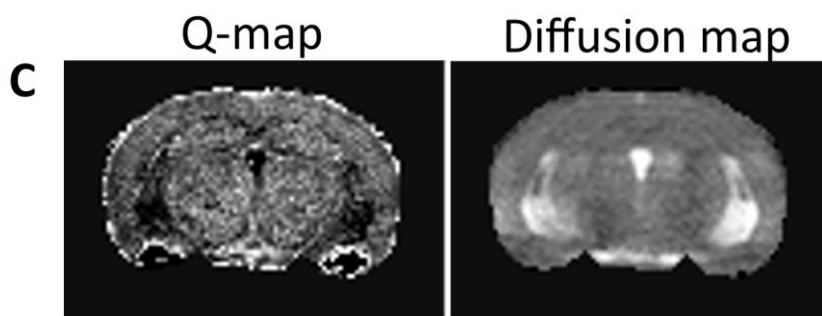
Contrast-enhanced T2* imaging was performed based on methods published by Klohs et al. 2015. Contrast is generated within the image by intravenous injection of a superparamagnetic iron oxide (SPIO) contrast agent, in this case ferumoxytol. Following intravenous administration, circulating macrophages phagocytose the iron oxide in the bloodstream and migrate to areas of inflammation. Accumulation of iron-containing macrophages in inflammatory sites then leads to a hypointense area on T2* weighted imaging. Alternatively, iron oxide in the bloodstream is able to enter the brain parenchyma through areas of leaky blood-brain barrier. In order to perform contrast-enhanced MRI of neuroinflammation, T2* images were acquired twice, once to obtain a baseline scan and then a second time 24 hours following the intravenous injection of the superparamagnetic iron oxide (SPIO) ferumoxytol to obtain the contrast-enhanced scan. A 3D gradient echo sequence with a field of view of 14x14x26mm and an acquisition matrix of 192x192x86 was performed with a TR and TE of 40ms and 8ms respectively. Acquisition time was 22 minutes with 2 signal averages. The flip angle was 30°. Following acquisition of the baseline scan, ferumoxytol was administered at 30mg/kg via the tail vein. The T2* sequence was then repeated 24 hours later. Areas of neuroinflammation can be identified as hypointense regions on the post-contrast scan that were

not present on the baseline scan (and are therefore due to accumulation of exogenous iron oxide).



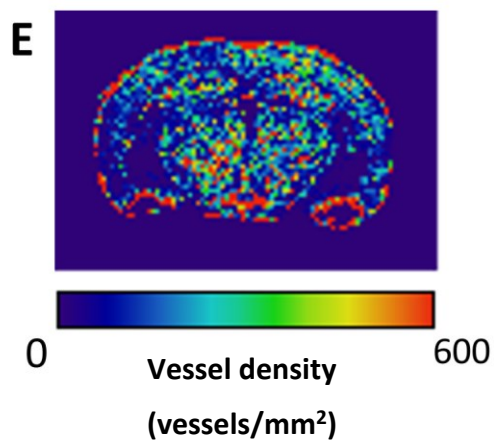
B

$$Q = \frac{\Delta R_2}{(\Delta R_2^*)^{2/3}}$$



D

$$N = 0.218(Q^3/D), [D] = \text{mm}^2\text{s}^{-1}, [Q] = \text{s}^{-1/3}$$



◀ **Figure 2.6 Q-map imaging.** Q-map imaging was performed based on methods published by Boehm-Sturm et al. 2013. (A) R2 and R2* sequences are acquired before and after the administration of the iron oxide contrast agent ferumoxytol. (B) Subtracting the post-contrast R2 and R2* values from pre-contrast values generates difference images ($\Delta R2$ and $\Delta R2^*$), which can be used to calculate the index 'Q' (C) (Jensen and Chandra, 2001). By taking into account tissue diffusivity (C), a value for 'N', vessel density, can be calculated using the equation shown in (D), in order to generate maps of vessel density as shown in (E). Equations taken from Boehm-Sturm et al. (2013).

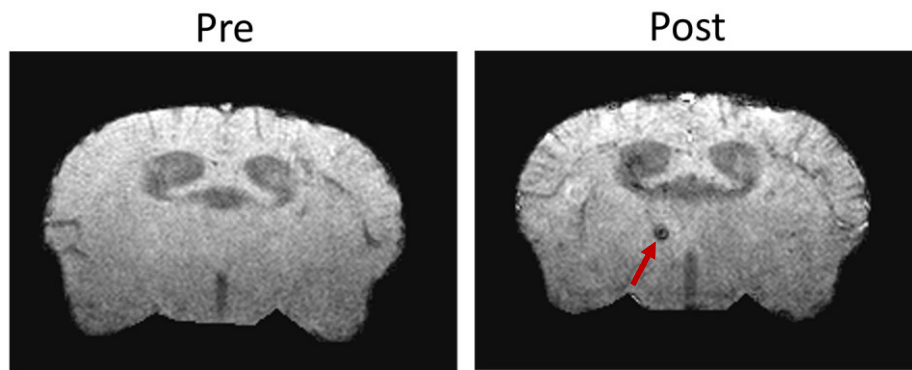


Figure 2.7 Contrast-enhanced T2* imaging. T2* images acquired from a hypoperfused mouse pre and 24 hours post intravenous administration of the iron oxide contrast agent ferumoxytol. In the post-contrast image, a hypointense region is detectable in the thalamic nuclei which is not seen on the pre-contrast image, indicating an accumulation of exogenous iron oxide.

2.10 Transcardial perfusion

Mice were anaesthetised with 5% isoflurane, maintained at 3.5% for perfusion. An incision was made down the midline and the heart exposed. A needle was inserted into the left ventricle of the heart and the right atrium was opened with scissors. Mice were then perfused with 30mls of 0.9% heparinised phosphate buffered saline at 2mls/min.

2.11 Tissue processing

Following perfusion, brain tissue was removed and fixed in 4% paraformaldehyde for 24 hours, after which it was processed for either paraffin embedding or freezing.

2.11.1 Paraffin

After fixation, tissue was then washed in PB for 1 hour before being sectioned into 3mm blocks using a mouse brain matrix. Tissue blocks were then processed for paraffin embedding on an automated Tissue Tek VIP 2 (Sakura) overnight. Paraffin embedded tissue sections were cut on a microtome (Leica RM2135) at 6µm and mounted on superfrost plus slides (VWR International). Anatomical levels for each study can be found in the relevant methods sections.

2.11.2 Frozen

Following fixation, brain tissue was cryoprotected in 30% sucrose in PBS for 72 hours, then frozen for 5 minutes in isopentane cooled to -42°C. Brains were stored at -20°C and sectioned on a cryostat (Leica CM1950). 12µm sections were mounted directly onto superfrost plus slides (VWR International) and 30µm sections were stored in 24 well plates in cryoprotective medium at -20°C.

2.12 Histology

2.12.1 Haematoxylin and eosin staining

Sections were rehydrated to running water and incubated in filtered haematoxylin (Thermo Fisher, UK) for 3 minutes. Sections were then rinsed in running water and added to 1% Acid Alcohol for 10 seconds before being placed in running tap water for 2 minutes. Sections were then incubated in Scott's tap water substitute for 2 minutes, washed in running tap water for 2 minutes and incubated in EosinY Alcoholic (Thermo Fisher, UK) for 2 minutes. Finally, sections were rinsed in running water, dehydrated through serial alcohols (70%, 90%, 100%) and incubated in xylene for 15 minutes before mounting with DPX.

2.12.2 DAB Enhanced Perls' Prussian Blue

Perl's staining was performed to detect the presence of iron using a kit (Sigma, UK) according to manufacturer's instructions. Sections were rehydrated to distilled water, then incubated in a 1:1 mix of potassium ferrocyanide and hydrochloric acid for 10 minutes at room temperature. Sections were then rinsed in distilled water and incubated in DAB/Metal concentrate diluted in peroxide buffer (Metal Enhanced DAB Substrate Kit, Thermo Fisher, UK) for 15 minutes. Sections were then rinsed in running tap water, dehydrated through serial ethanols (70%, 90%, 100%) to xylene and mounted using DPX (Thermo Fisher, UK).

2.13 Immunohistochemistry

All primary and secondary antibodies are listed in Table 2.1.

2.13.1 Immunoperoxidase labelling

Paraffin sections were deparaffinised at 60°C for 30 minutes followed by incubation in xylene. Frozen sections were removed from the freezer and allowed to air dry for 30 minutes. Slides were washed in phosphate-buffered saline (PBS) then dehydrated through serial ethanols (70%, 90% and 100%) and finally placed in xylene for 10 minutes.

Thereafter, paraffin and frozen sections underwent the same protocol. Sections were rehydrated in 100% ethanol and endogenous peroxidase was quenched using 3% hydrogen peroxide solution for 30 minutes. Antigen retrieval was performed as required. For citric acid retrieval, sections were incubated in 10mM citric acid (pH6) and heated to 100°C for 10 minutes. For proteinase K retrieval, sections were incubated in proteinase K (20µg/ml) for 10 minutes at room temperature (21°C). Following retrieval, sections were washed in PBS and incubated in blocking solution (10% normal serum, 0.5% bovine serum albumin) for 1 hour at room temperature followed by incubation in primary antibody solution overnight at 4°C. Sections were then washed in PBS and incubated with the secondary antibody for 1 hour at room temperature, before signal amplification using a Vector ABC Elite Kit (Vector Labs, UK) also for 1 hour at room temperature. After washing in PBS, peroxidase activity was visualised by incubation with 3,3' diaminobenzadine tetrahydrochloride (DAB, Vector Labs, UK) for 3 minutes. Finally, sections were washed in running water and dehydrated through serial ethanols (70%, 90%, 100%) before incubation in xylene and mounting with DPX (Thermo Fisher, UK).

2.13.2 Immunofluorescent labelling

Paraffin sections were deparaffinised at 60°C for 30 minutes followed by incubation in xylene. Frozen sections were removed from the freezer and allowed to air dry for 30 minutes. Slides were washed in phosphate-buffered saline (PBS) then dehydrated through serial ethanols (70%, 90% and 100%) and finally placed in xylene for 10 minutes. Thereafter, paraffin and frozen sections underwent the same protocol. Sections were rehydrated through serial ethanols (100%, 90%, 70%) and rinsed in distilled water prior to antigen retrieval if required as described above in Methods section 2.13.1. Subsequently, sections were washed in PBS and incubated in blocking solution (10% normal serum, 0.5% bovine serum albumin) for 1 hour at room temperature followed by incubation in the primary antibody solution overnight at 4°C. Sections

were washed in PBS and incubated in biotinylated secondary for 1 hour at room temperature if amplification was required. Sections were then washed in PBS and incubated with fluorescent secondaries for 1 hour at room temperature and protected from light. Sections were washed in PBS followed by TB, then allowed to air dry for 30 minutes prior to mounting with Vectashield Hardset with DAPI (Vector, UK).

2.14 Analysis of immunohistochemistry

DAB stained sections were imaged on an Olympus BX51 microscope (x10, Olympus UK, Southend-on-Sea, UK); immunofluorescent images were acquired using a laser scanning confocal microscope (x20, Zeiss 780, Carl Zeiss Microscopy, Cambridge, UK). Images were captured in cortical and thalamic regions according to Figure 2.4. All images were analysed

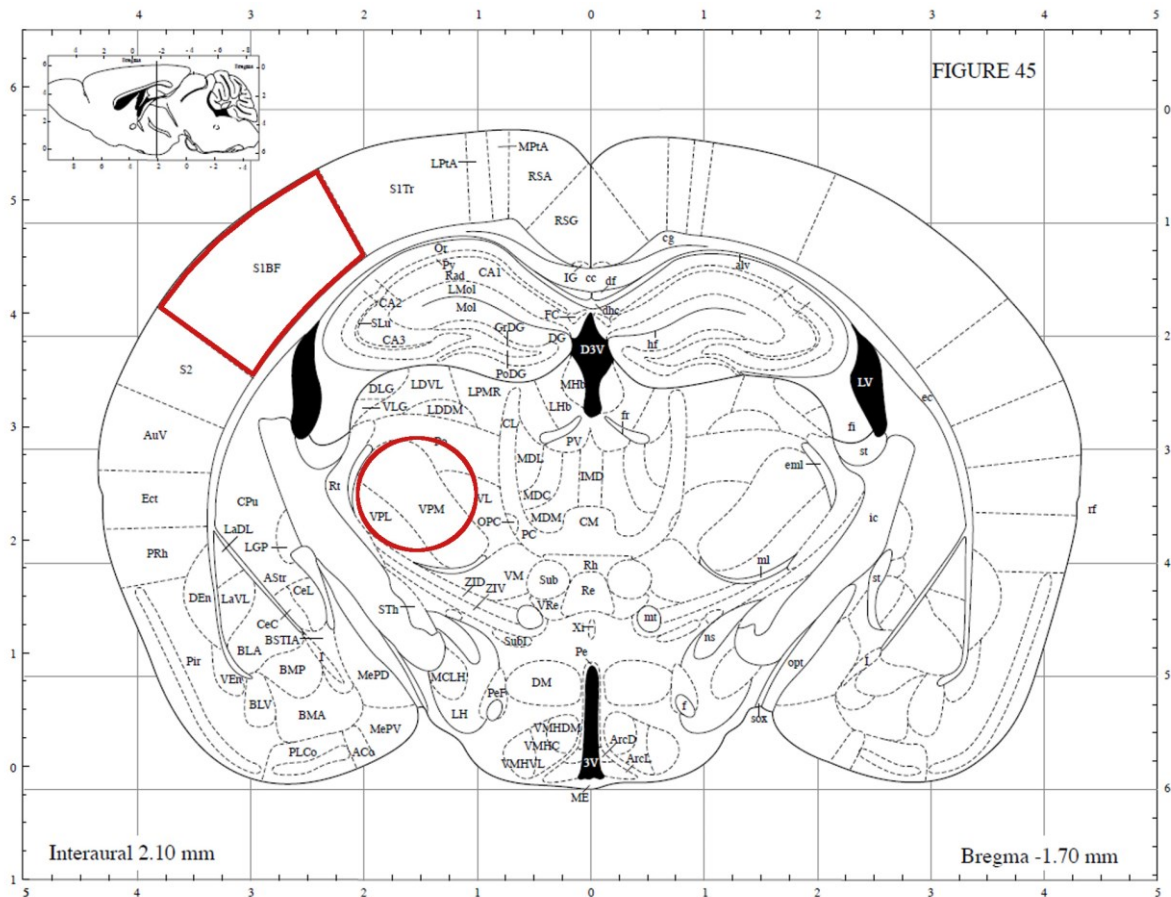


Figure 2.8 Cortical and thalamic ROIs used for image analysis. Unless otherwise stated, cortical and thalamic images were acquired at 1.7mm posterior to Bregma. Cortical images were acquired from the barrel cortex, thalamic images were acquired from the ventral posteromedial and posterolateral thalamic nuclei. Image adapted from Paxinos and Franklin (2001).

using ImageJ software (v1.46, NIH, Bethesda, MD, USA). Details of relevant methodology for individual analyses can be found in the corresponding chapter methods.

2.15 Tissue processing for biochemistry

Following transcardial perfusion with heparinised phosphate buffered saline, brain tissue was removed and hemibrains were snap frozen in liquid nitrogen. All subsequent steps were performed on ice or at 4°C. Hemibrains were homogenised in a dounce fit homogeniser in 1ml PBS on ice. 300µl was taken as a whole brain homogenate, and added to 300µl 50mM Tris-buffered saline containing 1% Triton-X 100 and 1% protease and phosphatase inhibitors. Homogenates were centrifuged at 3000rpm for 3 minutes to remove tissue debris. Generation of vessel-enriched fractions was performed based on methods by Yousif et al. (2007). Remaining whole brain homogenates were suspended in ficoll (17.5%) and centrifuged at 3200 g for 25 minutes. The supernatant was collected and respun, before both pellets were combined in 1% BSA and centrifuged at 2000g for 10 minutes. The pellet was then washed in PBS and centrifuged at 6000g for 15 minutes before being stored at -80°C. Total protein extraction was performed using RIPA buffer (50mM Tris, 1% NP-40, 150mM NaCl, 1mM EDTA, 0.1% SDS, 0.5% Sodium deoxycholate, 1% protease and phosphatase inhibitors) followed by sonication for 5 seconds at 10% amplitude and mixing for 2 hours at 4°C. Samples were centrifuged at 5000g for 2 minutes and the supernatant was retained for subsequent protein analysis.

2.16 Determination of protein concentration

Protein concentration was assessed using the Pierce BCA Protein Assay Kit (Thermo Scientific) and was performed according to manufacturer's instructions. Absorbance was measured at 562nm on a FilterMax microplate reader (Molecular Devices, CA, USA).

2.17 Dot blot assay

Dot blotting was performed for semiquantitative assessment of changes in protein levels, using a Bio-Rad Bio-Dot Microfiltration Unit (Bio-Rad Laboratories Ltd, UK). Nitrocellulose membrane was soaked in PBS for 10 minutes and placed in the 96-well microfiltration unit. Following assembly of the microfiltration unit, the membrane was rehydrated by applying 100µl filtered PBS (filter size 0.2µm) to all wells and drawing through under vacuum. Samples were loaded at 2µg of protein per well in 110µl filtered PBS and were loaded in triplicates. Samples were drawn through the membrane under vacuum, the membrane was then removed from the microfiltration unit and blocked in 1:1 Odyssey blocking buffer (LI-COR, UK):PBS for 1 hour on a shaker at room temperature. Primary antibodies were diluted in 1:1 Odyssey blocking buffer:PBS containing 0.1% Tween-20. Membranes were incubated in primary antibody solutions on a shaker overnight at 4°C. They were then washed in PBS containing 0.1% Tween-20 6 times for 5 minutes each, and incubated in secondary antibody solution for 45 minutes on a shaker at room temperature. Fluorescent infra-red secondary antibodies were diluted in 1:1 Odyssey blocking buffer:PBS containing 0.1% Tween-20 and 0.01% SDS. Membranes were then washed in PBS containing 0.1% Tween-20 6 times for 5 minutes each, followed by 3 washes in PBS. Membranes were visualised using a LI-COR Odyssey FC scanner in the 700 and 800 channels. All antibody concentrations used for dot blot assays can be found in Table 2.3.

2.18 Analysis of dot blot

Dot blots were analysed using Image Studio Lite software (LI-COR, UK). Circular shapes were applied to all dots and background subtraction was performed by the software using an outer border around each dot. Signal intensity from each dot in the target protein channel was normalised to loading control signal, and the results from triplicate values were averaged.

2.19 Enzyme-linked immunosorbent assay (ELISA)

Vascular NADPH-oxidase 2 (NOX2) levels were assessed using an ELISA kit (Cusabio CSB-EL006325MO) performed according to manufacturer's instructions. Vascular NOX2 expression was then normalised to total protein levels using results from the BCA protein assay.

2.20 Statistical analysis

All statistical analysis was performed using SPSS (v19, IBM Corp.) or GraphPad Prism software (v5.01, GraphPad Software Inc., La Jolla, USA). Details of statistical analysis performed for each measure can be found in the corresponding chapter methods. Unless otherwise stated, data are presented as mean \pm standard error of the mean and $p < 0.05$ was considered to be statistically significant.

Table 2.2 Primary and secondary antibodies used for immunohistochemistry							
Primary antibody	Label	Dilution	Retrieval	Supplier	Secondary antibody	Dilution	Supplier
6E10	A β	1:10,000 (IP) 1:750 (IF)	Citric acid	Covance SIG-39320	Biotinylated anti-mouse	1:100	Vector BA2000
Anti-Iba1	Microglia	1:1000	Citric acid	Menarini MP-290	Biotinylated anti-rabbit	1:100	Vector BA1100
Anti-collagen IV	Blood vessels	1:100	Citric acid, proteinase K	Millipore AB769	Anti-goat Alexa Fluor 546	1:500	Life-tech A11056
Anti-GFAP	Astrocytes	1:100	Citric acid, proteinase K	Life-tech 13-0300	Anti-rat Alexa Fluor 647	1:500	Stratech 712-605-150
Anti-PDGFR β	Pericytes	1:200	Citric acid, proteinase K	R&D Systems AF1042	Biotinylated anti-goat	1:100	Vector BA9500
					Streptavidin Alexa Fluor 488	1:100	Life-tech S-32354
Anti-aquaporin4	Aquaporin 4 (AQP4)	1:500	Citric acid, proteinase K	Millipore AB3594	Biotinylated anti-rabbit	1:100	Vector BA1100
					Streptavidin Alexa Fluor 488	1:100	Life-tech S-11223
Anti-p47	NOX	1:1000	Citric acid	Millipore ABN1480	Biotinylated anti-rabbit	1:100	Vector BA1000
Anti-collagen IV	Blood vessels	1:8000	Citric acid, proteinase K	Stratech 70R-CR013X	Biotinylated anti-rabbit	1:100	Vector BA1000

Table 2.3 Primary and secondary antibodies used for dot blot assays						
Primary antibody	Label	Dilution	Supplier	Secondary antibody	Dilution	Supplier
Anti-gp91	NOX2	1:500	BD Biosciences 611415	Anti-mouse IR680	1:10,000	LI-COR
Anti-3NT	3NT	1:750	Abcam ab61392	Anti-mouse IR680	1:10,000	LI-COR
Anti-NOX4	NOX4	1:750	Abcam ab133303	Anti-rabbit IR680	1:10,000	LI-COR
Anti-GAPDH	GAPDH (loading control)	1:20,000	Sigma G9545	Anti-rabbit IR800	1:10,000	LI-COR
Anti-tubulin	Tubulin (loading control)	1:10,000	Abcam ab7291	Anti-mouse IR800	1:10,000	LI-COR

Chapter 3.

Development and validation of MRI approaches to assess vascular parameters in vivo

Development and validation of MRI approaches to assess vascular parameters in vivo

3.1 Introduction

Cerebrovascular pathologies such as small vessel disease and ischaemic stroke are prominent contributors to cognitive impairment (Wang et al. 2014; Adiukwu, Ofori and Ugbomah, 2016). Cerebrovascular pathology observed in vascular cognitive impairment has included cerebral hypoperfusion (Hebert et al. 2013), decreased vascular density (Brown and Thore, 2011), development of ischaemic lesions and microbleeds (Kalaria, 2016; Valenti et al. 2016), and enhanced inflammation (Lenart, Brough and Denes, 2016). In order to study how vascular alterations may contribute to cognitive decline, experimental animal models were established, such as the mouse chronic cerebral hypoperfusion model and the TgSwDI mouse, which reproduce clinical features of small vessel disease and vascular cognitive impairment. Investigation of the cerebral vasculature using current immunohistochemical and biochemical approaches is limited by the requirement for post-mortem tissue. As such, there is a need to develop non-invasive techniques to allow the assessment of vascular parameters in vivo, and preclinical magnetic resonance imaging (MRI) represents an attractive alternative approach with translational value to clinical MRI findings. Key features of vascular disease such as alterations in resting blood flow, endothelial alterations and development of vascular lesions may all be identified using MRI. Arterial spin labelling allows the quantification of resting cerebral blood flow throughout the brain and has been used previously to detect age and amyloid-related changes in perfusion (Hebert et al. 2013; Lin et al. 2013). Q-map imaging has been used to detect alterations in vessel number in tumour and stroke models (Ullrich et al. 2011; Boehm-Sturm et al. 2013), and could be used to detect vascular degeneration in

experimental models of vascular cognitive impairment. Structural T2 imaging has already been validated as an approach to assess the development of microinfarcts and microbleeds following hypoperfusion (Holland et al. 2015) and is therefore a valuable tool to assess progression of small vessel disease pathology. Finally, inflammatory events related to cerebral amyloid angiopathy have been previously detected using a contrast-enhanced T2* imaging approach (Klohs et al. 2015), suggesting this technique may also have utility in assessing inflammatory processes relating to vascular pathology and following hypoperfusion.

Overall, the ability to perform sensitive, non-invasive evaluation of vascular parameters would provide an opportunity to track dynamic changes in the vasculature in experimental models. This will provide a basis on which to test future hypotheses and also to test the efficacy of potential therapeutic interventions. Therefore, developing imaging approaches was a key aspect in forming the basis of studies at the outset of this thesis.

3.1.1 Aims

To develop MRI techniques that allow the in vivo assessment of vessel number, resting cerebral blood flow and cerebral inflammation.

To assess the sensitivity of these techniques and validate MRI-derived measures using established in vivo and ex vivo methods.

3.2 Methods

3.2.1 Animals

C57Bl/6J and heterozygous TgSwDI mice were used for all optimisation and validation experiments. For Q-map imaging validation experiments, male wild type C57Bl6/J and TgSwDI mice were studied at 3 months (n=3 wild type), 6 months (n=7 wild type and 7 TgSwDI) and 24 months old (n=7 and 9 TgSwDI). For ASL optimisation experiments (slice thickness and slice thickness multiplier), male and female wild type mice were studied at 3-9 months old (n=6). For ASL validation experiments, male wild type mice were studied at 7-8 months old (n=21); and wild type and TgSwDI mice were studied at 12 months old (n=7 wild type and 18 TgSwDI). For contrast-enhanced T2*, male wild type and TgSwDI mice were studied at 12 months old (n=21 C57Bl6/J and n=20 TgSwDI). All experiments were performed and analysed blinded to age, genetic and surgical status of the mice. For ASL optimisation experiments, analysis was also performed blind to slice thickness and slice thickness multiplier values. N numbers were chosen based on retrospective analysis of pilot data to achieve a significance value of $p < 0.05$ at a power of 0.8.

3.2.2 Ibotenic acid lesion

Ibotenic acid lesions were performed in a subset of 3 wild type mice in order to validate Q-map imaging-derived measures of vascular density. Unilateral ibotenic acid lesions were induced according to Methods section 2.8. Q-map imaging was performed 1 day after induction of the lesion.

3.2.3 Cerebral hypoperfusion surgery

Cerebral hypoperfusion surgery was performed as described in Methods section 2.2 as part of ASL validation and contrast-enhanced T2* experiments. Unless otherwise stated, imaging was performed at 3 months following hypoperfusion surgery.

3.2.4 Magnetic resonance imaging

MRI was performed as described in Methods section 2.9. Structural T2 imaging was performed in order to detect vascular lesions and to provide a spatial guide for subsequent region of interest-based analysis in other imaging modalities. Q-map imaging was performed in order to determine vessel number; ASL was used to measure resting cerebral blood flow and contrast-enhanced T2* was performed to evaluate brain inflammation.

3.2.5 Optimisation of ASL parameters

Mice underwent ASL imaging according to Methods section 2.9.1. For optimisation of slice thickness, mice (n=2) were scanned once using a slice thickness of 1.5mm and once using a slice thickness of 1mm in the same imaging session. Blood flow was subsequently measured from the cortex and thalamus. For optimisation of slice thickness multiplier, each mouse was scanned once using the original slice thickness multiplier of 1.5 and once using a different value of either 2, 2.5, 3 or 3.5 in the same imaging session (n=4). Blood flow was measured from the cortex and thalamus. For both optimisation experiments, the sequence of scans was alternated to avoid confounding effects of prolonged anaesthesia on blood flow.

3.2.6 Validation of ASL using laser speckle contrast imaging

Laser speckle contrast imaging was performed as described in Methods section 2.4. Blood flow values obtained from sham and hypoperfused mice were compared to ASL-derived measures of cortical blood flow.

3.2.7 Validation of Q-map derived vessel number using collagen-IV immunohistochemistry

Following Q-map imaging, mice were removed from the scanner and perfused with 20mls 0.1M heparinised phosphate buffer. Brains were removed and placed in 4% paraformaldehyde for 24 hours followed by paraffin embedding. 6µm brain sections were cut and stained for collagen IV according to methods described in Methods section 2.13.1. For ibotenic acid studies, collagen density was then quantified in the lesion site and in the contralateral hemisphere using the area fraction function of ImageJ (v1.46, NIH, Bethesda, MD, USA). For correlational analysis, collagen density was quantified in the cortex and thalamus, and the results were compared to those obtained with Q-map imaging.

3.2.8 Validation of ce-T2* using Iba1 immunohistochemistry and enhanced Perl's stain

Three days following ce-T2* imaging, brain tissue was collected and processed according to Methods section 2.11.2. Iba1 staining was performed according to Methods section 2.13.1 in tissue sections corresponding to Figure 46 in the Mouse Brain Atlas (Paxinos and Franklin, 2001). Enhanced Perl's staining was performed according to Methods section 2.12.2, and in a subset of mice this was combined with Iba1 immunohistochemistry. In these cases, DAB was used to visualise the Perl's signal, and VIP was used to visualise Iba1.

3.2.9 Statistical analysis

A paired t-test was used to detect changes in blood flow measurements in ASL optimisation experiments for slice thickness and slice thickness multiplier; to detect changes in blood flow following hypoperfusion surgery for both ASL and laser speckle derived measures of rCBF; and was also used to compare vessel density between unlesioned and lesioned hemispheres for both Q-map and collagen IV immunohistochemistry derived measures. The Pearson r test was

used to test for correlation between ASL and laser speckle measures of cortical blood flow, and between Q-map and immunohistochemical measures of vessel density. A significance level of $p < 0.05$ was considered to be statistically significant.

3.3. Results

3.3.1 Arterial spin labelling can be used to assess resting cerebral blood flow in vivo

Alterations in resting cerebral blood flow are associated with ageing and vascular cognitive impairment. In experimental animal models, resting cerebral blood flow has also been shown to be altered, however existing techniques such as autoradiography and laser Doppler or speckle imaging can be invasive or restricted to superficial cortical brain regions. Arterial spin labelling was therefore developed in order to provide a non-invasive alternative with which to quantify alterations in resting cerebral blood flow (rCBF) in experimental models. ASL was performed in wild type mice and measures of rCBF were generated. The resulting maps of rCBF highlight regional variations in the mouse brain, with values of $559 \pm 138 \text{ ml/100g/min}$, $533 \pm 121 \text{ ml/100g/min}$ and $348 \pm 106 \text{ ml/100g/min}$ in the thalamus, cortex and corpus callosum respectively (Figure 3.1).

Results obtained from initial ASL scans were in agreement with those found by Kober et al. (2008) (on which the sequence was based) but higher than the majority of published literature. Optimisation of the slice thickness and slice thickness multiplier value were subsequently tested in a subset of mice, in order to determine if blood flow values were dependent on these parameters. Decreasing the slice thickness from 1.5mm to 1mm resulted in a significant reduction in regional cerebral blood flow values of approximately 35% (Figure 3.2) ($t=10.61$, $df=3$, $p<0.01$). Mice were also scanned using the original slice thickness multiplier value of 1.5 and a modified value of either 2, 2.5, 3 or 3.5. Increasing the slice thickness multiplier significantly reduced cerebral blood flow values by approximately 15% ($t=16.54$, $df=3$, $p<0.001$), however, using a slice thickness multiplier above 1.5 introduced asymmetry in the blood flow maps (Figure 3.3 A and B). Therefore, a

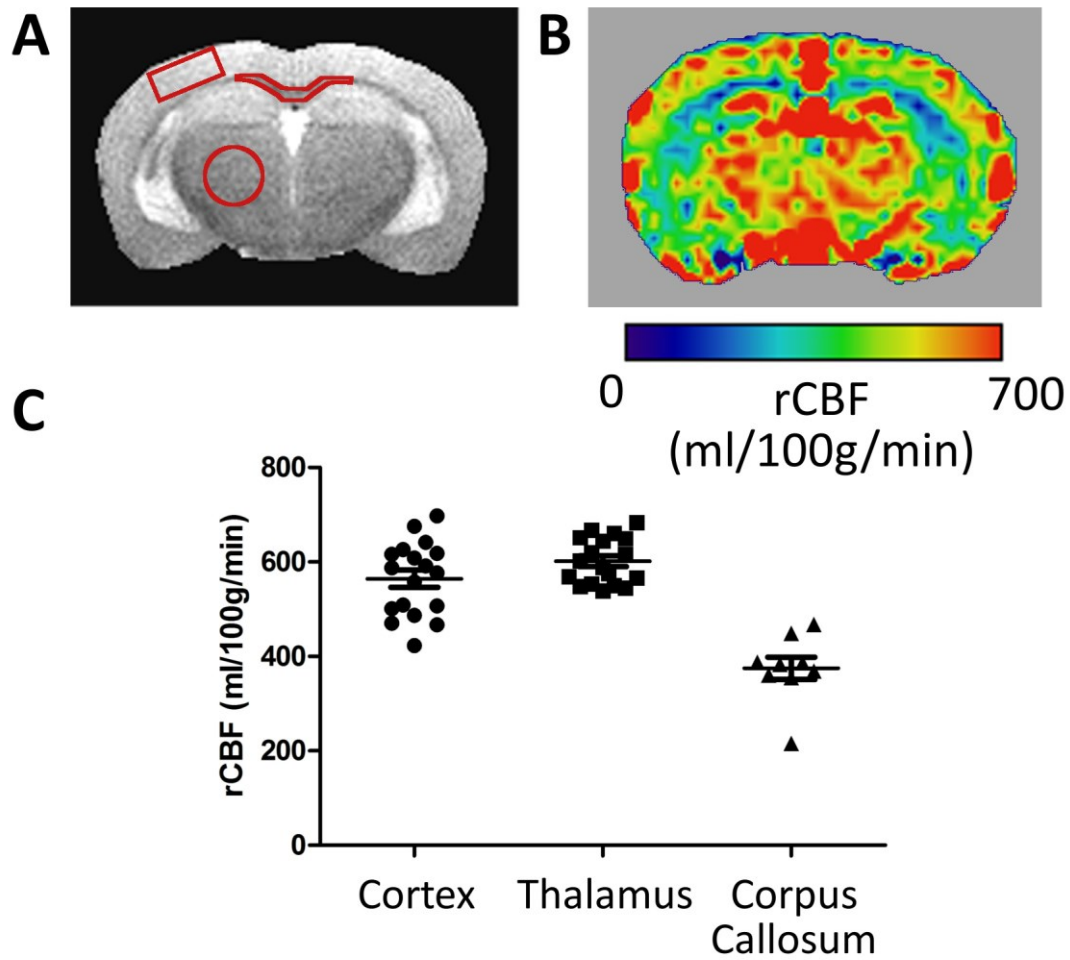


Figure 3.1 Arterial spin labelling can detect regional variations in resting cerebral blood flow. (A) Representative structural T2 scan showing regions of interest highlighted in red. (B) Arterial spin labelling derived pseudo-coloured image of resting cerebral blood flow. (C) Quantification of arterial spin labelling reveals regional differences in perfusion. Data presented as mean±SEM, n=9-14

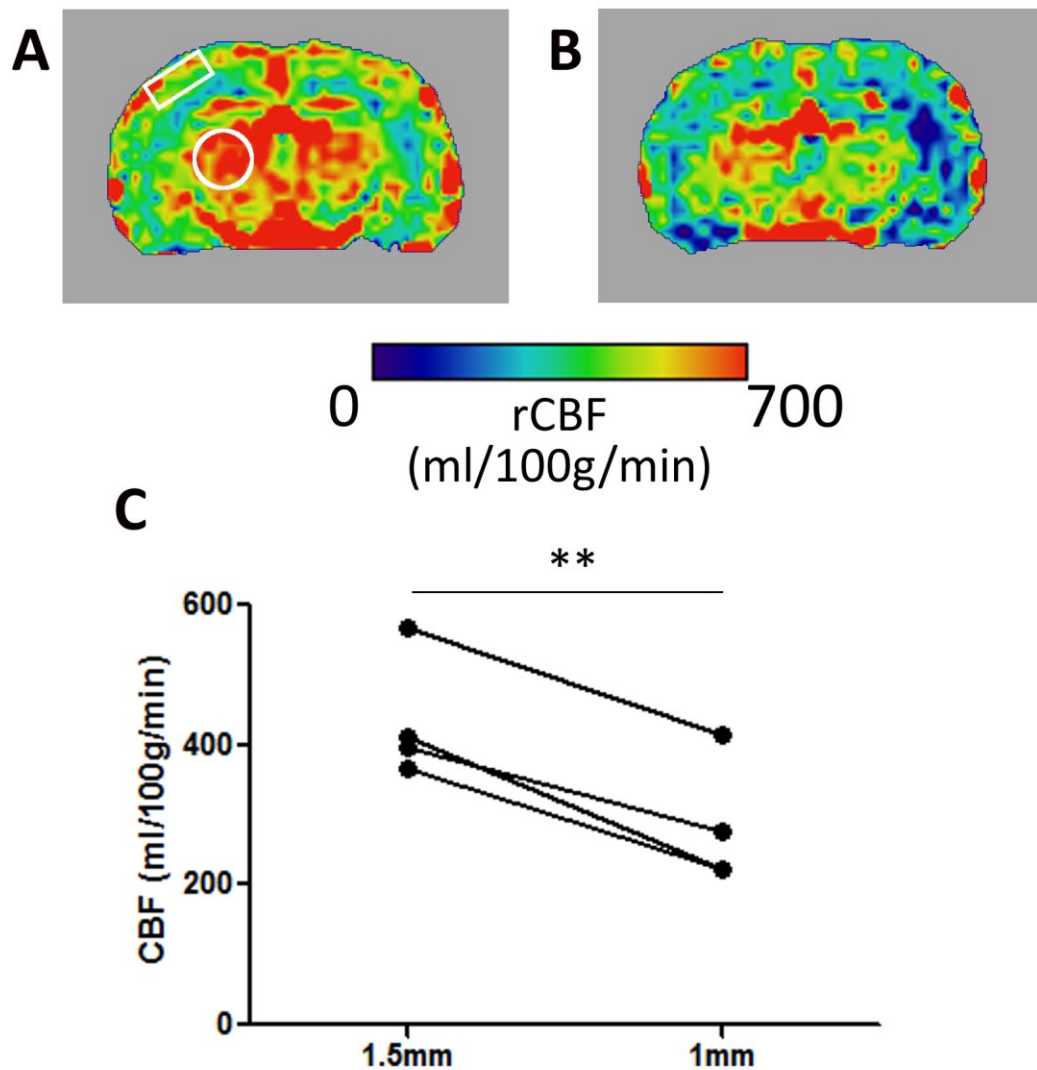


Figure 3.2 Reduction of CBF values obtained with slice thickness of 1mm. Representative arterial spin labelling derived pseudo-coloured images of resting cerebral blood flow measured in the same mouse over a slice thickness of (A) 1.5mm and (B) 1mm. Highlighted regions in white indicate cortical and thalamic regions of interest. (C) Cortical and thalamic measures of regional blood flow are significantly reduced when measured over a slice thickness of 1mm compared to 1.5mm. N=4. **p<0.01

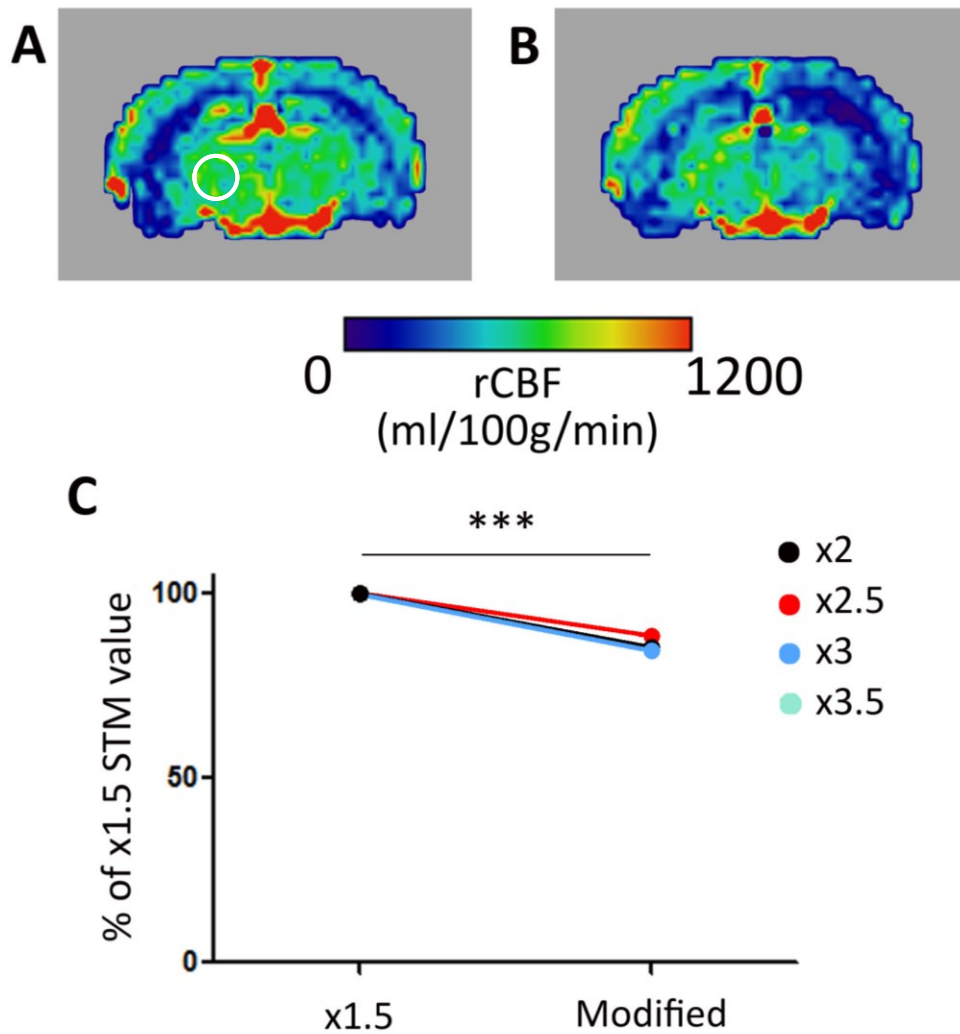


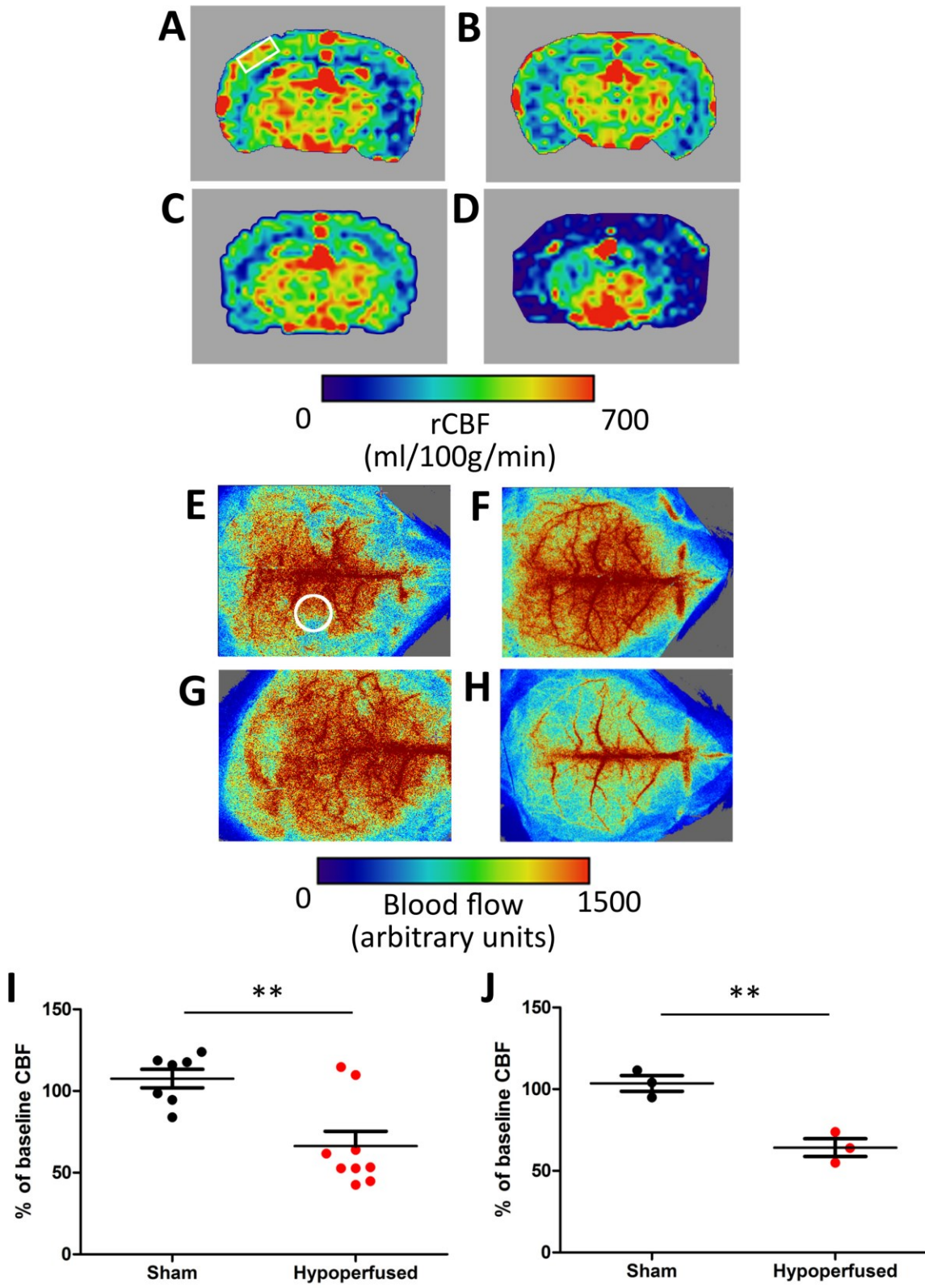
Figure 3.3 CBF values are reduced when measured using a slice thickness multiplier above 1.5. Representative CBF maps measured at (A) 1.5 and (B) 3. CBF was measured in the thalamus (highlighted in white on (A)) Although CBF values are significantly reduced when using a slice thickness multiplier above 1.5 (C), the resulting CBF maps show a pronounced asymmetry (B) and are thus unsuitable for inclusion in subsequent studies. N=3. ***p<0.01

slice thickness multiplier of 1.5 was used for subsequent experiments, and blood flow was calculated over a slice thickness of 1mm.

The reduction in blood flow observed in the chronic cerebral hypoperfusion mouse model is well characterised and has been shown by laser speckle imaging to reduce cortical perfusion by ~30-40% (Shibata et al. 2004a; McQueen et al. 2014). In order to determine if ASL is sensitive to alterations in rCBF, and to validate ASL measures with laser speckle imaging, rCBF was quantified in sham-operated and hypoperfused mice at baseline and 3 months following surgery using ASL and laser speckle contrast imaging (Figure 3.4). In sham-operated mice, rCBF assessed with ASL at 3 months was $107 \pm 15\%$ of baseline, indicating that blood flow had not been reduced over the course of the study. In contrast, rCBF of hypoperfused mice was significantly reduced by 33% to $66 \pm 30\%$ of baseline ($t=3.618$ $df=14$ $p<0.01$) when assessed with ASL (Figure 3.4). Using laser speckle imaging, rCBF was $103 \pm 8\%$ of baseline in sham-operated mice after 3 months, indicating that again blood flow had not changed over the course of the study in sham mice. In hypoperfused mice, rCBF was significantly reduced by 35% to $64 \pm 9\%$ of baseline ($t=5.418$ $df=4$ $p<0.01$) (Figure 3.4), in line with previously published data (Shibata et al. 2004a). Both ASL and laser speckle imaging were therefore able to detect reductions in blood flow following hypoperfusion, and the reductions in ASL were of the same magnitude as laser speckle imaging performed in the present study and previously published work.

In order to determine if ASL derived measures of rCBF were related to those obtained with laser speckle contrast imaging, both techniques were used to assess rCBF in the cortex of a

cohort of sham and hypoperfused mice. A significant correlation was observed between laser speckle and ASL-derived CBF measures ($r=0.7153$, $p<0.001$) (Figure 3.5).



◀ **Figure 3.4 Arterial spin labelling can detect reductions in cerebral blood flow following cerebral hypoperfusion surgery.** To validate arterial spin labelling (ASL), both ASL and laser speckle imaging were performed at baseline and 3 months following cerebral hypoperfusion, and the reductions in cerebral blood flow measures were compared. Representative images of resting cerebral blood flow from sham and hypoperfused mice at baseline (A, B) and at 3 months following surgery (C, D). Representative laser speckle images from sham and hypoperfused mice at baseline (E, F) and at 3 months following surgery (G, H). All regions of interest highlighted in white. (I) Quantification of arterial spin labelling revealed a significant 33% reduction in cortical resting blood flow following hypoperfusion surgery. (J) Analysis of rCBF using laser speckle imaging also revealed a significant 35% reduction in cortical blood flow following hypoperfusion. Data presented as mean±SEM, n=3-9 per group. **p<0.01

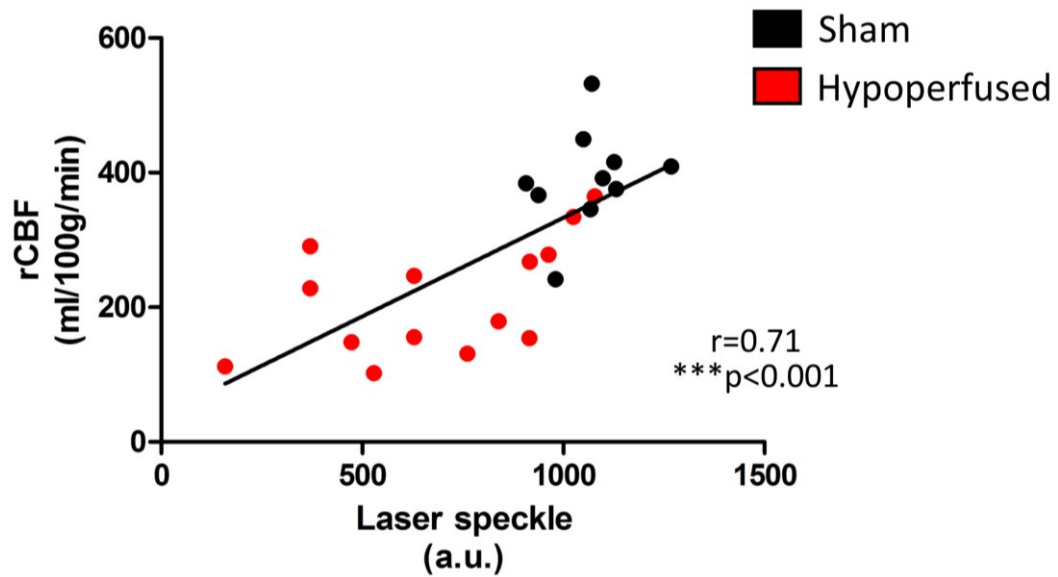


Figure 3.5 Significant correlation between arterial spin labelling and laser speckle imaging derived measures of cortical blood flow. In order to determine whether measures of rCBF obtained through ASL imaging were related to those obtained through laser speckle imaging, cortical blood flow was assessed using both techniques in the same mice. Correlational analysis indicated a significant association between the two measures ($r=0.71$, $p<0.001$). $N=10-14$ per group.

3.3.2 Q-map imaging can be used to measure vessel number in vivo

Alterations in vessel number have been reported in cerebral vascular disease and in experimental animal models using post-mortem histology. Q-map imaging was developed in order to non-invasively assess changes in vessel number in vivo in experimental mouse models. Q-map imaging was performed in wild type mice and regional values of vessel number were calculated using the resulting Q-maps. In the cortex, vessel number was shown to be 293 ± 67 vessels/mm², in the thalamus vessel number was 372 ± 63 vessels/mm² and in the hippocampus vessel number was 291 ± 30 vessels/mm²; indicating regional variation within the mouse brain (Figure 3.6).

In order to determine if Q-map imaging was sufficiently sensitive to detect pathological reductions in vessel number, a unilateral lesion was induced through administration of ibotenic acid into the subcortex. Quantification of Q-map images revealed a significant 60% reduction in vessel number in the lesion site relative to the contralateral hemisphere (147 ± 75 vessels/mm² vs 372 ± 54 vessels/mm² respectively; $t=13.78$ $df=2$ $p<0.01$). A significant 31% reduction in collagen staining density in the lesion site was also found using collagen IV immunohistochemistry ($1.82 \pm 0.1\%$ vs $2.67 \pm 0.1\%$ in lesion and contralateral hemispheres respectively; $t=5.940$ $df=2$ $p<0.05$) (Figure 3.7).

Having observed that Q-map imaging was able to detect pathological alterations in vessel number, we sought to determine whether Q-map derived measures of vessel number would correlate with values derived from collagen IV immunohistochemistry in control mice without the presence of pathology. A highly significant correlation was observed between the two measures ($r=0.5478$; $p<0.0001$) (Figure 3.8).

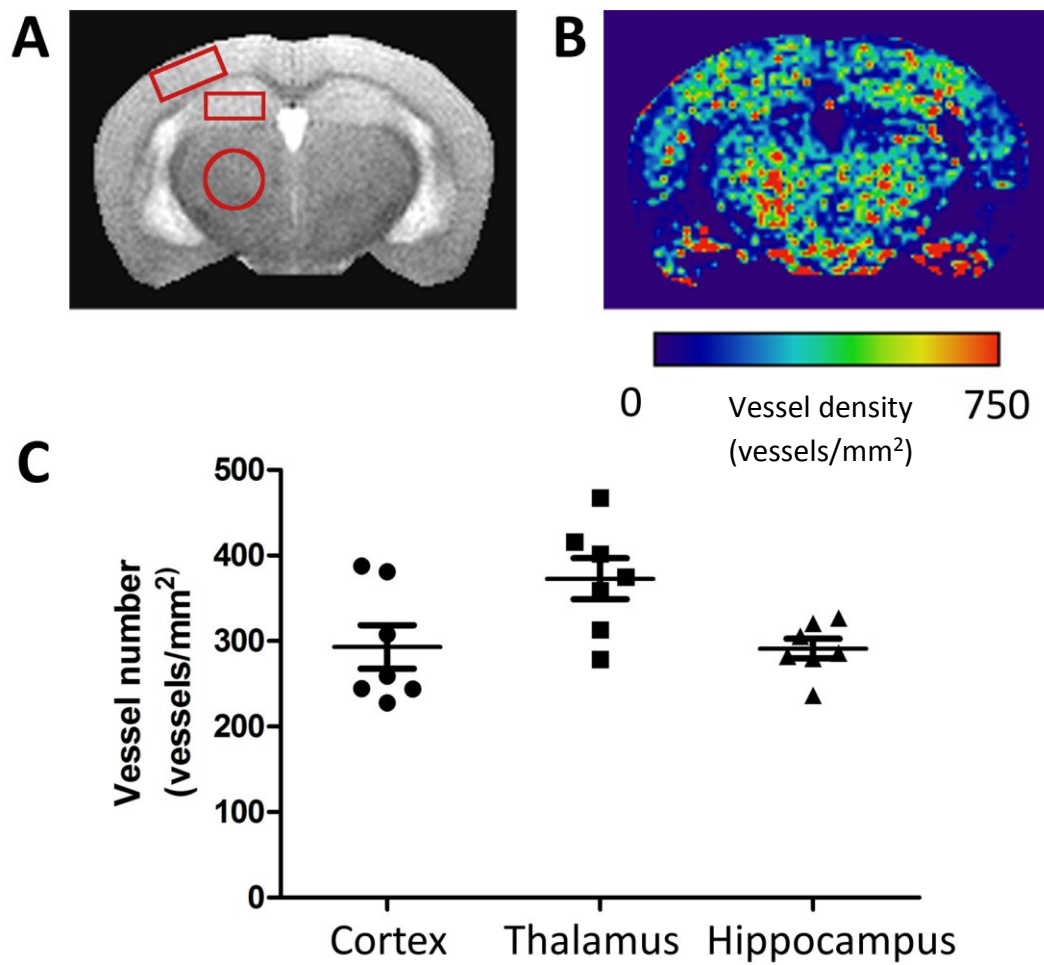


Figure 3.6 Q-map imaging can be used to measure vessel number in vivo. Representative images of (A) structural T2 scan and (B) Q-map of vessel number. Regions of interest are highlighted in red. (C) Quantification of vessel number reveals regional differences between cortex, thalamus and hippocampus. Data presented as mean \pm SEM, n=7.

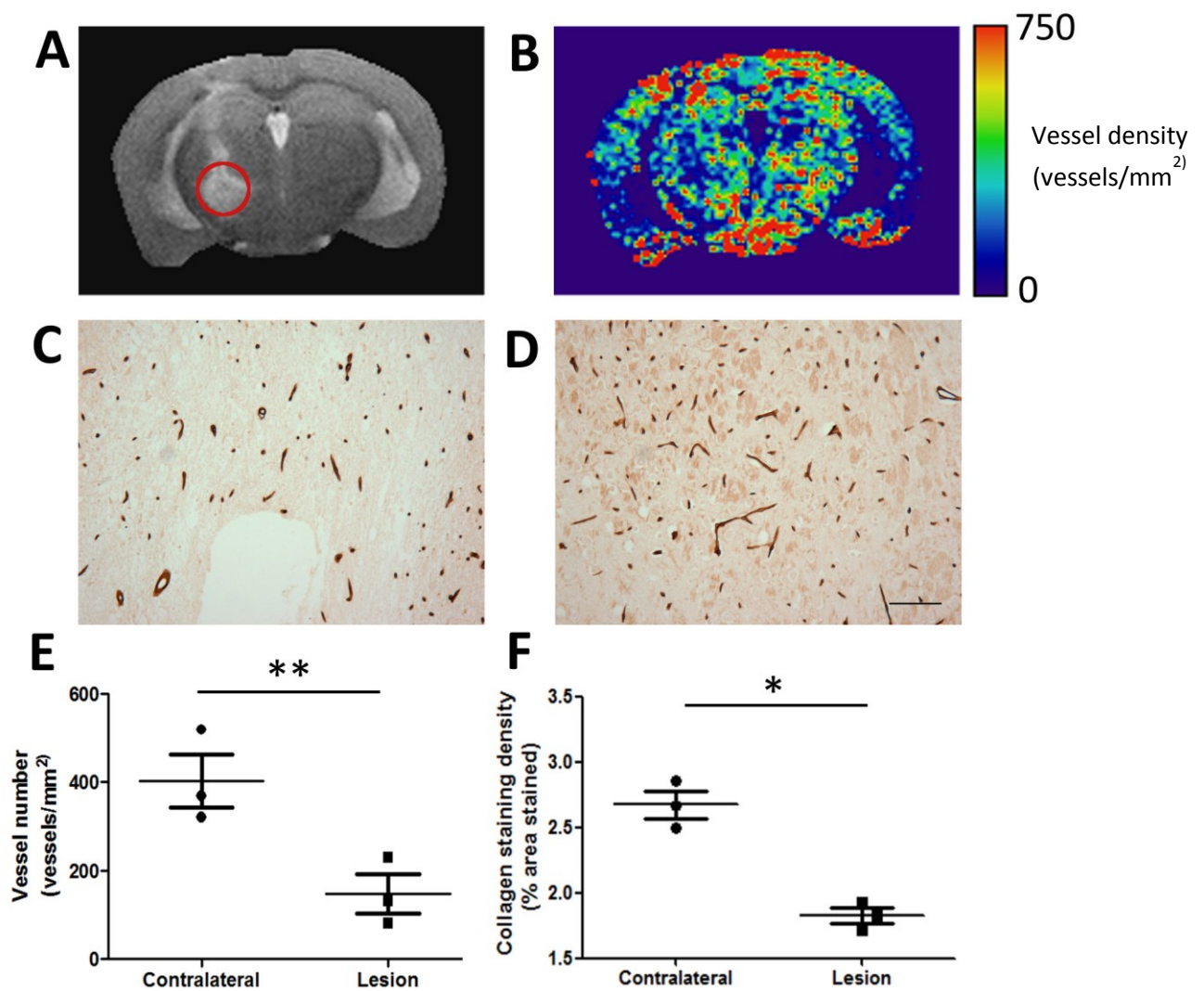


Figure 3.7 Q-map imaging can sensitively detect reductions in vessel number.

Unilateral ibotenic acid lesions were induced in a subset of mice to determine whether Q-map imaging could detect changes in vessel number. (A) Structural T2 scan depicting the hyperintense lesion. (B) Q-map image depicting low vessel number, shown in blue, in the site of the lesion. (C) Histological stain for collagen IV in the lesion site and (D) in the contralateral subcortex. (E) Quantification Q-map imaging and (F) collagen IV immunohistochemistry reveals vessel number is significantly reduced in the lesion site relative to the contralateral subcortex. Scale bar= 50 μ m. Data presented as mean \pm SEM, n=3. *p<0.05, **p<0.01

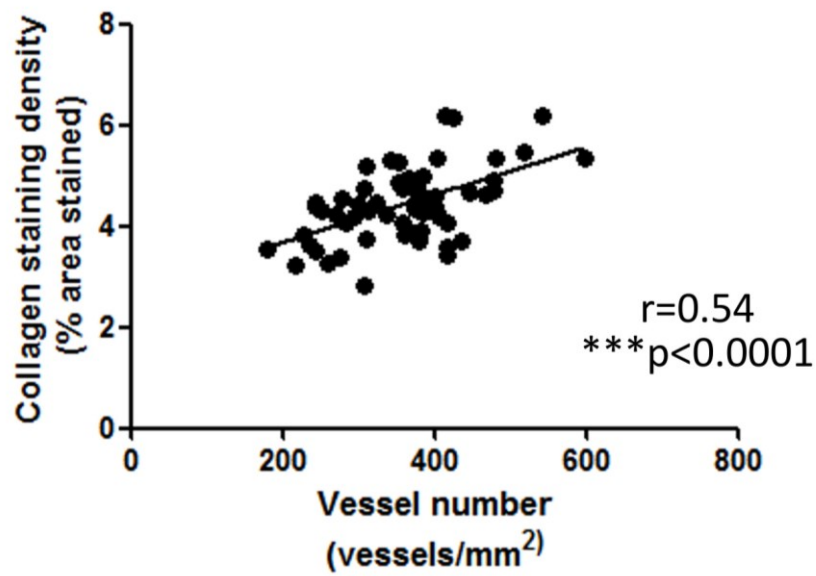


Figure 3.8 Q-map derived measures of vessel number correlate with immunohistochemical measures of vessel density. Vessel number was quantified using both Q-map imaging and collagen IV immunostaining in order to validate Q-map imaging as an in vivo tool for measuring vessel number. A significant correlation was detected between the two measures ($r=0.54$, $p<0.001$). $N=58$.

3.3.3 T2 imaging can be used for the detection of vascular lesions in vivo

Structural T2 imaging has been previously developed for use in detecting ischaemic and haemorrhagic lesions in vivo (Holland et al. 2015). This technique was utilised in imaging studies both for detection of vascular lesions and as a guide for region of interest based analysis of Q-map imaging. Examples of vascular lesions characterised according to Holland et al. (2015) are shown in Figure 3.9. Ischaemic lesions were classified as hyperintense signal with focal tissue loss, potentially cavitated with or without localized hypointense areas consistent with paramagnetic effects of iron/hemosiderin in the surrounding parenchyma. Haemorrhagic lesions were classified as areas of rounded predominantly hypointense signal. In control mice, no vascular lesions were detected. In order to validate the detection and classification of vascular lesions with structural T2 imaging, haemotoxylin and eosin (H&E) and Perls' Prussian Blue staining were performed in tissue sections corresponding to those assessed with MRI. Ischaemic lesions were identified as clearly delimited areas of tissue pallor on H&E staining, whilst haemorrhagic lesions were identified as blue-coloured cellular hemosiderin deposits on Perls' Prussian Blue stained sections. Hyperintense features on MRI were associated with areas of ischaemic pathology on H&E stained sections, whilst hypointense features on MRI were associated with areas of haemorrhagic pathology. H&E and Perls' Prussian Blue confirmed the absence of vascular lesions in control mice.

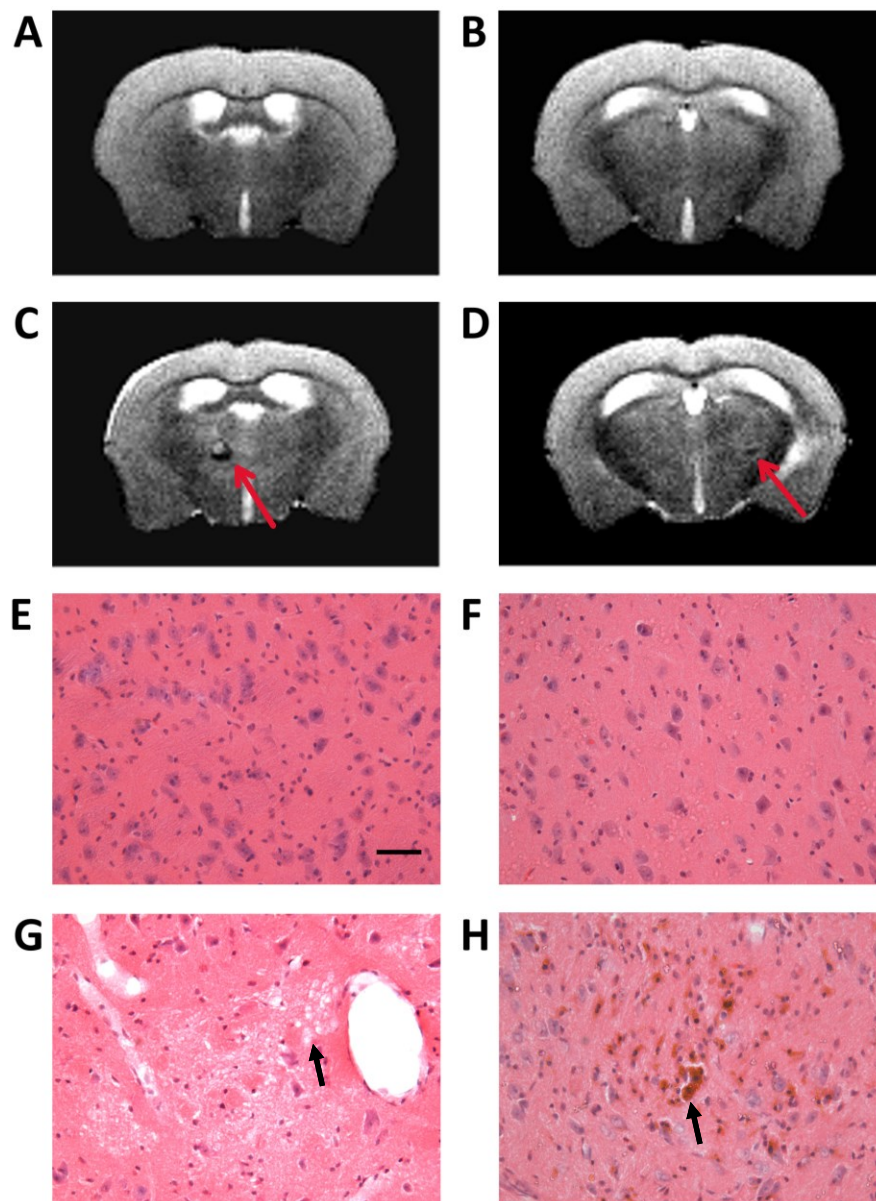
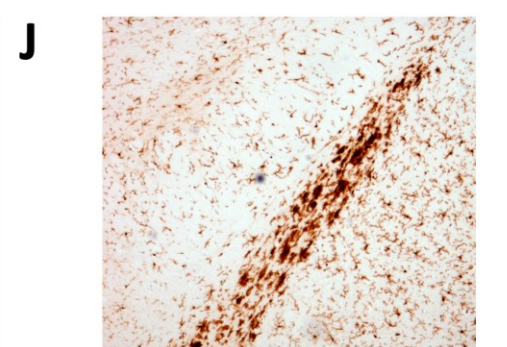
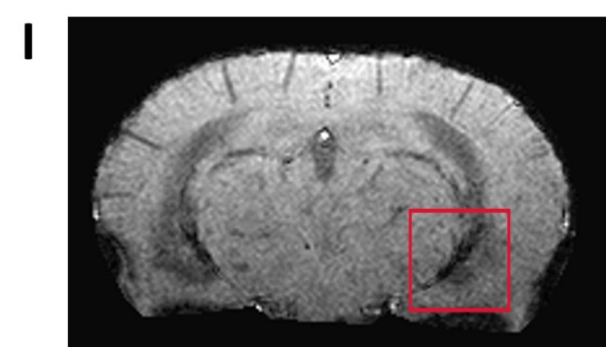
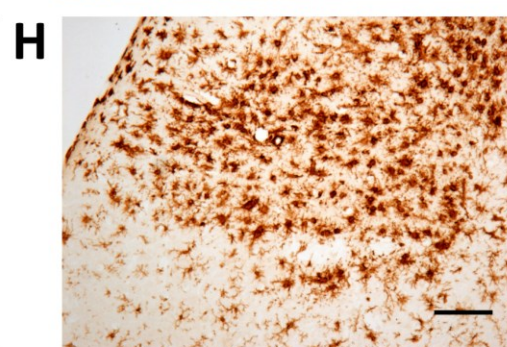
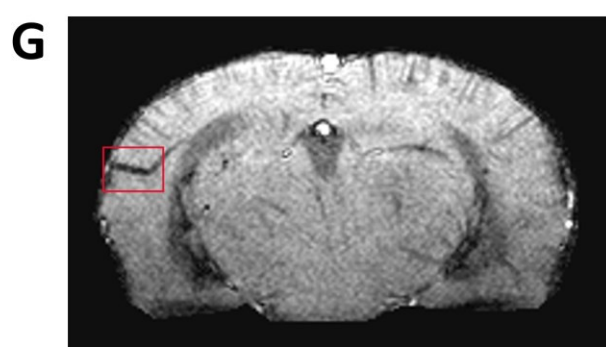
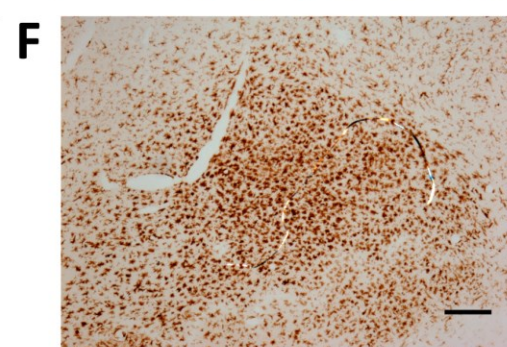
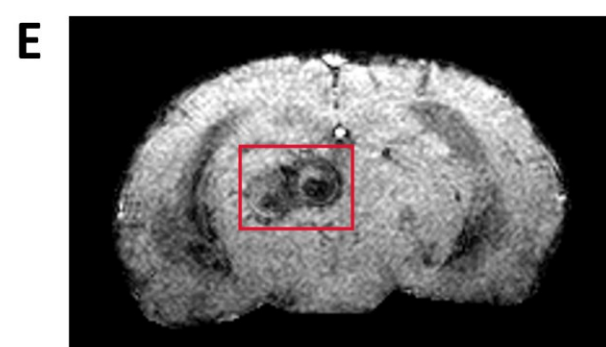
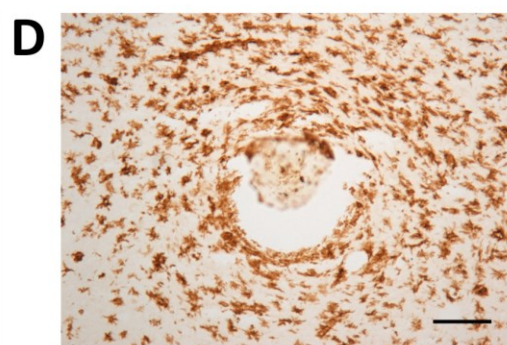
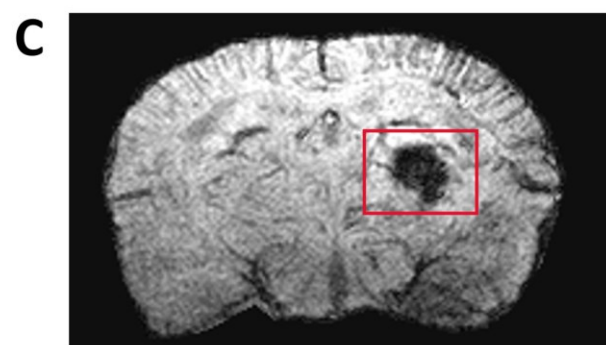
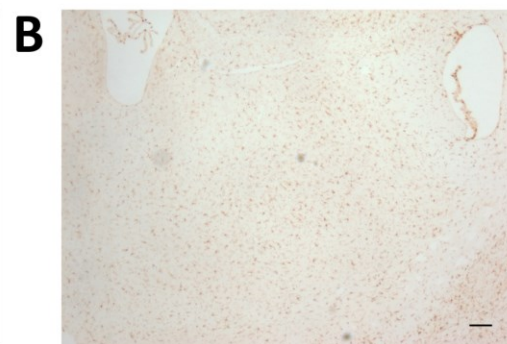
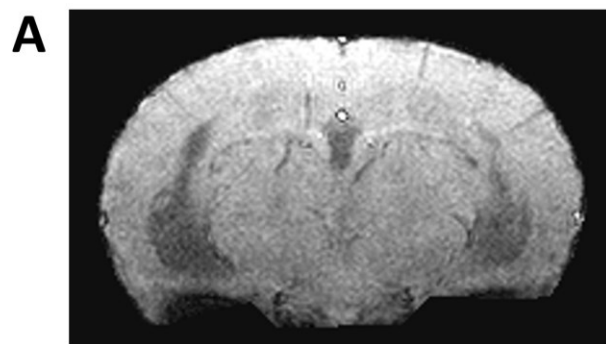


Figure 3.9 Detection of ischaemic and haemorrhagic lesions by structural T2 magnetic resonance imaging. T2 imaging has previously been developed and validated for the detection of vascular lesions in vivo. (A,B) Representative images from control mice that exhibit no imaging abnormalities. (C) Hyperintense signal in the thalamus (red arrow) indicative of an ischaemic lesion. (D) Hypointense signal in the thalamus (red arrow) indicative of a haemorrhagic lesion. (E,F) Representative H&E stained tissue sections from sham mice showing non-lesioned tissue. (G) H&E stained tissue section showing tissue pallor and vacuolation (arrow) in ischaemic lesion corresponding to (C). (H) H&E stained tissue section showing brown haemosiderin deposits (arrow) indicative of haemorrhagic pathology corresponding to (D). 126

3.3.4 Contrast-enhanced T2* imaging can detect areas of inflammation in vivo

Neuroinflammation is associated with the initiation and progression of cerebral vascular disease and has been identified as a key mediator of pathology in experimental models. In this study, the potential of contrast-enhanced T2* MRI for assessing inflammation in vivo was investigated. 3D gradient echo data was collected in order to measure accumulation of the ultrasmall superparamagnetic iron oxide (USPIO) contrast agent ferumoxytol in both sham and hypoperfused mice. In hypoperfused mice, but not in shams, ce-T2* revealed areas of signal loss that appeared as rounded, focal hypointensities in the thalamus and white matter, as well as vascular hypointensities observed in the penetrating vessels of the cortex and in larger vessels of the thalamus. Hypointense areas on T2* images corresponded to areas of increased Iba1 as assessed by immunohistochemistry, whereas areas of increased Iba1 were not detected in sham mice (Figure 3.10).

In order to determine if hypointense signal changes observed on contrast-enhanced T2* images were due to tissue accumulation of iron, DAB enhanced Perl's staining was performed in tissue sections. Positive Perl's staining was observed in hypoperfused mice, but not in shams, in perivascular cells and also in microglia on combined Perl's/Iba1 sections, indicating cellular uptake of iron following contrast-enhanced T2* imaging (Figure 3.11).



◀Figure 3.10 Use of contrast-enhanced T2* imaging to detect inflammation in vivo.

Contrast-enhanced T2* imaging and Iba1 immunohistochemistry were performed in sham and hypoperfused mice. In hypoperfused mice, but not in shams (A), focal hypointensities could be observed on ce-T2* images, and were observed in thalamus (C, E), cortex (G) and white matter tracts (I) (red boxes). In the same mice, Iba1 staining in tissue sections from the same anatomical location revealed focal areas of microgliosis in the corresponding regions of hypointensity detected with ce-T2* (D, F, H, J). In sham-operated mice, areas of increased Iba1 immunoreactivity were not detected (B). Scale bar=200 μ m (D, H), 100 μ m (B, F).

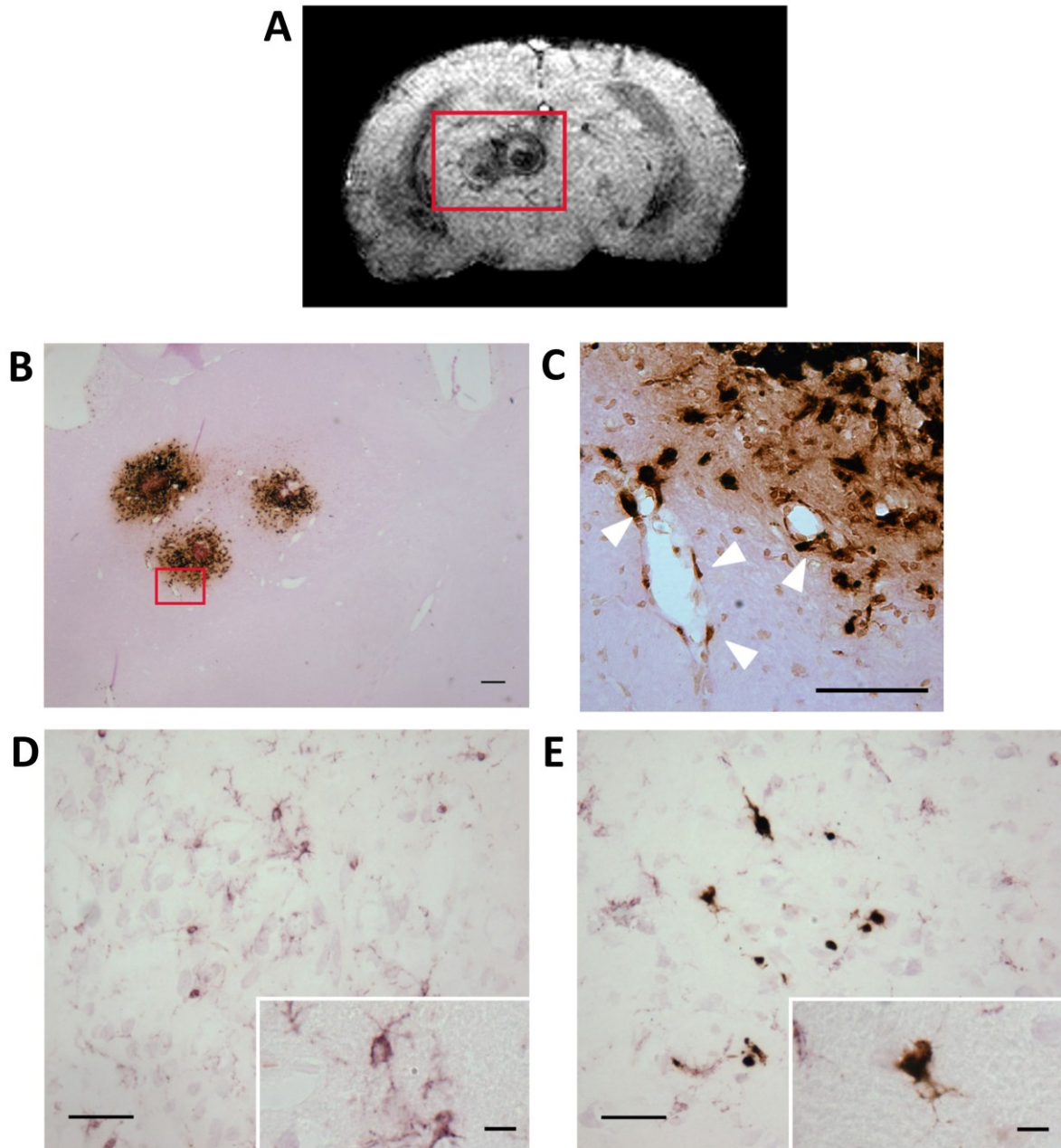


Figure 3.11 Detection of iron following contrast-enhanced T2* imaging. Enhanced Perl's was performed in brain tissue sections in order to investigate tissue retention of iron oxide contrast agent following contrast-enhanced T2* imaging. (A) T2* image depicting focal thalamic hypointensities (red box). (B) Positive Perl's staining in thalamus corresponds to the hypointense region observed on T2*. Red box indicates region of higher magnification in (C). (C) Perivascular cells (white arrowheads) are positively stained, indicating presence of iron within these cells. (D,E) Enhanced Perl's was also combined with Iba1 VIP immunohistochemistry to detect the presence of iron within microglia. (D) Inset: higher power image shows no iron deposits were detected in microglia of sham mice. (E) In hypoperfused mice, positive Perl's staining was observed to colocalise with Iba1 positive cells. Inset: higher power image showing presence of iron deposits within microglial cell. Scale bar=200µm (B), 100µm (C), 50µm (D,E), 10µm (D inset, E inset).

3.4 Discussion

MRI has the potential to provide in vivo, non-invasive measures of vascular parameters and therefore overcomes the requirement for post-mortem tissue used in techniques such as biochemistry and immunohistochemistry. Here, MRI techniques have been developed that enable the assessment of resting cerebral blood flow, vessel number, vascular lesions and inflammation, and these approaches have been validated using measures obtained from a range of other modalities.

3.4.1 Arterial spin labelling as a tool to assess resting cerebral blood flow

Changes in resting cerebral blood flow have been widely reported to occur with age and also in Alzheimer's disease and vascular dementia (Chen et al. 2011; Gao et al. 2013). In order to assess rCBF in experimental models, we developed an MRI arterial spin labelling approach based on published methodology (Kober et al. 2004, 2008) and validated this approach using surgical intervention and laser speckle imaging. ASL was able to successfully distinguish between sham and hypoperfused mice, detecting a 33% reduction in cortical blood flow following hypoperfusion, in line with previously published data (Shibata et al. 2004a, McQueen et al. 2014). Furthermore, this reduction in CBF assessed using ASL was also in good agreement with the assessment by laser speckle imaging in the same mice, which indicated a 35% reduction in cortical blood flow. There was also a significant positive correlation between the values obtained from the two measures, further indication of the agreement between these two techniques. These results are encouraging for the use of ASL in future studies, in which it may be preferential to laser speckle imaging as it allows the measurement of cerebral blood flow in deeper brain structures such as white matter and subcortex, whereas laser speckle imaging may only provide information related to superficial cortex. The relatively short scan duration (20mins) is also beneficial when considering

longitudinal studies that may require repeated periods of anaesthesia. Importantly, however, the variation in ASL measures was greater than that obtained for laser speckle imaging. Values of rCBF assessed by ASL in the cortex of wild type sham mice varied by almost 23%, therefore a minimum sample size of 10 per group is required in order to detect an rCBF reduction of 30% (i.e. for studies of cerebral hypoperfusion). In comparison, variability of cortical perfusion assessed by laser speckle was just 7%, meaning a minimum sample size of just 2 per group would be required to detect such a reduction.

A further limitation of the current technique is that blood flow values exceed those reported in the literature. Quantitative autoradiography reports thalamic blood flow values of 146ml/100g/min (Niwa et al. 2002) and 159ml/100g/min (Maeda et al. 2000) in non-anaesthetised mice, relative to 559ml/100g/min in the present study. However, measuring cerebral blood flow over a smaller slice thickness of 1mm instead of 1.5mm reduced blood flow values to be closer in line with those published in the literature (318ml/100g/min for thalamic blood flow). A potential reason for the overestimation of flow is the use of isoflurane anaesthesia during the scan. Isoflurane is a known vasodilator (Iida et al. 1998) and may increase brain blood flow to influence ASL measures. In order to minimise the contribution of isoflurane to blood flow measurements, in subsequent experiments steps were taken to standardise the inhaled concentration of isoflurane across animals and to ensure that ASL was performed after a standardised duration of anaesthesia for each mouse. Isoflurane administered at 1.8% has been shown to increase blood flow by 46% when assessed with laser Doppler (Kehl et al. 2002), so although isoflurane anaesthesia may contribute to overestimation of perfusion it is unlikely to entirely account for the differences observed between autoradiographical measures and blood flow values obtained in this study. Kober et al (2008) report thalamic blood flow measures of 440ml/100g/min using the same ASL protocol

at 4.7T, and suggest that arterial bulk flow may also contribute to overestimation of perfusion using this protocol. A final consideration is that T1 of arterial blood was not measured in the present study. A value of 2.25s was selected based on Dobre, Ugurbil and Marjanska (2007), who measured T1 of bovine blood at the same magnetic field strength (7T), however direct measurement would negate the need to make such an assumption in the mathematical modelling to calculate rCBF. Further investigation of the overestimation of perfusion values is warranted. Despite absolute values of perfusion being higher than those reported in the literature, the present ASL approach would still be suitable for detecting relative changes in perfusion, such as in the comparison between blood flow values before and after chronic cerebral hypoperfusion surgery.

In the present study, ASL was used to measure resting blood flow, however it could also be modified to incorporate measures of vascular responsiveness, for example to a hypercapnic challenge, in order to generate data on vessel function (Noth et al. 2006). The current method used in this study for measuring blood flow is too long to incorporate a hypercapnic challenge, as it would require that the mouse breathe CO₂ for the duration of the scan (20 minutes). However, the use of another, shorter ASL technique may be of considerable benefit for future studies as vascular responsiveness has been shown to be altered in vascular diseases and Alzheimer's disease (Jennings et al. 2005; Vetri et al. 2012; Vicenzini et al. 2007), and is associated with cognitive outcomes (Sorond et al. 2013).

3.4.2 Q-map imaging assessment of vessel number in vivo

Vessel number has been shown to be altered in human cerebral vascular disease (Brown and Thore, 2011) and in experimental animal models (Moore et al. 2015). In the present study, Q-map imaging was developed in order to measure vessel density in vivo, and allowed the calculation of vessel number in distinct regions of the brain. Measures of vessel number

obtained in this study are also in good agreement with those from other studies that utilise Q-map imaging. In the present study, vessel number was found to be 293 ± 67 vessels/mm², 372 ± 63 vessels/mm² and 291 ± 30 vessels/mm² for the cortex, thalamus and hippocampus respectively. This is in good agreement with data from Bosomtwi et al. (2008), who measure cortical vessel density as 313 ± 32 vessels/mm², whilst the cortical value is slightly less than that found by Wu et al. (2004) who measure vessel number as 444 ± 80 , 458 ± 59 and 238 ± 69 vessels/mm² for the cortex, thalamus and hippocampus respectively. Importantly, the results presented here are in good agreement with those obtained with histology: Weiss et al. (1982) reports vessel number as 256 vessels/mm², 345 vessels/mm² and 333 vessels/mm² in cortex, thalamus and hippocampus respectively. This further indicates the validity of Q-map imaging for detection of vessel number in vivo.

Q-map imaging was also sufficiently sensitive to detect pathological alterations in vessel number following ibotenic acid lesion. With Q-map imaging, vessel number in the lesion site was 60% less than in the contralateral hemisphere, although it was found to be only 30% less in the lesion site when assessed by collagen IV immunohistochemistry. This discrepancy may relate to the much larger volume of tissue measured using Q-map imaging, where vessel number was assessed in a slice covering 800µm, compared to just a 6µm tissue section that was used for immunohistochemistry. The ability to assess vessel number across the whole brain in one imaging session offers a distinct advantage over conventional immunohistochemistry, where to assess vessel number histologically over such a large volume of tissue would be relatively labour-intensive. Because the calculation of vessel number using Q-map imaging is reliant on an intravascular contrast agent, vessel numbers obtained with this method should only correspond to perfused, and therefore functional vessels. However, occluded or degenerating vessels will still be detected by antibodies directed against the basement

membrane, such as collagen IV as used here, and may result in an overestimation of vessel number by immunohistochemistry. Bosomtwi et al. (2008) reported that, whilst Q-map imaging measures correlated highly with histologic values of vessel number in healthy tissue, in the ischaemic core following embolic stroke the two measures did not correlate. In this case, vessel numbers measured by histology were found to be as little as 8 ± 3 vessels/mm², the low numbers of vessels present in ischaemic lesions may result in a much lower signal to noise ratio obtained from the intravascular contrast agent. This may not be a concern, however, for studies of vessel number in less severe experimental animal models, for example in models of ageing or amyloid deposition, where focal lesions are not typically induced. With ageing, a 15% loss in vessel number has been reported in wild type mice by 2 years old (Miao et al. 2005), this figure increases to 29% in an amyloid-expressing transgenic model (Miao et al. 2005). In the absence of focal ischaemic tissue loss, the agreement between measures of vessel number obtained through Q-map imaging and histology can be expected to be good. Indeed, in the present study measures of vessel number from Q-map imaging in young and aged mice from brain regions without ischaemic pathology correlated well with those obtained from collagen IV immunohistochemistry. This indicates the sensitivity of this technique in assessing non-pathological variations in vessel number, but the ability of Q-map imaging to assess vessel number in lesion sites requires further validation.

Some limitations of Q-map imaging still remain to be addressed. In the current study, administration of the contrast agent was performed via femoral vein cannulation, precluding recovery of the animals. The alternative use of tail vein cannulation would overcome this problem and permit repeated assessments in the same mice. The scan also has a relatively long total duration at 1hr 30 minutes, which may be problematic if used in combination with other techniques due to the length of time required for continued anaesthesia. It is also not clear from

the present study how Q-map-derived measures of vessel number would be affected by blood-brain barrier breakdown and leakage of the blood (and therefore the contrast agent) into the parenchyma. Large, focal haemorrhages or ischaemia may be detected by diffusion tensor imaging already incorporated into the Q-map paradigm (Whang et al. 2015), but the effect of smaller microbleeds was not assessed in this study and may represent a potential confound. Microbleeds and disruption of the blood vessel wall have been reported in response to both vascular amyloid deposition and chronic cerebral hypoperfusion (Dierksen et al. 2010, Holland et al. 2015), their effect on MRI measures should be an important consideration for future studies.

Another concern when incorporating Q-map imaging into future studies is the observed variability within mice from the same population. Vessel number in the cortex of young wild type mice varied by almost 23%, in the thalamus by 16% and in the hippocampus by 10%. The minimum sample size required to detect small changes in vessel number (i.e. 15% as reported previously (Miao et al. 2005)) would therefore be 37 to detect such a change in the cortex, 20 in the thalamus and 8 in the hippocampus. To detect slightly larger changes in vessel number, such as those reported in amyloid-transgenic mouse models of ~30%, the minimum sample sizes would be 10, 5, and 2 for cortex, thalamus and hippocampus respectively. Therefore, predicted regions in which blood vessel alterations are likely to occur, and what the magnitude of these changes will be, should be taken into account when designing future studies that incorporate Q-map imaging. Inter-mouse variation in anatomical MRI image slice location may also have contributed to the high variability observed. In order to address this issue, a standardised slice plan for all scans will be used in future experiments (centred on Bregma - 1.82mm in stereotactic coordinates of the Mouse Brain Atlas (Paxinos and Franklin, 2001), and a fast, low-resolution T2 scan will be performed at the outset in order to ensure uniform

placement of the mouse within the MRI scanner. This should ensure that all measurements are calculated in consistent regions of the brain in order to reduce variability.

3.4.3 Detection of vascular lesions using structural T2 imaging

T2 imaging has previously been developed and validated for the detection of ischaemic and haemorrhagic vascular lesions (Holland et al. 2015). In line with previously published work, hyperintense and hypointense features could be observed on T2 images from hypoperfused mice, in regions such as the thalamus which are known to be vulnerable to chronic cerebral hypoperfusion (Holland et al. 2015). Importantly, no abnormal MRI findings were detected on T2 images from sham-operated mice, highlighting the sensitivity of this technique to the pathological alterations that occur following chronic cerebral hypoperfusion in mice. MRI findings were further validated using histology, which confirmed the absence of lesions in sham mice and allowed the pathological basis of T2 signal alterations to be examined. Ischaemic and haemorrhagic pathology were found to have distinct signatures on T2 imaging as outlined previously, which will aid the detailed and precise classification of lesion burden in vivo in future studies. Both microinfarcts and microbleeds are prevalent neuroimaging features in clinical studies and are associated with cognitive performance (Kalaria, 2016; Valenti et al. 2016). Structural T2 imaging will therefore be used to provide useful translational evidence regarding the development of vascular lesions in experimental models, and can be combined with behavioural assays to allow mechanistic hypotheses of vascular cognitive impairment to be tested.

3.4.4 In vivo assessment of neuroinflammation using contrast-enhanced T2*

Neuroinflammation is implicated in the initiation and progression of cerebral vascular disease and may represent a promising target for reduction of vascular cognitive impairment (Lenart, Brough and Denes, 2016; Raz, Knoefel and Bhaskar, 2016). The ability to measure inflammation in vivo, and to monitor inflammation in response to therapeutics would be a highly valuable tool. In this study, a contrast-enhanced T2* approach was utilised in order to detect uptake of an iron oxide contrast agent by inflammatory cells. In hypoperfused mice, but not in shams, enhanced retention of iron oxide was observed in brain tissue, resulting in hypointense signals on T2* images. Focal hypointensities were predominantly observed in the thalamus and white matter, in line with previously published data highlighting prominent white matter disruption (Holland et al. 2011) and the vulnerability of subcortical regions to haemorrhage and infarction (Holland et al. 2015). In addition, cortical penetrating arterioles also appeared hypointense in hypoperfused mice and not in shams. Cortical ischaemic lesions have been reported previously (Holland et al. 2015), but a specific focus on pathology of the penetrating arterioles in the cortex may warrant further investigation. The microglial marker Iba1 was also increased in hypointense regions identified from T2* imaging, indicative of increased inflammation. T2* hypointensities following the administration of superparamagnetic iron oxide particles (SPIOs) are proposed to arise through phagocytosis of SPIOs by macrophages in areas of inflammation. In peripheral tissues, the small particle size of SPIOs allows them to exit the bloodstream through capillary walls and infiltrate inflamed tissue, where they accumulate due to phagocytosis by macrophages. By utilising this feature of SPIOs, contrast-enhanced T2* has been used as an indicator of inflammation in a number of models of peripheral infection (for review see Neuwelt et al. 2014), and the degree of signal change on T2* imaging has been shown to be related to the extent of iron accumulation in the

tissue (Sigovan et al. 2009; Seyfer et al. 2014). Contrast-enhanced imaging has also been used to investigate inflammation in the brain, however the origin of SPIO-induced signal changes in the central nervous system differs to that in peripheral tissue due to the presence of the blood-brain barrier, meaning that SPIOs cannot infiltrate parenchymal tissue as readily. Nevertheless, in the present study, hypointensities were observed on T2* in hypoperfused mice and not in shams. There are likely to be several mechanisms by which SPIO accumulation occurs, the first may be as a result of blood-brain barrier breakdown in which SPIOs can passively diffuse into the parenchyma from the bloodstream, in particular this may be the case for studies of cerebral stroke where large regions of the blood-brain barrier are likely to be compromised. SPIOs may also be phagocytosed by circulating macrophages in the bloodstream, which may then be recruited to the brain through adhesion to activated endothelial cells. Infiltration of circulating macrophages has been suggested to form the basis of hypointensities observed in animal models of multiple sclerosis, such as the experimental autoimmune encephalomyelitis (EAE) model (Linker et al. 2006). SPIO accumulation may further occur through uptake by perivascular macrophages and accumulation in the vessel wall, as has been shown in a mouse model of cerebral amyloid angiopathy (Klohs et al. 2015). The mechanism of SPIO accumulation in hypoperfused mice from the present study has not been determined, although it may be likely to occur through several mechanisms due to the diversity of pathology that exists in hypoperfused mice. Areas of ischaemic and haemorrhagic pathology may induce focal hypointensities as a result of blood-brain barrier compromise, rather than directly as a result of inflammation itself. Hypointense signal changes that appeared vascular in nature, for example those in the penetrating vessels of the cortex, may be due to uptake of SPIOs by perivascular macrophages- indeed, positive detection of iron could be observed in cells lining blood vessel walls, although further characterisation would be necessary to confirm the identity of these

cells as perivascular macrophages. In order to specifically detect areas of vascular inflammation, SPIOs have been developed that target inflammatory markers such as vascular cell adhesion molecule-1 (VCAM-1), and have been used to delineate core and penumbral regions in ischaemic stroke (Hoyte et al. 2010; Gauberti et al. 2013). The use of specially designed ligands that target specific proteins or enzymes is common in positron emission tomography (PET) imaging of neuroinflammation, where radiotracers that bind to markers of microglial or astrocytic activation (such as translocator protein (TSPO), and monoamine oxidase B) have been used clinically to demonstrate increased microglial inflammation following ischaemic stroke (Pappata et al. 2000) and in MCI and Alzheimer's disease (for review see Higuchi et al. 2016). PET approaches have also been used extensively in animal models. Mirzaei et al. (2016) demonstrate increased retention of a radioligand against TSPO in the cortex and hippocampus of the 5XFAD model of Alzheimer's disease, this retention coincided with increased amyloid deposition and microglial (but not astrocytic) activation in the same areas when validated with immunohistochemistry. Binding of the PET radiotracer to a specific ligand offers an advantage over ce-T2* in which positive signal may have distinct cellular origins, on the other hand a ce-T2* approach may be less restrictive when there is a need to assess a range of inflammatory processes. MRI is often cheaper than PET imaging and has a better spatial resolution, nevertheless, PET imaging is more sensitive than MRI and the use of specific ligands may be a useful approach to validate ce-T2*. Such an approach could be used to determine the contribution of vascular inflammation to signal changes observed on T2* in the hypoperfusion model. In the present study, an increase in Iba1 +ve cells was observed in areas corresponding to hypointense signal change, indicative of increased inflammation, although whether these cells are resident microglia or circulating macrophages that may have entered the brain from the bloodstream as a result of vascular activation cannot

be determined through the use of Iba1 alone. The inflammatory phenotype of these cells and the surrounding tissue was also not further examined, and currently it is not known whether SPIO accumulation can distinguish between pro and anti-inflammatory processes. It would be beneficial to know how signal changes on T2* correlate to the inflammatory state of the tissue, for instance the expression of pro-inflammatory markers such as CD68 on Iba +ve cells, as well as the levels of pro or anti-inflammatory cytokines and chemokines such as interleukin-1 β or interleukin-4. Nevertheless, contrast-enhanced T2* appears to be a useful method for detecting inflammation in vivo, and was able to distinguish between sham and hypoperfused mice. Future studies would determine whether it could also detect resolution of inflammation through treatment with therapeutic drugs.

3.4.5 Conclusions

Overall, MRI has potential to non-invasively monitor vascular parameters in vivo such as vessel number, resting cerebral blood flow and neuroinflammation. In future studies of experimental models these approaches may afford the use of lower n numbers, as mice can be studied at more than one timepoint. There is also clear translational value to human imaging experiments using the same or similar techniques, as preclinical MRI observations can be validated with pathological assessment of post-mortem brain tissue, whereas it is much more challenging to obtain a similar standard of pathological validation in human studies. Future studies within this thesis will utilise these validated MRI approaches to detect vascular alterations in vivo in response to ageing, amyloid deposition and chronic cerebral hypoperfusion.

Chapter 4.

The effect of ageing on neurovascular structure and function in wild type and TgSwDI mice

The effect of ageing on neurovascular structure and function in wild type and TgSwDI mice

4.1 Introduction

Ageing is one of the most significant risk factors for development of vascular cognitive impairment, and has been shown to disrupt neurovascular coupling and to alter components of the neurovascular unit. In clinical studies, neurovascular coupling becomes progressively impaired with age (Hutchison et al. 2013; Gauthier et al. 2013); in mice neurovascular coupling has been shown to be impaired as early as 8 months (Balbi et al. 2015) and also at 12 months (Park et al. 2007). Increasing age is also associated with reduced astrocyte number but increased activation, a reduction in pericyte number and reduced capillary density (Cerbai et al. 2012; Soto et al. 2015; Brown and Thore, 2011). Impairments in vascular reactivity have been suggested to precede the development of white matter lesions (Sam et al. 2016) and may be associated with small vessel disease (Yezhuvath et al. 2012). Age-related neurovascular dysfunction may therefore be an early pathological feature in the progression of vascular cognitive impairment, however the specific cell types that underlie such changes are still unknown. Cerebral amyloid angiopathy, a prominent feature of small vessel disease, has also been shown to impair neurovascular coupling (Han et al. 2015; Kimbrough et al. 2015), potentially mediated by reactive oxygen species (Hamel, 2015); and may exacerbate age-related vascular dysfunction. To address this, the present study sought to perform a comprehensive characterisation of the neurovascular unit and neurovascular function using in vivo MRI approaches and immunohistochemistry, and investigate the impact of ageing and amyloid accumulation using wild type and TgSwDI mice at different ages.

4.1.1 Hypothesis

This study tests the hypothesis that ageing impairs neurovascular coupling in association with reduced coverage of vessels by pericytes and astrocytic endfeet, and that age-related impairments are exacerbated in the TgSwDI mouse model of amyloid deposition.

4.1.12 Aims

The aim of the study is to assess resting cerebral blood flow, neurovascular coupling and structural integrity of the neurovascular unit in young and aged wild type and TgSwDI mice to assess the effect of age and genotype.

4.2 Methods

4.2.1 Animals

Male C57Bl/6J and heterozygous TgSwDI mice were studied at three age points: 6 months (n=7 C57Bl/6J, n=7 TgSwDI), 12 months (n=7 C57Bl/6J, n=5 TgSwDI) and 24 months (n=7 C57Bl/6J, n=9 TgSwDI). All data collection and analysis was performed blind to the age and genetic status of the mice. N numbers were chosen based on power analysis of previously collected neurovascular coupling data. In order to achieve a significance level of $p < 0.05$, a minimum group size of n=7 was required to reach a power of 0.8.

4.2.2 Magnetic resonance imaging to assess structural alterations, resting blood flow and vascular density

Magnetic resonance imaging was performed according to Methods section 2.9. Structural T2 imaging, arterial spin labelling and Q-map imaging were performed in 6 month and 24 month old mice.

4.2.3 Magnetic resonance imaging analysis

Relative CBF maps were constructed from ASL data in Matlab using in-house scripts. CBF maps were analysed in ImageJ (v1.46, NIH, Bethesda, MD, USA) using cortical and thalamic regions of interest selected from T1 maps acquired with the ASL sequence. Q-maps were generated using Matlab and Statistical Parametric Mapping 8 software (SPM8, <http://www.fil.ion.ucl.ac.uk/spm/software/spm8/>, Wellcome Trust Centre for Neuroimaging) and were analysed in ImageJ. Cortical and thalamic regions of interest were selected from T2-weighted structural scans.

4.2.4 Laser speckle imaging to assess neurovascular coupling

Following MRI, laser speckle imaging was performed according to Methods sections 2.5 to assess neurovascular coupling. Laser speckle imaging was performed in 6, 12 and 24 month old mice.

4.2.5 Tissue processing

Following laser speckle imaging, mice were transcardially perfused according to Methods section 2.10 and tissue was processed for paraffin embedding according to Methods section 2.11.1. 6µm coronal sections were collected corresponding to Bregma -1.82mm in stereotaxic mouse atlas (Paxinos and Franklin, 2001).

4.2.6 Immunohistochemistry to assess neurovascular unit structure

Immunohistochemistry using peroxidase labelling was performed according to Methods section 2.13.1. Amyloid deposition, blood vessels, microglia and the NOX subunit p47 were visualised using primary antibodies for 6E10, collagen IV, Iba1 and p47 respectively, according to concentrations listed in Table 2.2.

Immunohistochemistry with fluorescent labelling was performed according to Methods section 2.13.2. Amyloid deposition, blood vessels, pericytes, astrocytes and astrocytic endfeet were visualised using for 6E10, collagen IV, PDGFR-β, GFAP and aquaporin-4 respectively, according to concentrations listed in Table 2.2.

Images of DAB stained sections were captured on an Olympus BX51 microscope (x10, Olympus UK, Southend-on-Sea, UK); immunofluorescence images were acquired using a laser scanning confocal microscope (x20, Zeiss 780, Carl Zeiss Microscopy, Cambridge, UK). All images were analysed using ImageJ software (v1.46, NIH, Bethesda, MD, USA). Percentage area stained by 6E10, ColIV, Iba1 and p47 was used to calculate total amyloid load, vessel density, microglial density and p47 density respectively. GFAP-positive astrocytes were

manually counted. For quantification of vascular amyloid load, vascular AQP4 coverage and vascular PDGFR- β coverage, colocalisation between ColIV and either 6E10, AQP4 or PDGFR- β was calculated using Mander's coefficient. Analysis was performed in 2-6 images per region per animal.

4.2.7 Statistical analysis

Laser speckle imaging measures of vascular function and MRI measures of resting cerebral blood flow and vessel density were analysed by two way ANOVA with age and genotype as the factors. The percentage area stained by 6E10, collagen IV, Iba1 and p47, as well as Mander's coefficient of colocalisation between aquaporin-4, PDGFR- β and collagen IV, were compared using two-way ANOVA with age and genotype as the factors. Comparisons of Manders coefficients for colocalisation between young and aged TgSwDI mice was performed using Mann Whitney U test. Correlational analysis was performed using Spearman rank-order. All statistical analysis was performed using Prism GraphPad software (v5, GraphPad Software Inc, La Jolla, USA) and with $p < 0.05$.

4.3 Results

4.3.1 TgSwDI mice exhibit parenchymal and vascular amyloid deposition which is absent in wild-type mice

Amyloid deposition is thought to contribute to cerebrovascular dysfunction. In order to quantify the extent of amyloid deposition in the cortex of TgSwDI and wild-type mice, 6E10 immunohistochemistry was performed at 6 months and 24 months of age (Figure 4.1). At 6 months of age, amyloid was not detectable in TgSwDI or wild-type mice. However at 24 months, there was a marked accumulation of amyloid in the cortex of TgSwDI mice and as expected amyloid was not present in age-matched wild-type littermate controls. Overall, there was a significant effect of age and genotype ($F_{(1,29)} = 26.1$, $p < 0.0001$ and $F_{(1,29)} = 67.3$, $p < 0.0001$ respectively) and a significant interaction effect ($F_{(1,29)} = 24.9$, $p < 0.0001$). These differences were due to a significant increase in amyloid in 24 month old TgSwDI mice compared with 24 month wild type mice in which amyloid was not present ($p < 0.001$). Previously it has been shown that vascular amyloid has a pronounced effect on neurovascular coupling (Han et al. 2008). Thus, to determine the extent of vascular amyloid in TgSwDI mice, the co-localisation of amyloid to collagen IV-labelled vessels was examined in the barrel cortex (the region in which neurovascular coupling was measured) and the extent of parenchymal amyloid (i.e. amyloid outside vessels) also determined (Figure 4.2). The coverage of vascular amyloid was found to be low albeit the extent of vascular amyloid significantly increased from $0.02\% \pm 0.02$ to $0.06\% \pm 0.05$ in 6 month and 24 month TgSwDI mice respectively ($U=11$ $p < 0.05$). The percentage of cortical vessels which were found to have vascular amyloid also significantly increased with age, from $1.3\% \pm 2.5$ to $2.7\% \pm 2.4$ for 6 month vs 24 month old mice respectively ($U=12$ $p < 0.05$). The extent of parenchymal amyloid was overall much higher than vascular amyloid in the TgSwDI mice at both ages. The percentage area of parenchymal

amyloid staining significantly increased from $0.19\% \pm 0.11$ to $3.6\% \pm 0.72$ in 6 and 24 month TgSwDI mice respectively ($U=0$ $p<0.001$).

In TgSwDI mice, amyloid deposition is particularly prominent in the thalamus (Davis et al. 2004) and thus the extent of thalamic amyloid deposition was assessed in this brain region in TgSwDI mice and compared to wild-types (Figure 4.3). There were significant effects of age and genotype ($F_{(1,29)}= 294.5$, $p< 0.0001$ and $F_{(1,29)}= 300.4$, $p< 0.0001$ respectively) and a significant interaction effect ($F_{(1,29)}= 290.7$, $p< 0.0001$). Amyloid deposition was significantly increased in 24 month TgSwDI mice compared with 24 month wild type mice ($p<0.001$) whereas there was no significant difference at 6 months of age ($p>0.05$). Consistent with previous studies (Davis et al. 2004), the extent of vascular amyloid was found to be higher in the thalamus than in the cortex. Vascular amyloid also significantly increased from $0.003\% \pm 0.005$ to $0.65\% \pm 0.19$ ($U=0$ $p<0.001$) from 6 months of age to 24 months of age in TgSwDI mice (Figure 4.4). The proportion of vessels covered by amyloid also increased significantly from $0.13\% \pm 0.27$ to $28.6\% \pm 5.7$ for 6 month vs. 24 month old mice respectively ($U=0$ $p<0.001$). Again, parenchymal amyloid load was higher than vascular load in the thalamus. The percentage area of parenchymal amyloid significantly increased from $0.1\% \pm 0.2$ to $9.4\% \pm 2.8$ between 6 and 24 months ($U=0$ $p<0.001$).

4.3.2 Alterations in resting cerebral blood flow in wild-type and TgSwDI mice

In order to investigate whether ageing or amyloid deposition might affect baseline blood flow, arterial spin labelling was used to compare resting cerebral blood flow (rCBF) between groups. No significant differences in cortical blood flow were detected relative to 6 month wild type mice ($p>0.05$) (Figure 4.5). In the thalamus there were no significant effects of age or genotype, however there was a significant interaction effect ($F_{(1,29)}= 5.436$, $p<0.05$) (Figure 4.6).

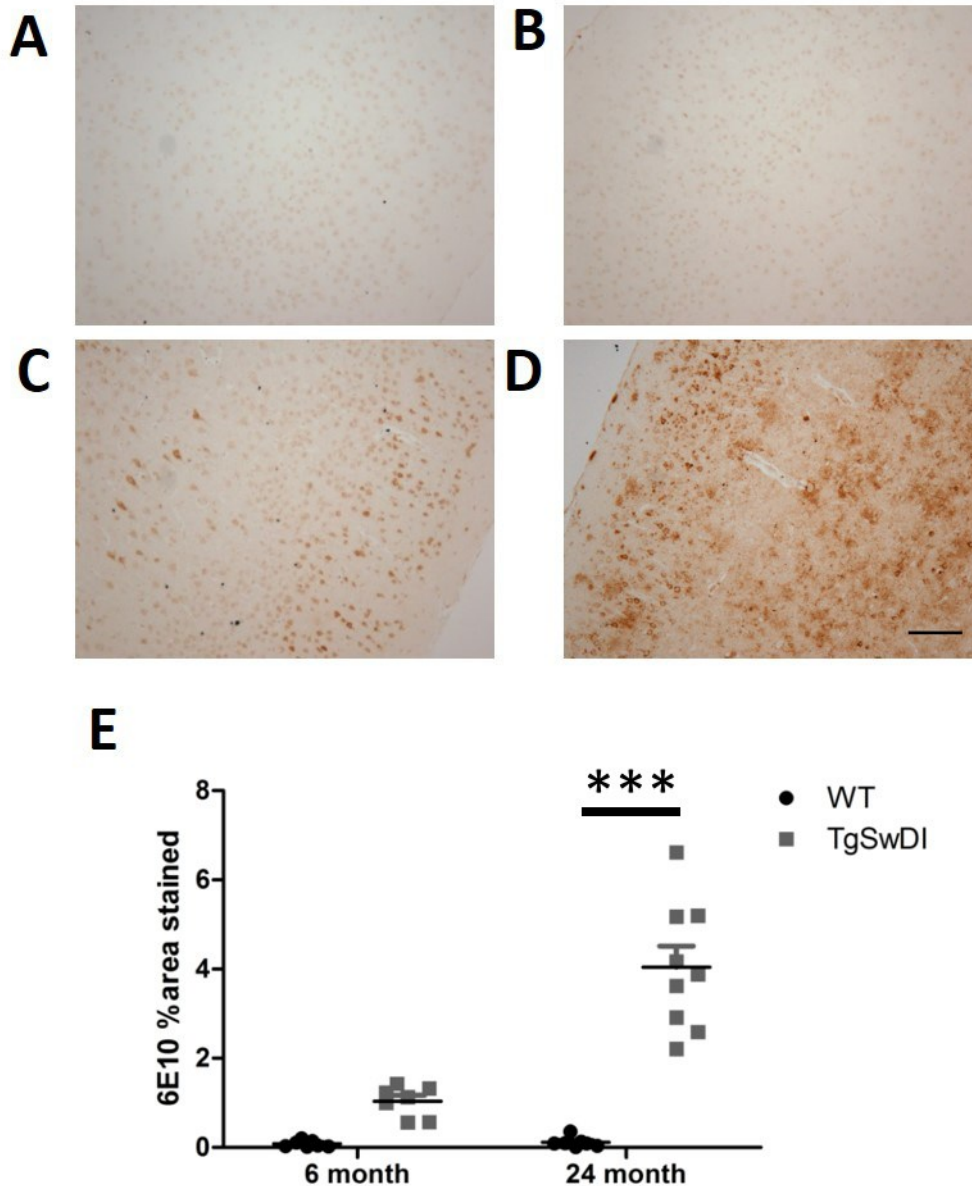


Figure 4.1 Aged TgSwDI mice develop extensive cortical amyloid deposition. Representative images of cortical 6E10 staining in (A) young wild type, (B) aged wild type, (C) young TgSwDI, and (D) aged TgSwDI mice. (E) At 24 months, TgSwDI mice display significantly increased cortical 6E10 staining compared to wild type mice, however this difference is not significant at 6 months. Scale bar= 100µm. Mean ±SEM n=7-9 per group. ***p<0.001

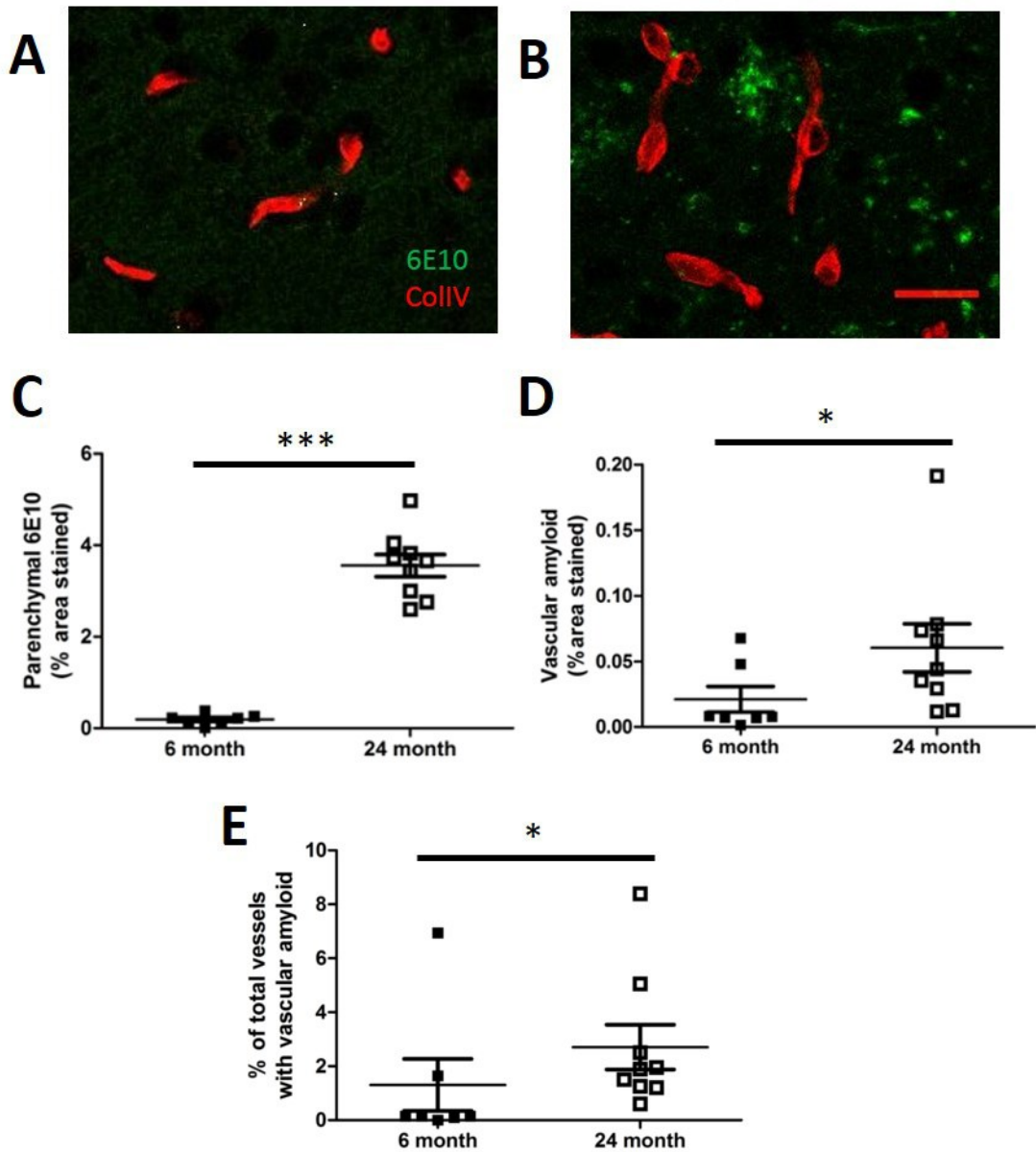


Figure 4.2 Pattern of cortical amyloid deposition in TgSwDI mice. Representative cortical images costained for 6E10 (green) and ColIV (red) in (A) young and (B) aged TgSwDI mice. (C,D) Both parenchymal and vascular amyloid are increased with age in TgSwDI mice. (E) The proportion of vessels containing vascular amyloid was increased with age in TgSwDI mice. Scale bar=20µm. Mean ±SEM n=7-9 per group. *p<0.05, ***p<0.001

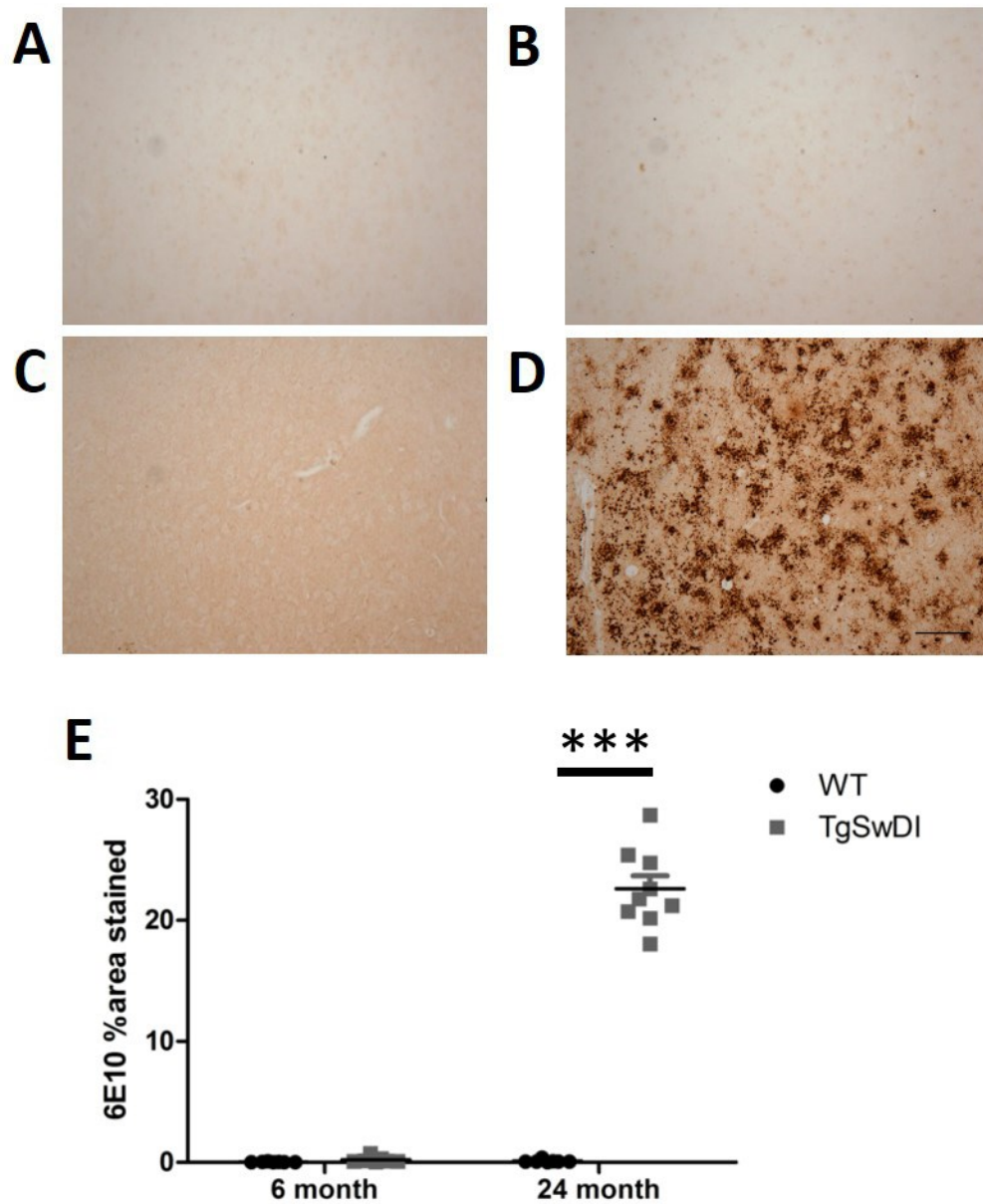


Figure 4.3 Aged TgSwDI mice develop extensive thalamic amyloid deposition. Representative images of thalamic 6E10 staining in (A) young wild type, (B) aged wild type, (C) young TgSwDI, and (D) aged TgSwDI mice. (E) At 24 months, TgSwDI mice display significantly increased cortical 6E10 staining compared to wild type mice. Scale bar= 100 μ m. Mean \pm SEM n=7-9 per group. ***p<0.001

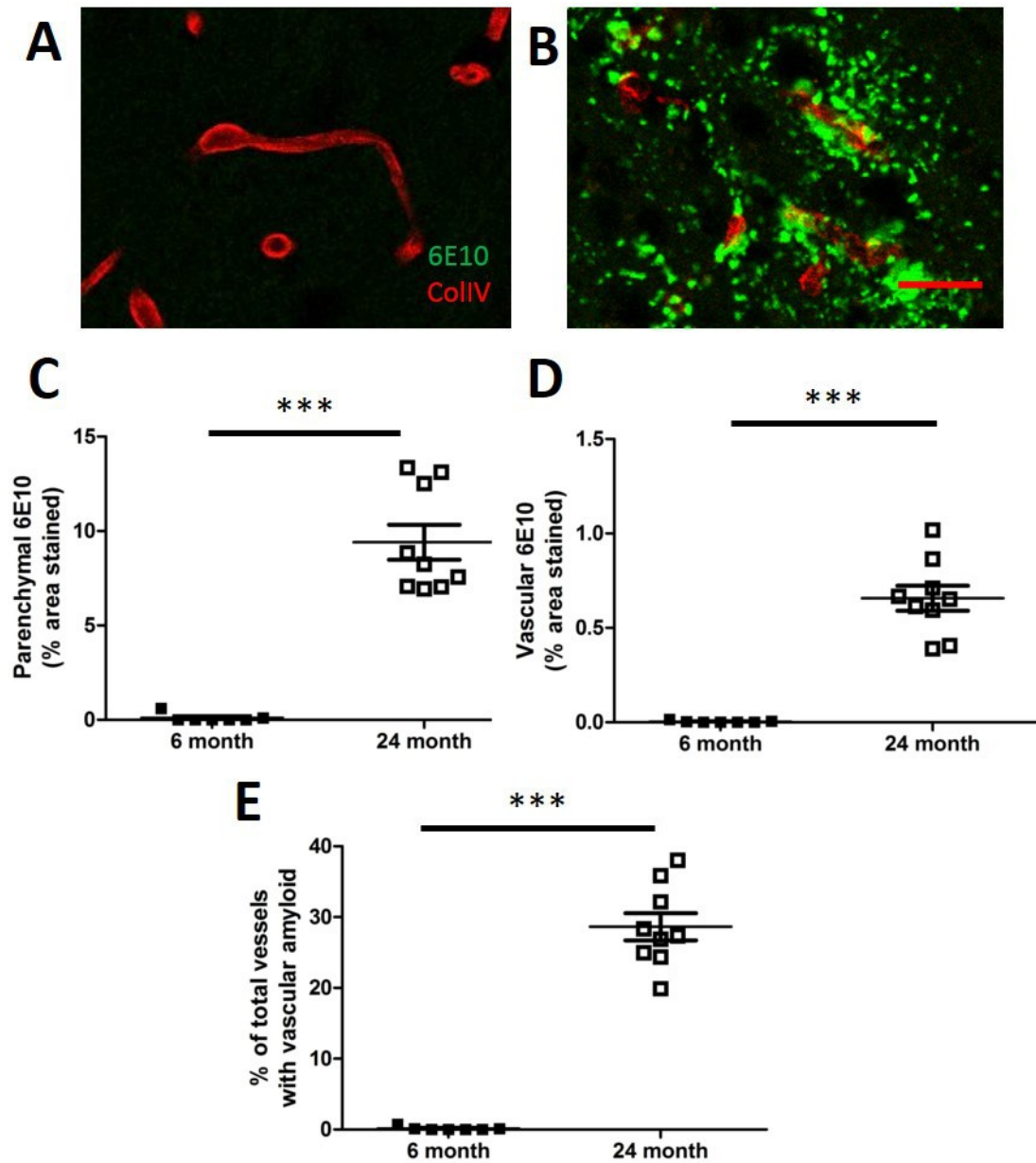


Figure 4.4 Pattern of thalamic amyloid deposition in TgSwDI mice. Representative thalamic images costained for 6E10 (green) and ColIV (red) in (A) young and (B) aged TgSwDI mice. (C,D) Both parenchymal and vascular amyloid are increased with age in TgSwDI mice. (E) The proportion of vessels containing vascular amyloid was increased with age in TgSwDI mice. Scale bar=20 μ m. Mean \pm SEM n=7-9 per group. ***p<0.001

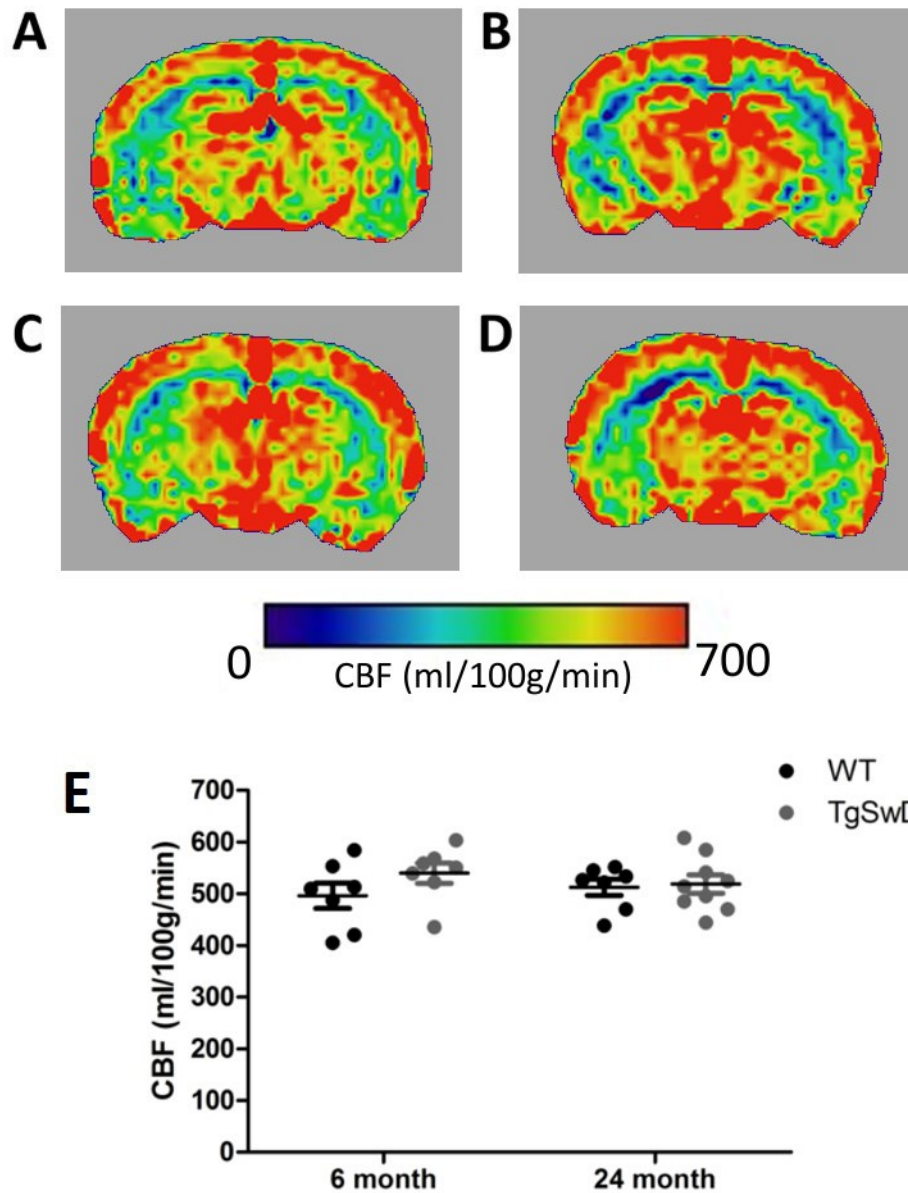


Figure 4.5 Cortical blood flow was unchanged with ageing or in TgSwDI mice. Arterial spin labelling was used to measure resting cerebral blood flow. Representative coronal ASL scans of resting blood flow from (A) young wild type, (B) aged wild type, (C) young TgSwDI, and (D) aged TgSwDI mice. (E) No significant differences in cortical resting cerebral blood flow were detected. Mean \pm SEM n=7-9 per group.

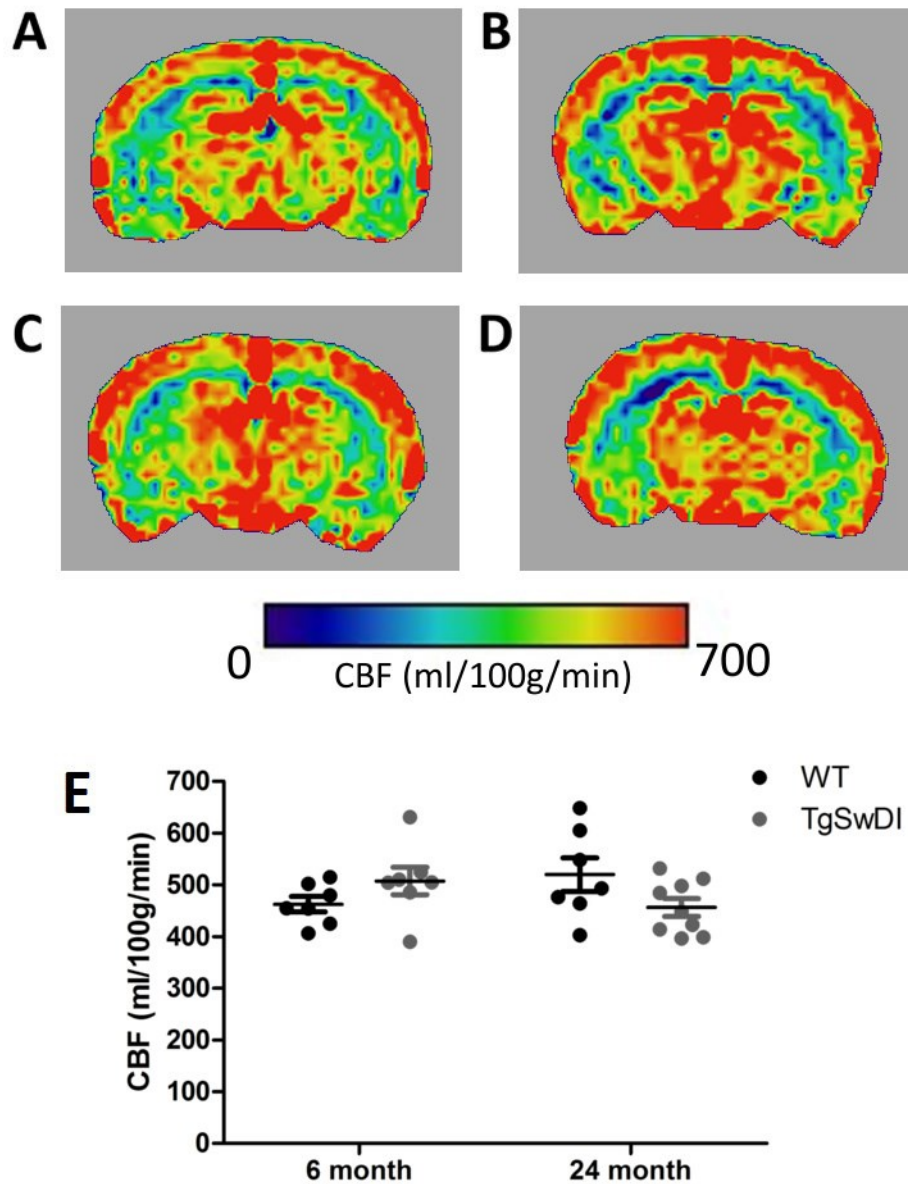


Figure 4.6 Alterations in thalamic resting blood flow. Arterial spin labelling was used to measure resting cerebral blood flow. Representative coronal ASL scans of resting blood flow from (A) young wild type, (B) aged wild type, (C) young TgSwDI, and (D) aged TgSwDI mice. (E) There was no significant effect of age or genotype on thalamic rCBF. Mean \pm SEM n=7-9 per group.

4.3.3 Alterations in vascular density in wild-type and TgSwDI mice

In order to determine if ageing or amyloid deposition would induce alterations in cerebral blood vessels, vascular density was assessed using both in vivo MRI and ex vivo immunohistochemical techniques. Q-map imaging was used to measure perfused vessel density in vivo, and collagen IV immunohistochemistry was used to measure vessel density in tissue slices. No significant differences in cortical vascular density were observed between groups with either Q-map imaging ($p>0.05$) or immunohistochemical measures ($p>0.05$) (Figure 4.7 and 4.8).

In the thalamus, collagen IV immunohistochemistry analysis revealed significant effects of age and genotype ($F_{(1,29)}= 4.416$, $p<0.05$ and $F_{(1,29)}= 7.917$, $p<0.01$ respectively), however no differences in vessel density were detected using in vivo Q-map imaging ($p>0.05$) (Figure 4.9 and 4.10).

4.3.4 CBF increases to whisker stimulation are significantly attenuated in aged wild-type and TgSwDI mice.

Laser speckle imaging was used to measure the vasodilatory response to whisker stimulation in the barrel cortex. Neurovascular coupling was significantly reduced in aged wild type and TgSwDI mice relative to young (Figure 4.11). We detected a significant effect of age ($F_{(2,38)}=14.315$, $p<0.001$) however there was no significant effect of genotype ($p>0.05$). Post hoc tests indicated that neurovascular coupling was significantly reduced in 12 and 24 month old mice relative to 6 month mice ($p<0.001$ and $p<0.001$ respectively).

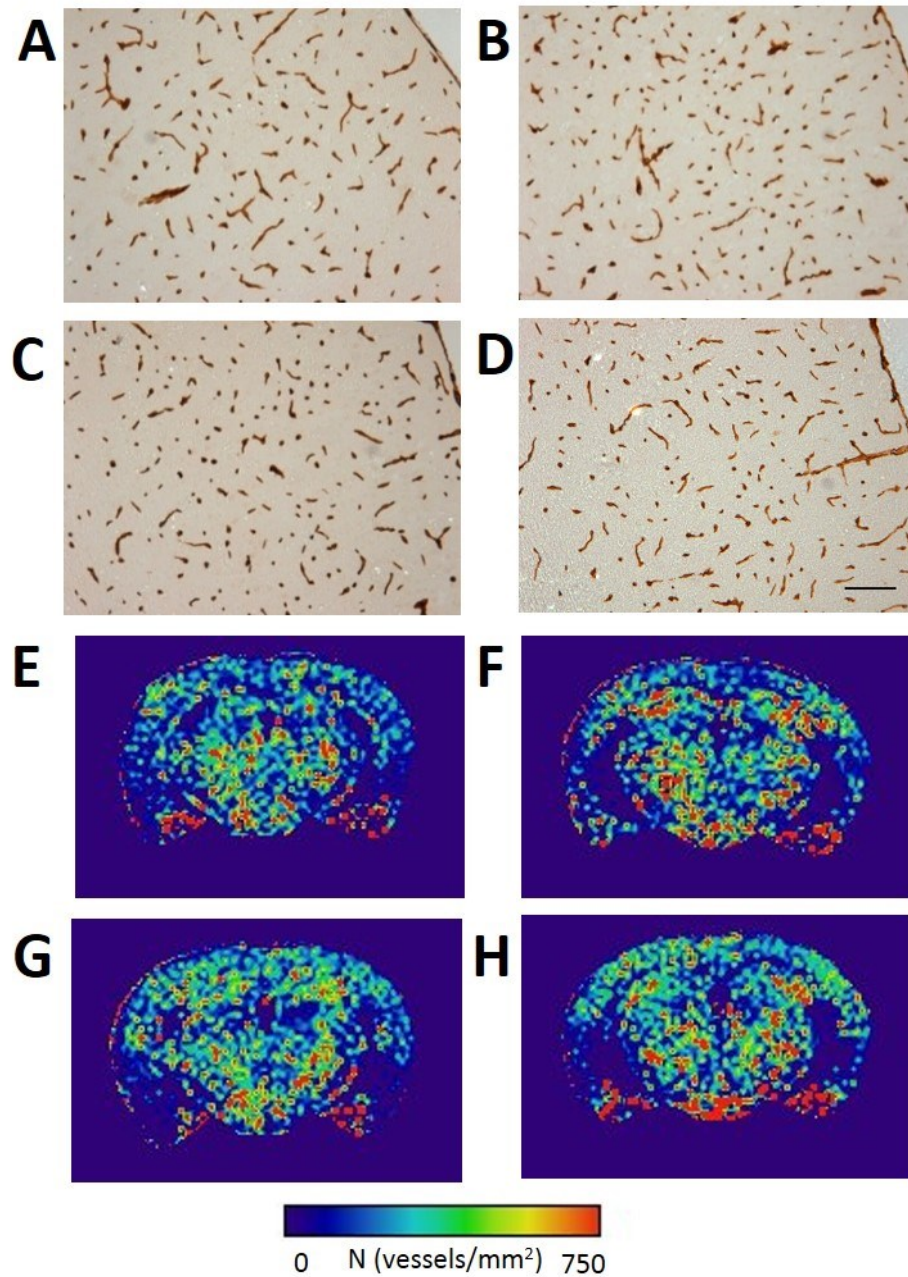


Figure 4.7 Cortical vessel density is unchanged with ageing or between wild type and transgenic mice. Vessel density was measured using two independent techniques. Representative images of collagen IV immunohistochemistry from (A) young wild type, (B) aged wild type, (C) young TgSwDI and (D) aged TgSwDI. Representative Q-map images of vessel density from (E) young wild type, (F) aged wild type, (G) young TgSwDI, and (H) aged TgSwDI. Scale bar: 100 μ m. Mean \pm SEM n=7-9 per group.

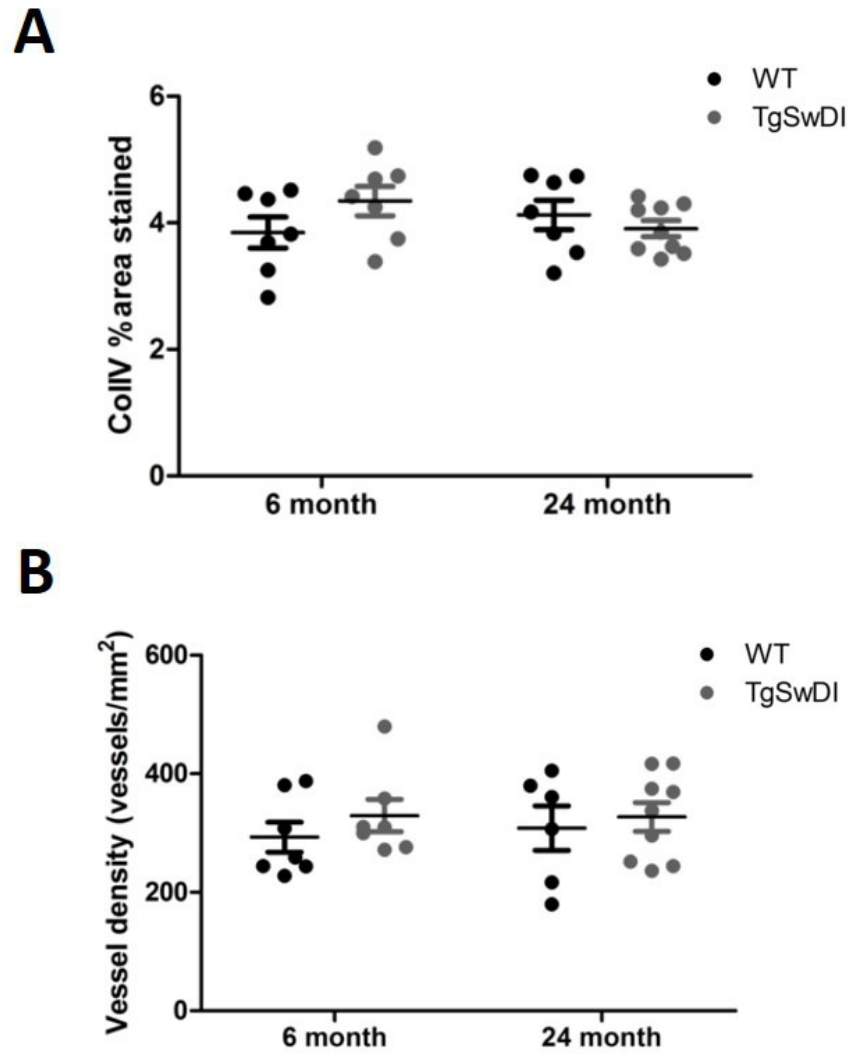


Figure 4.8 Cortical vessel density is unchanged with ageing or between wild type and transgenic mice. Vessel density was measured using two independent techniques. Neither collagen immunohistochemistry (**A**) nor in vivo Q-map imaging (**B**) detected a difference in cortical vessel density between groups. Mean \pm SEM n=7-9 per group.

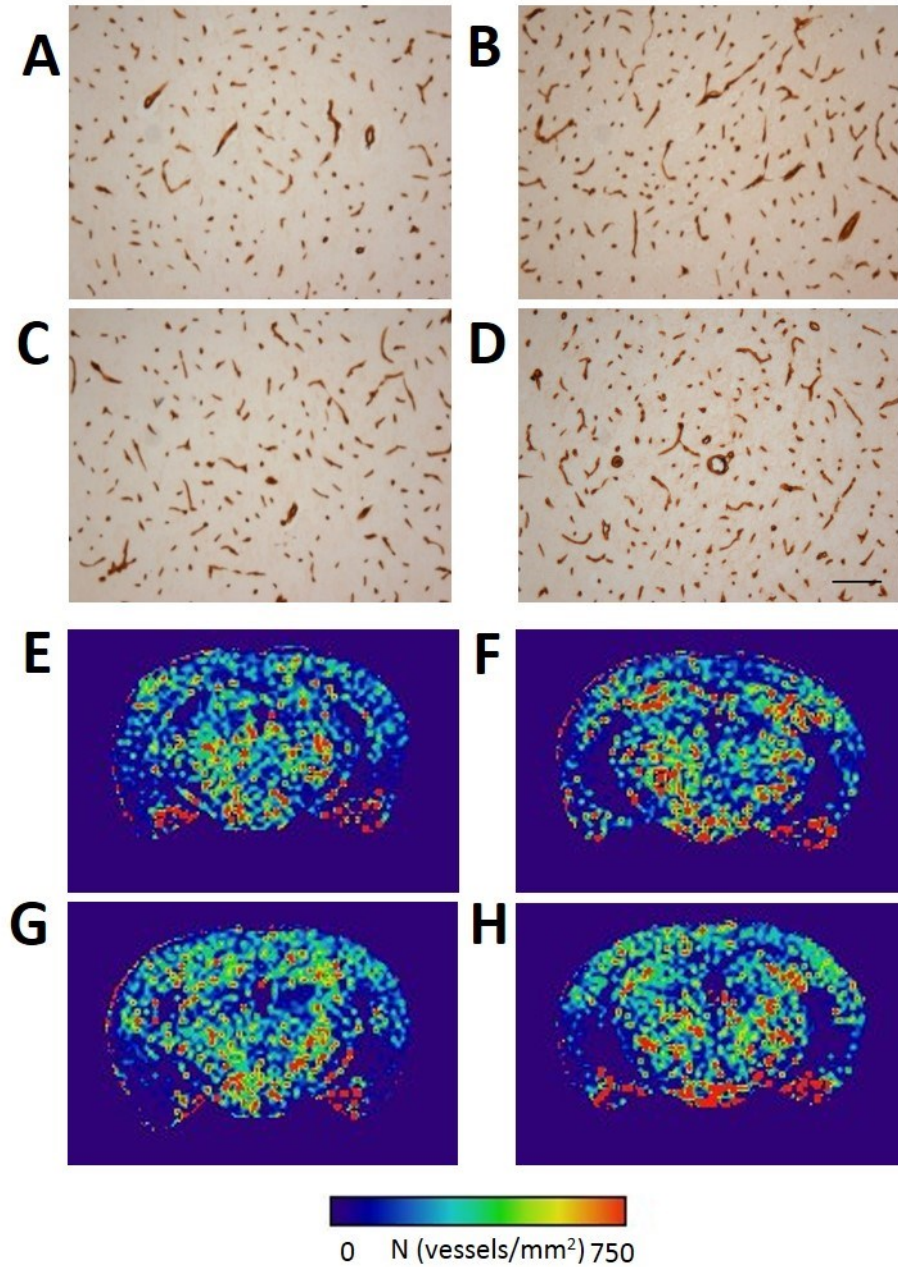


Figure 4.9 Thalamic vessel density is increased with age and in TgSwDI mice. Vessel density was measured using two independent techniques. Representative images of collagen immunohistochemistry from (A) young wild type, (B) aged wild type, (C) young TgSwDI, and (D) aged TgSwDI mice. Representative Q-map images from (E) young wild type, (F) aged wild type, (G) young TgSwDI, and (H) aged TgSwDI mice. Scale bar= 100 μ m

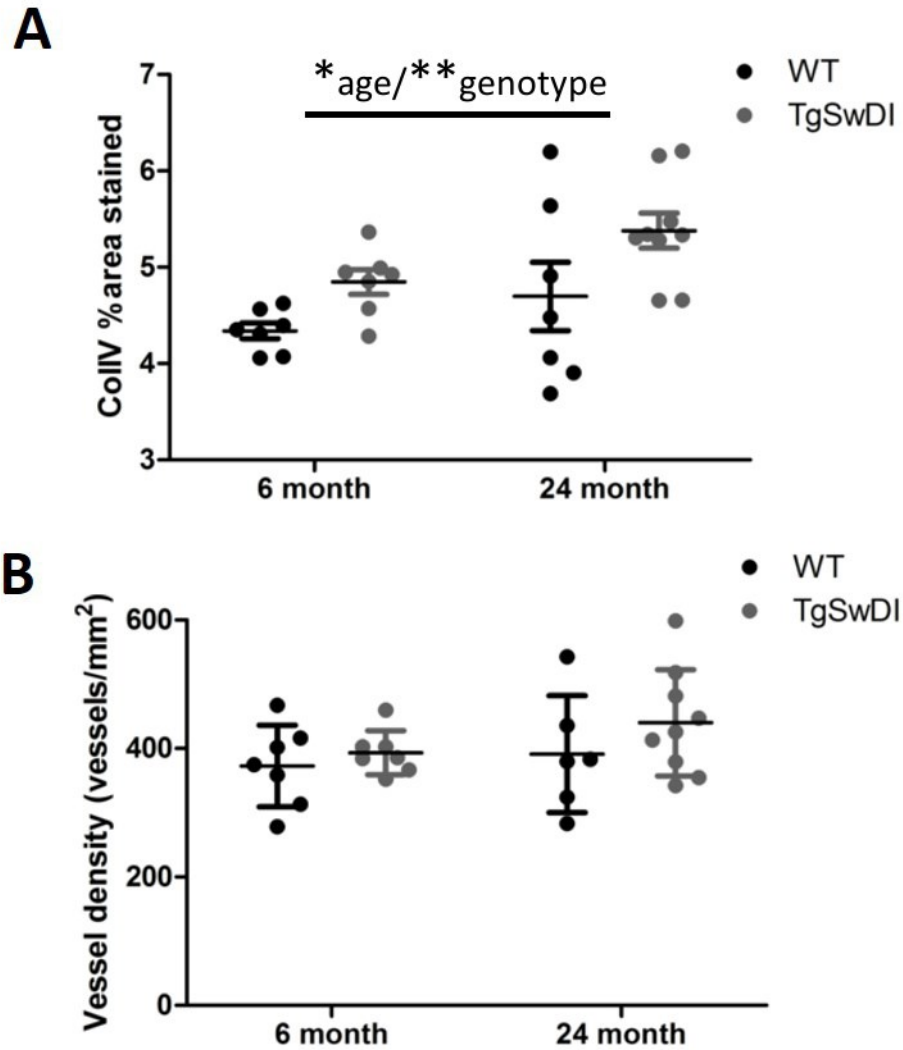


Figure 4.10 Thalamic vessel density is increased with age and in TgSwDI mice. Vessel density was measured using collagen IV immunohistochemistry and Q-map imaging. **(A)** Collagen IV immunohistochemistry detected a significant increase in thalamic vessel density in aged mice compared to young, and in TgSwDI mice compared to wild type. **(B)** In vivo Q-map imaging did not detect a difference in thalamic vessel density between groups. Mean \pm SEM n=7-9 per group. *p<0.05 **p<0.01.

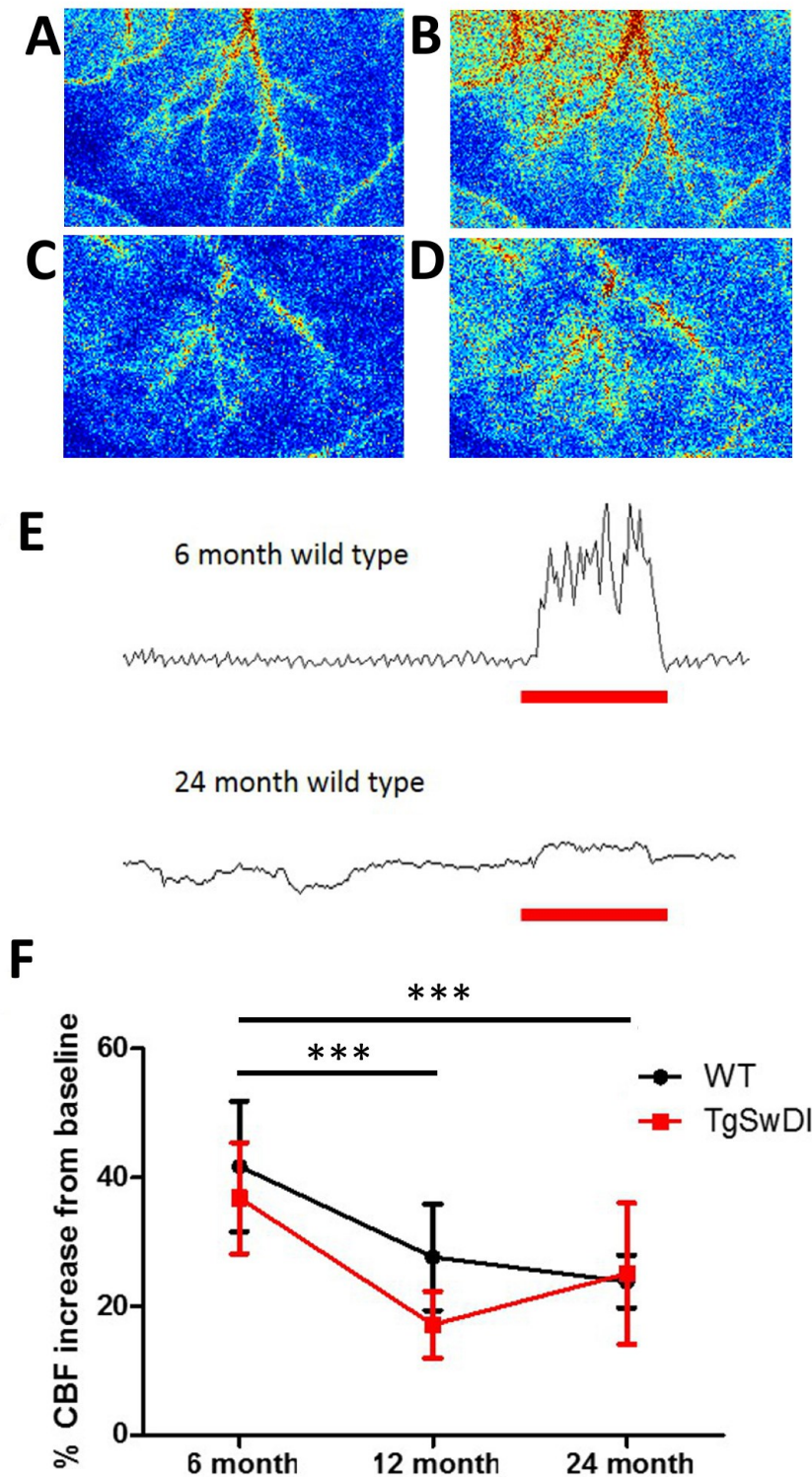
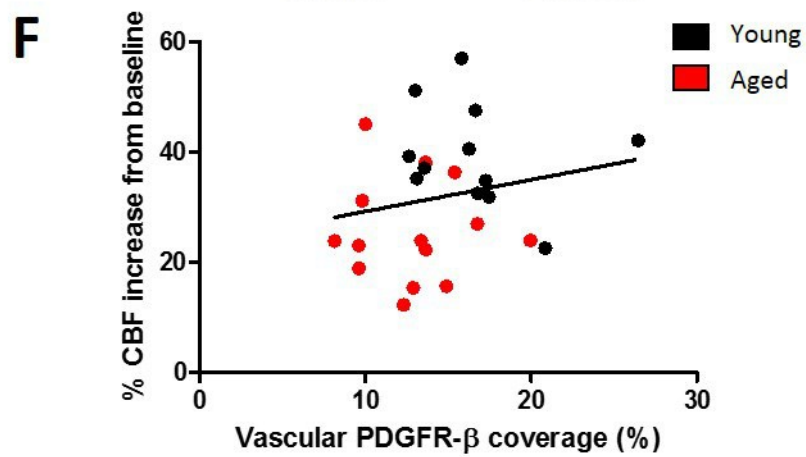
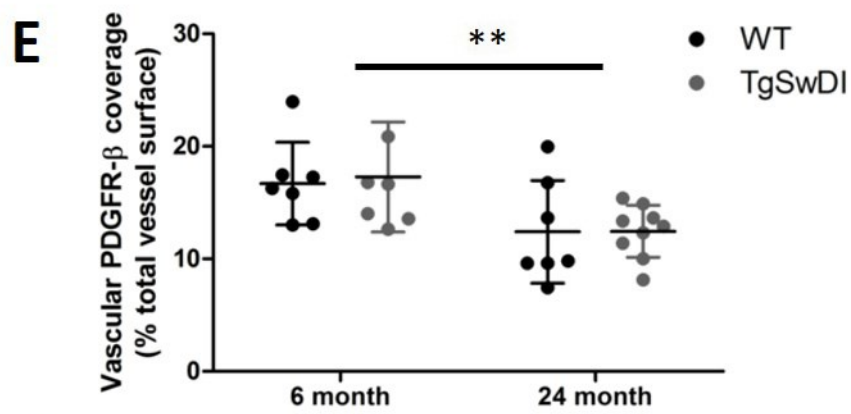
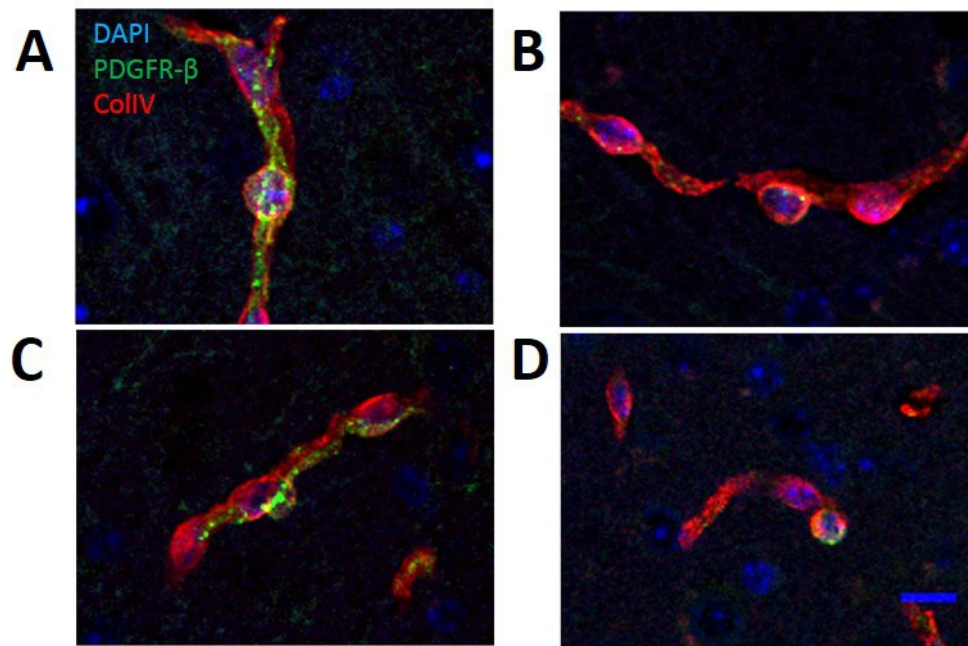


Figure 4.11 Vascular response to whisker stimulation is significantly impaired in aged mice. Representative laser speckle images from 6 month (A, B) and 24 month old (C, D) mice during baseline (A, C) and whisker stimulation (B, D). (E) shows representative traces from young and aged wild type mice. Whisker stimulation (red bar) elicits an increase in cerebral blood flow. (F) Vascular function is significantly impaired in aged mice compared to young mice, however there was no significant effect of transgene. Mean \pm SEM n=7-9 per group.

4.3.5 Reduced pericyte coverage of blood vessels in aged mice

Pericytes have been suggested to regulate cortical blood flow in capillaries (Hall et al. 2014), therefore we sought to determine whether changes in vascular pericyte coverage may underlie age-related reductions in neurovascular coupling. The extent to which cortical blood vessels are contacted by pericyte processes was assessed using co-localisation analysis of PDGFR- β , as a marker of pericytes, with collagen IV-labelled vessels. As predicted, aged mice displayed significantly reduced vascular pericyte coverage compared to young mice ($F_{(1,29)} = 10.21$, $p < 0.01$) but there were no significant genotype or interaction effects (Figure 4.12). Furthermore, vascular pericyte coverage was unrelated to the extent of neurovascular coupling ($r = 0.28$; $p > 0.05$).

In the thalamus, vascular pericyte coverage analysis revealed a significant age effect ($F_{(1,29)} = 13.05$, $p < 0.01$) with aged mice displaying reduced vascular pericyte coverage compared to young, but there was no effect of genotype (Figure 4.13).



◀ **Figure 4.12 Coverage of cortical vessels by PDGFR- β is significantly reduced in aged mice compared to young.** Representative cortical images of PDGFR- β (green) and collagen IV (red) from (A) young wild type, (B) aged wild type, (C) young TgSwDI, (D) aged TgSwDI. (E) Aged mice have significantly less vascular PDGFR- β coverage compared to young mice, however there were no differences between genotype. (F) Vascular PDGFR- β coverage does not correlate with vascular function ($p>0.05$). Scale bar= 10 μ m. Mean \pm SEM n=7-9 per group. ** $p<0.001$

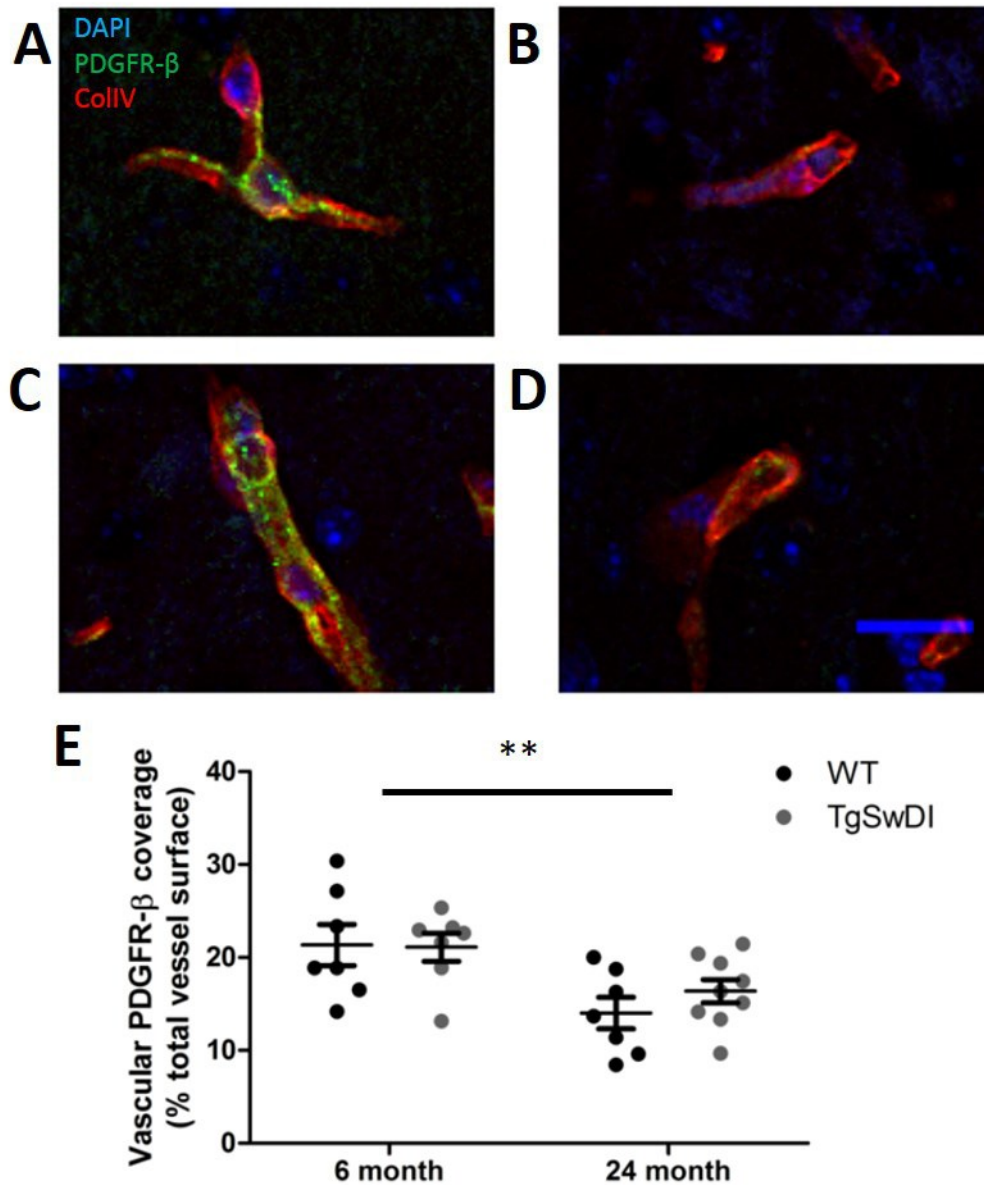


Figure 4.13 Vascular pericyte coverage in the thalamus is significantly reduced in aged mice. Representative thalamic images of PDGFR-β (green) and collagen IV (red) from (A) young wild type, (B) aged wild type, (C) young TgSwDI, (D) aged TgSwDI. (E) Aged mice have significantly less vascular PDGFR-β coverage compared to young mice, however there were no differences between genotype at either age. Scale bar= 20μm. Mean ±SEM n=7-9 per group. **p<0.01.

4.3.6 Reduced coverage of blood vessels by astrocytic endfeet AQP4 in aged mice

Neurovascular coupling is suggested to be mediated, in part, by contact between astrocytic endfeet and cerebral blood vessels (Bazargani and Attwell, 2016). To investigate whether alterations in neurovascular unit structure might underlie impairments in vascular function, the integrity of this contact was assessed using aquaporin-4 as a marker of astrocytic endfeet and the extent co-localised to vessels determined. Significant effects of age and genotype were detected, with aged mice displaying a significant reduction in astrocytic end-feet expression of AQP4 on cortical blood vessels compared to young mice ($F_{(1,29)} = 27.85$, $p < 0.0001$), and greater vascular AQP4 coverage in TgSwDI compared to wild type mice ($F_{(1,29)} = 13.41$, $p = 0.001$) (Figure 4.14). Interestingly, there was a significant positive correlation between neurovascular coupling and AQP4 localisation on cortical blood vessels ($r = 0.45$, $p = 0.01$). Having identified alterations in the contact between astrocytes and blood vessels, we also sought to determine if the number of GFAP+ve astrocytes was altered with age or amyloid deposition. Analysis of GFAP-positive astrocytes revealed significant effects of age and genotype ($F_{(1,29)} = 36.78$, $p < 0.0001$ and $F_{(1,29)} = 27.14$, $p < 0.0001$ respectively) and also a significant interaction effect ($F_{(1,29)} = 28.27$, $p < 0.0001$) (Figure 4.15). Aged TgSwDI mice had a significantly greater number of GFAP+ve astrocytes compared to aged wild type mice ($p < 0.001$).

The reduction with age in astrocytic end-feet expression of AQP4 on blood vessels was also found in the thalamus ($F_{(1,29)} = 33.78$, $p < 0.0001$), however there was no genotype effect (Figure 4.16). Additionally, a pronounced increase in parenchymal AQP4 expression in TgSwDI mice was noted. Analysis of parenchymal AQP4 expression revealed significant effects of age and genotype ($F_{(1,29)} = 78.24$, $p < 0.0001$ and $F_{(1,29)} = 27.81$, $p < 0.0001$ respectively) as well as a significant interaction effect ($F_{(1,29)} = 45.07$, $p < 0.0001$), whereby aged TgSwDI mice displayed

a significant increase in parenchymal AQP4 compared to aged wild type mice ($p < 0.001$). Similarly to cortical measures, there were significant effects of age and genotype on number of GFAP+ve astrocytes in the thalamus ($F_{(1,29)} = 339.8$, $p < 0.0001$ and $F_{(1,29)} = 184.2$, $p < 0.0001$ respectively) and also a significant interaction effect ($F_{(1,29)} = 168.6$, $p < 0.0001$) (Figure 4.17). Aged TgSwDI mice had significantly more GFAP-positive astrocytes compared to aged wild type mice ($p < 0.001$).

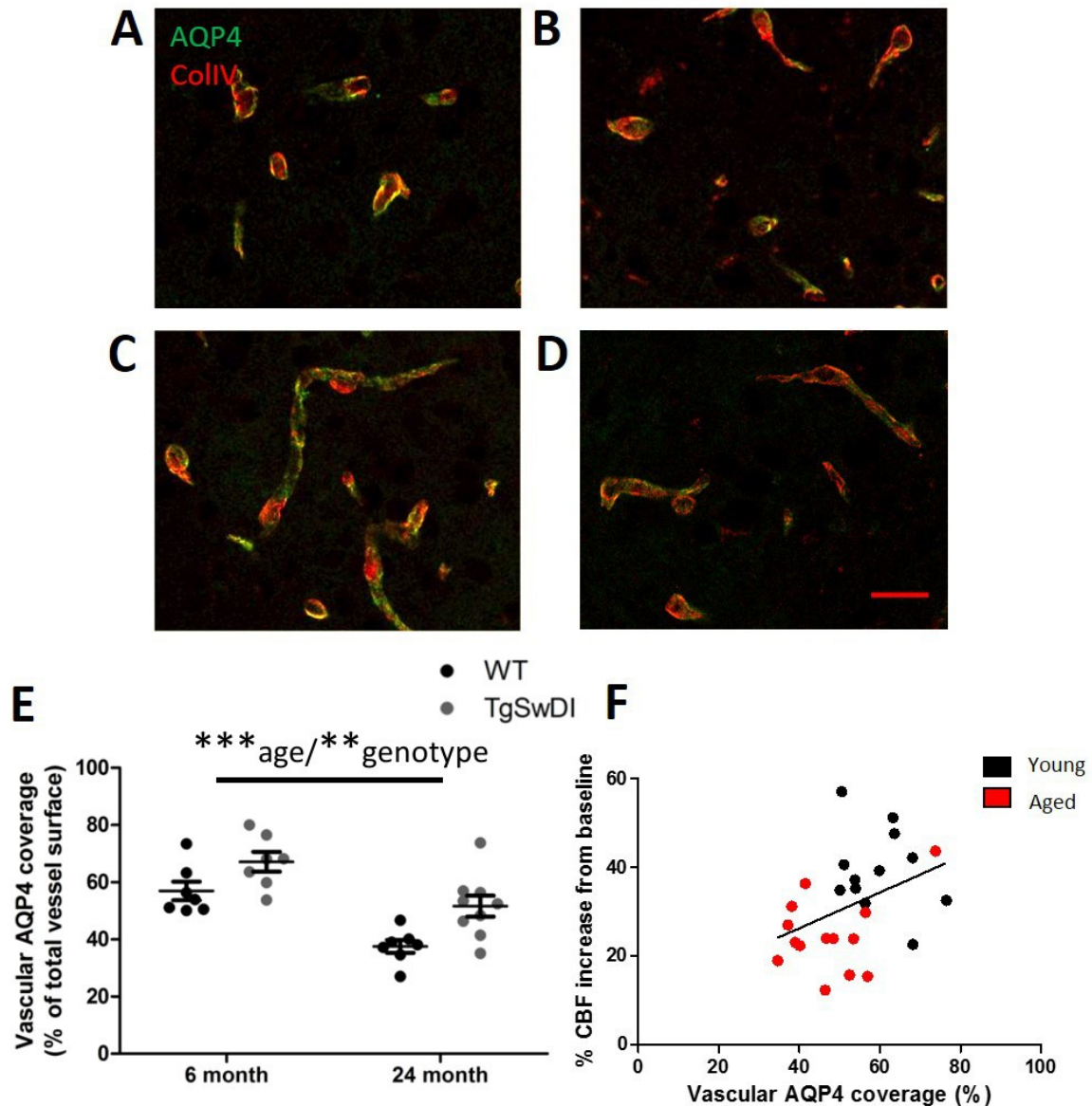


Figure 4.14 AQP4 expression on cortical blood vessels is significantly reduced in aged mice compared to young. (A) Representative cortical images of aquaporin-4 (AQP4) (green) and collagen IV (red) from (A) young wild type, (B) aged wild type, (C) young TgSwDI, and (D) aged TgSwDI. (E) Vascular coverage by AQP4 was assessed using Mander's coefficient. Aged mice have significantly reduced expression of AQP4 on cortical blood vessels compared to young mice, while TgSwDI mice have increased vascular AQP4 compared to wild type mice. (F) There was a significant correlation between vascular coverage by AQP4 and vascular function. Scale bar=20 μ m. Mean \pm SEM n=7-9 per group. **p=0.001, ***p<0.0001.

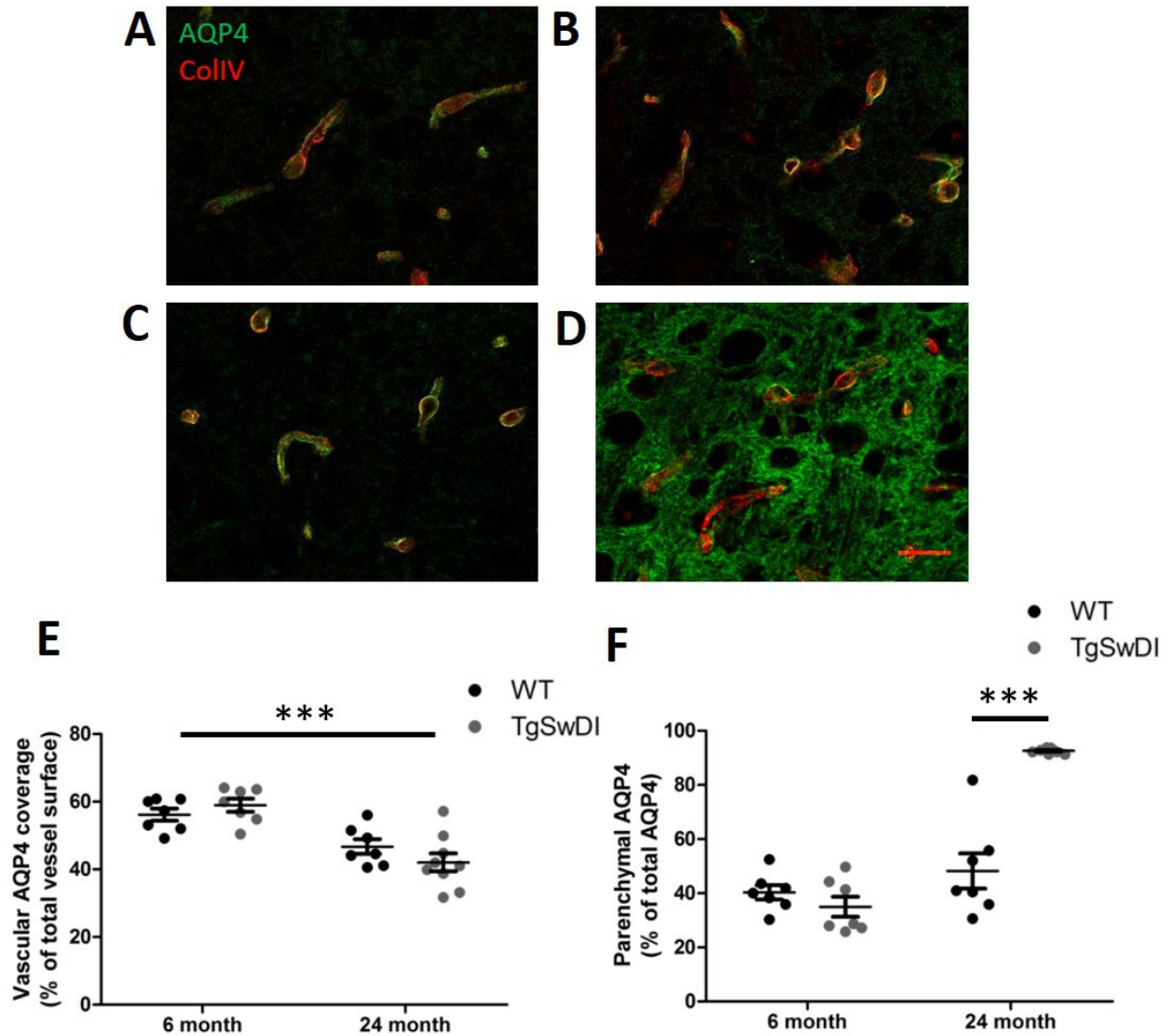


Figure 4.16 AQP4 expression on thalamic blood vessels is significantly reduced in aged mice compared to young. (A) Representative thalamic images of aquaporin-4 (AQP4) (green) and collagen IV (red) from (A) young wild type, (B) aged wild type, (C) young TgSwDI, and (D) aged TgSwDI. (E) Vascular coverage by AQP4 was assessed using Mander's coefficient. Aged mice have significantly reduced expression of AQP4 on thalamic blood vessels compared to young mice. (F) Parenchymal AQP4 expression is increased in aged TgSwDI mice. Scale bar= 20 μ m. Mean \pm SEM n=7-9 per group. ***p<0.0001.

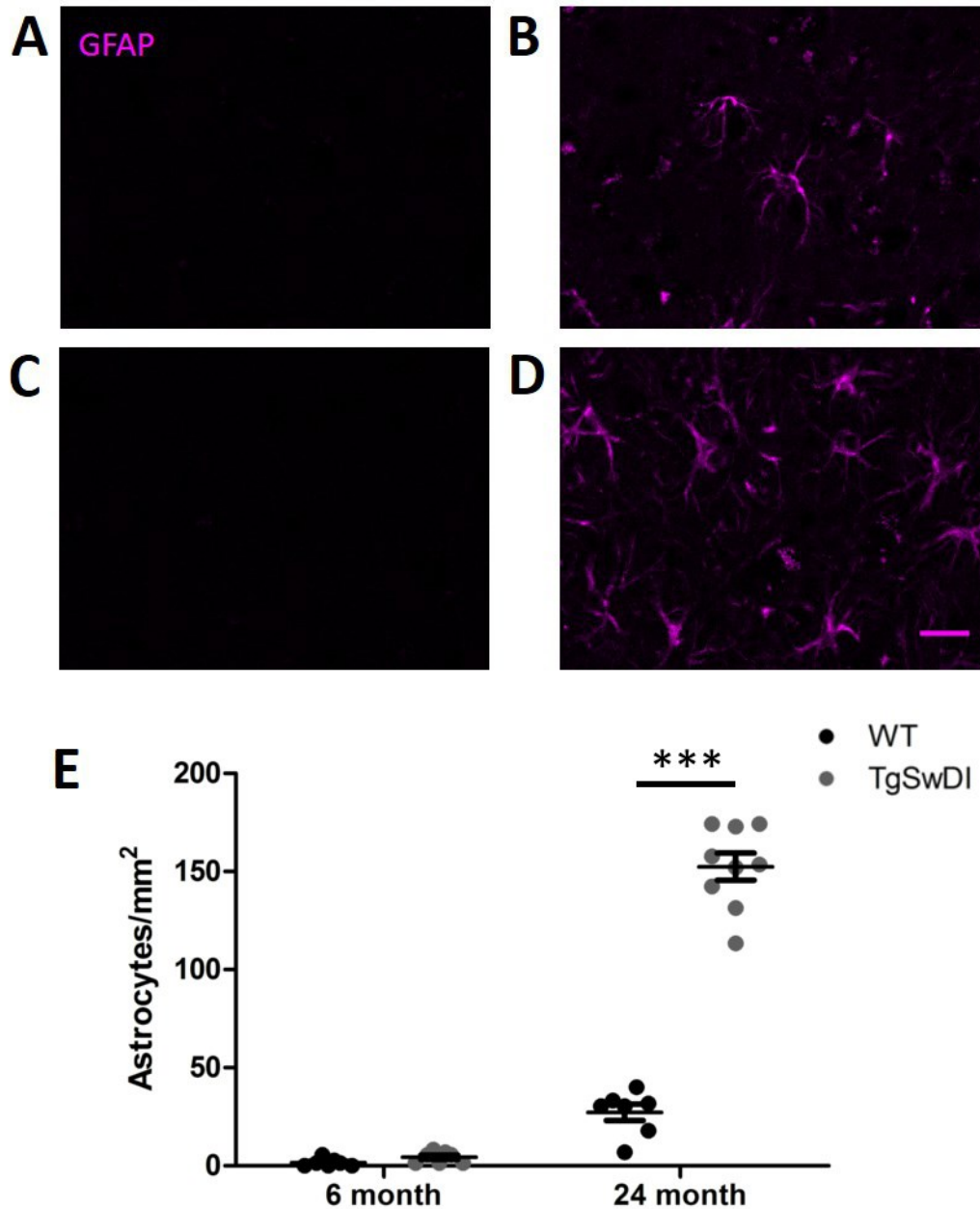


Figure 4.17 GFAP+ve astrocytes are increased in thalamus of aged mice and exacerbated in TgSwDI. Representative images of thalamic GFAP+ve astrocytes from (A) young wild type, (B) aged wild type, (C) young TgSwDI, and (D) aged TgSwDI. (E) Astrocytic activation was significantly increased in aged mice compared to young, and aged TgSwDI mice had significantly more astrocytes compared to aged wild type mice. Mean \pm SEM n=7-9 per group. ***p<0.001. Scale bar= 20 μ m.

4.3.7 Microglial activation/number is increased with ageing and exacerbated in TgSwDI mice

Following on from the demonstration that alterations in GFAP+ve astrocytes are associated with reduced vascular function, we sought to identify whether alterations in microglia may also be related to changes in neurovascular coupling. Quantification of Iba1-positive microglia was performed in the barrel cortex in adjacent sections to those used to identify astrocytic end feet processes. Significant effects of age and genotype were detected, with significantly greater Iba1 staining in aged mice compared to young ($F(1,29)= 17.97$, $p<0.001$), and in TgSwDI mice compared to wild type ($F(1,29)= 13.88$, $p<0.001$) (Figure 4.18). Further, the extent of Iba1+ve staining correlated significantly with the extent of neurovascular coupling ($r= -0.55$, $p<0.01$). In the thalamus, quantification of Iba1-positive microglia revealed significant effects of age and genotype ($F(1,29)= 133.9$, $p<0.0001$ and $F(1,29)= 82.57$, $p<0.0001$ respectively) and also a significant interaction effect ($F(1,29)= 48.09$, $p<0.0001$) (Figure 4.19). Iba-1+ve microglia density was significantly increased in aged TgSwDI mice compared to aged wild type mice ($p<0.001$) but there was no difference in microglial density between young mice.

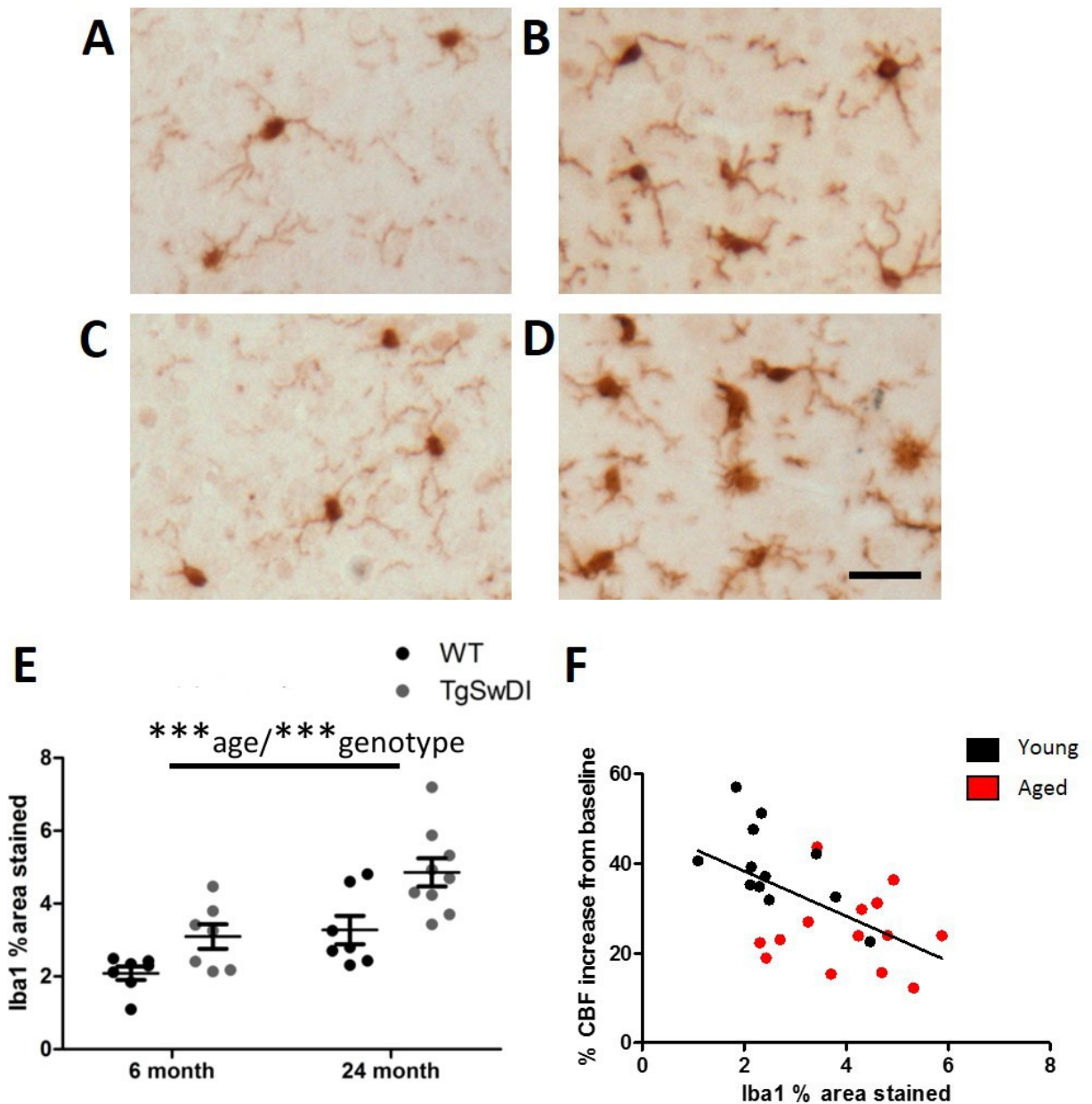


Figure 4.18 Cortical microglial activation is enhanced in aged mice and exacerbated in TgSwDI. Representative images of cortical Iba+ve microglia from (A) young wild type, (B) aged wild type, (C) young TgSwDI, and (D) aged TgSwDI. (E) Percentage area of Iba1 was significantly increased in aged mice compared to young, and further increased in aged TgSwDI compared to aged wild type mice. (F) Iba+ve microglia were negatively correlated with vascular function. Scale bar= 30 μ m. Mean \pm SEM n=7-9 per group. ***p<0.001.

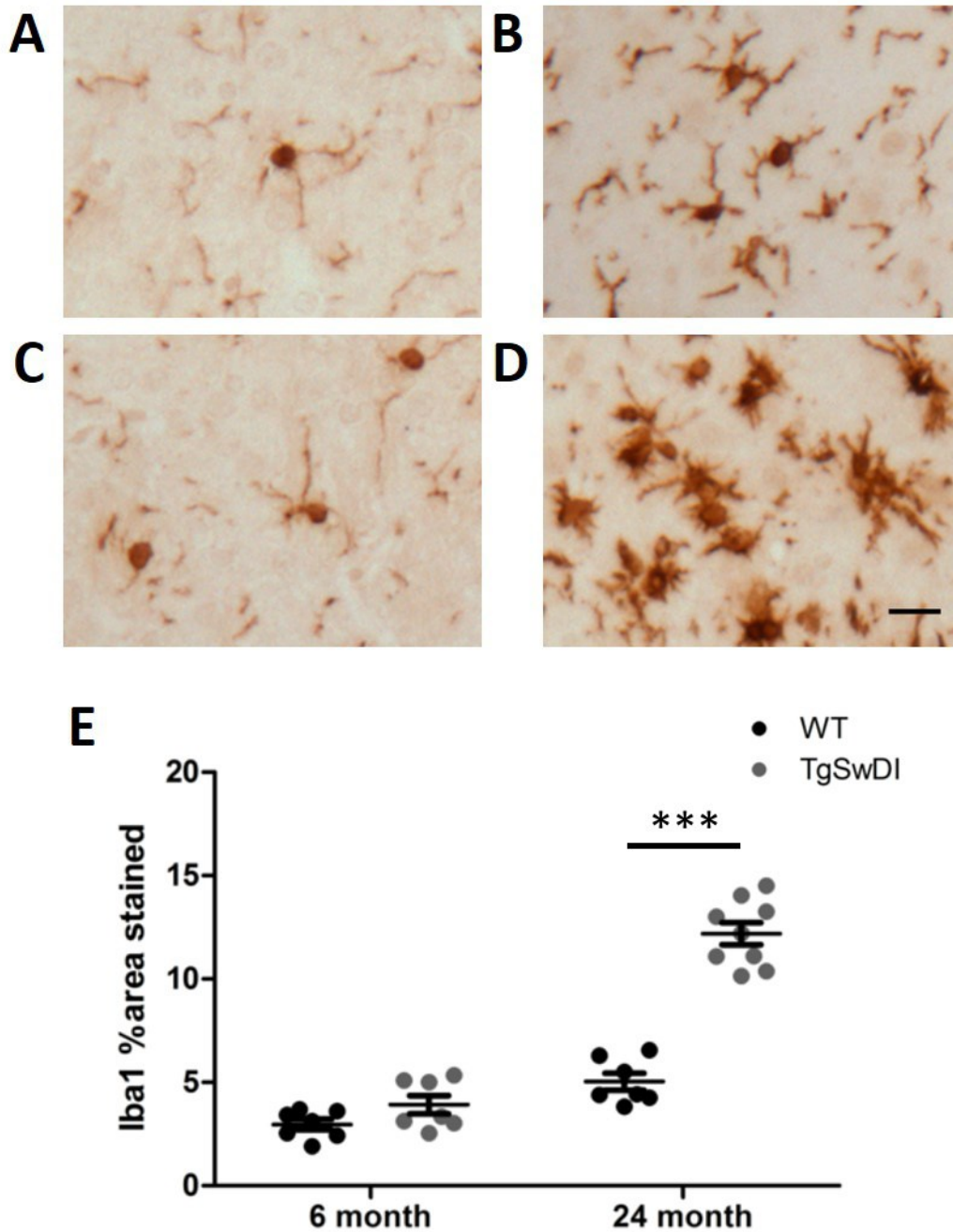


Figure 4.19 Thalamic microglial activation is enhanced in aged mice and exacerbated in TgSwDI. Representative images of thalamic Iba+ve microglia from (A) young wild type, (B) aged wild type, (C) young TgSwDI, and (D) aged TgSwDI. (E) Percentage area of Iba1 was significantly increased in aged mice compared to young, and further increased in aged TgSwDI compared to aged wild type mice. Scale bar= 20 μ m. Mean \pm SEM n=7-9 per group. ***p<0.001.

4.3.8 Alterations in expression of p47 subunit of NADPH oxidase 2

To further probe the mechanisms by which age may contribute to impaired neurovascular coupling we quantified immunostaining for p47, a subunit of the NADPH oxidase 2 (NOX2). This is a major contributor to reactive oxygen species, is highly expressed by glia (Bedard and Krause, 2007) and has been shown to become highly activated in response to amyloid (Han et al. 2015). In the cortex, there was a significant increase in NOX2 with age ($F_{(1,29)} = 6.906$, $p < 0.05$) but no effect of genotype and no interaction (Figure 4.20).

In the thalamus, there were significant effects of age and genotype ($F_{(1,29)} = 39.71$, $p < 0.001$ and $F_{(1,29)} = 19.4$, $p < 0.001$) respectively) and also a significant interaction effect ($F_{(1,29)} = 12.7$, $p < 0.01$) (Figure 4.21). Aged TgSwDI mice had significantly increased p47 expression compared to aged wild type mice ($p < 0.001$) consistent with more pronounced amyloid deposition in this brain region.

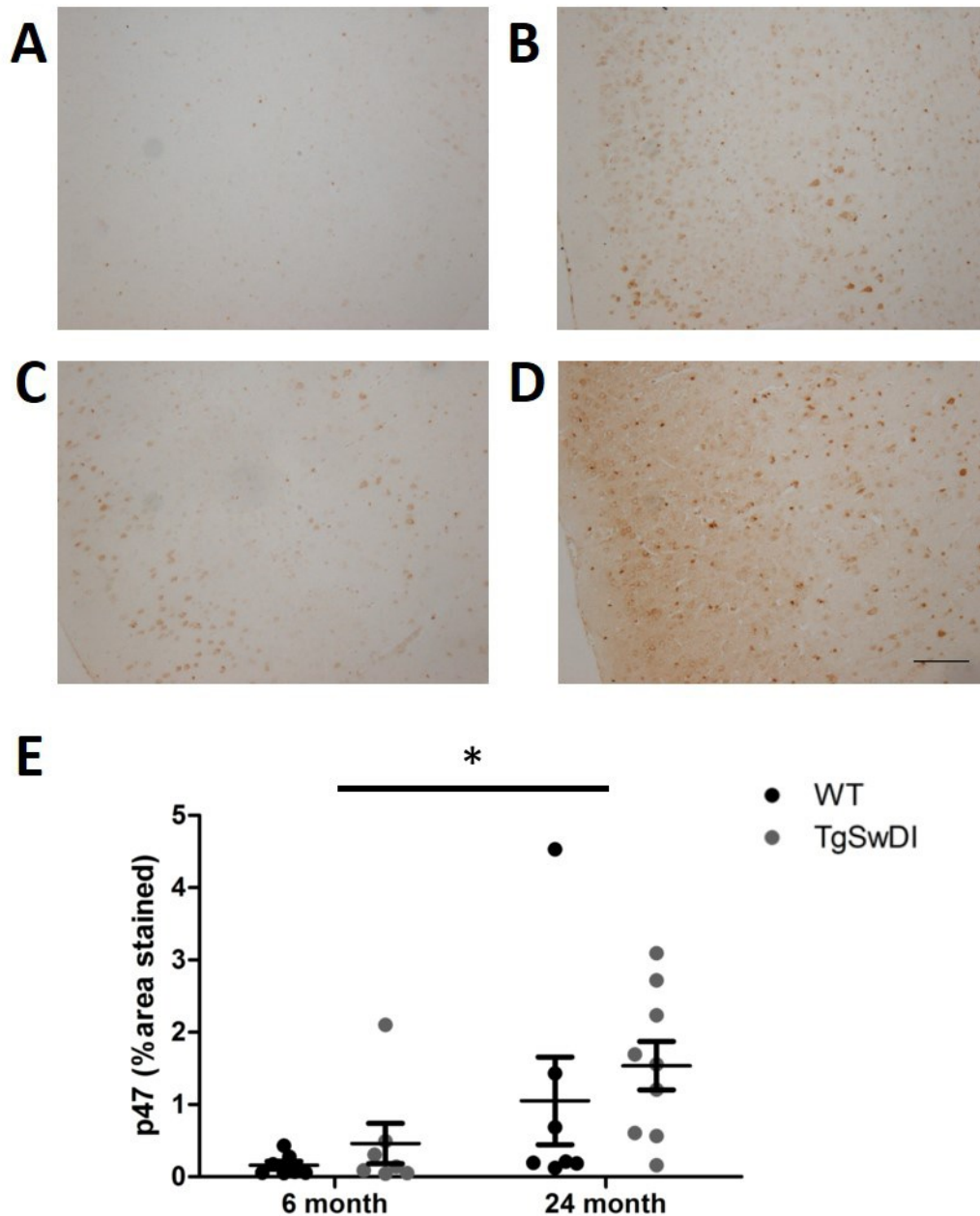


Figure 4.20 Cortical p47 expression is increased in aged mice compared to young. Representative images of cortical p47 staining from (A) young wild type, (B) aged wild type, (C) young TgSwDI, and (D) aged TgSwDI. (E) Aged mice display significantly increased cortical p47 expression compared to young mice, however there were no differences between wild type and TgSwDI mice. Scale bar= 100 μ m. Mean \pm SEM n=7-9 per group. *p<0.05.

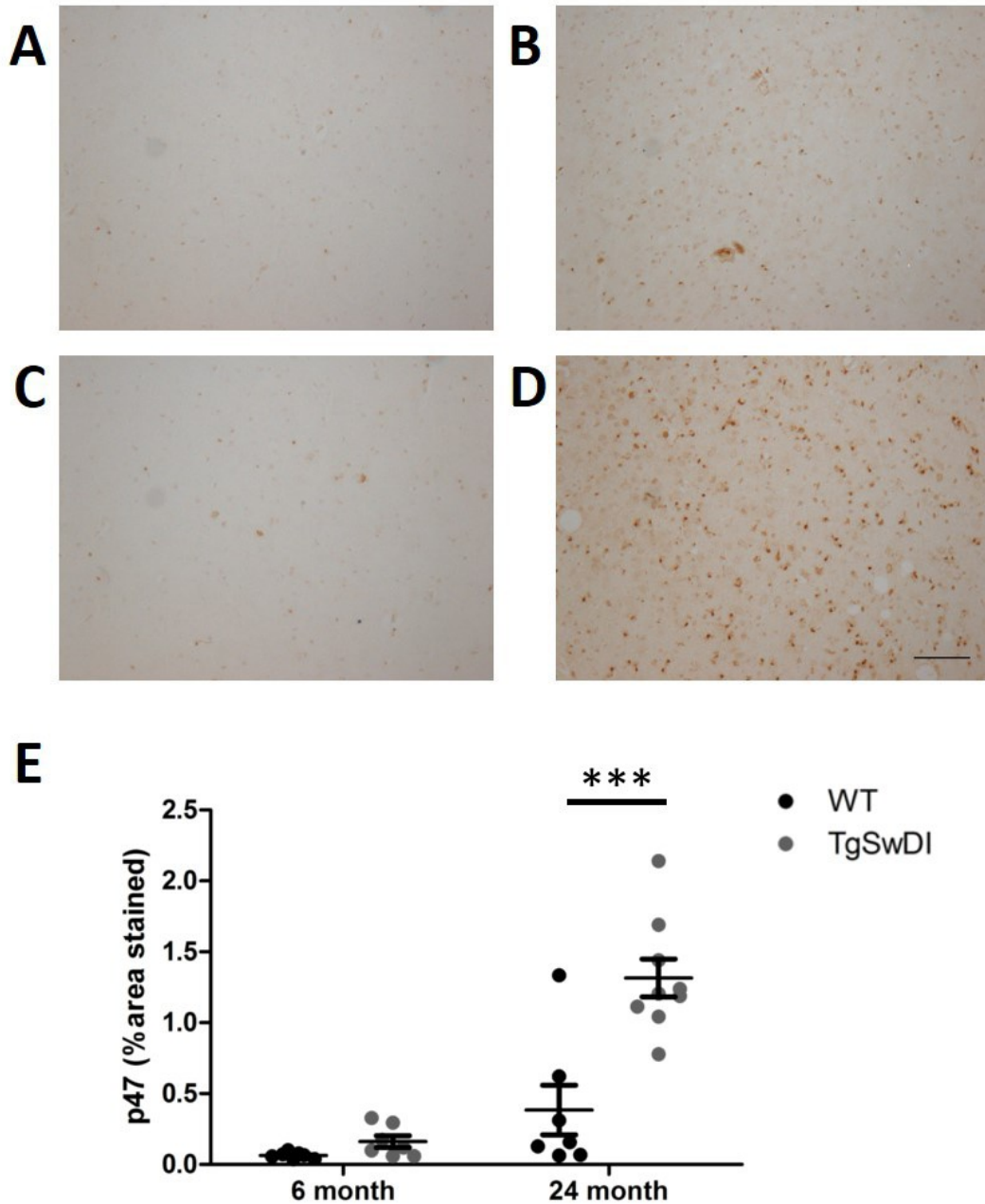


Figure 4.21 Thalamic p47 expression is increased in aged mice and exacerbated in TgSwDI. Representative images of thalamic p47 staining from (A) young wild type, (B) aged wild type, (C) young TgSwDI, and (D) aged TgSwDI. (E) Aged mice display significantly increased thalamic p47 expression compared to young mice, and this is further increased in aged TgSwDI. Scale bar= 100 μ m. Mean \pm SEM n=7-9 per group. ***p<0.001.

4.4 Discussion

The current study demonstrates that neurovascular coupling, in the cortex, is progressively impaired with advancing age and that these changes are closely related to disruption of astrocytic end feet contact on vessels and increased gliosis. However, contrary to the original predictions, the presence of extensive cortical amyloid deposition did not exacerbate the alterations in neurovascular unit function or structure.

4.4.1 Neurovascular coupling is impaired with age

Age-related impairments in neurovascular coupling in wild type mice were apparent at both 12 and 24 months of age (Fig 4.11). The extent of reduction in blood flow responses to whisker stimulation was marked and decreased by approximately 33% from 6 to 12 months of age. This data is in keeping with previously published work (Park et al. 2007), however another study has also shown that the cerebral vasculature may become impaired as early as 8 months of age (Balbi et al. 2015) when comparing blood flow responses to 6 week old mice. Clinical imaging studies have also demonstrated that increased age is related to reduced vascular responsiveness (Hutchison et al. 2013; Gauthier et al. 2013; Mohtasib et al. 2012). These differences have been reported in groups with an average age of 60 years, although it is not yet known when vascular functional impairments are first evident and there are likely to be differences between brain regions. Although reductions in vessel density have previously been reported with ageing in humans (Brown and Thore, 2011), cortical vessel number was not reduced in the present study (Fig 4.8), suggesting that impaired vascular function was not simply due to a reduced number of functional vessels, in agreement with other published work (Park et al. 2014). In the present study, impairments in neurovascular coupling were not accompanied by changes in resting cortical blood flow or cortical vessel density (Fig 4.5 and 4.8). Reductions in cerebral blood flow with age have been reported in both human and mouse imaging studies (Chen et al. 2011;

Hébert et al. 2013). The lack of change in resting blood flow to the barrel cortex in the present study may be attributed to the relative insensitivity of measuring from such a small area, and an alternative approach may be required in future to assess whether age-related vascular dysfunction also extends to resting cerebral blood flow. Matching neuronal activity to changes in blood flow via neurovascular coupling is essential to prevent hypoxia and preserve neuronal function. Measures of cognition were not performed in the present study but should be used to determine whether age-related impairments on neurovascular coupling, detectable from just 12 months of age, represent an early feature of vascular disruption that precedes cognitive impairment. In clinical studies, reduced vascular function is associated with cognitive impairment and even conversion from MCI to Alzheimer's disease (Viticchi et al. 2012; Mohtasib et al. 2012). Improving or preserving vascular function in mid to old age may therefore prove an effective, early timepoint for therapeutic intervention, prior to the onset of vascular cognitive impairment.

4.4.2 Neurovascular coupling was not further impaired in the presence of cortical amyloid

Although the present data demonstrated prominent age-related impairments in 12 and 24 month old mice, despite the presence of extensive cortical amyloid deposition in TgSwDI these mice were no more impaired on measures of neurovascular coupling than their wild type littermates (Fig 4.11). This was an unexpected finding since amyloid has been shown to have profound effects on vascular function (Dumas et al. 2012; Niwa et al. 2002). Further to this, previous work in transgenic mice that develop age-related amyloid deposition has also shown that neurovascular coupling is impaired relative to mice that do not develop amyloid pathology (Park et al. 2005, 2008). These discrepancies may be partly explained by differences in the particular amyloid species present in the models at the time of measurement of neurovascular

coupling and the extent of vascular amyloid. In TgSwDI mice, soluble, oligomeric amyloid levels are low and since oligomeric rather than fibrillar amyloid can have direct effects on vascular health (Park et al. 2005) there may, arguably, have been minimal impact of this amyloid species on cortical blood flow responses in the TgSwDI mice. However, using the same TgSwDI line, work published by Park et al. (2014) has shown blunted responses to whisker stimulation at just 3 months of age, prior to the accumulation of any amyloid deposition. The authors attribute this impairment to the presence of soluble amyloid, although this is not measured directly. Differences in experimental design may also influence the outcome measures between studies. In those by Park et al (2005, 2008, 2014) the authors perform a craniotomy with removal of the dura over the cortex in order to measure CBF responses. This relatively invasive procedure may disturb the underlying tissue and disrupt normal physiological responses. More recently, Kimbrough et al. (2015) used in vivo multiphoton imaging to elegantly demonstrate that in hAPPJ20 mice, neurovascular function was only impaired where there was evidence of vascular amyloid. Within the same vessel, segments in which there was an absence of vascular amyloid displayed vascular responses that were comparable to wild type mice. In the present study, the coverage of vessels by amyloid was low and at most was 2.7% of the vascular surface in the cortex (Fig 4.2). Therefore, the low burden of vascular amyloid in this cortical region may explain why vascular function was no different between wild-type and TgSwDI mice. Other models, such as J20 and APP23 mice with a greater burden of cortical vascular amyloid may exhibit greater neurovascular impairments relative to controls. The TgSwDI model does develop extensive microvascular amyloid deposition in the thalamus, with coverage in this region approaching almost 30% of the vascular surface (Fig 4.4). Assessing vascular reactivity in this region, for example utilising ASL with a hypercapnic challenge, may yield further information about whether vascular

amyloid exerts a detrimental effect on vascular function. Interestingly, in the thalamus, but not the cortex, TgSwDI mice exhibited greater vessel density relative to wild type mice when assessed by collagen IV immunohistochemistry, and vessel density was greater in aged mice compared to young (Fig 4.10). This difference was not detected by Q-map imaging (Fig 4.10), and may therefore represent an increase in basement membrane thickening rather than vessel number. Both ageing and vascular amyloid have previously been demonstrated to disrupt the basement membrane (Hawkes et al. 2013; Shimizu et al. 2009), but the impact of such changes on neurovascular coupling in this region have yet to be determined.

4.4.3 Contribution of pericytes to neurovascular coupling

In order to determine the potential mechanisms that may contribute to impairments in neurovascular coupling, alterations in components of the neurovascular unit were examined at 6 and 24 months of age, ages at which neurovascular coupling was normal and profoundly impaired, respectively. Since pericytes have been suggested to regulate cerebral blood flow, particularly at the capillary level (Hall et al. 2014), vascular coverage of pericytes was investigated as a potential mechanism by which neurovascular coupling may be impaired. In support of this, a pronounced reduction of the coverage of vessels with pericytes was found in aged brain as compared to young (Fig 4.12). Similar to the lack of differences in neurovascular coupling between TgSwDI and wild-type mice, there were no genotype differences in pericyte coverage. Previous studies have similarly shown a reduction of pericyte coverage in the frontal cortex and hippocampus of aged mice (Soto et al. 2015; Tucsek et al. 2014), suggesting that pericytes in multiple brain regions may be vulnerable to age-related degeneration. Findings from the present study support and extend this observation by demonstrating loss of pericyte coverage in the thalamus as well as the cortex (Fig 4.13). Pericytes are suggested to regulate cerebral blood flow at the capillary level (Hall et al. 2014), however the extent to which they

are able to contract and relax to modulate vascular diameter has recently come under scrutiny (Hill et al. 2015; Wei et al. 2016). We did not find any correlation between vessel function and cortical vascular pericyte coverage (Fig 4.12). However, pericyte loss may primarily effect the function of small-calibre vessels i.e. capillaries, which may be less significant when compared to arterioles or other larger vessels in controlling blood flow responses to whisker stimulation. In addition, the present study's use of laser speckle flowmetry provides only a gross measure of cortical blood flow responses, and may be a relatively insensitive method to detect the contributions of distinct vessel populations to perfusion (Ayata et al. 2004), therefore a role for pericyte loss in contributing to age-related vascular dysfunction cannot be ruled out. Loss of pericyte coverage may also indirectly lead to impaired vessel function through increased permeability of the blood-brain barrier (Montagne et al. 2015), infiltration of circulating neutrophils and enhanced neuroinflammation. In the thalamus, although vascular amyloid load was substantially increased relative to the cortex (Fig 4.2 and 4.4), pericyte coverage was not further reduced in TgSwDI mice relative to wild type (Fig 4.13). However, in the present study pericyte coverage was assessed in all vessels, in the future it may be beneficial to quantify pericyte coverage specifically in vessels containing vascular amyloid deposits, in order to more directly determine the effect of cerebral amyloid angiopathy on pericyte integrity.

4.4.4 Contact between astrocytes and blood vessels may be critical for normal neurovascular coupling

Astrocytes and their endfeet are known to have critical roles in regulating cerebral blood flow (Bazargani and Attwell, 2015), the present study therefore investigated whether alterations in the contact between astrocytic endfeet and blood vessels may be related to impairments in neurovascular coupling. In aged 24 month old mice there was a profound loss of vascular localisation of AQP4 labelling of astrocytic endfeet contacts in the cerebral cortex (Fig 4.14)

and thalamus (Fig 4.16), whereas 6 month old mice demonstrated extensive colocalisation between blood vessels and AQP4. Loss of vascular AQP4 localisation may therefore indicate disruption of the contact between vessels and astrocytes in aged mice. We also observed an age-related increase in the number of GFAP+ve astrocytes (Fig 4.15 and 4.17), suggestive of an increase in astrocytic activation. Process retraction following activation may contribute to the disruption of astrocyte/vessel contact. Neuronal activity elicits intracellular calcium increases in the soma of astrocytes (Bazargani and Attwell, 2016), which in turn results in the release of arachidonic acid-derived vasodilators such as prostaglandins and epoxyeicosatrienoic acids (EETs) from the astrocyte endfoot. Disruption of contact between astrocytic endfeet and vasculature, as reflected in loss of vascular AQP4 coverage, may result in loss of this vasodilatory input and lead to impairments in neurovascular coupling. Our findings are in line with those of Kress et al (2014), who previously showed reductions in vascular AQP4 expression on penetrating arterioles in 18 month old wild type mice compared to 2-3 month old mice. This reduction was associated with impaired function of the glymphatic pathway, driven by reductions in cerebrovascular pulsation. The present study demonstrates a significant relationship between AQP4 localisation on vessels and neurovascular coupling. Together, the data suggest a critical role for expression of AQP4 on cerebral vasculature in order to maintain normal vascular function. Additionally, in the thalamus of TgSwDI mice, AQP4 expression was not only reduced on the vascular surface but redistributed into the parenchyma (Fig 4.16), an effect that was only observed in this brain region with significant burden of vascular amyloid. The underlying cause of this redistribution may be related to the enhanced astrocytic activation in aged TgSwDI mice and retraction of endfeet processes, or through disruption of the vascular basement membrane and loss of interaction between AQP4 and its anchoring protein complex. Loss of AQP4 polarity is likely to influence the clearance

of CSF/ISF (Kress et al. 2014) and may contribute to enhanced accumulation of amyloid in this region. Age and cerebral amyloid angiopathy-related loss of vascular AQP4 may therefore predispose to vascular dysfunction and cognitive decline. Indeed, AQP4 expression has been shown to be reduced in Alzheimer's disease brain (Wilcock et al. 2009) and loss of vascular AQP4 has recently been shown to occur in post-stroke dementia (Chen et al. 2016).

4.4.5 Microglial activation is associated with reduced neurovascular coupling

Neuroinflammation is reported to be increased in the ageing brain (Luo, Ding and Chen, 2010) and in response to amyloid (for review see Heneka et al. 2015). In the present study, Iba1+ve microglia were quantified in order to investigate whether neuroinflammatory processes may also contribute to impaired neurovascular coupling. An increase in microglial activation was observed in aged mice relative to young, and this increase was further exacerbated in the presence of amyloid both in the cortex and thalamus (Fig 4.18 and 4.19), supporting the concept that amyloid elicits a strong neuroinflammatory response in microglia (Heneka et al. 2015). In the cortex, microglial activation was also related to measures of neurovascular coupling (Fig 4.18). Activation of microglia increases the activity of the superoxide-generating NADPH oxidase complex (Gao, Zhou and Hong, 2012). In line with this, we observed an increase in expression of the p47 subunit of NADPH oxidase 2 in aged mice compared to young (Fig 4.20). Interestingly, this increase was not further exacerbated in the cortex of TgSwDI mice relative to wild type, but was increased in the thalamus. It is unclear from present findings whether the increase in NADPH oxidase activation arises due to the greater total burden of amyloid in this region, or the greater load of vascular amyloid specifically, as has been reported previously (Han et al. 2015). Reactive superoxide species and downstream products such as peroxynitrite may significantly impair the vasodilatory capacity of the cerebral blood vessels (Zou, 2007; Barbosa-Sicard et al. 2009; Arunchalam et al. 2010). Direct targeting of superoxide production

may shed further light on whether this contributes to age-related impairments on neurovascular function.

4.4.6 Conclusions

Ageing, a strong risk factor for development of cognitive decline, leads to profound neurovascular dysfunction and disruption of the underlying structure of the neurovascular unit. The present findings highlight the vulnerability of the cerebral vascular system to age-related alterations, which in humans are likely to be further exacerbated due to the presence of multiple vascular risk factors that also occur with ageing i.e. hypertension. Sustained vascular dysfunction may cause localised hypoxia, leading to tissue degeneration and cognitive decline, therefore targeting vascular health as individuals age could prove an effective strategy to reduce cognitive decline and delay the onset of dementia. Subsequent studies will examine the impact of a prominent feature of ageing, chronic cerebral hypoperfusion, on vascular lesion development and cognition.

Chapter 5.

The impact of chronic cerebral hypoperfusion and amyloid deposition on vascular function and cognitive decline

The impact of chronic cerebral hypoperfusion and amyloid deposition on vascular function and cognitive decline

5.1 Introduction

Cerebral hypoperfusion is a prominent feature of cerebrovascular disease and vascular cognitive impairment (Gorelick et al. 2011), yet the molecular mechanisms that link chronic cerebral hypoperfusion to cognitive decline are unknown. Cerebral hypoperfusion can be modelled in mice using the bilateral carotid artery stenosis (BCAS) model, causing a reduction in blood flow to the brain (Shibata et al. 2004). Induction of cerebral hypoperfusion has been shown to cause white matter disruption and impairments on spatial working memory after 1-2 months (Shibata et al. 2007; Coltman et al. 2011), recapitulating some aspects of vascular cognitive impairment (Tullberg et al. 2004). However, long-term hypoperfusion has also been shown to induce more severe impairments on cognition, as well as disruption of the neurovascular unit and the development of vascular lesions such as microinfarcts and microhaemorrhage (Holland et al. 2015). The impact of hypoperfusion on neurovascular function and the mechanism by which hypoperfusion drives vascular disruption have not been assessed in the BCAS model, but may be critical to understanding how vascular lesions and cognitive decline are initiated. Furthermore, the impact of cerebral hypoperfusion on vascular function in transgenic amyloid precursor protein mice has also not been assessed. Amyloid deposition is a key pathological feature of Alzheimer's disease, but vascular pathology such as cerebral hypoperfusion, microinfarcts and microhaemorrhage are also commonly found in AD individuals (Love and Miners, 2016), and likely contribute to disease progression. This study therefore sought to determine the impact of cerebral hypoperfusion on vascular function and cognition, and whether these changes were exacerbated in TgSwDI mice. The processes that

initiate vascular disruption and the induction of vascular lesions following hypoperfusion are unknown. Increases in oxidative stress have been implicated as potential mediators of damage following hypoperfusion and in cerebrovascular diseases (Liu and Zhang, 2012). Soluble and vascular forms of amyloid protein also increase production of reactive oxygen species through the activity of NADPH oxidase 2 (Park et al. 2005; Han et al. 2015), and data from our lab suggests this is exacerbated by hypoperfusion (Salvadores, unpublished). Therefore, this study also sought to determine whether oxidative stress was increased following hypoperfusion and further increased in hypoperfused TgSwDI mice.

5.1.1 Hypothesis:

This study tests the hypothesis that cerebral hypoperfusion induces vascular dysfunction and impaired cognition, and that these changes are exacerbated in TgSwDI mice.

5.1.2 Aims:

The aim of the study is to assess oxidative stress, neurovascular coupling, vascular lesion development and spatial learning and memory following cerebral hypoperfusion, and to investigate whether these alterations are exacerbated in TgSwDI mice.

5.2 Methods

5.2.1 Animals

Male C57Bl/6J and heterozygous TgSwDI mice were used for in vivo experiments and histopathology (n=21 C57Bl/6J, n=20 TgSwDI). An additional cohort was also included for generation of tissue for biochemical assays (n=18 C57Bl6/J, n=17 TgSwDI). Two mice in the study had to be singly housed due to aggressive fighting behaviour, but wherever possible animals were group housed. Mice were maintained on a 12:12hr light/dark cycle and had access to food and water *ad libitum*. All experiments were conducted in accordance with the Animals (Scientific Procedures) Act 1986 and local ethical approval at the University of Edinburgh and were performed under personal and project licenses granted by the Home Office. All data collection and analysis was performed by experimenters blind to the surgical and genetic status of the mice. N numbers were selected based on power analysis of previously collected ASL-MRI data from the thalamus (as MRI is the most variable dataset). To achieve a significance value of $p < 0.05$ at a power of 0.8, a minimum group size of $n=8$ was required.

5.2.2 Cerebral hypoperfusion surgery

Hypoperfusion surgery was performed when mice were 8-9 months of age, after the onset of cerebral amyloid deposition. Surgery was performed according to Methods section 2.2. One TgSwDI mouse was culled during surgery due to excessive bleeding. Following surgery, mice were placed in an incubator to recover from anaesthesia, and their subsequent recovery from surgery was monitored closely over the next 3 days. Seven mice (2 wild type and 5 TgSwDI) showed poor recovery following the surgery and were culled.

5.2.3 In vivo vascular imaging

In vivo MRI was performed at 1 week prior to and 3 months following cerebral hypoperfusion surgery. At 1 week prior to surgery, mice underwent T2, ASL and T2* imaging (non-contrast-enhanced) according to methods described in Methods section 2.9. At 3 months following cerebral hypoperfusion surgery, mice underwent the same scans with the addition of ce-T2* imaging. 3 mice were excluded from ASL analysis due to breathing problems during the scan.

5.2.4 Analysis of in vivo MRI

The number of ischaemic and haemorrhagic lesions detected by structural T2 imaging was counted according to criteria published in Holland et al. (2015). ASL data was generated according to Methods section 2.9.1. For ASL measures, regions of interest were placed in the cortex, hippocampus and thalamus of a simultaneously acquired T1 image to avoid bias in region placement. T2* signal was measured in cortical and thalamic regions and normalised to CSF values from the dorsal third ventricle according to the method of Klohs et al. (2015). The contrast agent ferumoxytol does not enter the CSF and so none should be present within the ventricle. Normalising to this region therefore allows subtraction of baseline signal so as to only measure signal change due to presence of the contrast agent.

5.2.5 Laser speckle imaging of baseline blood flow

In a subset of 16 mice, laser speckle imaging was used to track changes in cortical blood flow. Laser speckle imaging was performed at 4 timepoints during the experiment: 24 hours before surgery, 24 hours post-surgery, 1 month post-surgery and 3 months post-surgery according to methods described in Methods section 2.4. One wild type mouse was subsequently excluded from the entire study as it experienced an acute ischaemic attack during the 24 hour laser speckle imaging session.

5.2.6 Barnes Maze

At 10 weeks following cerebral hypoperfusion surgery, mice underwent the Barnes maze test of spatial learning and memory, performed according Methods section 2.7. Mean speed was compared between groups to ensure rates of learning were not influenced by transgene or surgery effects on movement speed. For the learning phase, mice were assessed based on the time taken to enter the escape chamber (escape latency). For each day of the learning phase, escape latency data was averaged over two trials. For probe trials, mice were assessed based on the proportion of time spent in the target quadrant i.e. the quadrant of the maze that had previously contained the escape chamber.

Inclusion criteria

Performance in the Barnes maze is dependent on the mouse exploring the maze and being motivated to locate the escape chamber. Therefore, inclusion criteria were as follows: mice must enter a minimum of 3 quadrants in 2 of the learning phase trials. No mice were excluded from subsequent analysis.

5.2.7 Laser speckle imaging measures of neurovascular coupling

Assessment of neurovascular coupling was performed 14 weeks after surgery according to Methods section 2.5. Mean response amplitude during stimulation was expressed as percentage increase from baseline and averaged across a minimum of 3 stimulations.

5.2.8 Tissue collection and processing

Following laser speckle imaging assessment of neurovascular coupling, mice were transcardially perfused with PBS according to Methods section 2.10. Brain tissue was then collected and processed according to Methods section 2.11.2. In an additional cohort of mice, hemibrains were collected for biochemical assays according to Methods section 2.15.

5.2.9 Amyloid quantification

12µm coronal sections were collected corresponding to Bregma -1.82mm in stereotaxic mouse atlas (Paxinos and Franklin, 2001) and labelled with 6E10 antibody according to Methods section 2.13.1. Sections were imaged at x10 using an Olympus BX51 microscope (x10, Olympus UK, Southend-on-Sea, UK); taking two pictures per region in the cortex and thalamus, and percentage area stained by 6E10 was quantified using ImageJ.

5.2.10 Quantification of ischaemic and haemorrhagic lesion burden

Coronal brain tissue sections were collected at six stereotactic levels throughout the brain (anterior/posterior from Bregma: +0.86mm, +0.14mm, -0.46mm, -1.34mm, -1.82mm and -2.3mm) and were stained using H&E and Perls' Prussian Blue according to Methods sections 2.12.1 and 2.12.2 in order to detect ischaemic and haemorrhagic pathology respectively. Ischaemic lesions were defined as sharply delimited areas of tissue pallor on H&E stained sections. Haemorrhagic pathology was defined as blue cellular staining of haemosiderin deposits on Perls' Prussian Blue stained sections. Non-cellular blue deposits were not classified as haemorrhagic lesions. Ischaemic and haemorrhagic lesions were quantified in the cortex, hippocampus, thalamus and white matter (comprising corpus callosum, anterior commissure, fimbria, internal capsule and optic tract).

5.2.11 Dot blot assay

Dot blot assessment of protein alterations was performed according to Methods section 2.17 using whole brain homogenates. Assays were performed for NADPH oxidase 2 (using antibodies against the catalytic subunit gp91phox), NADPH oxidase 4 and for 3-nitrotyrosine, a marker of protein nitration.

5.2.12 Statistical analysis

A two-way ANOVA with surgery and genotype as the between-subjects factors was used to compare resting cerebral blood flow assessed by both laser speckle imaging and ASL, neurovascular coupling measures, ce-T2* signal changes, amyloid burden and levels of oxidative stress markers. Lesion burden was compared using the Pearson Chi-Squared test. For the learning phase of the Barnes maze, speed and escape latency were assessed by repeated measures ANOVA, with surgery as the between-subjects factor and trial day as the within-subjects factor. For the probe trials, performance of each group was compared to chance using a one sample t-test. Performance between the groups was then compared using a two-way ANOVA with surgery and genotype as the factors. Statistical analysis was performed in SPSS (v19, IBM Corp.).

5.3 Results

5.3.1 Blood flow is reduced following cerebral hypoperfusion

In order to investigate blood flow changes following cerebral hypoperfusion surgery, laser speckle contrast imaging was performed at baseline (prior to surgery) and 24 hours, 1 month and 3 months following surgery in a subset of mice. Blood flow data was calculated as % change from baseline flow values. Analysis of percentage change in blood flow from baseline revealed significant effects of time ($F_{(3,153)}=49.742$, $p<0.001$) and surgery ($F_{(1,51)}=216.468$, $p<0.001$), but there was no effect of genotype ($p>0.05$) (Figure 5.1 and 5.2). Further, a significant interaction between time and surgery was detected ($F_{(3,153)}=65.738$, $p<0.001$). Post-hoc analysis indicated that blood flow was significantly reduced in both wild type and TgSwDI hypoperfused mice compared to shams at 24 hours ($p<0.001$), 1 month ($p<0.001$) and 3 months ($p<0.001$) following surgery.

In order to quantify changes in resting cerebral blood flow in subcortical brain regions, arterial spin labelling was performed at baseline (prior to surgery) and 3 months following surgery, and the percentage change from baseline was calculated. In the thalamus, a significant effect of surgery was detected ($F_{(1,26)}=17.3$, $p<0.001$), where blood flow was reduced in hypoperfused mice compared to shams (Figure 5.3 and 5.4), but there was no significant effect of genotype ($p>0.05$). In the hippocampus, there was a significant effect of surgery ($F_{(1,26)}=27.85$, $p<0.0001$) but no effect of genotype ($p>0.05$).

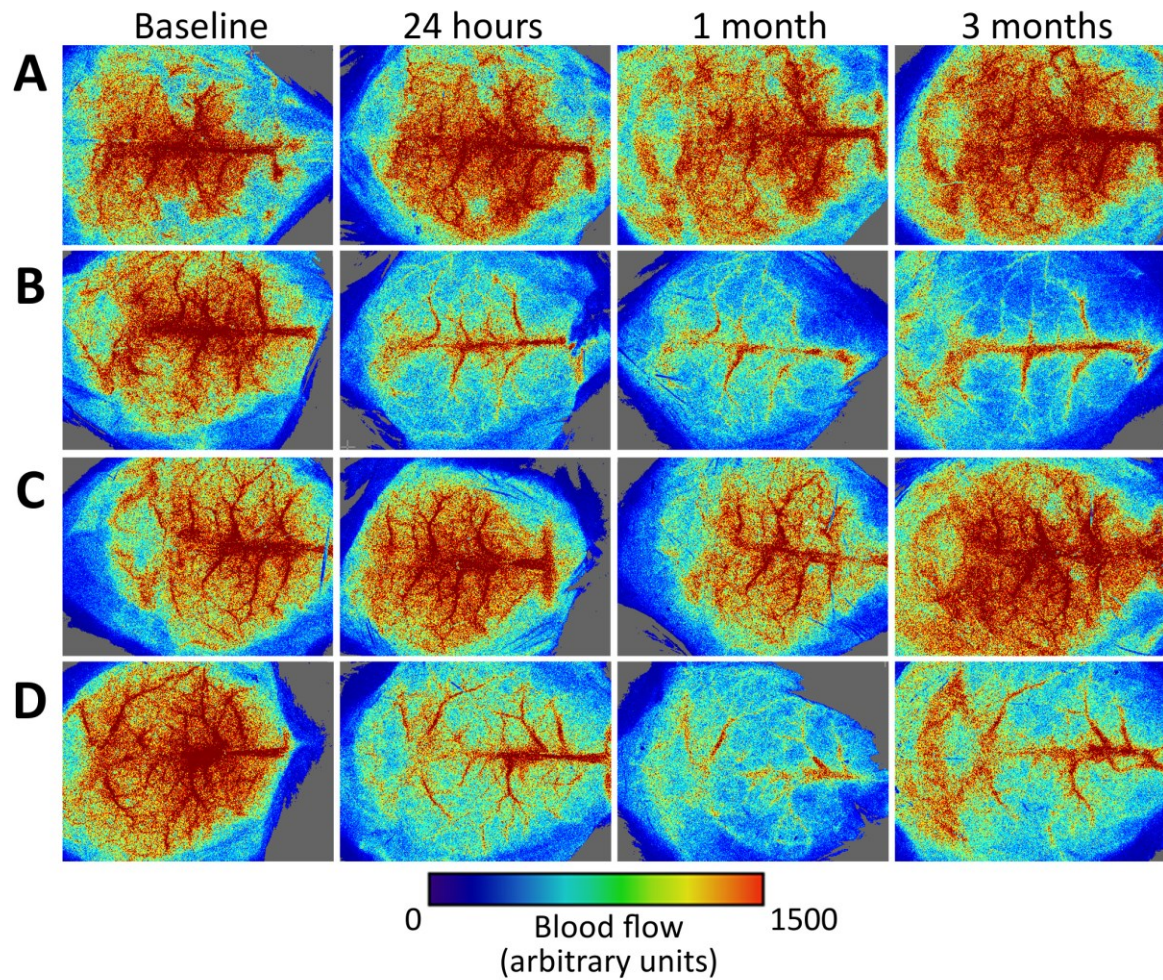


Figure 5.1 Cortical blood flow is persistently reduced following cerebral hypoperfusion. Laser speckle imaging was used to measure blood flow alterations from baseline at 24 hours, 1 month and 3 months following hypoperfusion surgery. Representative images of cortical blood flow at all timepoints from (A) wild type sham, (B) wild type hypoperfused, (C) TgSwDI sham and (D) TgSwDI hypoperfused mice.

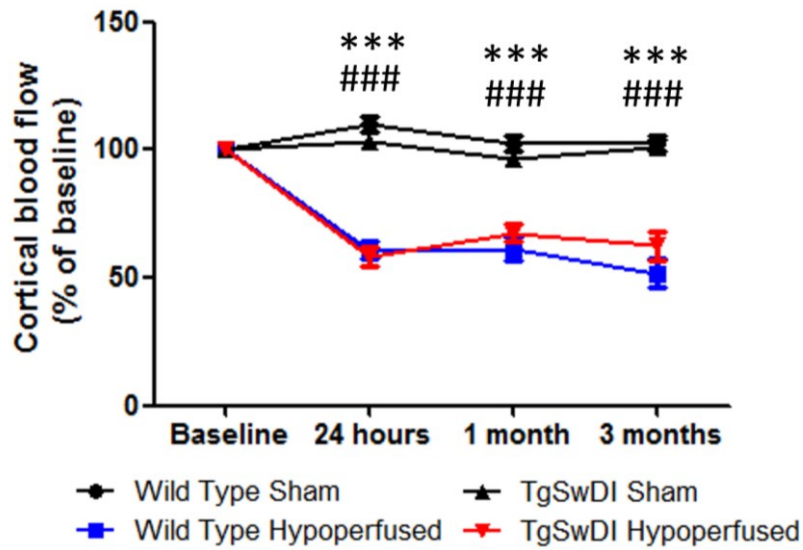


Figure 5.2 Cortical blood flow is persistently reduced following cerebral hypoperfusion. Laser speckle imaging was used to measure blood flow alterations from baseline at 24 hours, 1 month and 3 months following hypoperfusion surgery. Significant effects of time ($F_{(3,153)}=49.742$, $p<0.001$) and surgery ($F_{(1,51)}=216.468$, $p<0.001$) were detected, but there was no effect of genotype $p>0.05$). Further, a significant interaction between time and surgery was detected ($F_{(3,153)}=65.738$, $p<0.001$). Post-hoc analysis indicated that blood flow was significantly reduced in both wild type and TgSwDI hypoperfused mice compared to shams at 24 hours ($p<0.001$), 1 month ($p<0.001$) and 3 months ($p<0.001$) following surgery. $N=13-15$ per group. *** $p<0.001$ wild type hypoperfused vs wild type sham; #### $p<0.001$ TgSwDI hypoperfused vs TgSwDI sham.

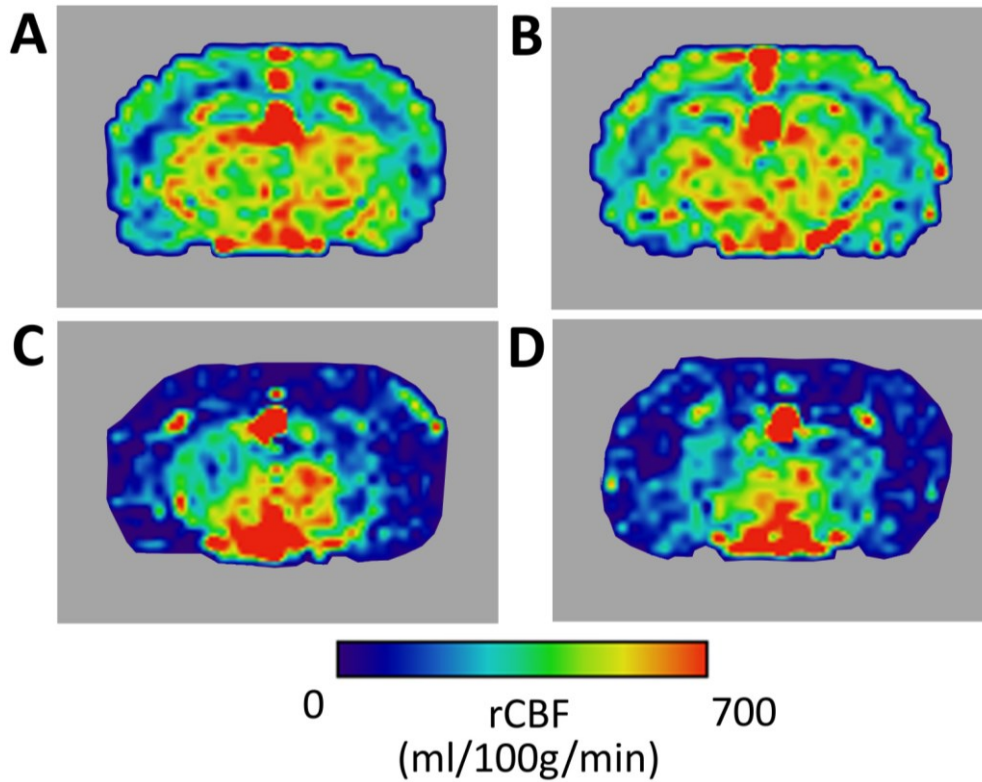


Figure 5.3 Arterial spin labelling was used to detect blood flow alterations at 3 months following hypoperfusion. Representative arterial spin labelling images from (A) wild type sham, (B) wild type hypoperfused, (C) TgSwDI sham and (D) TgSwDI hypoperfused mice.

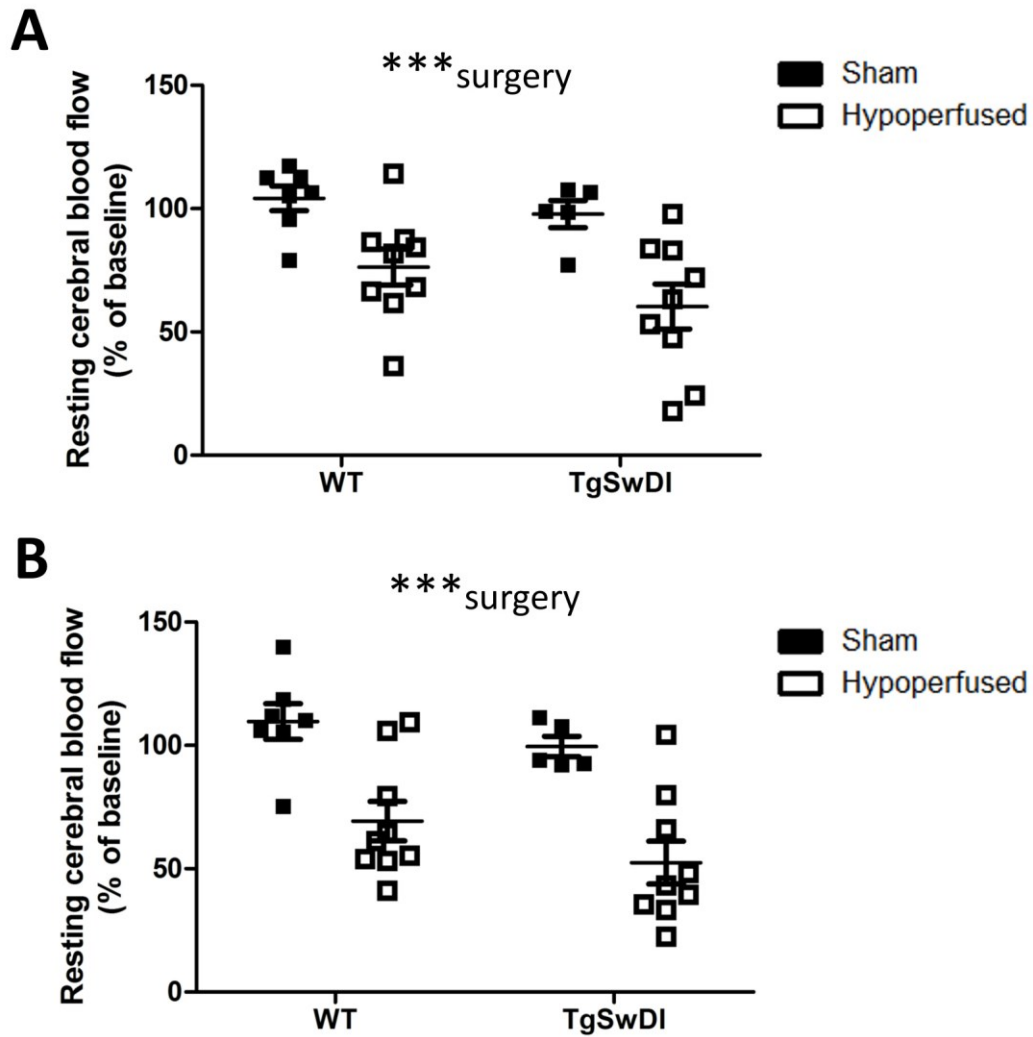


Figure 5.4 Thalamic and hippocampal blood flow remains reduced 3 months following cerebral hypoperfusion. Arterial spin labelling was used to measure blood flow in thalamus and hippocampus at baseline and 3 months following hypoperfusion surgery, and the percentage change from baseline was calculated. Resting blood flow was significantly reduced in hypoperfused mice in both thalamus ($F_{(1,26)}=17.35$, $p<0.001$) and hippocampus ($F_{(1,26)}=27.85$, $p<0.0001$). There was no significant effect of genotype in any brain region. Data presented as mean \pm SEM, $n=5-9$ per group. *** $p<0.001$.

5.3.2 TgSwDI mice develop amyloid deposition that is absent in wild type mice

6E10 immunohistochemistry was performed in order to determine the extent of amyloid deposition in brain tissue sections. Amyloid deposition was not detected in wild type mice, whereas TgSwDI mice had a significant amyloid load in the cortex and thalamus ($F_{(1,23)}=51.9$, $p<0.001$ and $F_{(1,23)}=42.3$, $p<0.001$ respectively) (Figure 5.5). Cerebral hypoperfusion did not influence amyloid load.

5.3.3 Neurovascular coupling is significantly impaired following cerebral hypoperfusion

In order to investigate whether hypoperfusion causes impairments on vascular function, neurovascular coupling was assessed using laser speckle contrast imaging with whisker stimulation, and the percentage increase in blood flow during stimulation was calculated. A significant effect of surgery was detected ($F_{(1,29)}=20.4$, $p<0.0001$), with hypoperfused mice exhibiting impaired responses to whisker stimulation relative to shams (Figure 5.6). No effect of genotype was detected ($p>0.05$).

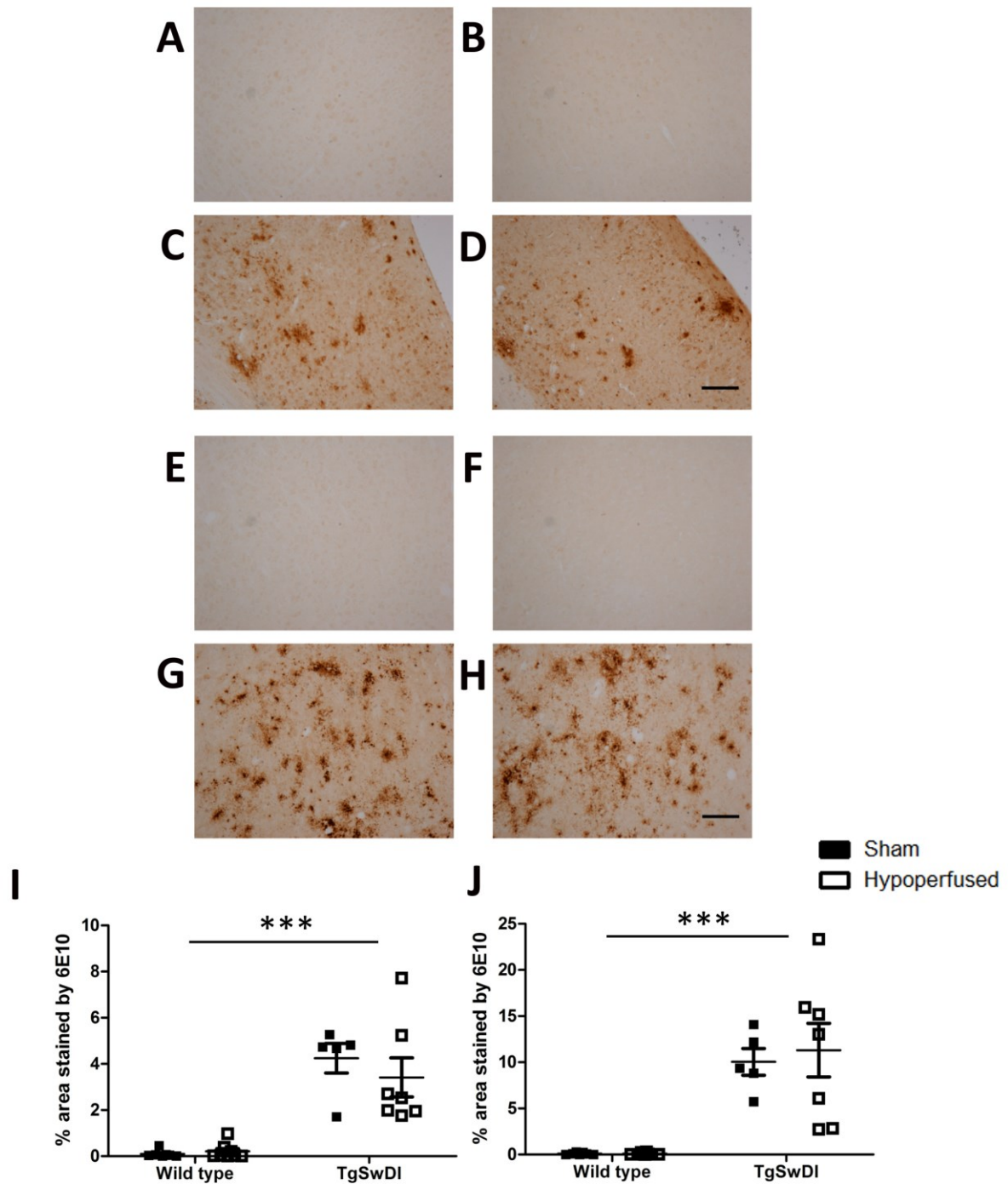


Figure 5.5 TgSwDI mice exhibit amyloid deposition that is not detectable in wild type mice. Representative images from (A, E) wild type sham, (B, F) wild type hypoperfused, (C, G) TgSwDI sham and (D, H) TgSwDI hypoperfused mice in cortex (A-D) and thalamus (E-H). Amyloid deposition is significantly greater in TgSwDI mice in both cortex (I) and thalamus (J). Data presented as mean±SEM, n=8-9 per group. ***p<0.001. Scale bar=100µm.

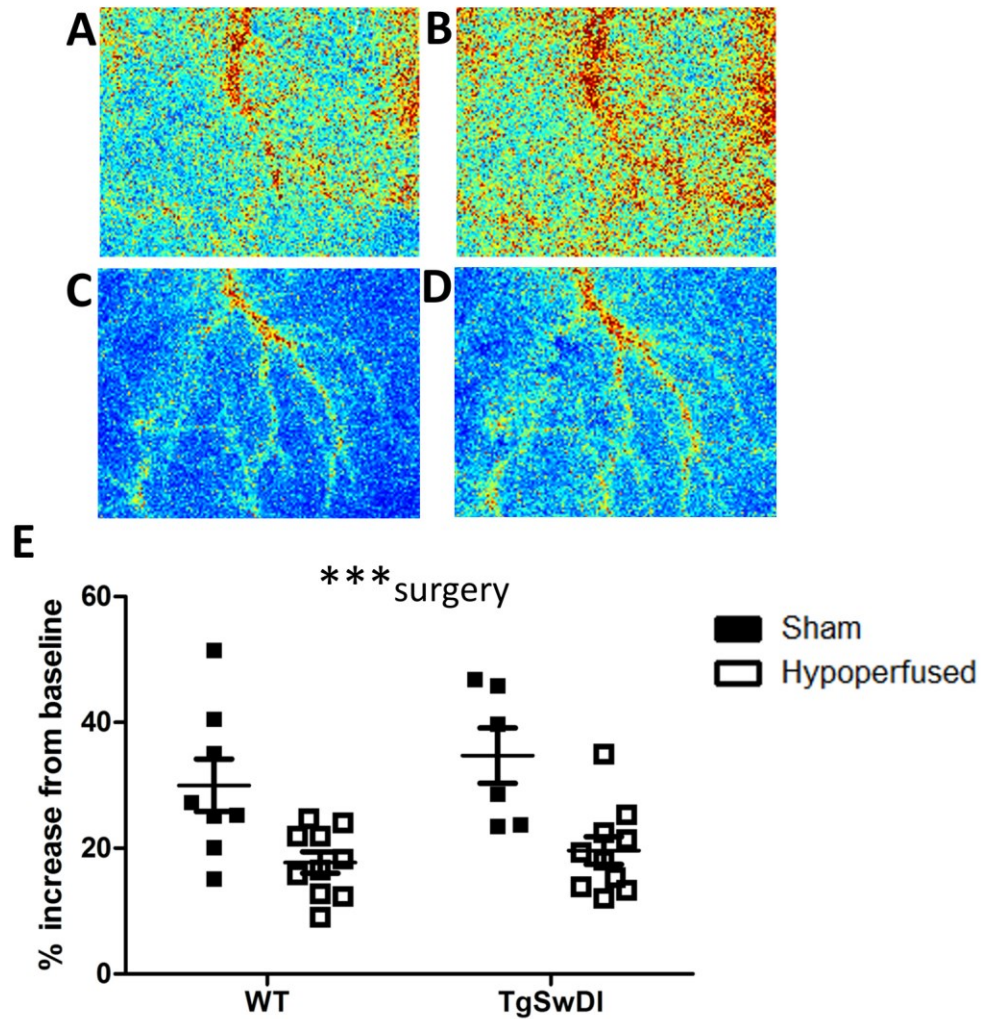
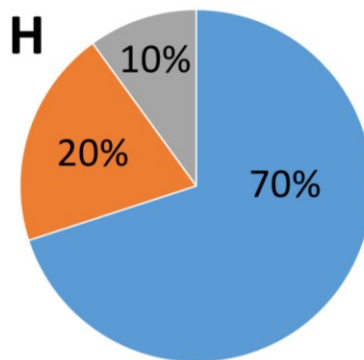
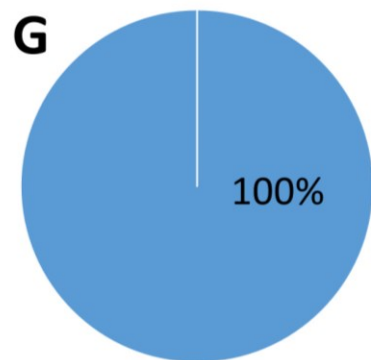
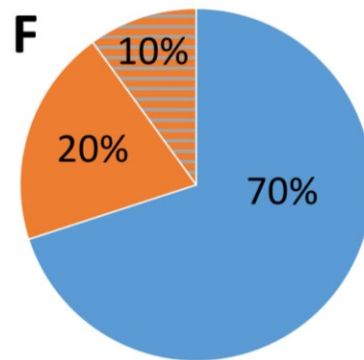
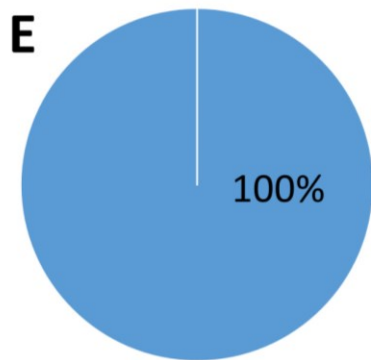
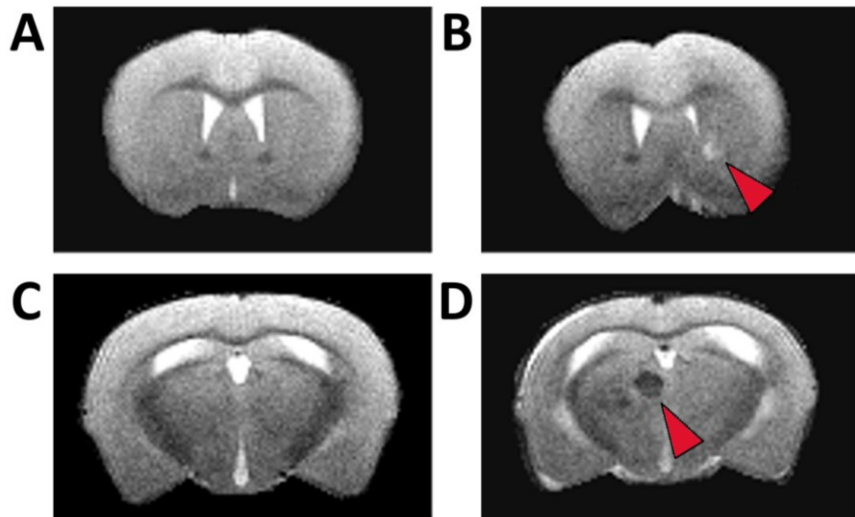


Figure 5.6 Neurovascular coupling is significantly impaired following cerebral hypoperfusion. Laser speckle imaging was performed with whisker stimulation in order to assess alterations in vascular function at 3 months following cerebral hypoperfusion. Representative images from sham (A, B) and hypoperfused (C, D) wild type mice during baseline (A, C) and whisker stimulation (B, D). (E) Neurovascular coupling was significantly impaired in hypoperfused mice relative to shams ($F_{(1,29)}=20.42$, $p<0.0001$), but there was no difference between wild type and TgSwDI mice. Data presented as mean \pm SEM, $n=6-10$ per group. *** $p<0.001$.

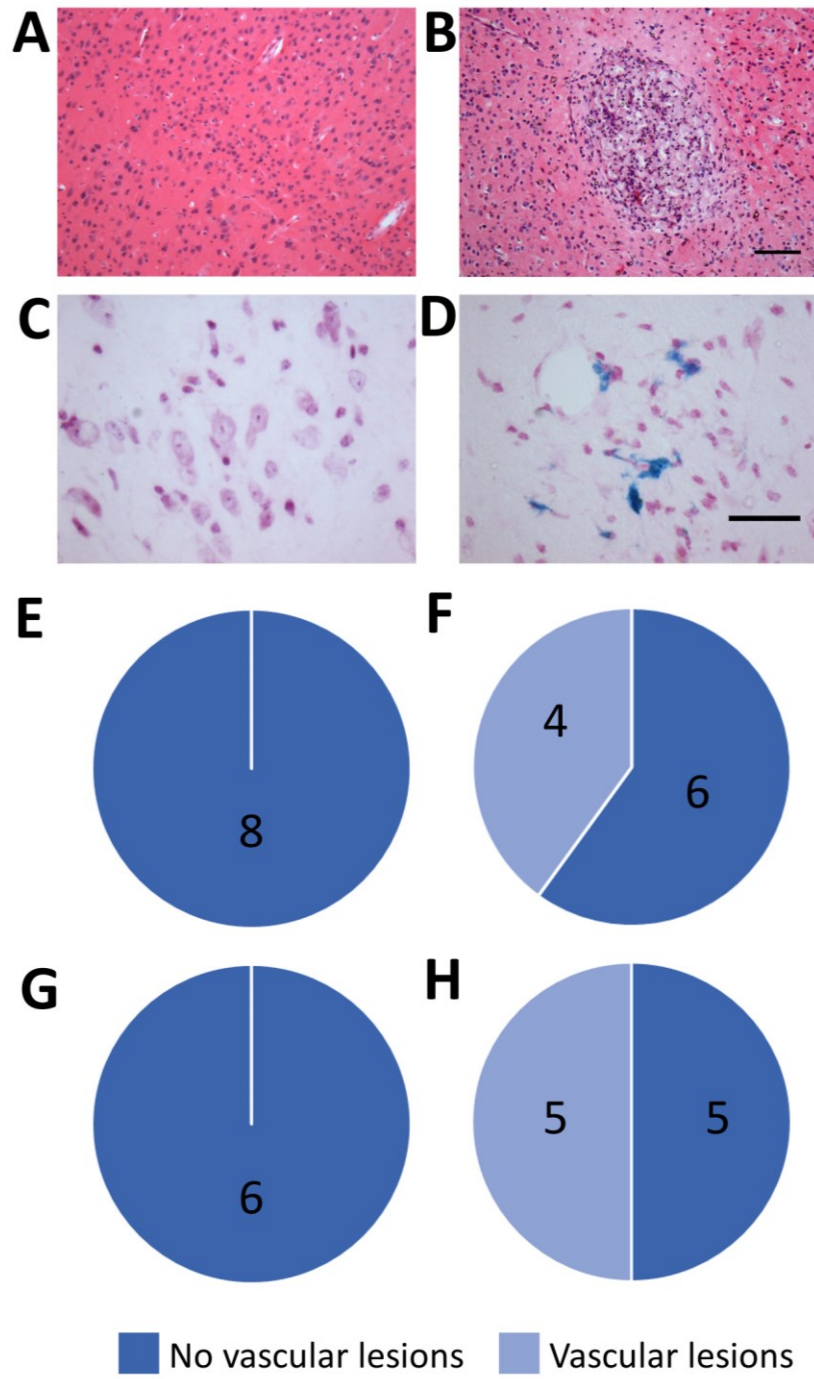
5.3.4 Hypoperfusion induces development of vascular lesions

Hypoperfusion has been shown previously to induce the development of vascular lesions at 6 months following surgery in wild type mice. In order to determine the effect of chronic cerebral hypoperfusion on the development of vascular lesions at 3 months, and to investigate whether TgSwDI mice would develop a greater lesion burden relative to wild types, T2 imaging was performed at 3 months following hypoperfusion surgery, and the number of mice with ischaemic and haemorrhagic lesions was counted according to previously published methods (Holland et al. 2015) (Figure 5.7). No vascular lesions were detectable in either wild type or TgSwDI sham mice. In hypoperfused wild type mice, 2 of 10 mice were found to have an ischaemic lesion (20%), 1 mouse was found to have both ischaemic and haemorrhagic lesions (10%), and the remaining 7 had no lesions (70%). In hypoperfused TgSwDI mice, 2 of 10 mice were found to have an ischaemic lesion (20%), 1 mouse was found to have a haemorrhagic lesion (10%) and the remaining 7 had no lesions. In order to further investigate the burden of ischaemic and haemorrhagic pathology in hypoperfused mice, H&E staining and Perls' Prussian Blue staining was performed in tissue sections throughout the brain and the number of mice with ischaemic or haemorrhagic pathology was quantified (Figure 5.8 and 5.9). The number of mice that developed ischaemic lesions was significantly greater in hypoperfused mice relative to shams for both wild type (0 of 8 wild type sham, 0%, vs 4 of 10 wild type hypoperfused, 40%; $\chi^2_{(1,18)}=4.114$, $p<0.05$) and TgSwDI mice (0 of 6 TgSwDI sham, 0%, vs 5 of 10 TgSwDI hypoperfused, 50%; $\chi^2_{(1,16)}=4.364$, $p<0.05$). However, the number of hypoperfused mice with ischaemic pathology was not significantly different between genotypes. The distribution of ischaemic pathology in regions throughout the brains of hypoperfused mice was also determined (Figure 5.9). No significant differences were found between the number of wild type or TgSwDI mice with ischaemic pathology in the cortex,

hippocampus, white matter, or thalamus ($p>0.05$). Haemorrhagic lesions were detectable only in the thalamus of hypoperfused mice, but there was no significant difference in the number of mice with haemorrhagic pathology between wild type (3 of 10, 30%) and TgSwDI mice (2 of 10, 20%). Therefore, hypoperfusion surgery was found to induce the development of vascular lesions, but TgSwDI mice did not develop a greater number of lesions relative to wild types.



◀ **Figure 5.7 Hypoperfusion induces development of vascular lesions.** Structural T2 imaging was performed at 3 months following hypoperfusion surgery. Representative images from sham (A,C) and hypoperfused mice indicating an ischaemic lesion in the anterior commissure (B) (red arrowhead) and a haemorrhagic lesion in the thalamus (D) (red arrowhead). No lesions were detected in sham-operated mice (E,G); whereas 20% of both wild type (F) and TgSwDI (H) hypoperfused mice were found to have ischaemic lesions. 10% of hypoperfused wild type mice had both ischaemic and haemorrhagic lesions, and 10% of hypoperfused TgSwDI mice had haemorrhagic lesions only.



◀ **Figure 5.8 Hypoperfusion induces development of vascular lesions.** H&E and Perls' Prussian Blue staining was performed to identify ischaemic and haemorrhagic lesions respectively. Representative H&E images showing normally appearing cortex from a sham mouse brain (A) and an ischaemic cortical lesion from hypoperfused mouse brain (B). Representative Perls stain from sham (C) and hypoperfused (D) mice. Blue cellular staining indicates a haemorrhagic lesion in hypoperfused mouse brain (D). No lesions were detected in sham-operated mice (E,G); whereas 40% of wild type (F) and 50% of TgSwDI (H) hypoperfused mice were found to have vascular lesions. Scale bar=100µm (B), 40µm (D).

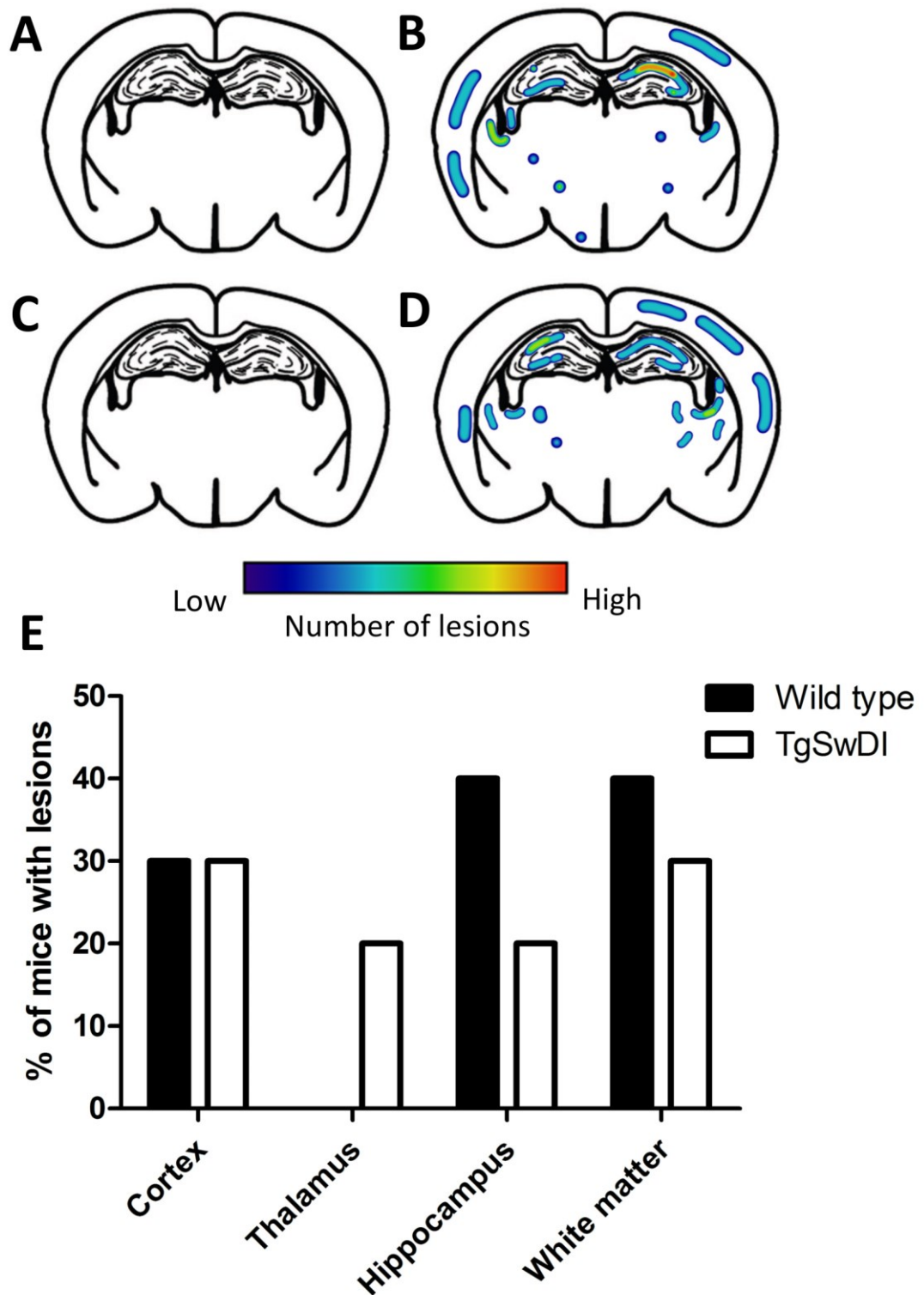
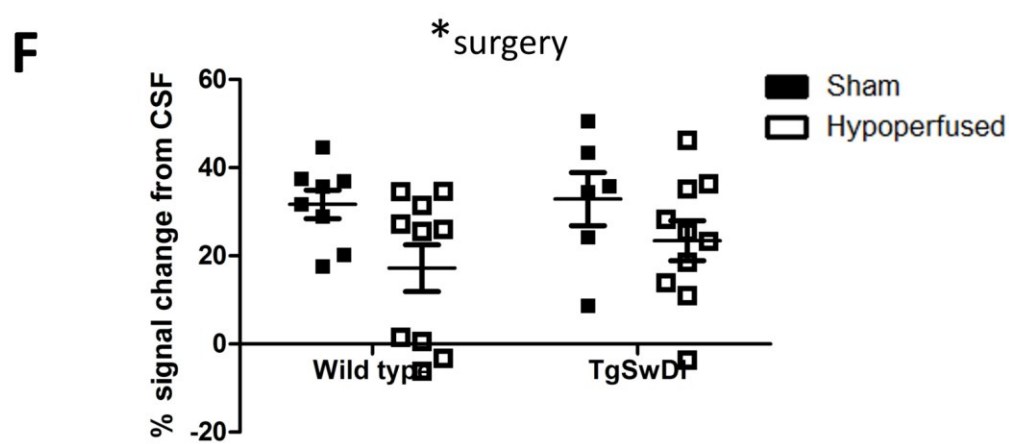
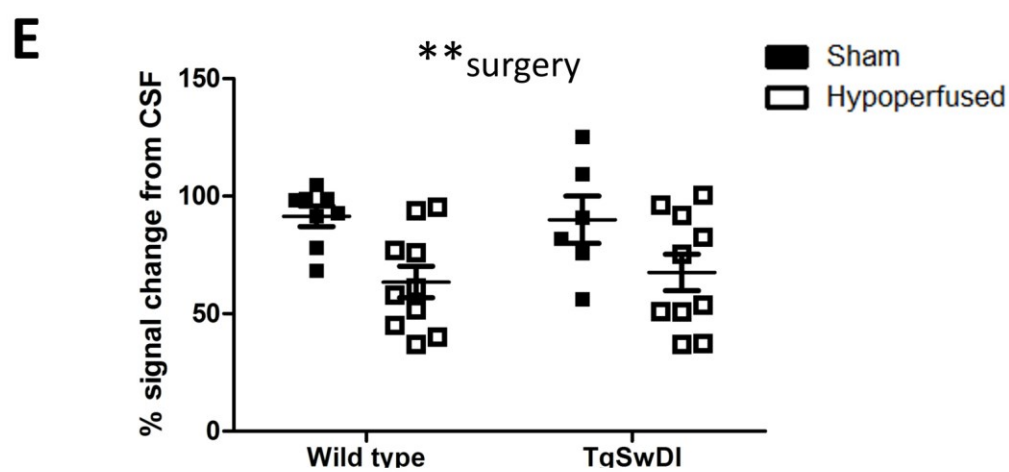
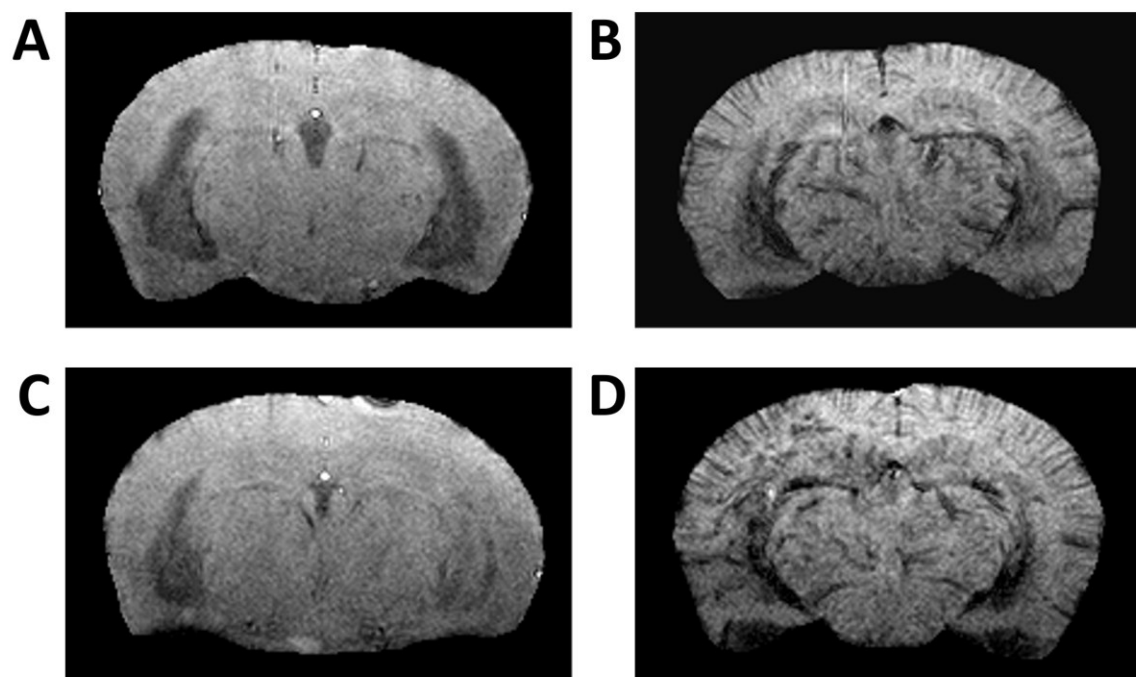


Figure 5.9 Distribution of vascular lesions following cerebral hypoperfusion. Maps indicating the distribution of vascular lesions in wild type sham (A), wild type hypoperfused (B), TgSwDI sham (C) and TgSwDI hypoperfused (D) mice. No significant differences in regional distribution of lesions were detected between wild type and TgSwDI hypoperfused mice (E).

5.3.5 Contrast-enhanced T2* signal is altered in hypoperfused mice

Having observed that chronic cerebral hypoperfusion was associated with an increase in the number of vascular lesions, contrast-enhanced T2* imaging was performed to determine if the development of vascular lesions also coincided with increased cerebral inflammation (Figure 5.10). T2* signal was measured from the cortex and thalamus and normalised to CSF T2* values, which should not be influenced by administration of the iron oxide contrast agent (Klohs et al. 2015). In the cortex, a significant effect of surgery was detected whereby tissue signal was significantly more hypointense in hypoperfused mice relative to shams ($F_{(1,30)}=11.47$, $p<0.01$). There was no overall genotype effect. In the thalamus, an overall effect of surgery was detected ($F_{(1,30)}=5.74$, $p<0.05$) indicating greater hypointensity in hypoperfused mice relative to shams, however there was again no overall genotype effect. Thus, in agreement with previous findings on lesion burden, inflammation is increased following hypoperfusion but not further exacerbated in TgSwDI mice.



◀ **Figure 5.10 The effect of hypoperfusion on contrast-enhanced T2* imaging.** Contrast-enhanced T2* MRI was performed in order to assess inflammation in vivo. T2* values from cortex and thalamus were normalised to the CSF and compared between groups. Hypointense tissue reflects greater retention of iron oxide and a higher degree of inflammation. Representative ce-T2* images from (A) wild type sham, (B) wild type hypoperfused, (C) TgSwDI sham and (D) TgSwDI hypoperfused mice. (E,F) Analysis of both cortical and thalamic regions of interest showed a greater degree of hypointensity in hypoperfused mice relative to shams, indicative of increased inflammation ($F_{(1,30)}=11.47$, $p<0.01$ and $F_{(1,30)}=5.74$, $p<0.05$ for cortex and thalamus respectively). There were no significant effects of genotype in either region studied. Data presented as mean \pm SEM, n=6-10 per group. * $p<0.05$, ** $p<0.01$.

5.3.6 Spatial learning, but not spatial memory, is impaired following hypoperfusion

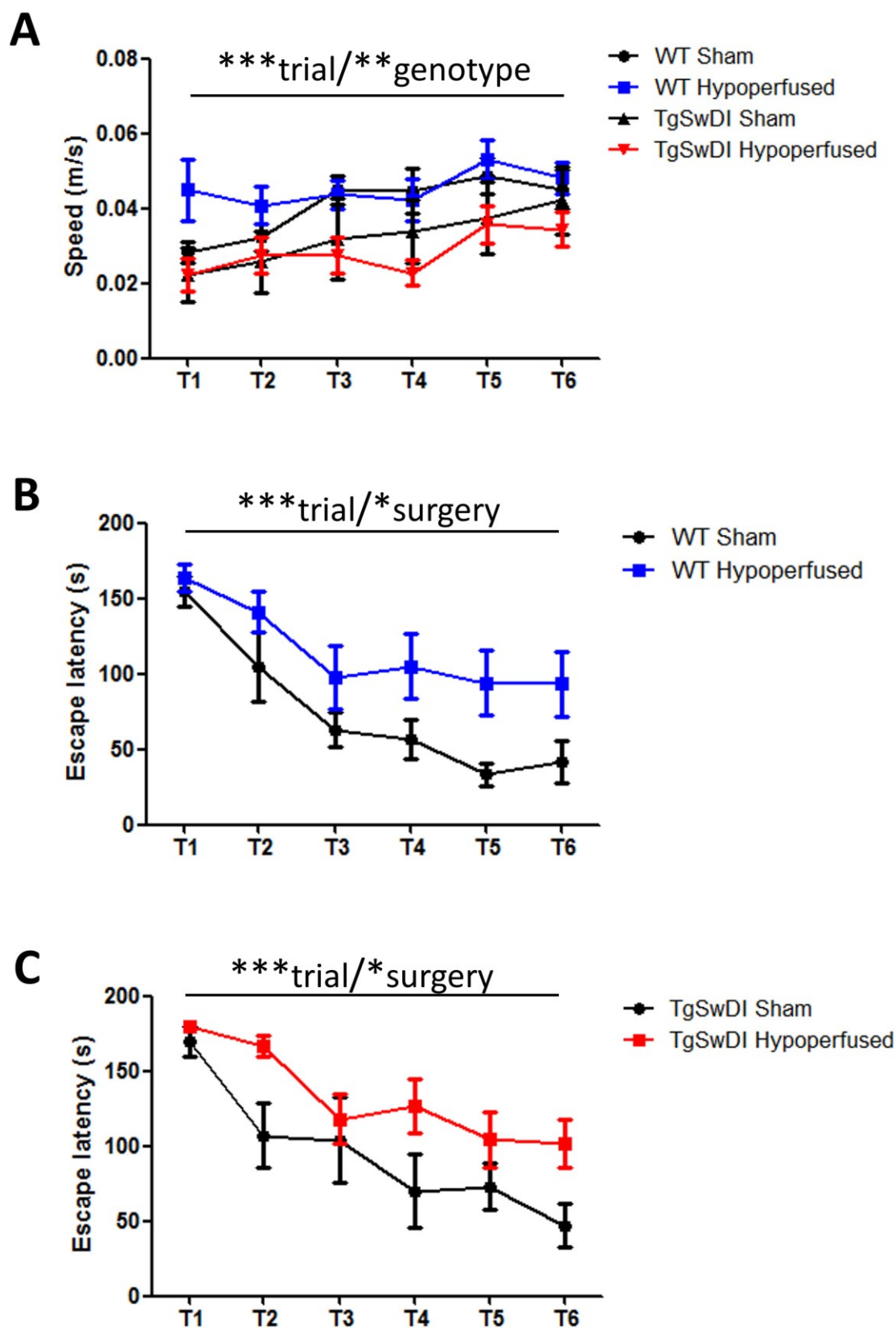
In order to determine if hypoperfusion also resulted in cognitive impairment in wild type and TgSwDI mice, mice were trained on the Barnes maze task of spatial learning and memory. Motor ability was first compared between groups to avoid confounds on subsequent measures. TgSwDI mice were found to move significantly slower than wild type mice ($F_{(1,30)}=8.239$, $p<0.01$) (Figure 5.11), therefore differences between wild type and TgSwDI could not be compared directly. There was no effect of hypoperfusion surgery on movement speed for either genotype. Time taken to enter the escape chamber (escape latency) was used as an index of learning. In wild type mice, there was a significant effect of trial ($F_{(3,149,8)}=19.216$, $p<0.001$), whereby escape latency decreased with increasing trial number; and a significant effect of surgery ($F_{(1,16)}=4.627$, $p<0.05$) whereby hypoperfused mice took longer to escape the maze relative to sham mice (Figure 5.11). Similar effects were observed in TgSwDI mice: there was a significant effect of trial ($F_{(3,4,47,9)}=4.627$, $p<0.05$) where escape latency decreased with increasing trial number; and a significant effect of surgery ($F_{(1,14)}=5.44$, $p<0.05$) whereby escape latency was increased in hypoperfused mice relative to shams (Figure 5.11). Therefore, whilst the performance of both hypoperfused and sham-operated mice improves over subsequent trials, reflected in decreasing escape latency, hypoperfused mice take longer to escape the maze, indicating an impairment on spatial learning.

In order to test long-term memory, a probe trial was performed 72 hours following the final training trial. The escape chamber was removed and mice were assessed based on their ability to remember the location of the escape hole (Figure 5.12). All groups spent significantly more time in the target quadrant relative to chance, with the exception of hypoperfused wild type mice ($46\pm 1\%$ vs 25% , $p<0.01$ for wild type shams; $43\pm 30\%$ vs 25% , $p>0.05$ for wild type

hypoperfused; $58 \pm 24\%$ vs 25% , $p < 0.05$ for TgSwDI shams; and $50 \pm 30\%$ vs 25% , $p < 0.05$ for TgSwDI hypoperfused mice). There were no significant overall effects of surgery or genotype on percentage time spent in the target quadrant. Together, these results indicate that long-term spatial memory was not impaired following hypoperfusion or in TgSwDI mice.

5.3.7 Reversal learning and memory are impaired in hypoperfused and TgSwDI mice

The reversal component of the Barnes maze task has been previously used to assess cognitive flexibility, through testing the ability of mice to forget a previously learned location and acquire a new location. In wild type mice, there was a significant effect of trial ($F_{(2,32)}=10.36$, $p < 0.05$) (Figure 5.13) whereby escape latency decreased with increasing trial; but no significant effect of surgery, indicating that the time taken to escape the maze was similar between sham and hypoperfused mice. In TgSwDI mice, there were no significant effects of trial or surgery, indicating that TgSwDI mice were unable to learn the reversal task. Analysis of the reversal probe indicated that only wild type sham mice spent significantly more time in the target quadrant than chance ($37 \pm 12\%$ vs 25% , $p < 0.05$), and that wild type hypoperfused, TgSwDI sham and TgSwDI hypoperfused mice all performed no better than chance ($27 \pm 11\%$ vs 25% , $p > 0.05$; $20 \pm 15\%$ vs 25% , $p > 0.05$; and $26 \pm 16\%$ vs 25% , $p > 0.05$ respectively) (Figure 5.14). Further comparison of time spent in the target quadrant indicated no significant overall effects of surgery or genotype. Together, the data suggests that although wild type hypoperfused mice are able to learn the reversal task, only wild type sham mice were able to learn and remember the new target location, and that all other groups are impaired on this measure of reversal memory.



◀ **Figure 5.11 Hypoperfusion causes deficits on spatial learning.** Performance on the Barnes maze task of spatial learning was assessed using escape latency at 10 weeks following hypoperfusion surgery. (A) Significant effects of trial and genotype were detected ($F_{(5,150)}=8.334$, $p<0.001$ and $F_{(1,30)}=8.239$, $p<0.01$) indicating that TgSwDI mice moved significantly slower than wild types, therefore wild type and TgSwDI mice were not compared. (B) In wild type mice, significant effects of trial and surgery on escape latency were detected ($F_{(3,1,49.8)}=19.216$, $p<0.001$ and $F_{(1,16)}=4.627$, $p<0.05$ respectively). (C) In TgSwDI mice, significant effects of trial and surgery on escape latency were detected ($F_{(3,4,47.9)}=4.627$, $p<0.05$ and $F_{(1,14)}=5.44$, $p<0.05$ respectively). Data presented as mean \pm SEM, n=6-10 per group. * $p<0.05$, ** $p<0.01$, *** $p<0.001$.

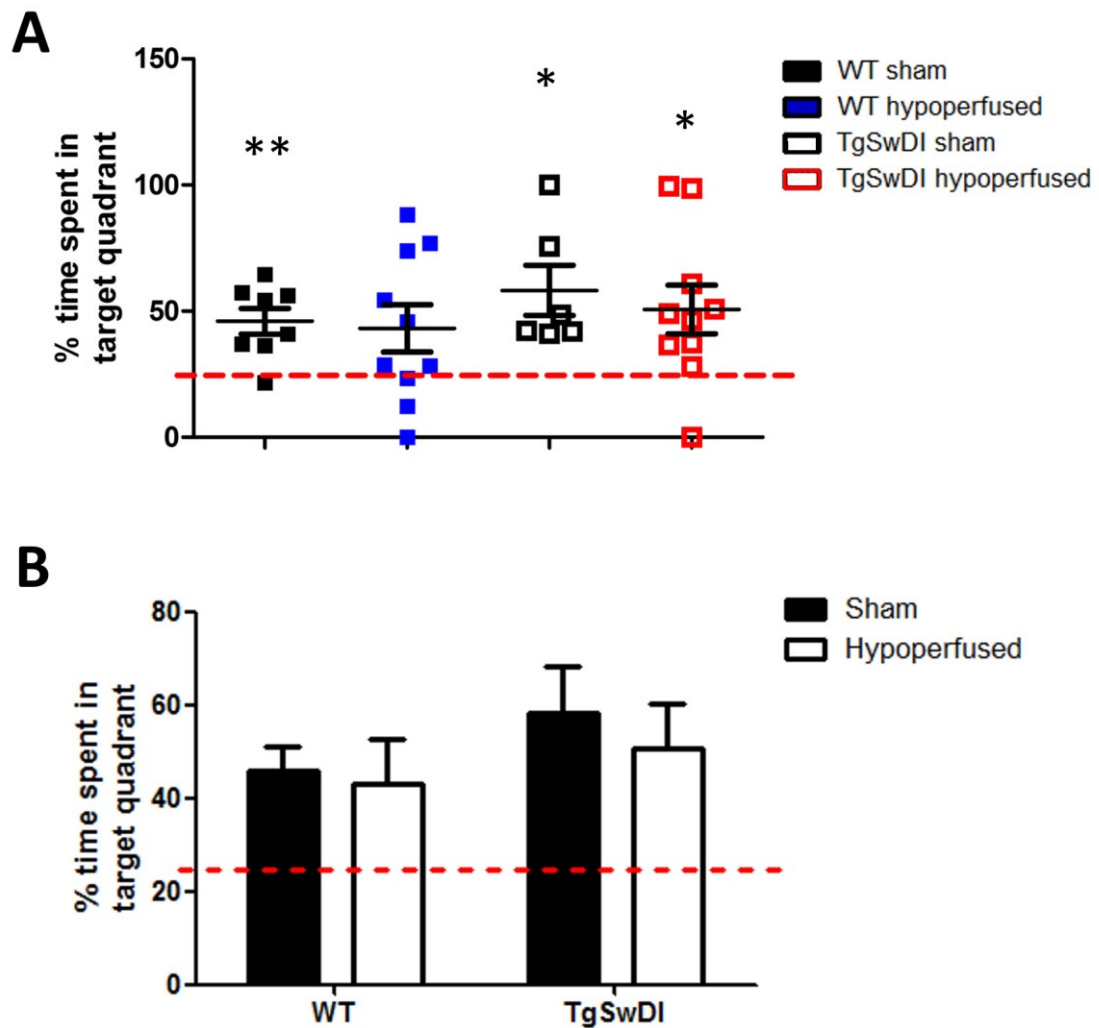


Figure 5.12 Hypoperfusion does not impair spatial memory. Spatial memory was assessed using a 72-hour delayed probe task, and mice were assessed based on percentage time spent in the target quadrant. (A) All groups performed significantly better than chance (indicated by dashed red line) and spent significantly more time in the target quadrant, with the exception of hypoperfused wild type mice. (B) No significant effects of hypoperfusion or genotype on percentage time spent in the target quadrant. Data presented as mean \pm SEM, n=6-10 per group. *p<0.05, **p<0.01.

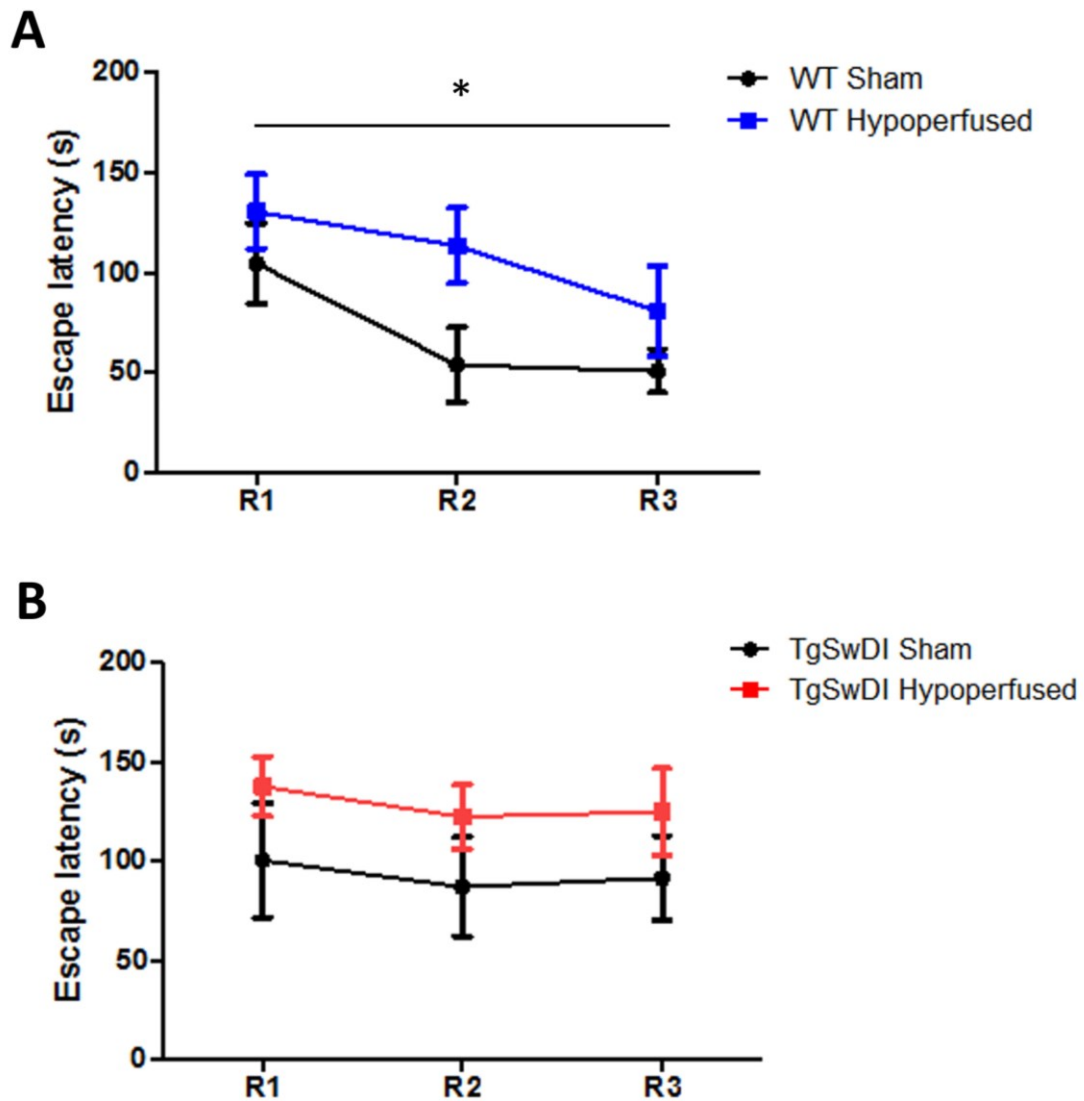


Figure 5.13 Reversal learning is impaired in TgSwDI mice. Mice were trained to learn a new escape chamber location in a reversal task on the Barnes Maze. (A) In wild type mice, a significant effect of trial was observed ($F_{(2,32)}=10.36$, $p<0.05$) indicating that escape latency decreased with increasing trial, however there was no effect of surgery. (B) In TgSwDI mice, no significant effects of trial or surgery were detected, indicating that TgSwDI mice were unable to learn the reversal task. Data presented as mean \pm SEM, n=6-10 per group. * $p<0.05$.

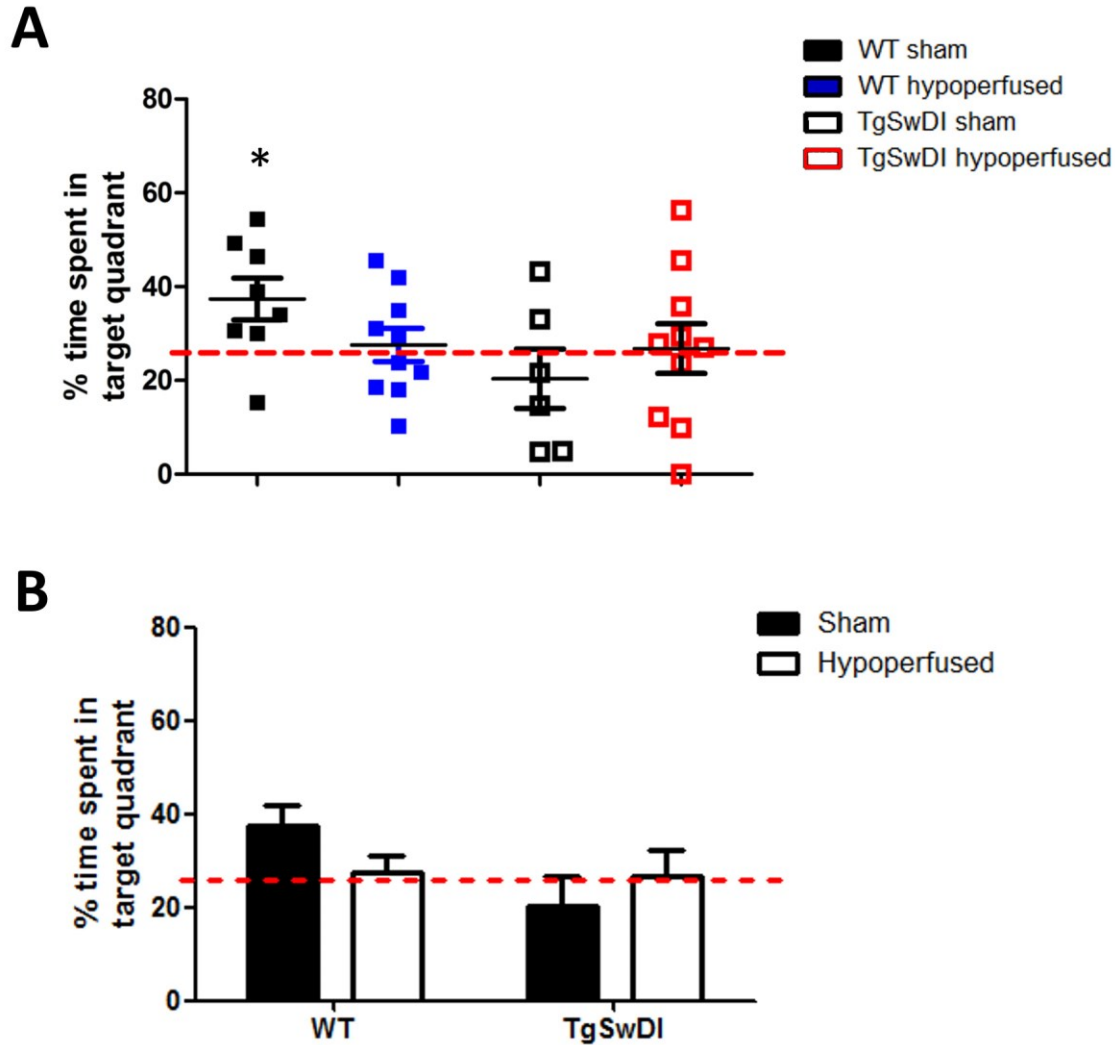


Figure 5.14 Reversal memory is impaired in hypoperfused and TgSwDI mice. Mice were assessed on percentage time spent in the target quadrant in a reversal probe task. (A) Only wild type sham mice performed better than chance (indicated by dashed red line) ($37 \pm 12\%$ vs 25% , $p < 0.05$; $27 \pm 11\%$ vs 25% , $p > 0.05$; $20 \pm 15\%$ vs 25% , $p > 0.05$; and $26 \pm 16\%$ vs 25% , $p > 0.05$ for wild type sham mice, wild type hypoperfused mice, TgSwDI sham mice and TgSwDI hypoperfused mice respectively). (B) There were no significant overall effects of surgery or genotype on percentage time spent in the target quadrant. Data presented as mean \pm SEM, $n = 6-10$ per group. $*p < 0.05$.

5.3.8 Markers of oxidative stress are increased following hypoperfusion

Oxidative stress is increased in cerebrovascular disease and is thought to contribute to disease progression (Liu and Zhang, 2012). In order to determine whether oxidative stress is increased following hypoperfusion and in TgSwDI mice, protein levels of several markers related to oxidative stress were assessed semiquantitatively using dot blot assay of total brain homogenates. All protein levels were normalised to a housekeeping gene loading control. Levels of NADPH oxidase 2 (NOX2) showed a significant increase following hypoperfusion surgery ($F_{(1,31)}=7.365$, $p<0.05$) but no effect of genotype (Figure 5.15). Analysis of levels of NADPH oxidase 4 (NOX4) revealed a significant interaction effect ($F_{(1,31)}=4.386$, $p<0.05$), post-hoc analyses indicated that NOX4 levels were significantly increased following hypoperfusion in wild type mice, but there was no effect of surgery in TgSwDI mice (Figure 5.16). Levels of 3-nitrotyrosine, a marker of oxidative damage, were also found to be significantly increased following hypoperfusion surgery ($F_{(1,31)}=5.061$, $p<0.05$) (Figure 5.17).

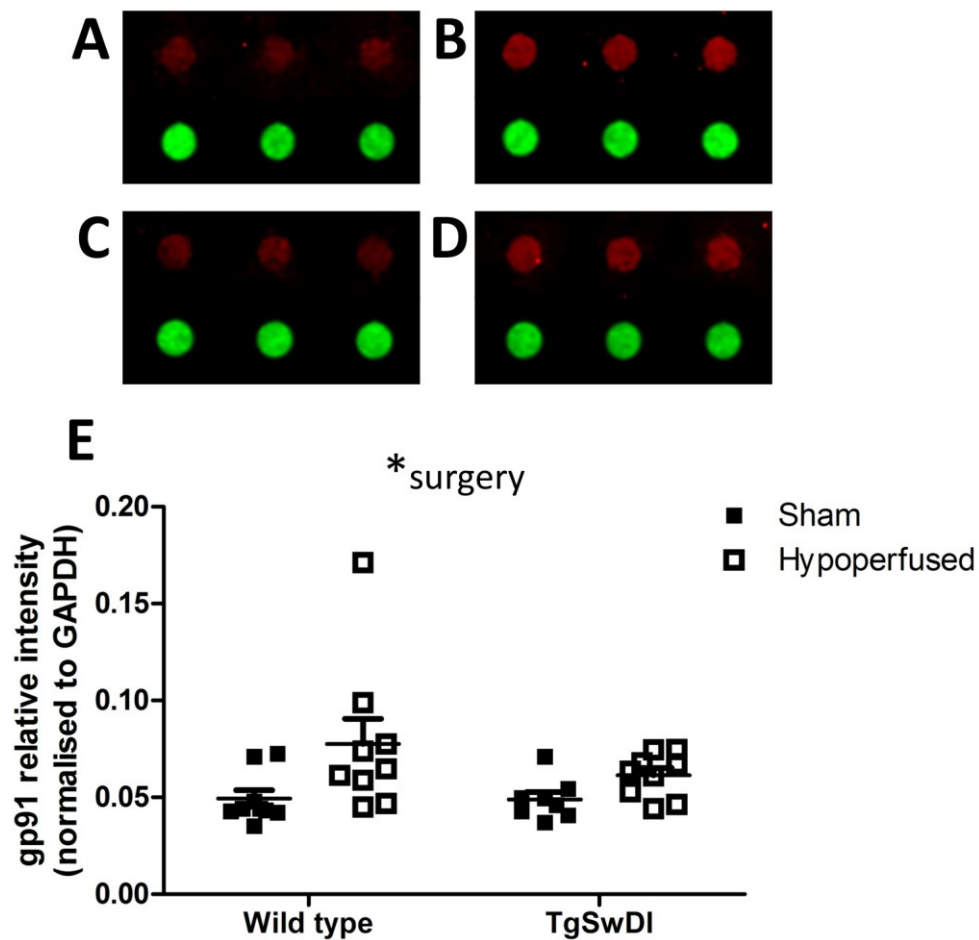


Figure 5.15 Hypoperfusion increases NOX2 expression. Levels of the NOX2 subunit gp91phox were assessed in whole brain homogenates using dot blotting. Representative dot blots showing NOX2 in red and GAPDH loading control in green from sham wild type mice (A), hypoperfused wild type mice (B), sham TgSwDI mice (C) and hypoperfused TgSwDI mice (D). (E) Hypoperfusion significantly increased the levels of NOX2 ($F_{(1,31)}=7.365$, $p<0.05$) but there was no effect of genotype. Data presented as mean \pm SEM, n=8-9 per group. * $p<0.05$.

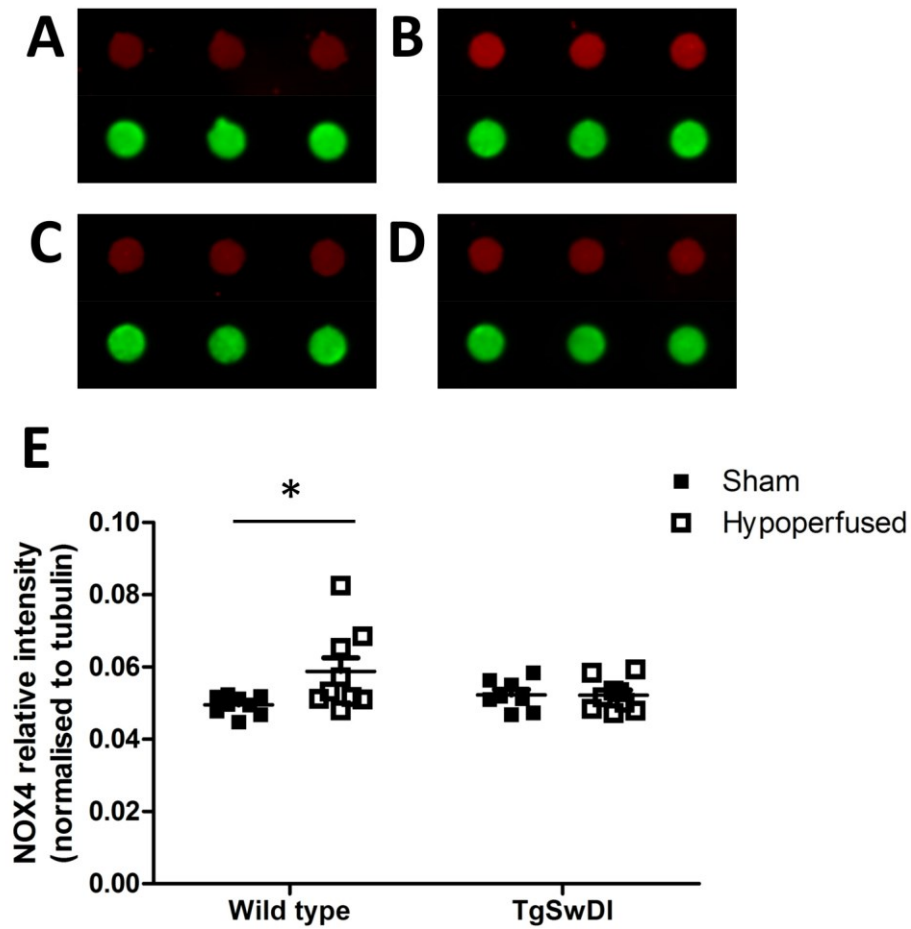


Figure 5.16 Hypoperfusion increases NOX4 expression in wild type mice. Expression of NOX4 was assessed in whole brain homogenates using dot blotting. Representative dot blots showing NOX4 in red and tubulin loading control in green from sham wild type mice (A), hypoperfused wild type mice (B), sham TgSwDI mice (C) and hypoperfused TgSwDI mice (D). (E) A significant interaction effect was detected ($F_{(1,31)}=4.386$, $p<0.05$). Post hoc analysis revealed a significant increase in NOX4 following hypoperfusion in wild type mice, but not in TgSwDI mice ($p<0.05$). Data presented as mean \pm SEM, n=8-9 per group. * $p<0.05$.

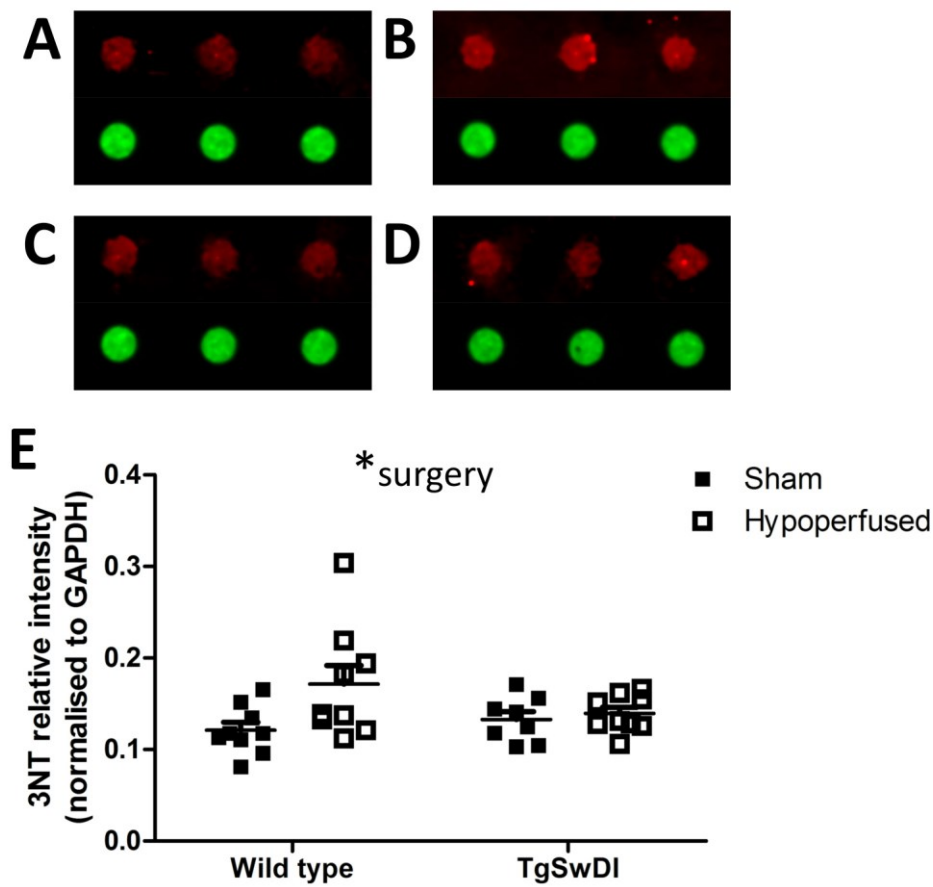


Figure 5.17 Hypoperfusion increases brain 3-nitrotyrosine content. Levels of 3-nitrotyrosine (3NT) were assessed in whole brain homogenates using dot blotting. Representative dot blots showing 3NT in red and GAPDH loading control in green from sham wild type mice (A), hypoperfused wild type mice (B), sham TgSwDI mice (C) and hypoperfused TgSwDI mice (D). (E) Hypoperfusion caused a significant increase in the levels of 3NT ($F_{(1,31)}=5.061$, $p<0.05$) but there was no effect of genotype. Data presented as mean±SEM, n=8-9 per group. * $p<0.05$.

5.4 Discussion

In the present study, modest reductions in cerebral blood flow were shown to induce cerebrovascular dysfunction, development of vascular lesions, inflammation and impairments on learning and memory in a mouse model. Contrary to the initial hypothesis, reducing cerebral blood flow in the TgSwDI mouse model of amyloid deposition did not result in further impairments on these measures. Finally, proteins related to oxidative stress were shown to be increased following hypoperfusion, and may be responsible for the induction of cerebrovascular pathology caused by reductions in cerebral blood flow.

5.4.1 Cerebral hypoperfusion surgery induces sustained reductions in cerebral blood flow

The reduction in blood flow following bilateral common carotid artery stenosis has been well characterised using laser speckle imaging and the results here agree with previously published findings of an approximately 30% reduction in flow from baseline (Shibata et al. 2004; McQueen et al. 2014). In the present study, ASL-MRI was also performed in order to detect blood flow changes in the thalamus and hippocampus, regions that are inaccessible with laser speckle imaging that only allows measurements from superficial cortex. Data from the hippocampus and thalamus indicated a reduction in flow of 30% and 24% respectively at 3 months following surgery in wild type mice. Measures of hippocampal perfusion obtained here with ASL are in good agreement with those from a recently published report of perfusion changes at early timepoints following hypoperfusion surgery. Hattori et al. (2016) used ASL to measure blood flow at 1 day through to 28 days following hypoperfusion surgery in the cortex and hippocampus. In the hippocampus Hattori et al. report an acute blood flow reduction of 50% at 1 day post surgery, which recovers to approximately 30% at 28 days. The findings presented here build on this work to include an even later timepoint of 3 months, and together demonstrate that although there is recovery from the initial acute phase of blood flow reduction,

this does not seem to continue past 28 days, and blood flow remains persistently reduced up to 3 months later. In addition, thalamic perfusion was also measured in the present study and was also found to be significantly reduced 3 months following hypoperfusion surgery, although the reduction was less pronounced. This may reflect differences in the vascular supply of this region, the thalamus is well supplied by both the ventral and dorsolateral thalamic arteries but also receives blood via the thalamoperforating artery (Dorr, Sled and Kabani, 2007), which originates from the vertebral artery and is thus not affected by the hypoperfusion procedure; although it is interesting to note that despite the milder reduction in flow, the thalamus is still vulnerable to vascular disruption (Holland et al. 2015). ASL perfusion data from this study and that of Hattori et al. (2016) confirm the ability of the hypoperfusion model to recapitulate the sustained pathological hypoperfusion that is observed on clinical imaging studies of cerebrovascular disease.

5.4.2 Hypoperfusion impairs neurovascular coupling

In the present study, cortical neurovascular coupling was found to be significantly attenuated at 3 months following cerebral hypoperfusion surgery. In response to whisker stimulation, perfusion in the barrel cortex increased by approximately 30% in sham-operated mice, but the magnitude of this increase was less than 20% in hypoperfused mice. Relatively few studies have examined the effect of chronic cerebral hypoperfusion on neurovascular function. One study that has utilised the permanent unilateral common carotid artery occlusion model (UCCAO) in mice showed using laser Doppler that blood flow responses to whisker stimulation were reduced from 18% of baseline in shams to just 6% in hypoperfused mice (Nishino et al. 2016). In the same UCCAO model, Tajima et al. (2014) also showed attenuated vasodilation of pial arteries in response to hypercapnia. Matin et al. (2016) also found that isolated penetrating arterioles showed decreased responses *ex vivo* to the vasodilator carbachol

following 8 weeks of BCAS in rat. Overall, hypoperfusion attenuates the ability of the cerebral vessels to modulate blood flow in response to a variety of vasoactive mediators. Matin et al. (2016) suggest a potential mechanism for this hypoperfusion-induced vascular impairment may be due to decreased expression of TRPV4 receptors on blood vessels, which bind epoxyeicosatrienoic acids (EETs) to modulate vessel diameter. EETs are released by astrocytic endfeet in response to neuronal activity (Bazargani and Attwell, 2016), and recent evidence suggests that expression of the astrocytic endfoot marker aquaporin-4 becomes reduced on cerebral blood vessels following hypoperfusion (Holland et al. 2015). In this thesis it was also shown that advanced age reduces the expression of aquaporin-4 on blood vessels (see Section 4.3.6), which was strongly associated with a reduction in neurovascular function. This age-related loss of astrocytic end foot contacts may be exacerbated by hypoperfusion to further impair neurovascular coupling. Disruption of the interface between astrocytes and blood vessels may impede the ability of vasoactive substances, secreted by astrocytes, to reach their vascular targets. Combined with a reduction in the expression of their receptors (such as TRPV4 above) on endothelial cells, this may contribute to the impairment on neurovascular coupling observed following hypoperfusion. This may be further exacerbated by astrocytic activation (Saggu et al. 2016; Holland et al. 2015).

An important consideration when reviewing data on neurovascular coupling is whether the findings reflect a true impairment of the cerebral vasculature or whether the neuronal signalling itself is reduced as a result of cerebral hypoperfusion. Although neuronal activity in response to whisker stimulation was not assessed in this study, evidence from 18F-FDG PET has shown that in the cortex, glucose uptake is not altered from baseline at 2 months following BCAS surgery (Nishio et al. 2010), an indication that neuronal activity does not change at this timepoint as a result of hypoperfusion. However, the same study did show reduced glucose

uptake at 6 months following hypoperfusion. Histological analysis of cortical neuronal density indicates that the number of neurons is unchanged following cerebral hypoperfusion (ElAli et al. 2013; Saggu et al. 2016). Nevertheless, given the longer duration of hypoperfusion and the more advanced age of the mice in this study, further measurements of neuronal activity or metabolism are warranted.

The finding that chronic cerebral hypoperfusion results in vascular dysfunction is also in agreement with findings from clinical studies. Disruption of cerebrovascular reactivity has been reported in carotid artery stenosis (Balucani et al. 2012), hypertension (Hajjar et al. 2014), leukoaraiosis (Sam et al. 2016a), vascular dementia (Vicenzini et al. 2007) and Alzheimer's disease (Glodzik et al. 2013). Furthermore, many studies report an association between the degree of vascular impairment and decline of cognitive performance (Balucani et al. 2012; Hajjar et al. 2014). Viticchi et al. (2012) report that decreased cerebrovascular reactivity could predict conversion from mild cognitive impairment to Alzheimer's disease. The relationship between vascular function and cognition is also supported by the findings in the present study, where spatial learning was also significantly impaired. Overall, this study is the first to present in vivo data on neurovascular coupling from the BCAS model of hypoperfusion, which strongly supports the idea that hypoperfusion impairs vascular function and is associated with cognitive decline.

5.4.3 Hypoperfusion induces vascular lesions and increased inflammation

Using a well-characterised structural T2 imaging approach, hypoperfusion was shown to induce the development of ischaemic and haemorrhagic lesions that were absent in sham mice. MRI findings were also subsequently confirmed using histological approaches. Together, this data extends the findings of Holland et al. (2015), who showed that the onset of lesion development was delayed, with very few lesions detectable at 1 month following surgery but

significant lesion burden at 6 months. The findings of the present study demonstrate that lesion onset is detectable at 3 months following hypoperfusion, indicating a progressive pattern of lesion development. The findings differ slightly from those of Holland et al. (2015) in that few haemorrhagic lesions were detected in hypoperfused mice in the present study, whereas haemorrhages were present in 15 out of 20 mice in Holland et al. It is plausible that haemorrhagic lesions exhibit a later onset relative to ischaemia, therefore the reduced duration of hypoperfusion in this study may be responsible for this difference. In conjunction with the development of vascular lesions, an increase in inflammation was also observed on contrast-enhanced T2* imaging, indicated by greater hypointensity in tissue due to retention of iron oxide by inflammatory cells. Microgliosis and astrogliosis are widely reported features of cerebral hypoperfusion models (Du et al. 2016; Saggu et al. 2016) and are likely to contribute to the onset of vascular lesions. Increasing reactive gliosis results in production of pro-inflammatory cytokines such as TNF- α , IL-1 β and IL-6 (Shi et al. 2016). Other pro-inflammatory mediators are also increased, in particular matrix metalloproteinases (MMPs) MMP-2 and MMP-9 are expressed by microglial, oligodendroglial and endothelial cells following cerebral hypoperfusion (Ihara et al. 2001, Seo et al. 2013). These degrade the basement membrane, leading to disruption of the blood-brain barrier and potentially contributing to the development of haemorrhagic lesions. Breakdown of the blood-brain barrier allows circulating leukocytes to infiltrate brain parenchyma, potentiating the pro-inflammatory tissue environment. Several studies have targeted inflammatory pathways to reduce the development of white matter lesions. Knockout of the adenosine A2A receptor increased mRNA levels of pro-inflammatory cytokines, resulting in more severe white matter lesions and greater cognitive impairment compared to wild type mice following BCAS surgery (Duan et al. 2009). Inhibition of the chemoattractant MCP-1 was also shown to reduce microglial

activation, secretion of pro-inflammatory cytokines and white matter rarefaction following hypoperfusion (Shi et al. 2016). However, less is known about the impact of inflammation on the development of vascular lesions, which occurs in the more chronic phase of hypoperfusion relative to the studies detailed above. Holland et al. (2015) demonstrated an increase in Iba1+ve microglia surrounding areas of vascular disruption, as well as an increase in reactive astrogliosis at 6 months following hypoperfusion. In this study, a contrast-enhanced T2* imaging approach was used for the first time in the BCAS model to detect ongoing inflammation in the cortex and thalamus, areas that have previously been shown to be vulnerable to ischaemic and haemorrhagic lesions. In the same mice, development of vascular lesions was also shown to increase following hypoperfusion. Increased inflammatory processes and the activation of inflammatory cells may therefore precede and contribute to the development of vascular lesions.

5.4.4 Behavioural deficits are induced following cerebral hypoperfusion

In the present study, hypoperfusion was shown to cause an impairment on spatial reference learning, but not spatial memory. Hypoperfused mice were also impaired on a more challenging reversal memory task. Current literature suggests that hypoperfusion induces progressive impairments on cognitive tasks that increase with increasing duration of hypoperfusion. Coltman et al. (2011) found that after 1-2 months hypoperfusion, mice were impaired on measures of spatial working memory in the radial arm maze, but that spatial reference learning was intact when assessed with the Morris water maze. The Barnes maze used in the present study is considered a dry land version of the Morris water maze, but spatial reference learning was significantly impaired in hypoperfused mice in the present study. In another study, Nishio et al. (2010) measured spatial reference learning in mice at 5-6 months following hypoperfusion and show that hypoperfused mice take longer to reach the target and make more

mistakes, indicating an impairment on spatial reference learning at this duration. The current data provides an intermediate timepoint of 3 months hypoperfusion and suggests this is the duration at which deficits on spatial reference learning start to appear. When assessed with a 72 hour delayed probe task, spatial reference memory was not impaired in hypoperfused mice in the present study, and was also not impaired on a 24 hour probe in that of Coltman et al. (2011). After 6 months of hypoperfusion however, spatial reference memory was impaired on a water maze probe task (Holland et al. 2015). The data suggest that spatial reference memory is more robust to cerebral hypoperfusion and that deficits may only become apparent following chronic hypoperfusion. Vulnerability of the underlying circuitry may contribute to these differences. Short durations of hypoperfusion result in white matter damage but not hippocampal pathology. Measures of spatial working memory rely on rapid communication between brain regions and so are dependent on white matter integrity; whereas reference learning is suggested to be a hippocampal-dependent task (Nishio et al. 2010). Hippocampal pathology was not assessed in the present study so contributions of the circuitry involved for each task cannot be determined directly. However, in line with progressive onset of pathological lesions, the burden of cognitive deficits also increases at longer durations of hypoperfusion.

In addition to spatial reference learning and memory tasks, an additional reversal task was performed in the present study. Reversal learning and memory has been used to test executive function and cognitive flexibility (O’Leary and Brown, 2013) by assessing the ability of the mice to learn a new location of the escape chamber. Both sham and hypoperfused wild type mice were able to learn the new location indicating that reversal learning was not impaired, despite impairments on the original spatial learning task. This may reflect the shorter duration of the reversal task, as after day 3 on the original spatial learning task hypoperfused mice

plateau in their performance and do not show further improvement, whilst sham-operated mice continue to reduce the time it takes to escape the maze. However, when memory for the new location is tested, hypoperfused mice are impaired relative to sham mice. The use of this more challenging reversal memory task therefore uncovers a deficit in cognition that is not detectable using a spatial memory task alone. This deficit may reflect the reductions in blood flow that affect the anterior regions of the brain involved in executive function, such as the frontal cortices and striatum.

5.4.5 Amyloid did not exacerbate vascular disruption, inflammation or cognitive abilities following cerebral hypoperfusion

In addition to investigating the effects of hypoperfusion on the cerebral vasculature, the current study also aimed to determine whether the presence of amyloid deposition would exacerbate vascular pathology in hypoperfused mice. TgSwDI mice were not further impaired than wild type mice on any measure assessed in the study, but appeared to be impaired to the same extent as wild type mice despite hypoperfusion occurring after the onset of amyloid deposition.

Studies looking at the effect of hypoperfusion in amyloid-expressing lines have predominantly focused on the interaction between hypoperfusion and the processing of APP and formation of A β plaques. Previous reports indicate that the induction of hypoperfusion, hypertension or hyperhomocysteinemia induces a redistribution of amyloid from the parenchyma to the vasculature (Okamoto et al. 2012; Sudduth et al. 2014; Kruyer et al. 2015); however changes in total amyloid burden are inconsistently reported, having been shown to either increase (Zhiyou et al. 2009), decrease (Yamada et al. 2011) or remain constant (Okamoto et al. 2012; Sudduth et al. 2014; Kruyer et al. 2015). Findings from the present study utilising 6E10 immunohistochemistry indicate that hypoperfusion did not alter the total deposition of amyloid, however, a more in depth biochemical quantification of distinct amyloid species is required.

This would allow investigation of the vascular pool of amyloid, as well as any changes in soluble amyloid or A β 1-40/A β 1-42 that would not have been detected using the current method. In the present study, the primary focus was the impact of amyloid pathology on vascular parameters, and was investigated using the well-characterised TgSwDI model, which develops diffuse parenchymal plaques in the cortex, as well as both vascular and parenchymal fibrillar amyloid deposition in the thalamus (Davis et al. 2004, Miao et al. 2005). Previous work in the TgSwDI model has indicated that neurovascular coupling is not impaired at 12 months of age relative to wild type mice (Section 4.3.4), although amyloid deposition in this model was associated with prominent microgliosis and astrogliosis (Sections 4.3.6 and 4.3.7) which may predispose TgSwDI mice to subsequent vascular disruption. The present study sought to determine whether hypoperfusion would impair neurovascular coupling to a greater extent in TgSwDI mice than wild type mice, but this was not found to be the case. The lack of vascular amyloid accumulation in the cortex, and the low concentration of soluble amyloid in this model may underlie this finding. The lack of synergistic effect observed between vascular pathology and amyloid deposition in this model is also in agreement with the study by Faraco et al. (2016), who showed that inducing hypertension using slow-pressor angiotensin-II administration in TgSwDI mice did not exacerbate neurovascular dysfunction. When an acute dose of angiotensin-II was administered intravenously, further disruption of the vascular response to whisker stimulation was observed, although this acute insult is arguably not representative of clinical cerebrovascular disease. Okamoto et al. (2012) demonstrate that 3 months following BCAS surgery, the number of microinfarcts is increased in TgSwDI mice but no microinfarcts were detectable in wild type mice. However, in the present study, the number of lesions detected with MRI was similar between wild type and TgSwDI mice. The more advanced age of the mice in this study (9 months at surgery vs 5 months in Okamoto et al. 2012) may have

made wild type mice more vulnerable to vascular damage following hypoperfusion, however an important note is that blood flow reductions in wild type mice in the study by Okamoto et al. were very subtle, at just 15% reduction from baseline. This is much less than typically reported for the BCAS model (~30% reduction), so it is possible that wild type mice were not subjected to the same degree of hypoperfusion from the outset of the study. Okamoto et al. also report an increase in vascular amyloid deposition following cerebral hypoperfusion. The TgSwDI model develops microvascular amyloid accumulation in the thalamus and it may be reasonable to expect that an increase in microvascular amyloid may result in an increased burden of microhaemorrhage in this region (Yates et al. 2013). Structural T2 imaging may not be sufficiently sensitive to detect small areas of blood-brain barrier breakdown, and future histological assessment of IgG extravasation or Perl's staining would confirm whether hypoperfusion induced any subtle haemorrhagic pathology. Inflammation, as assessed in vivo using contrast-enhanced T2* imaging, was also not found to be exacerbated in TgSwDI mice following hypoperfusion. It is also worth noting that inflammation in sham TgSwDI mice was not different to sham wild type mice. This is surprising, as the presence of amyloid has been shown to cause an increase in Iba1 +ve microglia and GFAP +ve astrocytes (Section 4.3.7 and 4.3.6); however it is an indication that hypointensities measured with T2* may represent a distinct inflammatory phenotype that is only induced following hypoperfusion. The iron accumulation detected with T2* may occur through phagocytosis by perivascular macrophages or infiltration of circulating leukocytes, rather than through microglial dependent processes, in which case it may not be exacerbated by the increased number of Iba1 +ve cells in the brains of TgSwDI mice. The observation that lesion burden is also not different between wild type and TgSwDI mice following hypoperfusion indicates that a similar degree of blood-brain barrier breakdown has occurred, and therefore accumulation of iron due to passive diffusion into the

parenchyma would also be expected to be similar between genotypes. In TgSwDI mice, it may be expected that the increased microglial and astrocyte numbers may lower the threshold for vascular lesions following hypoperfusion through secretion of proinflammatory cytokines which disrupt the blood-brain barrier and neurovascular unit. Further analysis of cytokine and chemokine secretion from these cell populations would yield valuable information about the interaction between amyloid and vascular pathology on the inflammatory response.

In line with the lack of exacerbated pathology in TgSwDI mice following hypoperfusion, there was also no impairment observed on spatial memory in hypoperfused TgSwDI mice. Differences in motor ability meant that spatial learning could not be compared between wild type and TgSwDI mice, however there was still a significant effect of hypoperfusion on escape latency for both genotypes. Escape latency was used as the dependent measure for this Barnes maze task as it is straightforward to quantify and does not require interpretation by the assessor so is less susceptible to experimenter bias. However, in this particular experiment differences in movement speed precluded the use of this measure to directly compare wild type and TgSwDI groups. In future, an alternative measure of choice accuracy, such as search strategy or number of errors, could be used to detect differences in spatial learning that are independent of motor ability. On the reversal learning task, both sham and hypoperfused TgSwDI mice were impaired and unable to learn the new location of the escape chamber, however this was not exacerbated by hypoperfusion. Since TgSwDI mice were unable to learn the new location, deficits on reversal memory are difficult to assess. Pimentel-Coehlo, Michaud and Rivest (2013) demonstrate a small synergistic effect of one vessel occlusion and APPSwe/PS1 genotype on spatial learning. APPSwe/PS1 one vessel occlusion mice were initially impaired on measures of spatial learning but further training ameliorates this difference. Yamada et al. (2011) performed the Barnes maze 6 months following BCAS surgery in wild type and J20

mice aged 8 months, and showed impaired performance in combined J20/BCAS mice relative to other groups, although motor differences were not assessed. No effect of the combination of J20 and BCAS was observed on long-term memory in this study, in line with findings reported here. An important difference between the transgenic models used in the present study and those reported in the literature is the extent of APP expression. The TgSwDI model is not an overexpressing line, and expression of the human mutated form of APP is 50% below that of endogenous mouse APP (Davis et al. 2004). J20 mice and APPSwe/PS1 both overexpress APP (Mucke et al. 2000; Jankowsky et al. 2004). In addition, hypoperfusion has been shown to further increase APP expression (Salvadores, unpublished; Bennett et al. 2000) leading to subsequent amyloidogenic cleavage by β -secretase (Sun et al. 2006). If the synergistic effect of hypoperfusion and APP genotype is mediated through APP or amyloid toxicity, the differences in baseline expression of APP may explain why no further effect of hypoperfusion was observed in TgSwDI mice.

5.4.6 Vascular dysfunction following cerebral hypoperfusion may be mediated by increased oxidative stress

Overall, the data presented in this study suggest that chronic cerebral hypoperfusion results in activation of inflammatory processes, impaired neurovascular function and the development of vascular lesions, to ultimately result in impaired cognitive ability. In order to investigate what pathological processes may underlie this cascade of events, the extent of oxidative stress was determined. The protein levels of NADPH oxidase 2 (NOX2), NADPH oxidase 4 (NOX4) and 3-nitrotyrosine (3NT) were all increased following hypoperfusion, indicating oxidative stress is increased in brain tissue following 3 months cerebral hypoperfusion. In a rat model of bilateral common carotid artery occlusion (BCCAO), Lapi et al. 2012 showed that ROS production was increased immediately following the occlusion, and increased further upon

removal of the occluding clamps and reperfusion. In the BCAS model, at 3 weeks following the hypoperfusion surgery Dong et al. (2011) detected increased levels of 3-nitrotyrosine and increased NADPH oxidase activity in mouse brain, although it was not investigated which isoform(s) was responsible for this increase. Lipid peroxidation and oxidative DNA damage were also shown to progressively increase over 28 days following ligation of both common carotid arteries in rat, although this model shows a more severe initial reduction in blood flow of 90%, recovering to approximately 70% of baseline by 28 days (Ueno et al. 2015). The initial increase in ROS/RNS production may be mediated by changes in shear stress as a result of reductions in blood flow (Rochfort et al. 2015). In vitro experiments have highlighted that following shear stress alterations, lectin-like oxidized low density lipoprotein receptor-1 (LOX-1) on endothelium can activate NOX, resulting in the release of superoxide and pro-inflammatory cytokines (Lubrano and Balzan, 2016). Importantly, findings from the present study indicate that increased oxidative stress persists into the chronic phase, and was still detectable 3 months after hypoperfusion surgery. Investigation at this later timepoint is vital to understanding the effects of chronic, sustained hypoperfusion, and better recapitulates human cerebrovascular disease where pathology may evolve over many years.

Expression of both NOX2 and NOX4 was found to be increased following hypoperfusion, although the roles of NOX2 and NOX4 may be quite distinct. NOX2 is one of the main producers in the brain of the free radical superoxide. Superoxide is highly reactive and can rapidly sequester nitric oxide (NO), a molecule that is critically important for vasodilation. The increased expression of NOX2 may therefore provide a mechanism by which neurovascular coupling can become impaired, through reduced activity of NO on endothelium and therefore impaired vasodilation. NOX2 is expressed in astrocytes and may be upregulated following ischaemia (Li et al. 2014), increased production of superoxide by astrocytes and in astrocytic

endothelium is therefore likely to have a direct effect on endothelial reactivity, given their close structural association and direct role in neurovascular coupling (Otsu et al. 2015). As outlined in Section 4.3.6, functional communication between astrocytes and endothelial cells appears critical for neurovascular function, and establishing the impact of increased superoxide production by astrocytes may be an important avenue for future exploration. Superoxide is also able to oxidatively inactivate tetrahydrobiopterin (BH₄), a cofactor that is critical for eNOS activity (Landmesser et al. 2003). This results in eNOS uncoupling, causing a switch in eNOS activity whereby NO production is reduced and superoxide radicals are generated instead (Santhanam et al. 2015). The reaction of superoxide with NO results in the formation of peroxynitrite, a potent mediator of oxidative damage and protein nitration. Peroxynitrite has been shown to nitrate prostacyclin synthase (Zou, 2007), a precursor for the vasodilator prostaglandin. Interestingly, substantial evidence implicates the activity of NOX2 as a key mediator of amyloid-induced toxicity. Application of soluble amyloid to cerebral vasculature has been shown to induce ROS production through NOX2 and attenuate vascular function (Park et al. 2005). Han et al. (2015) also demonstrate that cerebral amyloid angiopathy exerts detrimental effects on vascular function through increased NOX2 activity. Antioxidant therapy has also been shown to attenuate pathology in amyloid transgenic mice (Jiao et al. 2015). In the present study, although there was an overall increase in NOX2 following hypoperfusion, we did not observe increased levels of NOX2 expression in TgSwDI mice relative to wild type mice, as might be predicted from the literature. However, there are two likely reasons for this finding. The first is that the levels of soluble amyloid in this model are low and therefore unlikely to cause large changes in NOX2 expression. The second is that vascular amyloid in this model is predominantly restricted to the thalamus. For quantification of oxidative stress markers, whole brain homogenates were used, which may dilute the effect of thalamic vascular

amyloid on NOX2 expression. Previous work using vessel-enriched fractions has indicated an increase in NOX2 in TgSwDI mice that was exacerbated following hypoperfusion (Salvadores), and immunostaining for the p47 subunit of NOX2 has already indicated a significant increase in thalamic expression relative to wild type (Section 4.3.8). The observation that NOX2 was not increased in this study may therefore arise through technical limitations of the approach used to measure NOX2 levels. Parenchymal amyloid is deposited in the cortex of these mice, although previous analysis indicated that this did not increase the expression of p47 relative to wild type, in line with findings that vascular amyloid is the more potentially toxic species (Kimbrough et al. 2015). The lack of difference in NOX2 levels between genotypes also supports the observation that neurovascular coupling was not further impaired in TgSwDI mice relative to wild types.

Whilst there is a clear association between NOX2 and pathological production of ROS, the contribution of NOX4 is less clear, with some reports indicating NOX4 as a potent producer of superoxide, while others suggest a neuroprotective role. Basuroy et al. (2009) identify NOX4, and not NOX2, as the primary source of superoxide production in cultured endothelial cells in response to the pro-inflammatory cytokine TNF- α . Kuroda et al. (2014) demonstrate strong NOX4 expression in pericytes in culture and also in the peri-infarct region of mice subjected to middle cerebral artery occlusion. They go on to demonstrate that in cultured pericytes, NOX4, and not other NOX isoforms, mitochondria or xanthine oxidase, produces superoxide which is increased in response to hypoxia. NOX4 expression in pericytes was also associated with cellular proliferation, in keeping with a role for NOX4 in angiogenesis. Following cerebral ischaemia in mice NOX4 is detected in capillaries in the peri-infarct region (Vallet et al. 2005), and microarray data from our lab has indicated that pro-angiogenic pathways are strongly upregulated 72 hours following hypoperfusion (Reimer et al. 2011).

Despite the established physiological role of NOX4 in angiogenic processes (Craig et al. 2011), it is unclear what the impact of pathologically increased NOX4 expression is on the cerebral vasculature. Nishimura et al. (2016) show that genetically overexpressing NOX4 in pericytes increases infarct volume and BBB breakdown following middle cerebral artery occlusion, mediated by increased phosphorylation of NFκB leading to increased activity of MMP-9. Inhibition of NOX4 either genetically or pharmacologically also offered significant protection from oxidative stress and neuronal apoptosis following ischaemic stroke in mice (Kleinschnitz et al. 2010). However, evidence also suggests that NOX4 activity may be protective (Guo and Chen, 2015), owing to the production of hydrogen peroxide rather than superoxide, which does not form peroxynitrite but has instead been shown to induce eNOS activity to produce NO (Cai et al. 2003). Studies looking at NOX4 following hypoperfusion are limited. Choi et al. (2014) found that levels of NOX4 were unchanged in hippocampal neurons after 15 weeks in the 2VO model, but did not investigate expression in the vasculature. In the present study, NOX4 was increased in whole brain homogenates after 3 months, but the cellular localisation was not determined. NOX4 is reported to induce angiogenesis through activation of eNOS (Craig et al. 2011), however the additional presence of NOX2 and increased production of superoxide may deplete the eNOS cofactor BH₄, resulting in eNOS uncoupling. Production of superoxide (rather than NO) by eNOS may contribute to further oxidative damage and explain why typically vasoprotective NOX4 may become pathogenic. Clearly, there is a need for further characterisation of NOX4 responses to hypoperfusion, and whether its effects are protective or not. Interestingly, NOX4 was not found to be increased in TgSwDI mice following hypoperfusion. The reason for this difference is currently unclear, although it may reflect a loss of the protective angiogenic response caused by vascular disruption as a result of amyloid accumulation.

It is conceivable that although expression of NOX isoforms is increased, their activity and production of superoxide may remain unchanged following cerebral hypoperfusion. However, the levels of nitrated proteins assessed with 3-nitrotyrosine were also increased following hypoperfusion, indicative of nitrosative damage caused by peroxynitrite. Peroxynitrite is a product of superoxide and NO, and is not specific to NOX activity. It is also plausible that superoxide may be generated from mitochondria or xanthine oxidase activity following hypoperfusion, rather than NOX isoforms. The use of a NOX inhibitor following hypoperfusion would enable the contribution of this specific superoxide source to be determined.

5.4.7 Conclusions

Based on the data presented in this study, a cascade of pathological events leading to cognitive decline can be proposed (Figure 5.18). Following hypoperfusion, the upregulation of NOX2 and NOX4 result in the increased production of reactive oxygen species and a state of oxidative stress. ROS/RNS induce endothelial dysfunction and inflammation, which in turn is able to generate more ROS/RNS. Continued disruption of endothelial function leads to impairment of neurovascular coupling, exacerbates tissue hypoperfusion and leads to ischaemic events. Additional ROS/RNS and inflammatory mediators also disrupt the blood-brain barrier causing haemorrhagic pathology. The accumulation of vascular lesions and progressively disrupted cerebrovascular function finally results in cognitive impairment. Targeting sources of ROS/RNS following hypoperfusion may prevent the onset of vascular dysfunction. Reduction of oxidative stress may therefore represent a promising therapeutic target to prevent the development of vascular lesions and cognitive impairment in chronic cerebral hypoperfusion. In the next study, the effect of apocynin, a proposed NOX inhibitor, on vascular dysfunction and cognition was investigated in the cerebral hypoperfusion model.

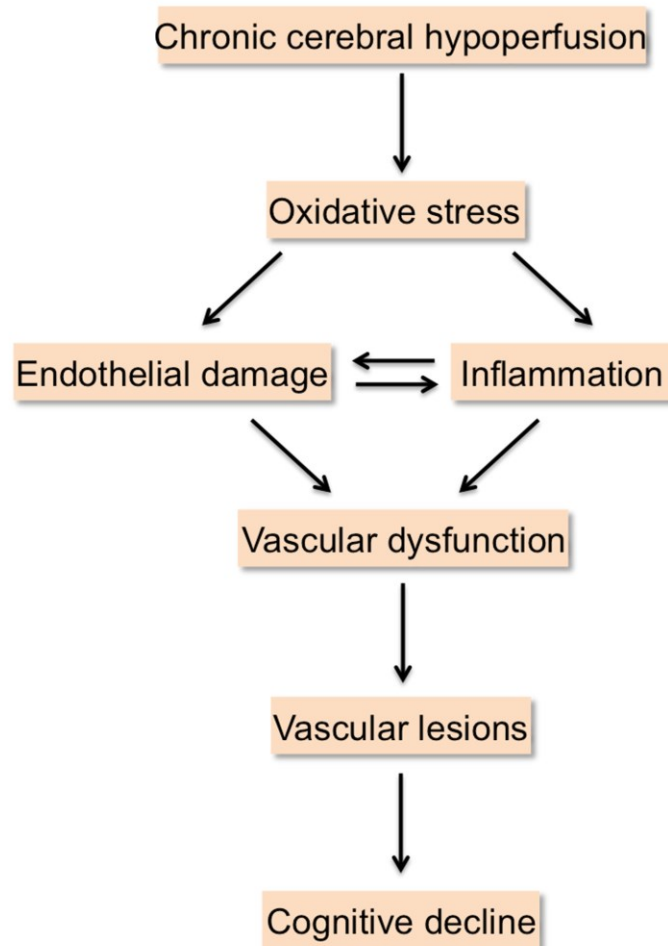


Figure 5.18 Proposed pathway of pathological events following chronic cerebral hypoperfusion.

Chapter 6.

The effect of apocynin on vascular function and cognition following cerebral hypoperfusion in TgSwDI mice

The effect of apocynin on vascular function and cognition following cerebral hypoperfusion in TgSwDI mice

6.1 Introduction

In the previous studies in the thesis it was demonstrated that chronic cerebral hypoperfusion in the TgSwDI mouse model causes impaired neurovascular coupling, promotes the development of vascular lesions and results in cognitive decline. Vascular impairments were associated with a concurrent increase in oxidative stress markers NADPH oxidase 2 and 3-nitrotyrosine, indicating ongoing oxidative stress in the brains of chronically hypoperfused TgSwDI mice. Mouse models of cerebral amyloid angiopathy such as the TgSwDI and the Tg2576 have been consistently associated with an increase in NOX2 activity, and NOX2 is considered a key driver of amyloid-mediated vascular dysfunction (Han et al. 2015; Park et al. 2014). Whilst cerebral hypoperfusion is associated with increased production of ROS (Liu and Zhang, 2012), the source of ROS production has not been proven. Reactive oxygen species induce endothelial dysfunction by disrupting nitric oxide signalling, which may eventually lead to impairments of neurovascular coupling and initiate the onset of vascular lesions and cognitive decline. Previous studies have indicated that antioxidant therapy may be beneficial in models of hypoperfusion (Xu et al. 2010), and that targeting NOX2 may be beneficial in mouse models of vascular amyloid (Han et al. 2015). Apocynin, a natural organic compound isolated from the native medicinal plant *Picrorhiza kurroa*, is reported to inhibit the assembly of the active NOX complex, thus preventing its activation and production of reactive oxygen species (Johnson et al. 2002). Given the evidence linking NOX activity and vascular dysfunction in amyloid-expressing transgenic mouse lines, the present study sought to determine whether NOX activity may also drive pathological ROS production and vascular dysfunction following

cerebral hypoperfusion. This study investigated whether pharmacological inhibition of NOX activity in TgSwDI mice would result in improved vascular function and protection from vascular lesion development and cognitive impairment.

6.1.1 Hypothesis

This study tests the hypothesis that activation of NOX following cerebral hypoperfusion drives neurovascular dysfunction, development of vascular lesions and cognitive decline; and that treatment with the NOX inhibitor apocynin will ameliorate these pathological alterations.

6.1.2 Aims

The aim of the study is to compare non-treated and apocynin-treated TgSwDI mice on measures of neurovascular coupling, vascular lesion development, inflammation and cognition following cerebral hypoperfusion.

6.2 Methods

6.2.1 Animals

Male heterozygous TgSwDI mice were used in this study for in vivo experiments and histopathology (n=38). An additional cohort was also included for generation of tissue for biochemical assays (n=17). Five mice in the study had to be singly housed due to aggressive fighting behaviour, but wherever possible animals were group housed. Mice were maintained on a 12:12hr light/dark cycle and had access to food and water *ad libitum*. All experiments were conducted in accordance with the Animals (Scientific Procedures) Act 1986 and local ethical approval at the University of Edinburgh and were performed under personal and project licenses granted by the Home Office. All data collection and analysis was performed by experimenters blind to the surgical, genetic and treatment status of the mice. N numbers were selected based on power analysis of previously collected ASL-MRI data from the thalamus (as MRI is the most variable dataset). To achieve a significance value of $p < 0.05$ at a power of 0.8, a minimum group size of n=8 was required.

6.2.2 Chronic cerebral hypoperfusion surgery

Hypoperfusion surgery was performed when mice were 8-9 months of age, after the onset of cerebral amyloid deposition. Surgery was performed according to Methods section 2.2. One TgSwDI mouse was culled during surgery due to excessive bleeding. Following surgery, mice were placed in an incubator to recover from anaesthesia, and their subsequent recovery from surgery was monitored closely over the next 3 days. Five mice showed poor recovery following the surgery and were culled. One sham-operated mouse was also found dead 9 weeks following surgery. Final numbers for in vivo experiments were n=6 (sham non-treated mice), n=10 (hypoperfused non-treated mice), n=6 (sham apocynin-treated mice) and n=9 (hypoperfused

apocynin-treated mice). Final numbers for the biochemistry cohort were n=8 (hypoperfused non-treated) and n=9 (hypoperfused apocynin-treated).

6.2.3 Apocynin administration

Apocynin treatment commenced immediately following hypoperfusion surgery. Apocynin was administered to the mice via their drinking water at a dose of 30mg/kg/day. Apocynin stock solution was prepared by dissolving apocynin (Sigma, UK) in drinking water heated to 60°C to aid dissolution. Aliquots of apocynin stock solution were then frozen at -20°C for storage. Working apocynin solution was then prepared using thawed stock solution diluted to 1.5mM. Non-treated mice were given regular drinking water provided by the animal house. Apocynin and non-treated drinking water was replaced every 2-3 days and water consumption of each cage was recorded simultaneously.

6.2.4 In vivo vascular imaging

In vivo MRI was performed at 1 week prior to and 3 months following cerebral hypoperfusion surgery. At 1 week prior to surgery, mice underwent T2, ASL and T2* imaging (non-contrast-enhanced) according to methods described in Methods section 2.9. At 3 months following cerebral hypoperfusion surgery, mice underwent the same scans with the addition of ce-T2* imaging. 2 mice were excluded from ASL analysis due to breathing problems during the scan.

6.2.5 Laser speckle imaging of baseline blood flow

In a subset of 18 mice, laser speckle imaging was used to track changes in cortical blood flow. Laser speckle imaging was performed at 4 timepoints during the experiment: 24 hours before surgery, 24 hours post-surgery, 1 month post-surgery and 3 months post-surgery according to methods described in Methods section 2.4

6.2.6 Barnes Maze

At 10 weeks following cerebral hypoperfusion surgery, mice underwent the Barnes maze test of spatial learning and memory, performed according to methods described in Methods section 2.7. Mean speed was compared between groups to ensure rates of learning were not influenced by transgene or surgery effects on movement speed. For the learning phase, mice were assessed based on the time taken to enter the escape chamber (escape latency). For each day of the learning phase, escape latency data was averaged over two trials. For probe trials, mice were assessed based on the proportion of time spent in the target quadrant i.e. the quadrant of the maze that had previously contained the escape chamber.

Inclusion criteria

Performance in the Barnes maze is dependent on the mouse exploring the maze and being motivated to locate the escape chamber. Therefore, inclusion criteria were as follows: mice must enter a minimum of 3 quadrants in 2 of the learning phase trials. This highlighted three mice for exclusion, however two of these mice failed to explore and meet the criteria because they were already escaping the maze. One mouse was excluded from further analyses.

6.2.7 Laser speckle imaging of neurovascular coupling

Assessment of neurovascular coupling was performed 14 weeks after surgery according to methods described in Methods section 2.5. Mean response amplitude during stimulation was expressed as percentage increase from baseline and averaged across a minimum of 3 stimulations.

6.2.8 Tissue collection and processing

Following laser speckle imaging assessment of neurovascular coupling, mice were transcardially perfused with PBS according to Methods section 2.10. Brain tissue was then

collected and processed according to Methods section 2.11.2. For the biochemistry cohort, tissue was collected and processed according to Methods section 2.15.

6.2.9 Quantification of ischaemic and haemorrhagic lesion burden

Coronal brain tissue sections were collected at six stereotactic levels throughout the brain (anterior/posterior from Bregma: +0.86mm, +0.14mm, -0.46mm, -1.34mm, -1.82mm and -2.3mm) and were stained using H&E and Perls' Prussian Blue according to Methods sections 2.12.1 and 2.12.2 in order to detect ischaemic and haemorrhagic pathology respectively. Ischaemic lesions were defined as sharply delimited areas of tissue pallor on H&E stained sections. Haemorrhagic pathology was defined as blue cellular staining of haemosiderin deposits on Perls' Prussian Blue stained sections. Non-cellular blue deposits were not classified as haemorrhagic lesions. Ischaemic and haemorrhagic lesions were quantified in the cortex, hippocampus, thalamus and white matter (comprising corpus callosum, anterior commissure, fimbria, internal capsule and optic tract).

6.2.10 Amyloid quantification

12µm coronal sections were collected corresponding to Bregma -1.82mm in stereotaxic mouse atlas (Paxinos and Franklin, 2001) and labelled with 6E10 antibody according to Methods section 2.13.1. Sections were imaged at x10 using an Olympus BX51 microscope (x10, Olympus UK, Southend-on-Sea, UK); taking two pictures per region in the cortex and thalamus, and percentage area stained by 6E10 was quantified using ImageJ.

6.2.11 Analysis of vascular NOX2 in vessel-enriched tissue fractions

Vascular NOX2 was assessed by ELISA according to Methods section 2.19.

6.2.12 Statistical analysis

A two-way ANOVA with surgery and treatment as the between-subjects factors was used to compare resting cerebral blood flow assessed by both laser speckle imaging and ASL, neurovascular coupling measures, amyloid burden and ce-T2* signal changes. Lesion burden was compared using the Pearson Chi-Squared test. Vascular NOX2 expression levels were compared using an unpaired t-test. For the learning phase of the Barnes maze, speed and escape latency were assessed by repeated measures mixed ANOVA, with surgery and treatment as between-subjects factors and trial day as the within-subjects factor. For the probe trials, performance of each group was compared to chance using a one sample t-test. Performance between the groups was then compared using a two-way ANOVA with surgery and treatment as the factors. Statistical analysis of all data was performed in SPSS (v19, IBM Corp.).

6.3 Results

6.3.1 Water consumption is similar between non-treated and apocynin-treated mice

Water consumption was monitored to investigate whether administration of apocynin in drinking water would affect water intake. No differences in water consumption were found between non-treated and apocynin-treated mice ($t=1.568$ $df=78$ $p>0.05$) (Figure 6.1).

6.3.2 Apocynin does not protect against cortical blood flow reductions following cerebral hypoperfusion

In order to investigate cortical blood flow changes, laser speckle imaging was performed at baseline (prior to surgery), and again at 24 hours, 1 month and 3 months following hypoperfusion surgery (Figure 6.2 and 6.3). Blood flow data was calculated as % change from baseline flow values. Significant effects of time ($F_{(2,3,73.9)}=17.895$, $p<0.001$) and surgery ($F_{(1,32)}=64.684$, $p<0.001$) were detected, but no effect of treatment. Further, there was a significant interaction between time and surgery ($F_{(2,3,73.9)}=23.206$, $p<0.001$). Post-hoc analysis indicated that blood flow was significantly reduced in non-treated hypoperfused mice compared to shams at 24 hours ($p<0.001$), 1 month ($p<0.001$) and 3 months ($p<0.001$) following surgery. In apocynin-treated mice, blood flow was significantly reduced at 24 hours ($p<0.001$) and 1 month ($p<0.001$) following surgery, but not at 3 months ($p>0.05$). In order to account for potential variations in sham blood flow, blood flow data was also normalised to the corresponding sham group values and the magnitude of blood flow reductions were compared (Figure 6.3). There were no significant differences in the magnitude of change between non-treated and apocynin-treated mice.

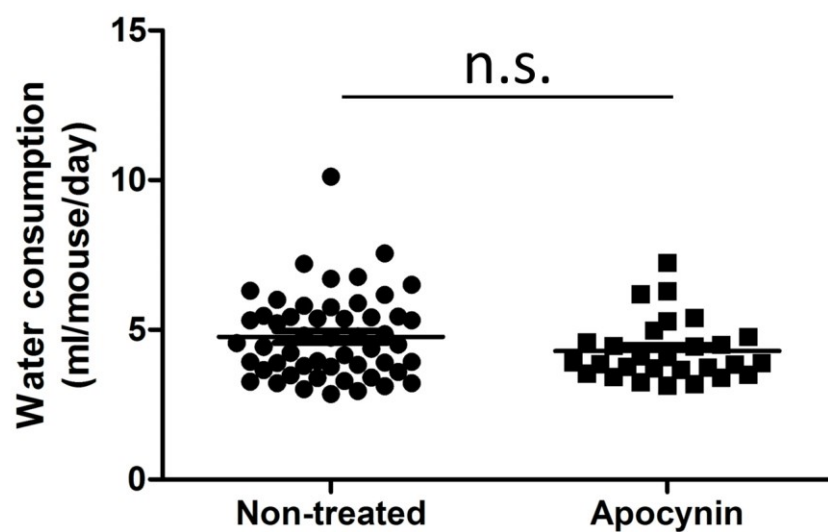


Figure 6.1 Apocynin administration does not affect water consumption. Water consumption was monitored to ensure that administration of apocynin in the drinking water did not alter normal drinking habits. No significant difference in water consumption was found between non-treated and apocynin-treated mice. Data presented as mean \pm SEM n=28-52 per group.

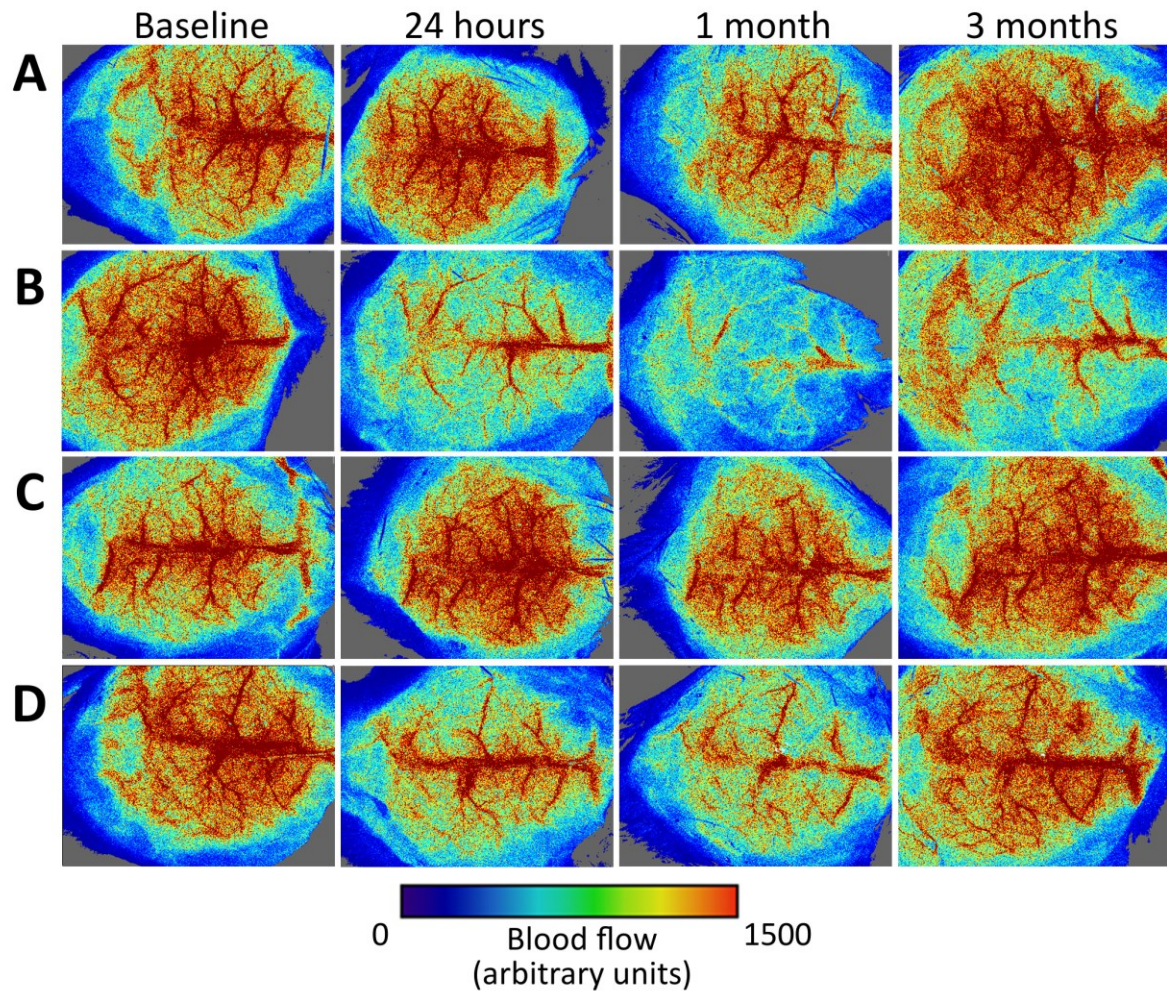


Figure 6.2 Apocynin treatment does not protect against cortical blood flow reductions following hypoperfusion surgery. Laser speckle imaging was used to measure blood flow alterations from baseline at 24 hours, 1 month and 3 months following hypoperfusion surgery. Representative images of cortical blood flow at each timepoint from (A) sham non-treated, (B) hypoperfused non-treated, (C) sham apocynin and (D) hypoperfused apocynin-treated mice.

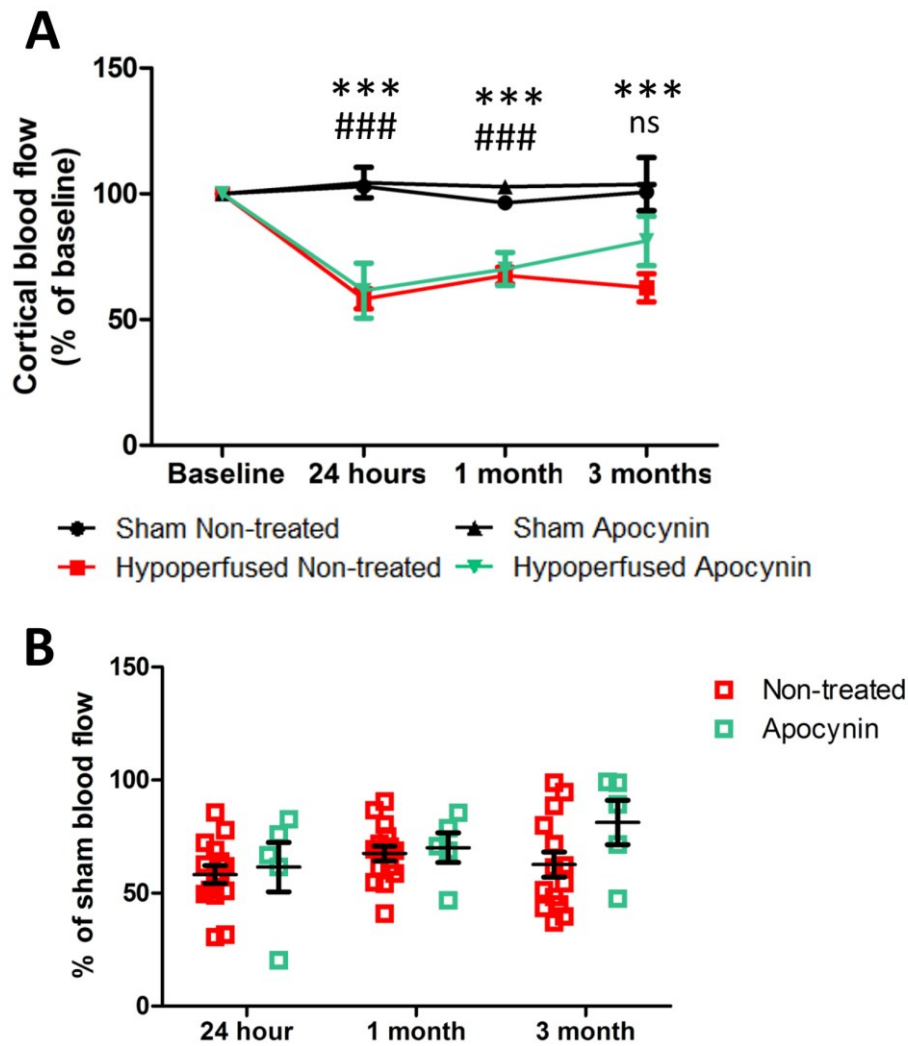


Figure 6.3 Apocynin treatment does not protect against cortical blood flow reductions following hypoperfusion. Laser speckle imaging was used to measure blood flow alterations from baseline at 24 hours, 1 month and 3 months following hypoperfusion surgery (A). Significant effects of time ($F_{(2,3,73.9)}=17.895$, $p<0.001$) and surgery ($F_{(1,32)}=64.684$, $p<0.001$) were detected, but there was no effect of treatment ($p>0.05$). A significant interaction between time and surgery was detected ($F_{(2,3,73.9)}=23.206$, $p<0.001$). Post-hoc analysis indicated that blood flow was significantly reduced in non-treated hypoperfused mice compared to shams at 24 hours ($p<0.001$), 1 month ($p<0.001$) and 3 months ($p<0.001$) following surgery. In apocynin-treated mice, blood flow was significantly reduced at 24 hours ($p<0.001$) and 1 month ($p<0.001$) following surgery, but not at 3 months ($p>0.05$). (B) Normalisation of blood flow to corresponding sham group revealed no significant differences in the magnitude of change between non-treated and apocynin-treated mice. *** $p<0.001$ sham non-treated vs hypoperfused non-treated, ### $p<0.001$ sham apocynin vs hypoperfused apocynin. N=5-15 per group

6.3.3 Baseline regional cerebral blood flow is not altered by apocynin after three months of treatment

In hypoperfused mice blood flow has been shown to be persistently reduced for 3 months following surgery in cortex, hippocampus and thalamus. In order to determine whether apocynin treatment was able to improve blood flow over the course of the study, arterial spin labelling was performed at baseline (prior to surgery) and 3 months following surgery, and the percentage change from baseline was calculated. In the thalamus there was a significant effect of surgery ($F_{(1,25)}=14.21$, $p<0.001$) but no significant effect of treatment (Figure 6.4 and 6.5). Similarly in the hippocampus, there was a significant effect of surgery ($F_{(1,25)}=15.44$, $p<0.001$) but no overall effect of treatment (Figure 6.4 and 6.5). Blood flow data was also normalised to the corresponding sham group values and the magnitude of blood flow reductions were compared (Figure 6.6). There were no significant differences in the magnitude of change between non-treated and apocynin-treated mice.

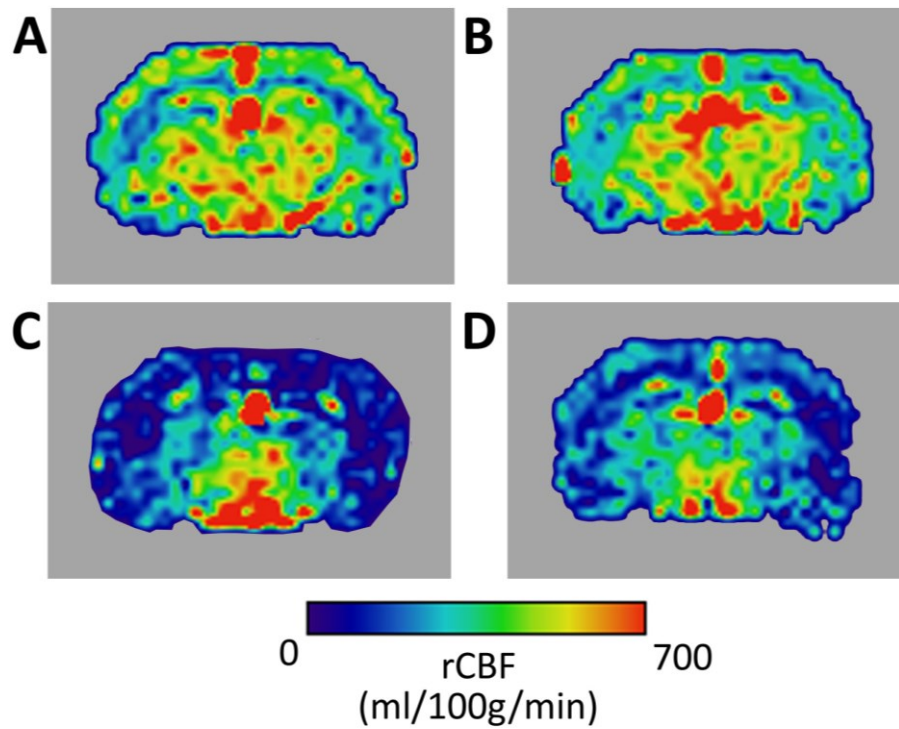


Figure 6.4 Arterial spin labelling was used to detect blood flow alterations at 3 months following hypoperfusion. Representative arterial spin labelling images from (A) sham non-treated, (B) hypoperfused non-treated, (C) sham apocynin and (D) hypoperfused apocynin-treated mice.

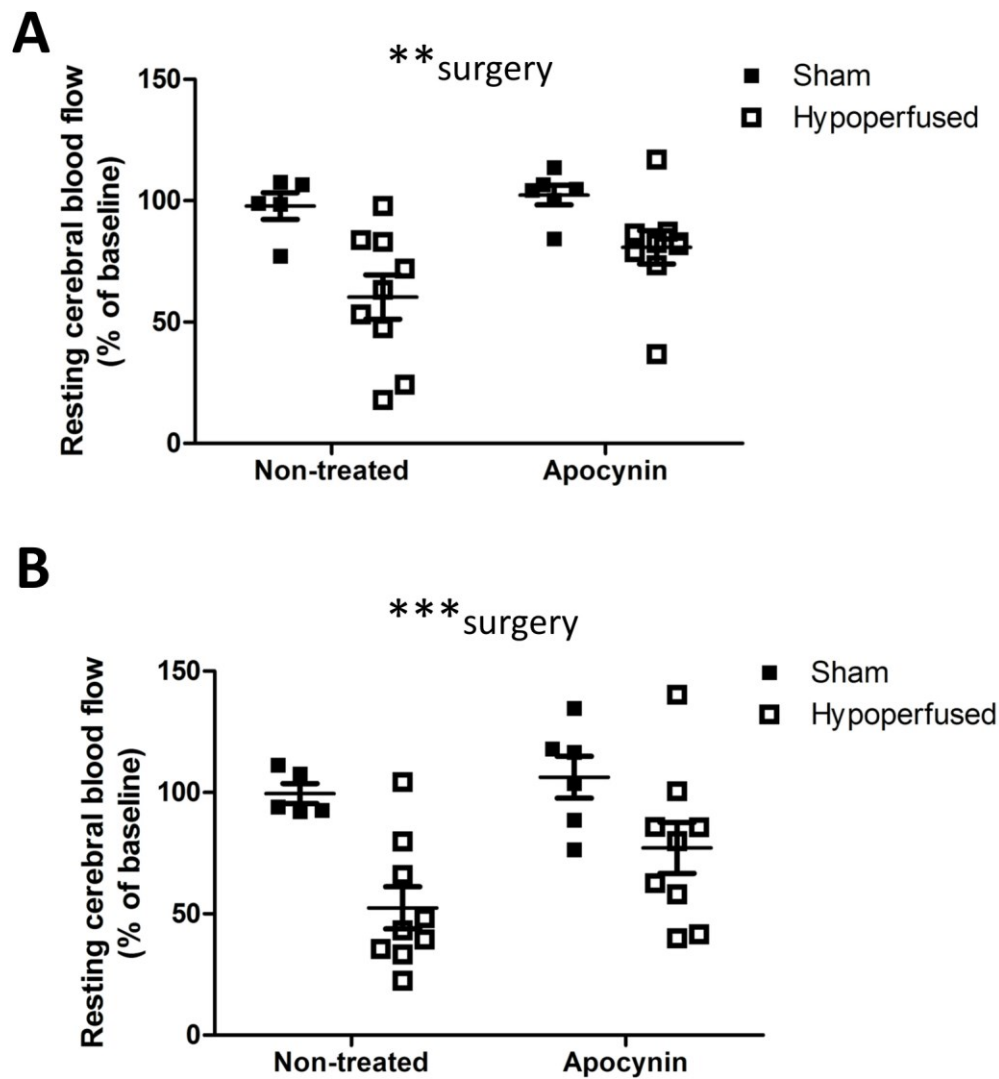


Figure 6.5 Effect of apocynin on recovery of resting cerebral blood flow. Arterial spin labelling was used to measure blood flow in subcortical brain regions at baseline and 3 months following hypoperfusion surgery, and the percentage change from baseline was calculated. An overall effect of surgery was detected, in which blood flow was significantly reduced following hypoperfusion in (A) thalamus ($F_{(1,25)}=14.21$, $p<0.001$) and (B) hippocampus ($F_{(1,25)}=15.44$, $p<0.001$), however post-hoc analyses revealed no differences in blood flow between sham and apocynin-treated hypoperfused mice for either thalamus (A) or hippocampus (B). Data presented as mean \pm SEM, $n=5-9$ per group. ** $p<0.01$, *** $p<0.001$

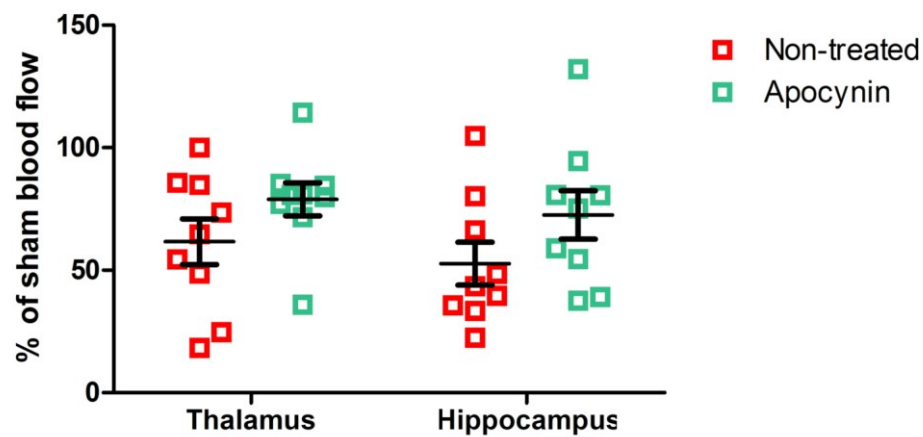


Figure 6.6 Effect of apocynin on recovery of resting cerebral blood flow. Arterial spin labelling was used to measure blood flow in subcortical brain regions at baseline and 3 months following hypoperfusion surgery, and the percentage change from baseline was calculated. Normalisation of blood flow to corresponding sham group values revealed no significant differences in the magnitude of change between non-treated and apocynin-treated mice. Data presented as mean \pm SEM, n=9 per group.

6.3.4 Apocynin rescues the impairment in neurovascular coupling following cerebral hypoperfusion

In order to determine if apocynin treatment could improve the impairment on neurovascular coupling induced by cerebral hypoperfusion, laser speckle imaging with whisker stimulation was performed at 3 months following surgery, and the increase in blood flow during stimulation was calculated. A significant interaction effect was observed ($F_{(1,27)}=4.865$, $p<0.05$), post-hoc analyses revealed significantly impaired neurovascular coupling following cerebral hypoperfusion in non-treated mice ($p<0.01$), but not in apocynin-treated mice (Figure 6.7), indicating that apocynin treatment was able to ameliorate deficits on neurovascular coupling.

6.3.5 Apocynin does not prevent the development of vascular lesions but may selectively reduce cortical ischaemic pathology

Having observed that apocynin treatment was able to improve vascular function, T2 MRI was performed in order to investigate whether apocynin was also able to prevent the development of vascular lesions induced by chronic cerebral hypoperfusion. Structural T2 imaging was performed at 3 months following hypoperfusion surgery, and the number of mice with ischaemic and haemorrhagic lesions was counted (Figure 6.8). No vascular lesions were detectable in either non-treated or apocynin-treated sham mice. In hypoperfused non-treated mice, 2 of 10 mice were found to have an ischaemic lesion (20%), 1 mouse was found to have a haemorrhagic lesion (10%) and the remaining 7 had no lesions. In hypoperfused apocynin-treated mice, 3 of 9 mice were found to have an ischaemic lesion (33%) whilst the remaining 6 mice had no lesions (67%). In order to further investigate the burden of ischaemic and haemorrhagic pathology in hypoperfused mice, H&E staining and Perls' Prussian Blue staining was performed in tissue sections throughout the brain and the number of mice with ischaemic or haemorrhagic pathology was quantified (Figure 6.9). In non-treated mice, the number of

mice that developed ischaemic lesions was significantly greater in hypoperfused mice relative to shams (0 of 6 sham, 0%, vs 5 of 10 hypoperfused, 50%) ($\chi^2_{(1,16)}=4.364$, $p<0.05$). In apocynin-treated mice, 3 of 9 hypoperfused mice were found to have ischaemic lesions (33%) whilst no lesions were detected in sham apocynin-treated mice (0%), however this difference was not significant ($p>0.05$). The number of mice with ischaemic pathology was also not significantly different between non-treated and apocynin-treated hypoperfused mice ($p>0.05$). The distribution of ischaemic pathology in regions throughout the brains of hypoperfused mice was also determined (Figure 6.10). No significant differences were found between the number of apocynin or non-treated mice with ischaemic pathology in the hippocampus, white matter, or thalamus ($p>0.05$). In the cortex, 3 of 10 non-treated mice were found to have ischaemic lesions compared to 0 of 9 apocynin-treated mice, however this difference just missed statistical significance ($p=0.07$). Therefore, although apocynin treatment did not reduce overall burden of ischaemic pathology, there was a trend toward a reduction in cortical lesion burden. Haemorrhagic lesions were detectable only in the thalamus of hypoperfused mice, but there was no significant difference in the number of mice with haemorrhagic pathology between non-treated (2 of 10, 20%) and apocynin-treated mice (1 of 10, 10%).

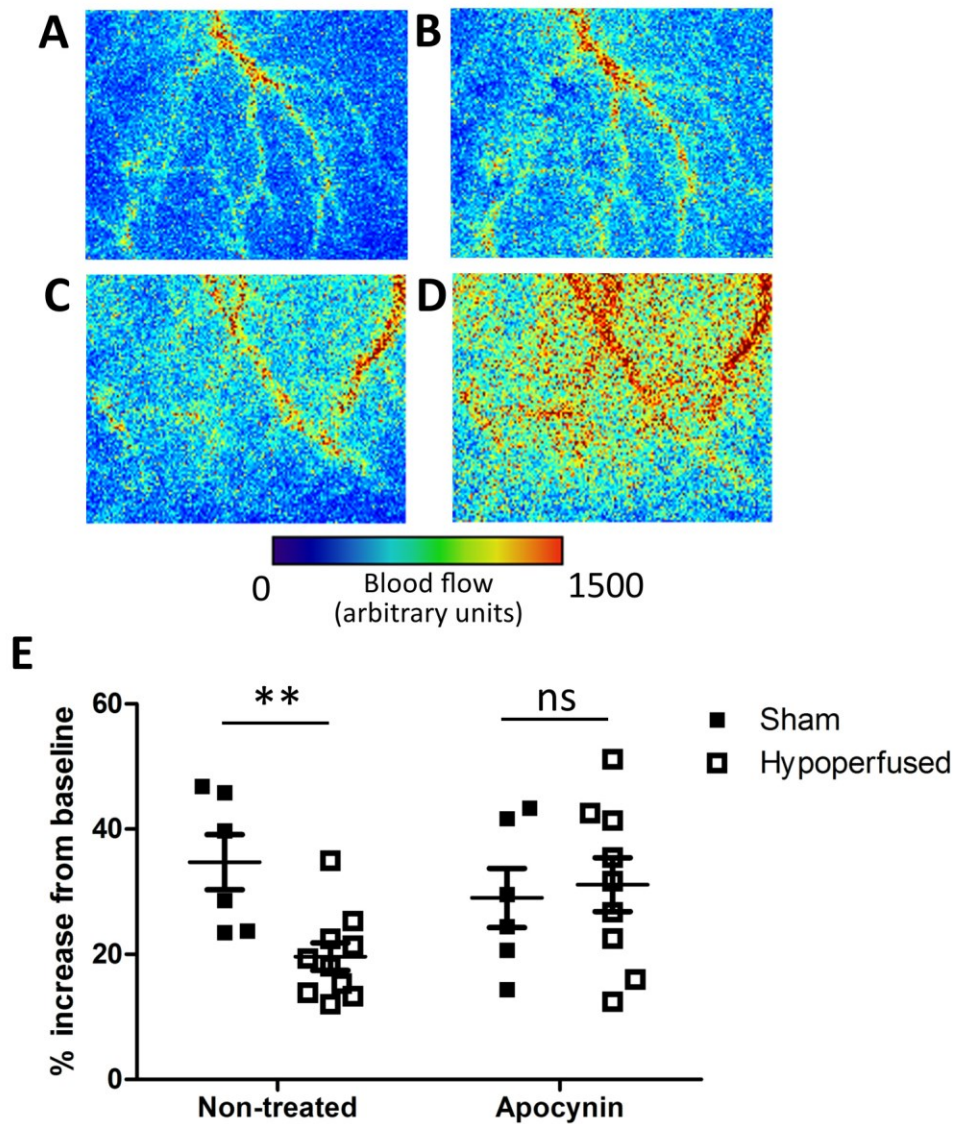
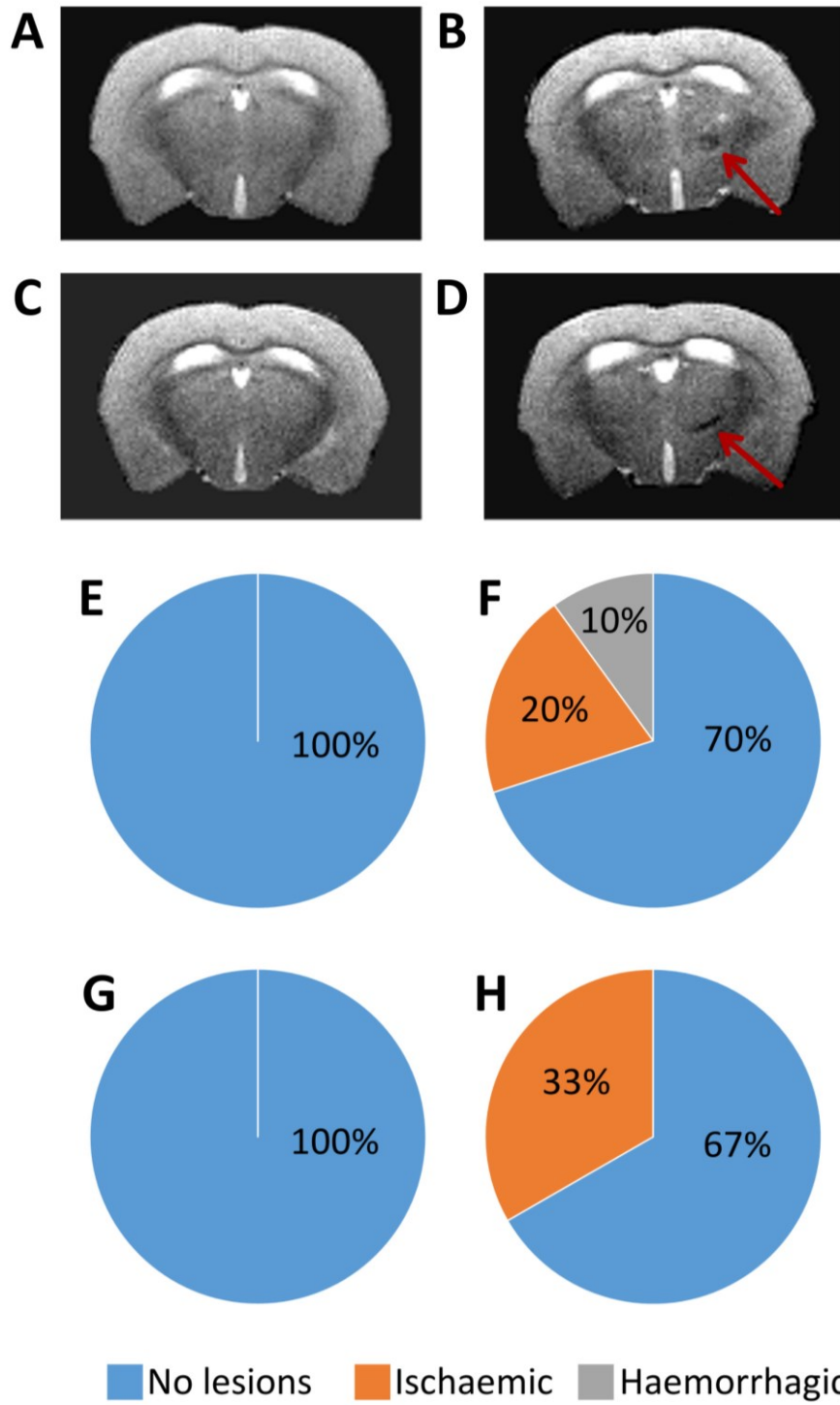
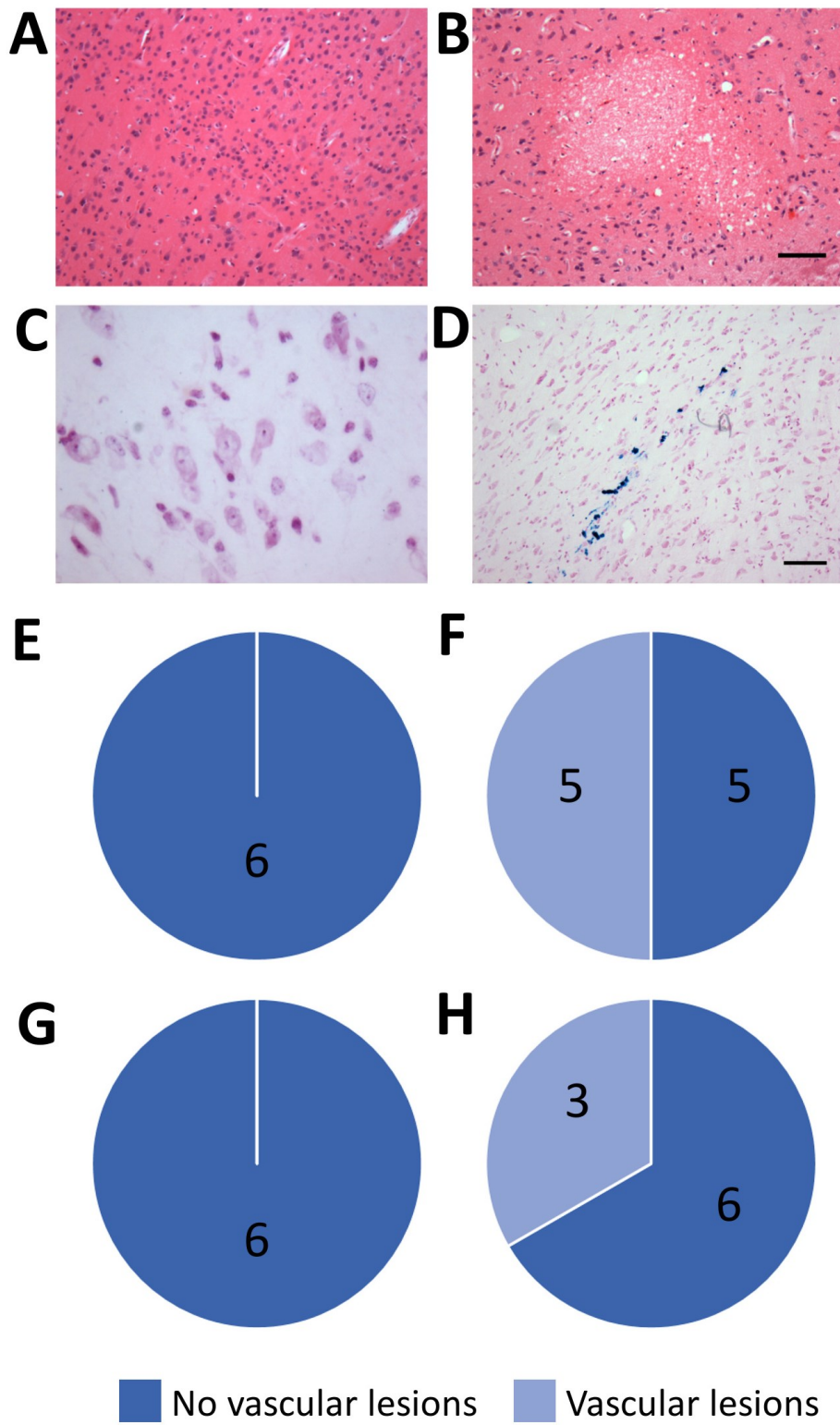


Figure 6.7 Apocynin rescues the impairment in neurovascular coupling following cerebral hypoperfusion. Laser speckle imaging was performed 3 months following hypoperfusion in order to assess vascular function. Representative images from non-treated (A, B) and apocynin-treated (C, D) mice during baseline (A, C) and whisker stimulation (B, D). (E) Analysis of neurovascular coupling responses revealed a significant interaction effect ($F_{(1,27)}=4.865$, $p<0.05$). Post-hoc analyses detected significantly impaired neurovascular coupling responses following hypoperfusion in non-treated mice ($p<0.01$), but not in apocynin-treated mice. Data presented as mean \pm SEM, $n=6-10$ per group. ** $p<0.01$



◀ **Figure 6.8 Apocynin does not protect against the development of vascular lesions.**

Structural T2 imaging was performed at 3 months following hypoperfusion surgery to determine if treatment with apocynin could prevent the development of vascular lesions. Representative T2 scans from sham (A,C) and hypoperfused mice indicating an ischaemic lesion in the corpus callosum (B) (red arrowhead) and a haemorrhagic lesion in the thalamus (D) (red arrowhead). No lesions were detected in sham-operated mice (E,G). In hypoperfused non-treated mice, 20% were found to have ischaemic lesions and 10% were found to have haemorrhagic lesions (F); whilst in hypoperfused apocynin-treated mice 33% were found to have ischaemic lesions but none exhibited any haemorrhagic lesions (H).



◀ **Figure 6.9 Apocynin does not protect against development of vascular lesions.** H&E and Perls' Prussian Blue staining was performed to identify ischaemic and haemorrhagic lesions respectively. Representative H&E images showing normally appearing cortex from a sham mouse brain (A) and an ischaemic cortical lesion from hypoperfused mouse brain (B). Representative Perls stain from sham (C) and hypoperfused (D) mice. Blue cellular staining indicates a haemorrhagic lesion in hypoperfused mouse brain (D). No lesions were detected in sham-operated mice (E,G); whereas 50% of non-treated (F) and 33% of apocynin-treated (H) hypoperfused mice were found to have vascular lesions. Scale bar=100µm (B), 50µm (D).

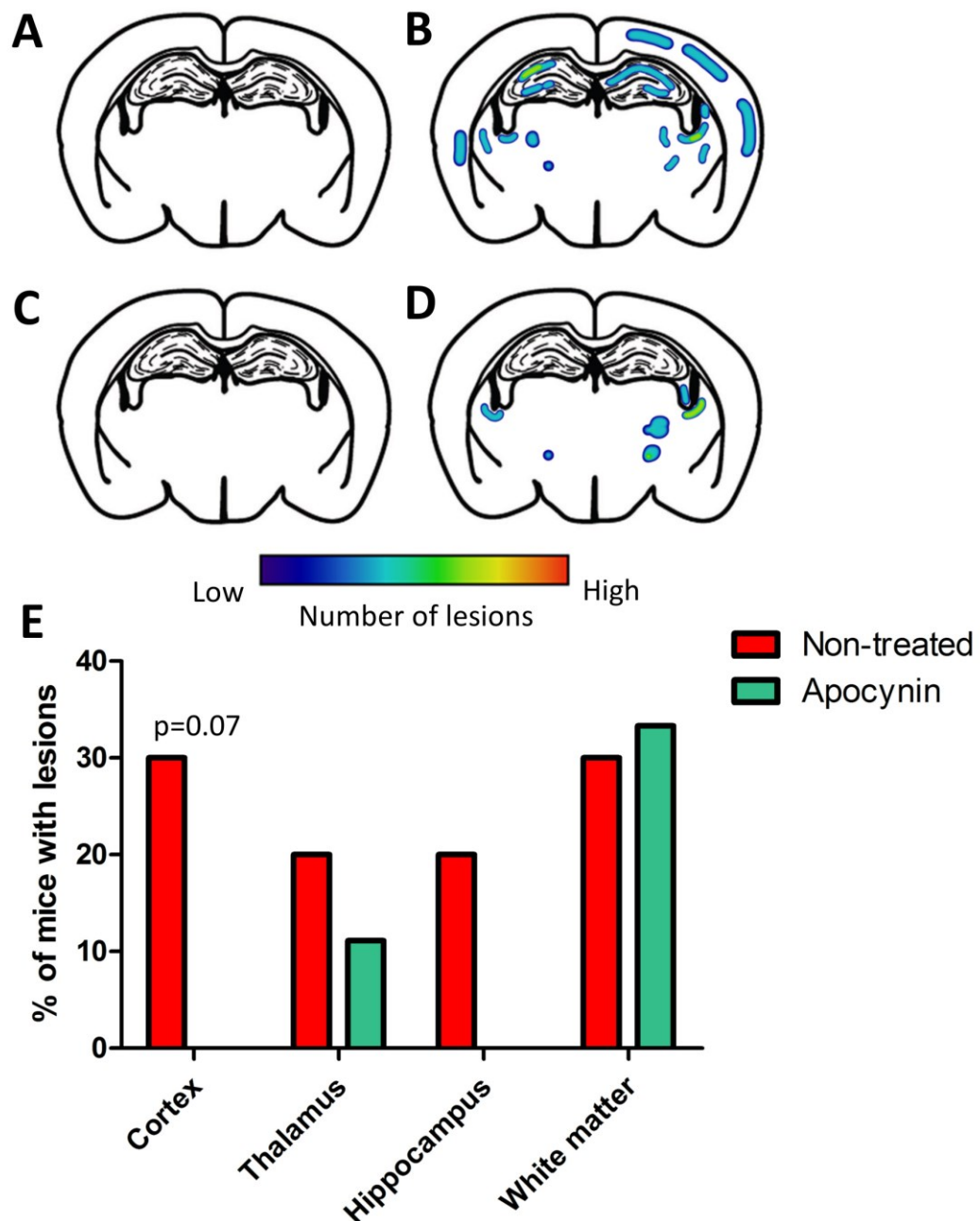


Figure 6.10 Apocynin treatment may selectively protect against cortical ischaemic lesions. Maps indicating the distribution of vascular lesions in non-treated sham (A), non-treated hypoperfused (B), apocynin-treated sham (C) and apocynin-treated hypoperfused (D) mice. No significant differences in regional distribution of lesions were detected between non-treated and apocynin-treated hypoperfused mice (E), although there was a trend towards a reduction in cortical ischaemic pathology following apocynin treatment ($p=0.07$).

6.3.6 Vascular NOX2 expression is not reduced in apocynin-treated mice

Hypoperfusion was previously shown to induce the upregulation of NOX2 (Figure 5.15). In order to determine if the improvements on neurovascular coupling and reduction of cortical ischaemic pathology as a result of apocynin treatment were due to reduced expression of NOX2 in cerebral vasculature, vessel-enriched brain homogenates were assayed for expression of the NOX2 subunit gp91phox. No significant differences were found in the expression levels of gp91phox between hypoperfused non-treated mice and hypoperfused apocynin-treated mice ($t=0.8254$ $df=15$ $p>0.05$) (Figure 6.11).

6.3.7 Inflammation is not reduced following treatment with apocynin

Hypoperfusion was shown to induce inflammation following cerebral hypoperfusion. Contrast-enhanced T2* (ce-T2*) imaging was performed to detect inflammation *in vivo* and to determine whether apocynin treatment could reduce inflammation following cerebral hypoperfusion (Figure 6.12). In the cortex, a significant overall effect of surgery was detected ($F_{(1,27)}=5.56$, $p<0.05$), in which hypoperfused mice exhibited greater tissue hypointensity relative to shams, but there was no effect of treatment. In the thalamus, no significant effects of either surgery or treatment were detected.

6.3.8 Apocynin administration does not reduce amyloid deposition

Amyloid deposition was assessed using 6E10 immunohistochemistry in the cortex and thalamus of brain tissue sections. No significant differences of either surgery or apocynin treatment were observed (Figure 6.13).

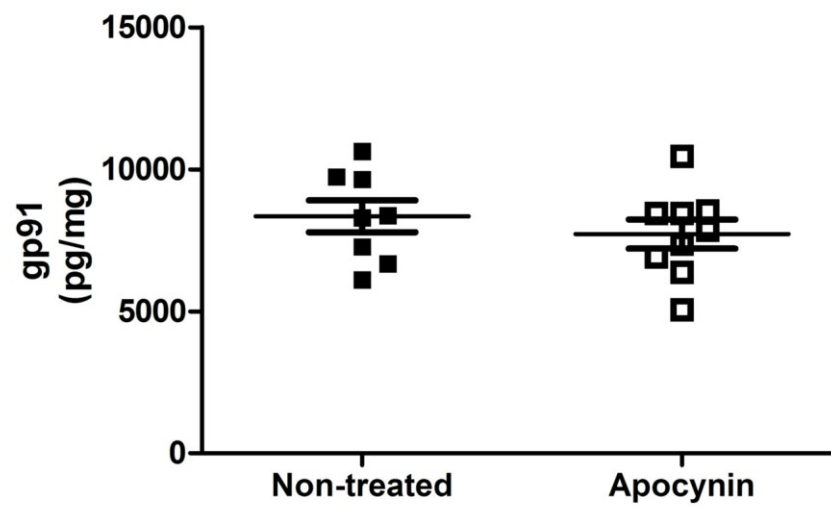
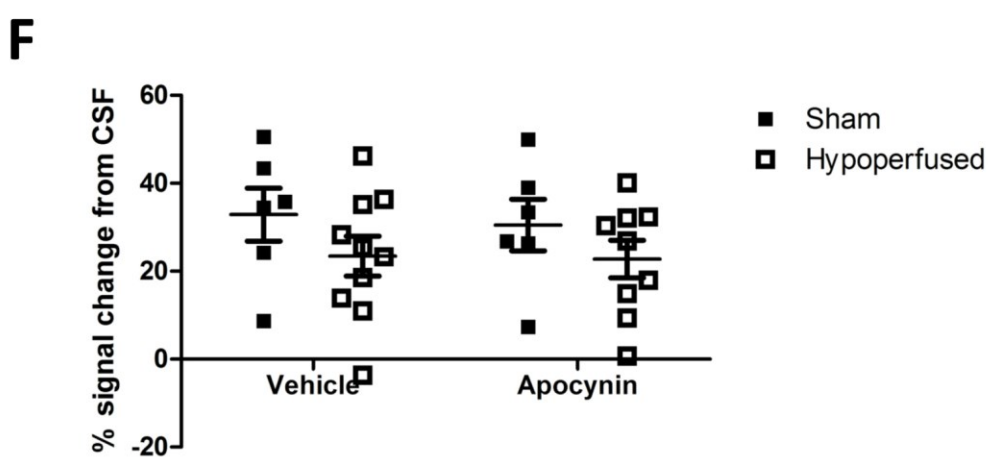
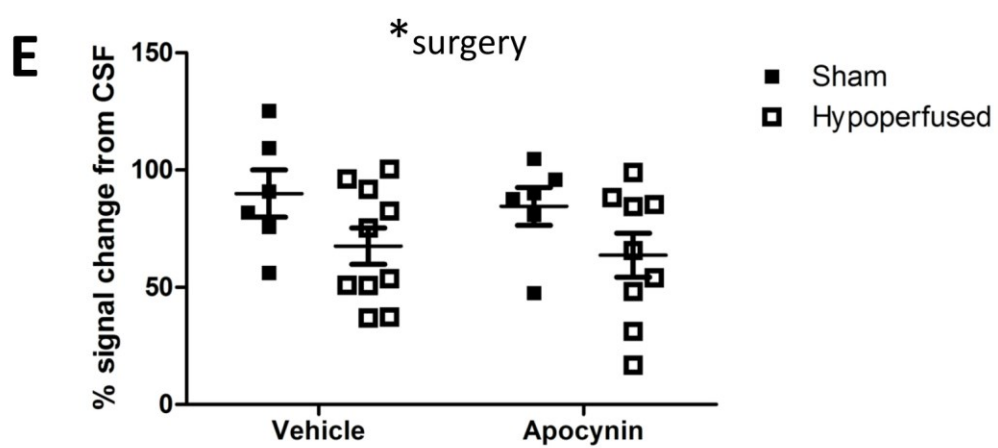
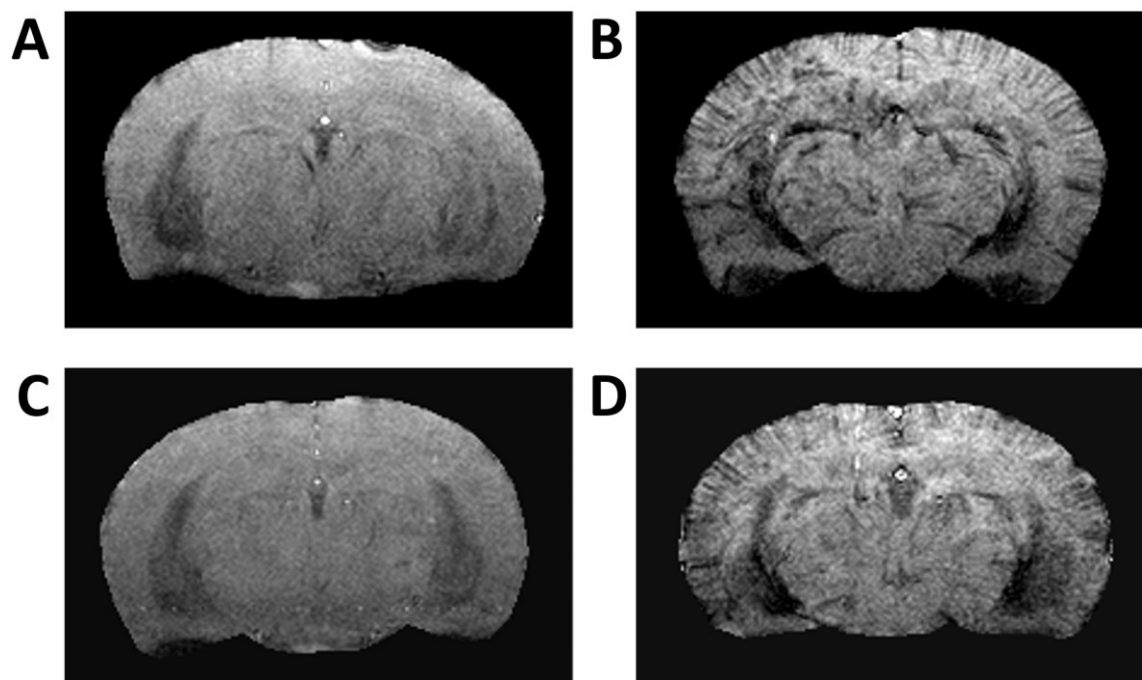


Figure 6.11 Apocynin treatment does not reduce vascular expression of NOX2. Vascular NOX2 protein expression levels were assessed by ELISA using vessel enriched brain tissue homogenates at 3 months following hypoperfusion surgery. No significant difference in NOX2 levels was detected between non-treated and apocynin-treated mice. Data presented as mean \pm SEM, n=8-9 per group.



◀ **Figure 6.12 The effect of apocynin on contrast-enhanced T2* imaging.** Contrast-enhanced T2* MRI was performed in order to assess inflammation in vivo. T2* values from cortex and thalamus were normalised to the CSF and compared between groups. Hypointense tissue reflects greater retention of iron oxide and a higher degree of inflammation. Representative ce-T2* images from (A) non-treated sham, (B) non-treated hypoperfused, (C) apocynin sham and (D) apocynin treated hypoperfused mice. (E,F) Analysis of cortical regions of interest showed a greater degree of hypointensity in hypoperfused mice relative to shams, indicative of increased inflammation that was not rescued by treatment with apocynin ($F_{(1,27)}=5.56$, $p<0.05$). No significant changes in T2* signal were observed in the thalamus. Data presented as mean \pm SEM, n=6-10 per group. * $p<0.05$.

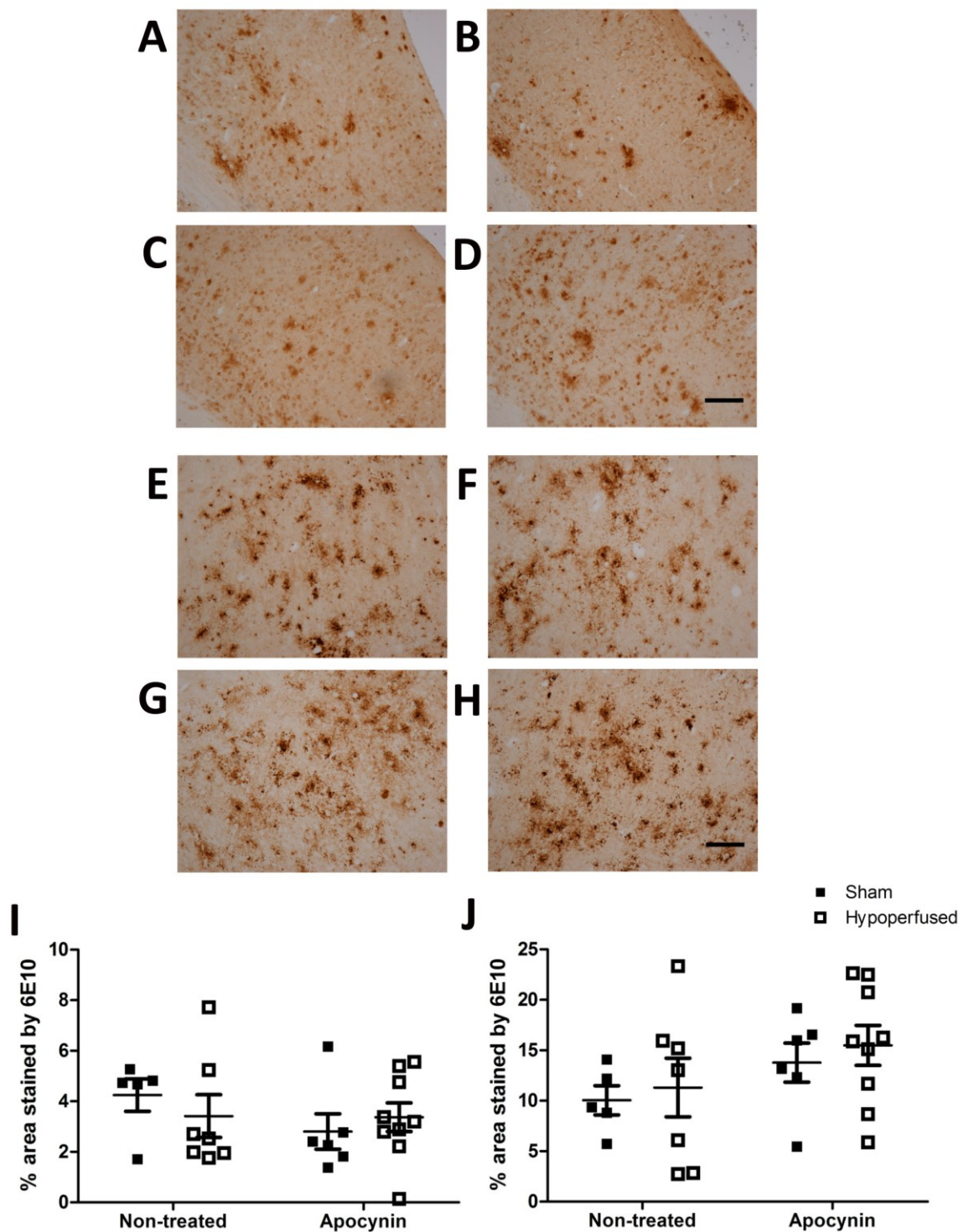


Figure 6.13 Apocynin administration does not affect amyloid deposition.

Representative images from from (A, E) non-treated sham, (B, F) non-treated hypoperfused, (C, G) apocynin-treated sham and (D, H) apocynin-treated hypoperfused mice in cortex (A-D) and thalamus (E-H). No differences in amyloid deposition were observed in either cortex (I) or thalamus (J). Data presented as mean \pm SEM, n=5-9 per group. Scale bar=100 μ m

6.3.9 Spatial learning and memory deficits are not rescued by treatment with apocynin

In order to see if apocynin could rescue the deficit in spatial learning caused by hypoperfusion, non-treated and apocynin-treated mice underwent the Barnes maze behavioural task. Analysis of movement speed revealed no significant effects of hypoperfusion or apocynin treatment, so all groups were subsequently analysed together on measures of spatial learning. Analysis of escape latency data revealed significant main effects of trial ($F_{(5,130)}=26.11$, $p<0.001$) and surgery ($F_{(1,26)}=9.54$, $p<0.01$), indicating that while all groups took less time to enter the escape chamber with increasing trial, hypoperfused mice took significantly longer relative to sham mice (Figure 6.14). There was no significant effect of apocynin treatment. Performance on the 72hour probe test was significantly better than chance for all groups except the hypoperfused apocynin-treated mice, possibly due to the high level of variation within this group ($58\pm24\%$ vs 25% , $p<0.05$ for sham non-treated mice; $50\pm30\%$ vs 25% , $p<0.05$ for hypoperfused non-treated mice; $60\pm33\%$ vs 25% , $p<0.05$ for sham apocynin mice and $40\pm38\%$ vs 25% , $p>0.05$ for hypoperfused apocynin mice) (Figure 6.15). There were no significant overall effects of surgery or genotype on time spent in the target quadrant.

On the reversal learning task, no significant effects were detected for either trial, surgery or treatment, indicating that mice were unable to learn the new location of the escape chamber and apocynin did not rescue this behavioural deficit (Figure 6.16). In the reversal probe, all groups performed no better than chance ($20\pm15\%$ vs 25% , $p>0.05$ for sham non-treated mice; $26\pm16\%$ vs 25% , $p>0.05$ for hypoperfused non-treated mice; $20\pm26\%$ vs 25% , $p>0.05$ for sham apocynin mice and $17\pm17\%$ vs 25% , $p>0.05$ for hypoperfused apocynin mice) (Figure 6.17). Together, these results suggest that apocynin is not able to rescue deficits on spatial learning and memory caused by hypoperfusion.

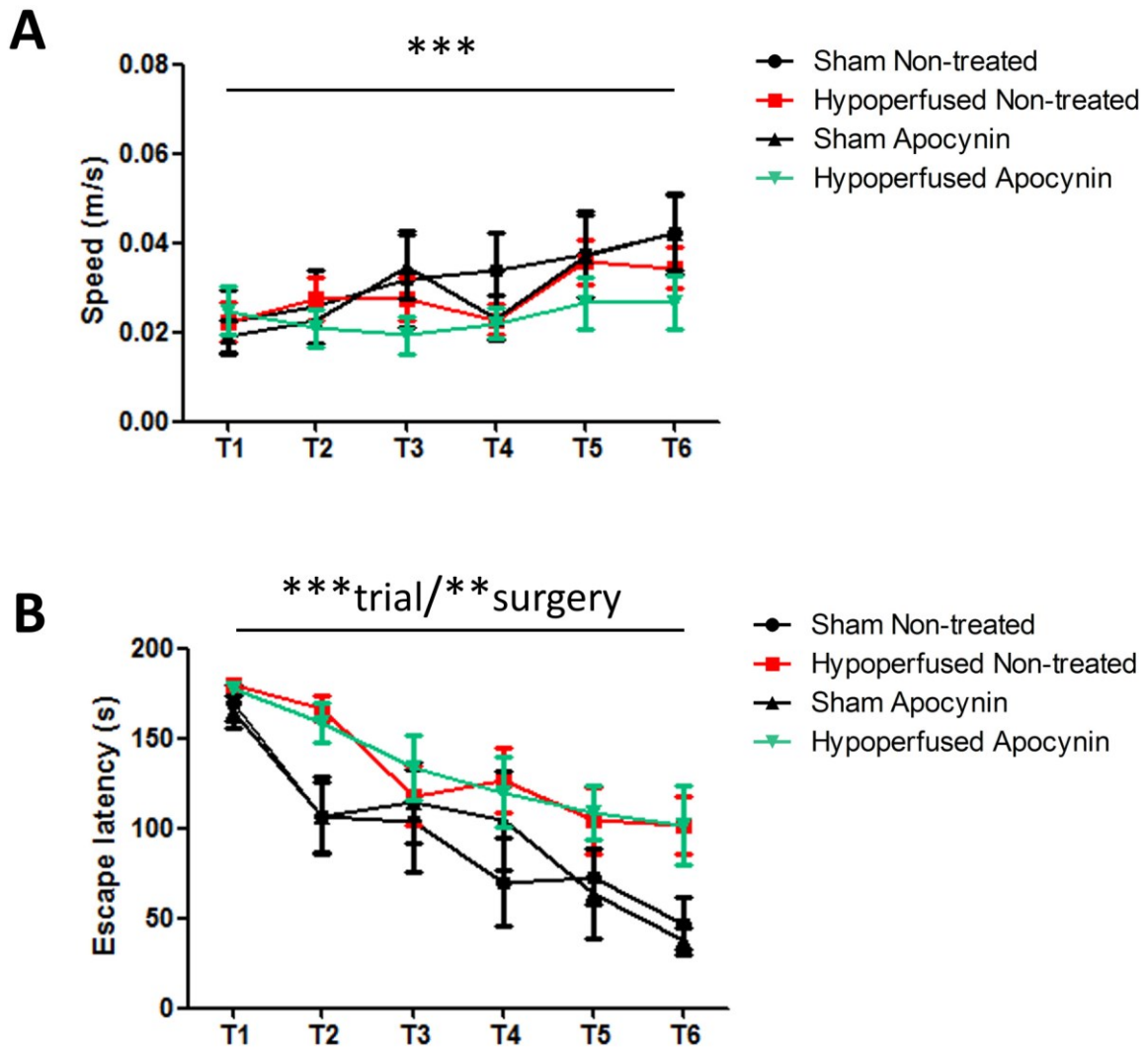


Figure 6.14 Apocynin does not rescue deficits on spatial learning. Spatial learning was assessed using the Barnes maze task. Movement speed was initially checked to ensure no differences in speed were caused by surgery or drug treatment. (A) There was a significant effect of trial ($F_{(3.4,90.3)}=7.031$, $p=0.001$) but there were no significant effects of hypoperfusion or apocynin treatment. (B) Significant effects of trial and hypoperfusion on escape latency were detected ($F_{(5,130)}=26.11$, $p<0.001$ and $F_{(1,26)}=9.54$, $p<0.01$ respectively). There was no significant effect of apocynin treatment. Data presented as mean \pm SEM, $n=6-10$ per group. ** $p<0.01$, *** $p<0.001$.

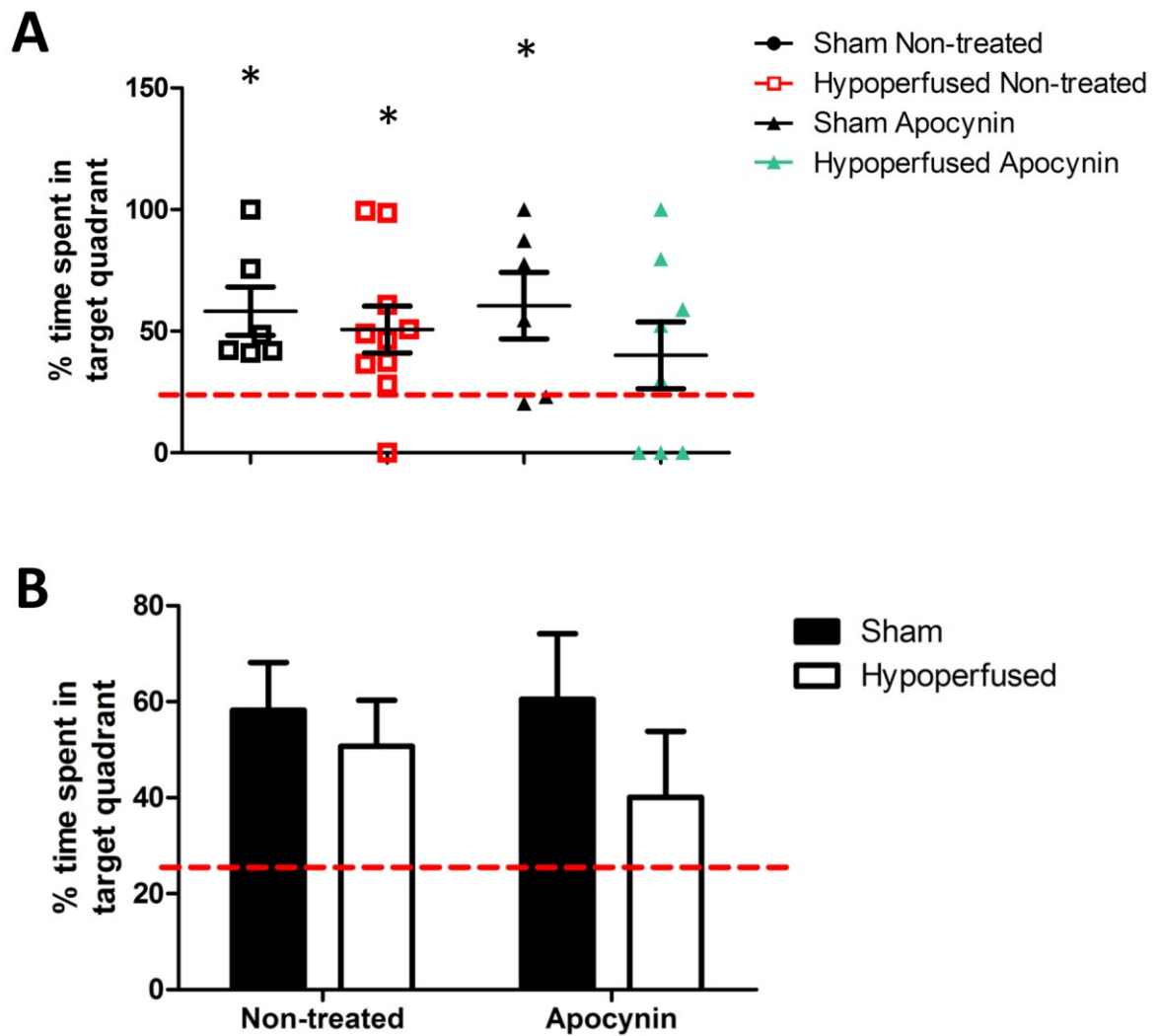


Figure 6.15 Apocynin does not improve performance on spatial memory. Spatial memory was assessed using a 72-hour delayed probe task. (A) All groups spent significantly more time in the target quadrant compared to chance (indicated by dashed red line), except the hypoperfused apocynin-treated mice ($58 \pm 24\%$ vs 25% , $p < 0.05$; $50 \pm 30\%$ vs 25% , $p < 0.05$; $60 \pm 33\%$ vs 25% , $p < 0.05$ and $40 \pm 38\%$ vs 25% , $p > 0.05$ for sham non-treated mice, hypoperfused non-treated mice, sham apocynin mice and hypoperfused apocynin mice respectively). (B) There were no significant overall effects of surgery or apocynin treatment on time spent in the target quadrant. Data presented as mean \pm SEM, $n = 6-10$ per group. * $p < 0.05$

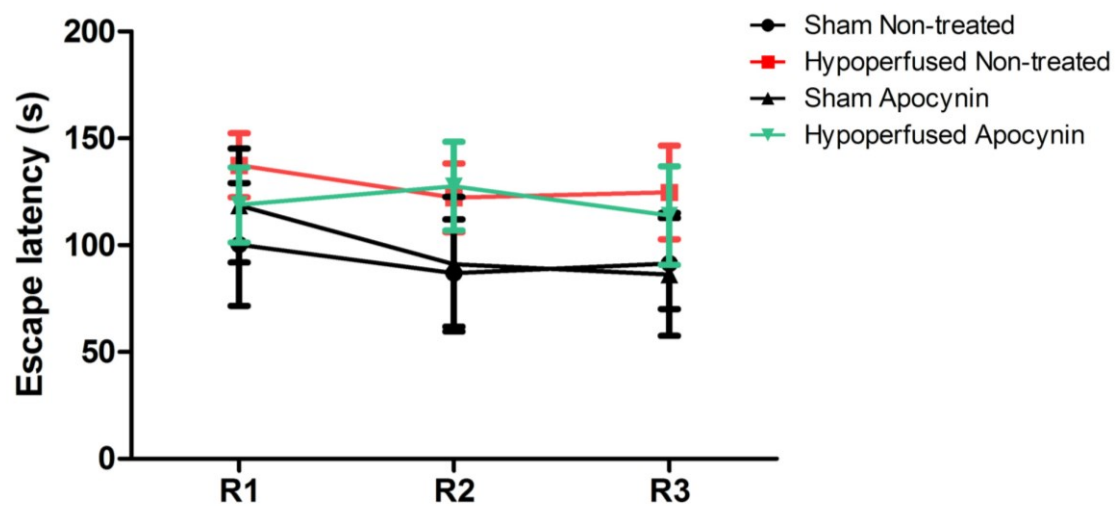


Figure 6.16 Apocynin does not improve performance on reversal learning. A reversal learning task was performed in order to assess executive function and cognitive flexibility. No significant effects of trial, surgery or treatment were detected on measures of reversal learning, indicating that mice were unable to learn the new location of the escape chamber and this deficit was not rescued by treatment with apocynin. Data presented as mean±SEM, n=6-10 per group. *p<0.05

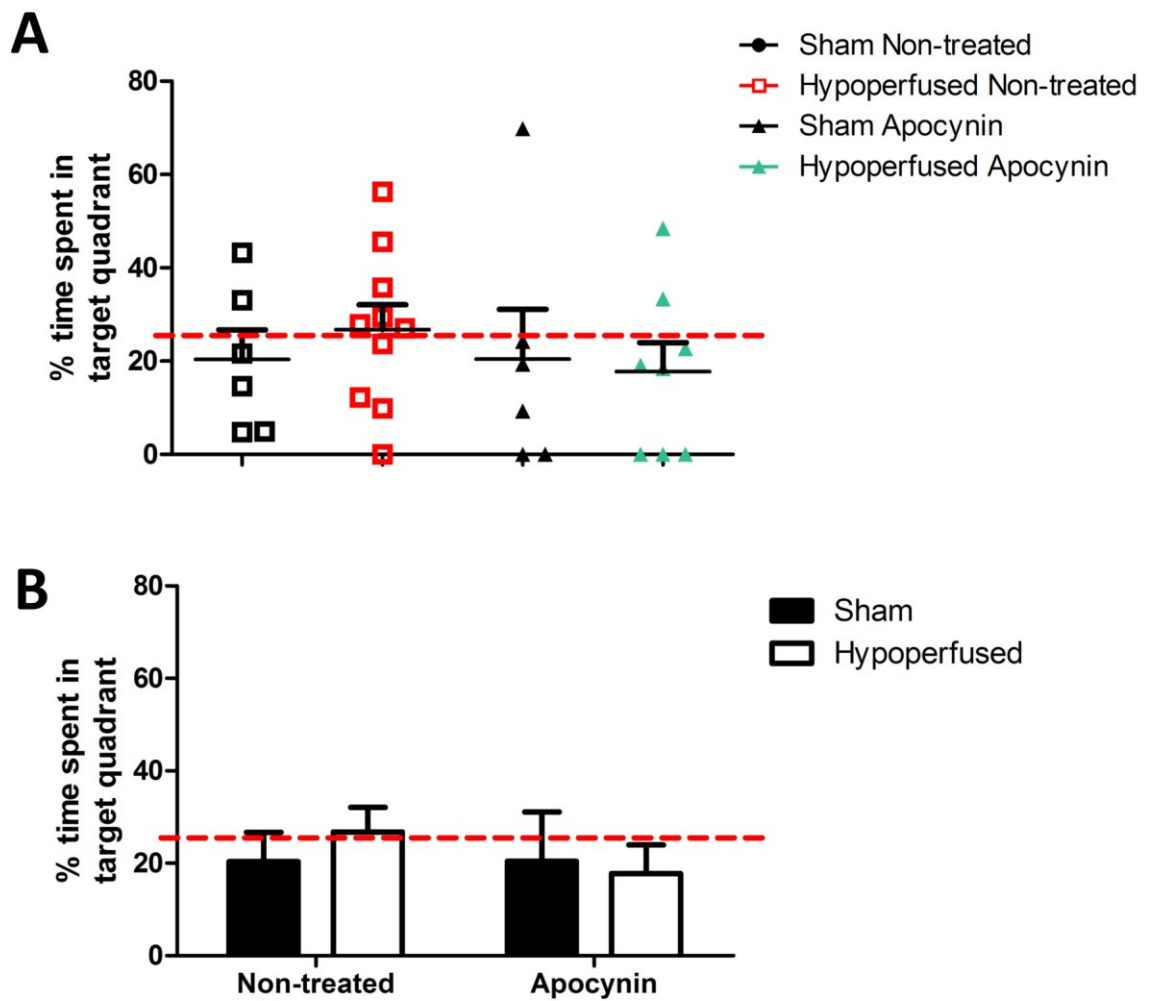


Figure 6.17 Apocynin does not improve performance on reversal memory. Cognitive flexibility was assessed using a reversal probe task, and mice were assessed on the percentage time spent in the target quadrant. (A) All groups performed no better than chance (indicated by dashed red line) ($20 \pm 15\%$ vs 25% , $p > 0.05$; $26 \pm 16\%$ vs 25% , $p > 0.05$; $20 \pm 26\%$ vs 25% , $p > 0.05$ and $17 \pm 17\%$ vs 25% , $p > 0.05$ for sham non-treated mice, hypoperfused non-treated mice, sham apocynin mice and hypoperfused apocynin mice respectively). (B) There were no significant overall effects of surgery or apocynin treatment on time spent in the target quadrant in the reversal memory probe task. Data presented as mean \pm SEM, $n = 6-10$ per group.

6.4 Discussion

In the present study, the NADPH oxidase inhibitor apocynin was shown to improve cortical neurovascular coupling following cerebral hypoperfusion in TgSwDI mice. Apocynin-treated mice also tended to have improved recovery of cortical blood flow and reduction of cortical ischaemic pathology. However, apocynin treatment did not prevent the development of vascular lesions elsewhere in the brain, nor did it prevent inflammation or cognitive decline.

6.4.1 Apocynin treatment does not protect against blood flow reductions following cerebral hypoperfusion but may improve recovery of cortical blood flow

Reductions in resting cerebral blood flow are induced by bilateral common carotid artery stenosis (BCAS) and remain reduced at 3 months following surgery. Treatment with apocynin did not protect against reductions in flow at 24 hours following surgery or at 3 months following surgery in subcortical regions, however, cortical blood flow did show a tendency to improve by 3 months after surgery in apocynin-treated mice. Lapi et al. (2012) showed a dose-dependent response to antioxidant treatment in blood flow during BCCAO, remarkably intravenous pretreatment 10 minutes prior to BCCAO with the highest dose of quercetin was able to increase cortical blood flow during the occlusion, and avoid the 60% reduction in flow that was observed in non-treated rats. This effect has also been demonstrated with several other antioxidant flavonoids (Mastantuono et al. 2015). In the present study, mice were not pre-treated with apocynin prior to the surgery, instead treatment was initiated in the drinking water after the BCAS surgery. Therefore it is perhaps not surprising that BCAS mice were not protected from blood flow reductions following the surgery. This allows the investigation of pathology that is downstream of blood flow reductions, rather than effects that are purely due to prevention of the acute, initial reduction in flow, and better mimics the clinical situation as vascular dysfunction is already likely to be present when an individual begins therapeutic

treatment. Dong et al. (2011) administered tempol, a superoxide scavenger, for 3 weeks following BCAS surgery in mice and found no change in resting cerebral blood flow relative to non-treated treated mice. These findings are in line with those from the present study, in which apocynin had no effect on recovery of cerebral blood flow at 1 month following BCAS surgery. Dong et al. (2011) demonstrate that in the absence of blood flow recovery, oxidative stress and spatial working memory were still improved; indicating that, at least in the short-term, recovery of blood flow may not be a requirement for functional improvement.

6.4.2 Neurovascular coupling is improved following treatment with apocynin

In the present study, treatment with apocynin was shown to ameliorate the impairment on neurovascular coupling induced by cerebral hypoperfusion. Neurovascular coupling was restored in the absence of a restoration in baseline cerebral blood flow, indicated by arterial spin labelling data. Although improvements in neurovascular coupling through apocynin treatment have been demonstrated previously in amyloid-expressing transgenic lines, this is the first study to present data on apocynin treatment in the BCAS model. Previous work has demonstrated that NOX expression is upregulated in response to hypoperfusion in TgSwDI mice (Section 5.3.8), the present study demonstrates that increases in NOX may be responsible for the observed impairment on neurovascular function. There are multiple mechanisms by which apocynin could improve neurovascular coupling. The inhibition of NOX results in reduced production of reactive superoxide species, and should therefore increase the biological half life of nitric oxide (NO). NOX inhibition should also reduce the inactivation or uncoupling of endothelial nitric oxide synthase (eNOS), leading to greater production of NO. Peroxynitrite formation will also be reduced, increasing the availability of vasodilators such as prostaglandins. It is important to bear in mind that although NOX2 was shown to increase following cerebral hypoperfusion, apocynin is a non-specific NOX inhibitor and may target

other NOX isoforms in addition to NOX2. The levels of NOX1 were not assessed in this study but have been shown to increase following 2 vessel occlusion (2VO) in rats, and inhibition using shRNA targeting NOX1 was also shown to improve pathological and cognitive outcomes (Choi et al. 2014). Therefore, the specific contribution of each NOX isoform to the deficit on neurovascular coupling cannot be determined from this study. It is also unclear which cells mediate the increased expression of NOX to induce vascular dysfunction. NOX1 is reported to be primarily expressed in neurons following hypoperfusion (Choi et al. 2014). NOX2 is expressed in neurons, microglia and endothelium, with endothelial NOX2 reported to mediate vascular dysfunction caused by vascular amyloid accumulation. The increased inflammation observed following hypoperfusion may also drive increased NOX2 activity in microglia and exacerbate vascular ROS production. Cell-specific genetic knockouts of NOX isoforms such as the endothelial NOX2 knockout mouse (Weissmann et al. 2012) would enable the contribution of individual cell types and NOX isoforms to be determined.

6.4.3 Apocynin treatment does not protect against overall vascular lesion development or inflammation

Treatment with apocynin did not prevent the overall development of vascular lesions, however, in agreement with the improvement of cortical vascular function, there was a trend towards a reduction in cortical ischaemic pathology. Cortical resting blood flow in apocynin-treated mice also showed a greater tendency to recover after 3 months relative to non-treated mice when assessed by laser speckle imaging. Together, the data indicate that apocynin may exert region-specific protection in the cortex. However, in other regions throughout the brain, apocynin-treated mice developed ischaemic and haemorrhagic lesions to nearly the same extent as non-treated mice following cerebral hypoperfusion. In line with this finding, *in vivo* measures of inflammation were also not reduced following apocynin treatment. This is in contrast to the

improvements observed in white matter lesions and inflammation following antioxidant therapy in short term hypoperfusion studies, and may indicate distinct pathways to white matter disruption or vascular dysfunction following chronic hypoperfusion. Toyama et al. (2014) provide evidence that treatment with apocynin for 3 weeks following BCAS in 9 week old mice can reduce white matter lesions and astrocytic activation in white matter tracts. They also demonstrate that blood-brain barrier disruption is improved by apocynin treatment, as leakage of the fluorescent tracer Evans blue is reduced. Dong et al (2011) also demonstrate reduction in white matter lesions following treatment with the free radical scavenger tempol for 2 weeks following cerebral hypoperfusion. Differences between the two studies may be explained by the difference in age of the mice, the use of a smaller diameter microcoil for induction of BCAS (0.16mm used by Toyama et al. vs 0.18mm used here), the increased duration of hypoperfusion in the present study and the additional burden of vascular and parenchymal amyloid deposition in the model. Further histological investigation of white matter lesions, for example myelin loss and axonal degeneration, may reveal whether NOX inhibition was able to protect against white matter disruption specifically, as has been reported in the studies described above. No other studies have aimed to also reduce grey matter vascular lesion burden by targeting oxidative stress during chronic cerebral hypoperfusion. Whilst antioxidant therapy may be successful in the short-term, sustained hypoperfusion and the resulting neuroinflammatory response may eventually overwhelm the antioxidant capacity of therapeutics. This may be particularly true for the TgSwDI model, where pre-existing microglial and astrocytic activation caused by the presence of amyloid deposition may exacerbate the release of pro-inflammatory mediators following hypoperfusion.

Reactive oxygen species have been shown to induce the activation of microglia and the production of pro-inflammatory mediators (Li et al. 2013; Brown, 2007). Despite this, in the

present study targeting NOX activity did not prevent an increase in inflammation, suggesting that inflammation occurs upstream of NOX activity following hypoperfusion. It is also conceivable that, following hypoperfusion, another source of ROS, for example mitochondrial ROS or xanthine oxidase activity, may induce microglial proliferation and cytokine production as has been demonstrated previously (Mander, Jekabsone and Brown, 2006; Naik and Dixit, 2011). Neuroinflammation may also be directly mediated by cytokine release from the endothelium in response to conditions of altered shear stress following hypoperfusion. Disturbed shear stress has been shown to induce the expression of endothelial inflammatory markers such as platelet endothelial cell adhesion molecule (PECAM1) and vascular cell adhesion molecule (VCAM1), and also to stimulate the release of TNF- α and IL-1 β from endothelial cells (Qin et al. 2015; Li et al. 2016). Together this enhances the recruitment of circulating leukocytes from the bloodstream and induces the activation of microglia within brain parenchyma, which may occur independently of NOX activity. Activated microglia further contribute to inflammatory cytokine production (e.g. of TNF- α and IL-6) that acts on the endothelium to reduce tight junction protein expression and disrupt the blood-brain barrier (Rochfort et al. 2014), contributing to the development of microbleeds. Production of reactive oxygen species by activated microglia is thought to induce endothelial dysfunction, due to disruption of NO signalling. Impaired endothelial function may result in localised areas of severe hypoperfusion and lead to the development of microinfarcts. NOX2 is critical to infarct development and progression following cerebral ischaemia, as inhibition or genetic deletion of NOX2 results in smaller infarct volumes and improved recovery (Jackman et al. 2009a; McCann, Dusting and Roulston, 2014). Overall, despite evidence for involvement of NOX activity in vascular lesion development, targeting NOX activity in the present study did not prevent development of ischaemic or haemorrhagic pathology 3 months following

hypoperfusion. Either neuroinflammation or an alternative ROS source may initiate vascular lesion development independently of impaired vascular function.

6.4.4 Vascular NOX2 expression is not reduced following apocynin treatment

In the present study, NOX2 expression was not reduced in the cerebral vasculature following apocynin treatment. Whilst this may explain the lack of protection conferred against development of vascular lesions, this is an interesting finding given that neurovascular coupling was found to be restored in the cortex. One potential explanation may be that microglial NOX2, rather than endothelial NOX2 may be more critical to neurovascular function, although microglial NOX2 was not assessed in this study. Apocynin is thought to inhibit NOX2 activation by preventing the translocation of its cytosolic subunits to the membrane, therefore it is also conceivable that apocynin is able to inhibit NOX2 activity without affecting the expression of the gp91 subunit detected by ELISA in the present study. Indeed, Nediani et al. (2007) showed that NOX-dependent superoxide production in human heart tissue was increased in the absence of detectable changes in gp91 subunit expression. Instead, they note that p47 translocation and an increase of p47phox in the membrane-bound fraction was responsible for the increase in NOX activity. In the present study, vessel-enriched homogenates were prepared from whole brains, although it would be interesting to determine whether regional variations in vascular NOX2 expression exist in hypoperfused TgSwDI mice, and whether, for instance, cortical NOX2 expression is reduced in line with neurovascular coupling improvements. Immunohistochemistry could be used in future to investigate distinctions in regional or cellular expression of NOX isoforms within tissue from the present study.

6.4.5 Apocynin treatment did not reduce amyloid burden

In the present study, apocynin administration did not reduce amyloid burden when assessed by 6E10 immunohistochemistry. A recent study by Han et al. (2015) using the Tg2576 mouse model found that apocynin treatment selectively reduced vascular amyloid load but had no effect on parenchymal plaque burden. Other studies using non-specific ROS scavengers, however, have found no effect on vascular amyloid load (Garcia-Alloza et al. 2009; Hartman et al. 2006). In contrast, parenchymal amyloid burden may be influenced by mitochondrial ROS, rather than that produced by NOX enzymes, as genetic deletion or overexpression of superoxide dismutase 2 has been shown to influence parenchymal amyloid deposition (Massaad et al. 2009; Esposito et al. 2006). However, increased mitochondrial ROS has been associated with both an increase (Massaad et al. 2009) and decrease (Esposito et al. 2006) in amyloid burden, therefore the nature of the interaction between ROS formation and amyloid deposition requires further investigation. There are several reasons why the current investigation may not detect any differences in amyloid load as a result of apocynin treatment. The present study is limited in that the current approach was performed over a small volume of the brain, is non-quantitative and does not allow a distinction between vascular and parenchymal amyloid burden. Future studies should utilise biochemical assays in order to quantify the concentration of different amyloid species within the brains of non-treated and apocynin-treated mice.

6.4.6 Behavioural impairments are not rescued by apocynin treatment

Chronic cerebral hypoperfusion induces deficits on spatial learning in TgSwDI mice. Treatment with apocynin was not able to rescue this cognitive deficit, in line with the lack of protection conferred against inflammation and the development of vascular lesions. Both

neuroinflammation and the presence of ischaemic or haemorrhagic pathology are associated with poorer cognitive outcomes (Suridjan et al. 2015; Arvanitakis et al. 2011; Meier et al. 2014), therefore it is unsurprising that apocynin did not improve cognition since vascular lesions were still present. In several studies, improvements on spatial learning and memory have been demonstrated in conjunction with improved white matter integrity following treatment with antioxidants (Korani et al. 2014; Peng et al. 2007; Xu et al. 2010). Critically, these studies induce hypoperfusion in young mice and for short durations. However, another important consideration regarding apocynin treatment is the dosing regimen, specifically the optimal dose concentration and the onset and duration of treatment. A wide range of concentrations are found in the literature regarding apocynin treatment, and may depend on the route of administration. In neurodegenerative models, doses in the range of 5mg/kg/day to 300mg/kg/day have been shown to be effective (Ferreira et al. 2013; Ghosh et al. 2012), and several studies report dose dependent effects. In superoxide dismutase 1 (SOD1) amyotrophic lateral sclerosis (ALS) mutant mice, Harraz et al. (2008) demonstrate progressive increases in survival rates with increasing doses of apocynin treatment from 0 (control) to 30, 150 or 300mg/kg/day. Whilst the dose of 30mg/kg used in the present study was shown to be effective in improving lifespan in this model, the greatest improvement was seen with the highest dose of 300mg/kg/day. Ghosh et al. (2012) also report only moderate neuroprotection in a mouse model of ALS with doses of 100 or 150mg/kg/day, but substantial reductions in neuroinflammation, neuronal loss and cognitive impairment with a dose of 300mg/kg/day of dimerised apocynin (diapocynin). Several papers report significant improvements in ROS production, neurodegeneration and cognition at doses of 30mg/kg/day, as used in the present study (Han et al. 2015; Kim et al. 2013; Beswick et al. 2001). A dose of 10mg/kg/day was sufficient to reduce inflammation in an APP mutant mouse line, but did not rescue behavioural

impairments (Lull et al. 2011). Whilst many studies report higher doses as more effective, others demonstrate a negative effect at higher concentrations of apocynin. Jackman et al. (2009a) demonstrate that administration of apocynin at 5mg/kg induced significantly greater mortality in mice following MCAO compared to treatment with 2.5mg/kg or to vehicle-treated mice. Tang et al. (2008) also showed that while treatment with 2.5mg/kg was effective for reducing infarct volume and neurological function following MCAO, higher doses of 3.75 and 5mg/kg increased the incidence of cerebral haemorrhage and had no protective effect on other measures. The variation in the literature may reflect underlying differences in the severity of the models used and the routes of administration. However, ROS signalling plays a fundamental physiological role in the control of vascular tone, and it is reasonable to expect that disruption of ROS signalling through NOX inhibition may also interfere with homeostatic functions of ROS. In line with this, Choi et al. (2014) report that administration of apocynin to sham mice caused deficits on spatial learning. Careful titration may be required in future to determine the dose needed to inhibit pathologically increased NOX activity, whilst sparing physiological NOX. Apocynin lacks specificity for individual NOX isoforms, which may also underlie the lack of improvement on vascular integrity and cognition observed in this study. Whilst inhibiting the activity of NOX2 may be beneficial for neurovascular coupling through reduction of superoxide production, the ability of apocynin to inactivate NOX4, or to react with its product, H₂O₂ (Petronio et al. 2013), may inhibit the protective angiogenic response of NOX4 and contribute to further hypoperfusion and the development of vascular lesions. Jackman et al. (2009b) also demonstrate a potentially protective role for NOX1 following ischaemic stroke, as genetic deletion of NOX1 resulted in significantly larger cortical infarct volumes relative to wild type mice following transient MCAO. Again, inhibition of NOX1 by apocynin may therefore result in loss of protection from vascular disruption and the

development of vascular lesions. A further consideration is the ability of apocynin to inhibit NOX in distinct cell populations. Apocynin requires oxidation in order to become activated, in neutrophils this occurs through the action of myeloperoxidase (Ximenes et al. 2007). However, myeloperoxidase expression is thought to be negligible in endothelial cells (Heumuller et al. 2008). It is possible that the lack of myeloperoxidase expression prevents the activity of apocynin in vascular cells, and therefore apocynin is unable to modulate NOX activity in the endothelium. This may explain why apocynin administration was unable to prevent the development of ischaemic and haemorrhagic vascular lesions in the present study. However, additional peroxidases may exist in the cerebral endothelium, further studies are warranted to investigate apocynin oxidation and NOX activity in the vasculature specifically. Interestingly, astrocytes have been shown to express myeloperoxidase (Chang et al. 2013; Maki et al. 2009). Apocynin may therefore modulate NOX activity in astrocytes, and preserve neurovascular coupling through reduction of ROS/RNS in this cell population. The fact that apocynin is able to reach the CNS when administered orally (Han et al. 2015; Trumbull et al. 2012), and its low toxicity (Stefanska and Pawliczak, 2008) make it an attractive therapeutic option for treating cerebrovascular dysfunction. However, lack of specificity for pathogenic rather than physiological ROS/RNS sources may mean that potential benefits are outweighed by unwanted deleterious effects on physiologic ROS/RNS signalling, and the efficacy of apocynin to inhibit NOX in the vasculature is unclear.

6.4.7 Conclusions

Oxidative stress has been previously targeted in vivo using antioxidant therapy to improve outcomes following hypoperfusion, however, antioxidants have met with little success in clinical trials for vascular disease or dementias, as they are challenging to deliver to the brain in meaningful doses and may be converted to pro-oxidant species in vivo. Targeting the

production of ROS/RNS rather than scavenging superoxide may therefore prove a more effective approach for therapeutic intervention. In an effort to identify the specific source of pathological ROS/RNS production induced by hypoperfusion, activity of NOX enzymes was pharmacologically inhibited using apocynin. Whilst administration of apocynin rescued neurovascular coupling, this did not result in the prevention of vascular lesions or cognitive decline. Inflammation was still prominent following apocynin treatment and may represent an additional important therapeutic target. Further characterisation of the impact of apocynin treatment on NOX activity is required in order to draw conclusions about the role of NOX in the pathological alterations induced by chronic cerebral hypoperfusion. Future work should aim to elucidate the specific contributions of individual NOX isoforms, and the expression of those isoforms in distinct cell populations, as non-specific inhibition may produce disruption of physiological NOX signalling.

Chapter 7.

Discussion and Conclusions

Discussion and Conclusion

7.1 Summary

In conclusion, the studies presented here demonstrate that ageing and cerebral hypoperfusion, both prominent risk factors for vascular cognitive impairment, result in profound impairment of neurovascular coupling, the disruption of the neurovascular unit and the development of vascular lesions. This accumulating burden of vascular pathology ultimately drives tissue degeneration and cognitive decline. Results from the present studies indicate increased oxidative stress and increased inflammation as prominent pathological features of vascular risk factors, but suggest that targeting oxidative stress through reducing NOX alone may not be sufficient to protect against cognitive decline.

7.2 Future directions

Future studies should delineate the specific contributions of individual NOX isoforms to vascular oxidative stress, as the relative contributions of each isoform to physiological or pathological signalling are ill-defined, particularly in disease states. Genetic deletion of individual NOX isoforms under a cell-specific promoter in mouse models would be of benefit here, particularly if inducible models are available to avoid confounding effects of genetic loss during development. The use of validated, specific inhibitors of NOX isoforms such as GSK2795039 for NOX2 (Hirano et al. 2015) should also be considered, although there is a relative paucity of truly specific isoform inhibitors. In addition, it cannot be ruled out that NOX activity is merely a secondary event that perpetuates vascular dysfunction, and may not be the main driver of vascular pathology. Microglial and astrocytic activation has been documented in the present studies and throughout the existing literature- notably, inflammation persisted even when NOX activity was inhibited. In conditions of low or disturbed blood flow,

endothelial cells are capable of producing pro-inflammatory cytokines and may signal directly to other inflammatory cells in the brain, in addition to recruiting leukocytes from the periphery. The inflammatory cascade leading to blood-brain barrier breakdown and the development of vascular lesions may therefore be more critical to cognitive impairment. Currently available drugs to inhibit microglial proliferation, such as colony stimulating factor 1 receptor inhibitors, would allow assessment of the contribution of microglial activation to progression of vascular lesions. Although vascular cognitive impairment may arise from heterogeneous vascular pathology, the identification of common pathways from vascular dysfunction to cognitive decline would provide invaluable targets for potential therapeutic interventions, in a condition for which there are currently no approved treatments.

7.3 Future implications for treatment of vascular cognitive impairment

Recent studies have reported a fall in the percentage of new cases of dementia (Matthews et al. 2016; Qiu et al. 2013). Whilst this is an encouraging trend, the absolute number of individuals affected may continue to rise as the global population ages. As such, the identification of effective therapeutic strategies to prevent or treat vascular cognitive impairment and dementia remains a critical issue due to the significant social and economic costs involved in caring for affected individuals. Studies have suggested that modification of vascular risk factors in mid-life can be protective against vascular cognitive impairment (Firbank et al. 2007; Tolppanen et al. 2015; Moorhouse and Rockwood, 2008), however there are currently no effective treatments once vascular cognitive impairment has been diagnosed. The same is also true for individuals affected by Alzheimer's disease. There is increasing recognition of the prevalence of cerebrovascular pathology in Alzheimer's disease cases, which may also explain why numerous clinical trials have failed to slow or treat Alzheimer's disease when underlying vascular pathology remains untreated. The results described in the present study demonstrate

that ageing, cerebral amyloid angiopathy and cerebral hypoperfusion exert a profound impact on the structure and function of the cerebral vasculature, resulting in small vessel disease-like pathology and cognitive impairment. Thus, they lend support to primary prevention strategies aimed at improving vascular health for reducing the incidence of vascular cognitive impairment. Currently, clinical trials are ongoing as to the efficacy of targeting vascular disease- one study involving 600 participants with vascular dementia will investigate the benefits of amlodipine, a calcium channel blocker used for the treatment of hypertension (Greenan et al. 2016); another smaller study will gather preliminary data on the use of cilostazol (a vasodilator and antiplatelet agent used for treatment of peripheral vascular disease and prevention of recurrent stroke) and isosorbide mononitrate (a vasodilator used for treatment of angina) (clinical trial:NCT02481323). Results of these trials may indicate whether improving overall vascular health is sufficient to slow cognitive decline, or whether a more specific approach targeting precise molecular pathways may be required. Building on the findings of the present study, dissemination of the molecular signalling that initiates and maintains vascular dysfunction may prove invaluable for the identification of novel therapeutic targets for the treatment of vascular cognitive impairment.

Chapter 8. References

References

- Abraham, H.M., Wolfson, L., Moscufo, N., Guttmann, C.R., Kaplan, R.F., White, W.B. 2016. Cardiovascular risk factors and small vessel disease of the brain: Blood pressure, white matter lesions, and functional decline in older persons. *J Cereb Blood Flow Metab* 36(1), 132-42. doi:10.1038/jcbfm.2015.121.
- Adair, J.C., Charlie, J., Dencoff, J.E., Kaye, J.A., Quinn, J.F., Camicioli, R.M., Stetler-Stevenson, W.G., Rosenberg, G.A. 2004. Measurement of gelatinase B (MMP-9) in the cerebrospinal fluid of patients with vascular dementia and Alzheimer disease. *Stroke* 35(6), e159-62. doi:10.1161/01.STR.0000127420.10990.76.
- Ai, Q., Pu, Y.H., Sy, C., Liu, L.P., Gao, P.Y. 2014. Impact of regional white matter lesions on cognitive function in subcortical vascular cognitive impairment. *Neurol Res* 36(5), 434-43. doi:10.1179/1743132814Y.0000000354.
- Akinyemi, R.O., Mukaetova-Ladinska, E.B., Attems, J., Ihara, M., Kalaria, R.N. 2013. Vascular risk factors and neurodegeneration in ageing related dementias: Alzheimer's disease and vascular dementia. *Curr Alzheimer Res* 10(6), 642-53.
- Alosco, M.L., Gunstad, J., Jerskey, B.A., Xu, X., Clark, U.S., Hassenstab, J., Cote, D.M., Walsh, E.G., Labbe, D.R., Hoge, R., Cohen, R.A., Sweet, L.H. 2013. The adverse effects of reduced cerebral perfusion on cognition and brain structure in older adults with cardiovascular disease. *Brain Behav* 3(6), 626-36. doi:10.1002/brb3.171.
- Alvarez, J.I., Dodelet-Devillers, A., Kebir, H., Ifergan, I., Fabre, P.J., Terouz, S., Sabbagh, M., Wosik, K., Bourbonnière, L., Bernard, M., van Horssen, J., de Vries, H.E., Charron, F., Prat, A. 2011. The Hedgehog pathway promotes blood-brain barrier integrity and CNS immune quiescence. *Science* 334(6063), 1727-31. doi:10.1126/science.1206936.
- Amantea, D., Nappi, G., Bernardi, G., Bagetta, G., Corasaniti, M.T. 2009. Post-ischemic brain damage: pathophysiology and role of inflammatory mediators. *FEBS J* 276(1), 13-26. doi:10.1111/j.1742-4658.2008.06766.x.
- Anderson, J.M., Van Itallie, C.M. 2009. Physiology and function of the tight junction. *Cold Spring Harb Perspect Biol* 1(2), a002584. doi:10.1101/cshperspect.a002584.
- Arbel-Ornath, M., Hudry, E., Eikermann-Haerter, K., Hou, S., Gregory, J.L., Zhao, L., Betensky, R.A., Frosch, M.P., Greenberg, S.M., Bacskaï, B.J. 2013. Interstitial fluid drainage is impaired in ischemic stroke and Alzheimer's disease mouse models. *Acta Neuropathol* 126(3), 353-64. doi:10.1007/s00401-013-1145-2.
- Arrighi, H.M., Barakos, J., Barkhof, F., Tampieri, D., Jack, C., Melançon, D., Morris, K., Ketter, N., Liu, E., Brashear, H.R. 2016. Amyloid-related imaging abnormalities-haemosiderin (ARIA-H) in patients with Alzheimer's disease treated with

- bapineuzumab: a historical, prospective secondary analysis. *J Neurol Neurosurg Psychiatry* 87(1), 106-12. doi:10.1136/jnnp-2014-309493.
- Arunachalam, G., Yao, H., Sundar, I.K., Caito, S., Rahman, I. 2010. SIRT1 regulates oxidant- and cigarette smoke-induced eNOS acetylation in endothelial cells: Role of resveratrol. *Biochem Biophys Res Commun* 393(1), 66-72. doi:10.1016/j.bbrc.2010.01.080.
- Arvanitakis, Z., Leurgans, S.E., Barnes, L.L., Bennett, D.A., Schneider, J.A. 2011a. Microinfarct pathology, dementia, and cognitive systems. *Stroke* 42(3), 722-7. doi:10.1161/STROKEAHA.110.595082.
- Arvanitakis, Z., Leurgans, S.E., Wang, Z., Wilson, R.S., Bennett, D.A., Schneider, J.A. 2011b. Cerebral amyloid angiopathy pathology and cognitive domains in older persons. *Ann Neurol* 69(2), 320-7. doi:10.1002/ana.22112.
- Asllani, I., Habeck, C., Scarmeas, N., Borogovac, A., Brown, T.R., Stern, Y. 2008. Multivariate and univariate analysis of continuous arterial spin labeling perfusion MRI in Alzheimer's disease. *J Cereb Blood Flow Metab* 28(4), 725-36. doi:10.1038/sj.jcbfm.9600570.
- Attems, J., Jellinger, K., Thal, D.R., Van Nostrand, W. 2011. Review: sporadic cerebral amyloid angiopathy. *Neuropathol Appl Neurobiol* 37(1), 75-93. doi:10.1111/j.1365-2990.2010.01137.x.
- Attems, J., Jellinger, K.A. 2014. The overlap between vascular disease and Alzheimer's disease--lessons from pathology. *BMC Med* 12, 206. doi:10.1186/s12916-014-0206-2.
- Attwell, D., Laughlin, S.B. 2001. An energy budget for signaling in the grey matter of the brain. *J Cereb Blood Flow Metab* 21(10), 1133-45. doi:10.1097/00004647-200110000-00001.
- Ayata, C., Dunn, A.K., Gursoy-OZdemir, Y., Huang, Z., Boas, D.A., Moskowitz, M.A. 2004. Laser speckle flowmetry for the study of cerebrovascular physiology in normal and ischemic mouse cortex. *J Cereb Blood Flow Metab* 24(7), 744-55. doi:10.1097/01.WCB.0000122745.72175.D5.
- Back, S.A., Kroenke, C.D., Sherman, L.S., Lawrence, G., Gong, X., Taber, E.N., Sonnen, J.A., Larson, E.B., Montine, T.J. 2011. White matter lesions defined by diffusion tensor imaging in older adults. *Ann Neurol* 70(3), 465-76. doi:10.1002/ana.22484.
- Bailey, E.L., McCulloch, J., Sudlow, C., Wardlaw, J.M. 2009. Potential animal models of lacunar stroke: a systematic review. *Stroke* 40(6), e451-8. doi:10.1161/STROKEAHA.108.528430.
- Balbi, M., Ghosh, M., Longden, T.A., Jativa Vega, M., Gesierich, B., Hellal, F., Lourdopoulos, A., Nelson, M.T., Plesnila, N. 2015. Dysfunction of mouse cerebral arteries during early aging. *J Cereb Blood Flow Metab* 35(9), 1445-53. doi:10.1038/jcbfm.2015.107.

- Baloyannis, S.J., Baloyannis, I.S. 2012. The vascular factor in Alzheimer's disease: a study in Golgi technique and electron microscopy. *J Neurol Sci* 322(1-2), 117-21. doi:10.1016/j.jns.2012.07.010.
- Balucani, C., Viticchi, G., Falsetti, L., Silvestrini, M. 2012. Cerebral hemodynamics and cognitive performance in bilateral asymptomatic carotid stenosis. *Neurology* 79(17), 1788-95. doi:10.1212/WNL.0b013e318270402e.
- Banerjee, G., Wilson, D., Jäger, H.R., Werring, D.J. 2016. Novel imaging techniques in cerebral small vessel diseases and vascular cognitive impairment. *Biochim Biophys Acta* 1862(5), 926-38. doi:10.1016/j.bbadis.2015.12.010.
- Barbosa-Sicard, E., Frömel, T., Keserü, B., Brandes, R.P., Morisseau, C., Hammock, B.D., Braun, T., Krüger, M., Fleming, I. 2009. Inhibition of the soluble epoxide hydrolase by tyrosine nitration. *J Biol Chem* 284(41), 28156-63. doi:10.1074/jbc.M109.054759.
- Barnes, C.A. 1979. Memory deficits associated with senescence: a neurophysiological and behavioral study in the rat. *J Comp Physiol Psychol* 93(1), 74-104.
- Basuroy, S., Bhattacharya, S., Leffler, C.W., Parfenova, H. 2009. Nox4 NADPH oxidase mediates oxidative stress and apoptosis caused by TNF-alpha in cerebral vascular endothelial cells. *Am J Physiol Cell Physiol* 296(3), C422-32. doi:10.1152/ajpcell.00381.2008.
- Bath, P.M., Wardlaw, J.M. 2015. Pharmacological treatment and prevention of cerebral small vessel disease: a review of potential interventions. *Int J Stroke* 10(4), 469-78. doi:10.1111/ijvs.12466.
- Bazargani, N., Attwell, D. 2016. Astrocyte calcium signaling: the third wave. *Nat Neurosci* 19(2), 182-9. doi:10.1038/nn.4201.
- Beason-Held, L.L., Moghekar, A., Zonderman, A.B., Kraut, M.A., Resnick, S.M. 2007. Longitudinal changes in cerebral blood flow in the older hypertensive brain. *Stroke* 38(6), 1766-73. doi:10.1161/STROKEAHA.106.477109.
- Beauquis, J., Homo-Delarche, F., Giroix, M.H., Ehses, J., Coulaud, J., Roig, P., Portha, B., De Nicola, A.F., Saravia, F. 2010. Hippocampal neurovascular and hypothalamic-pituitary-adrenal axis alterations in spontaneously type 2 diabetic GK rats. *Exp Neurol* 222(1), 125-34. doi:10.1016/j.expneurol.2009.12.022.
- Beckmann, N., Stirnimann, R., Bochen, D. 1999. High-resolution magnetic resonance angiography of the mouse brain: application to murine focal cerebral ischemia models. *J Magn Reson* 140(2), 442-50. doi:10.1006/jmre.1999.1864.
- Bedard, K., Krause, K.H. 2007. The NOX family of ROS-generating NADPH oxidases: physiology and pathophysiology. *Physiol Rev* 87(1), 245-313. doi:10.1152/physrev.00044.2005.

- Bell, R.D., Deane, R., Chow, N., Long, X., Sagare, A., Singh, I., Streib, J.W., Guo, H., Rubio, A., Van Nostrand, W., Miano, J.M., Zlokovic, B.V. 2009. SRF and myocardin regulate LRP-mediated amyloid-beta clearance in brain vascular cells. *Nat Cell Biol* 11(2), 143-53. doi:10.1038/ncb1819.
- Bell, R.D., Winkler, E.A., Sagare, A.P., Singh, I., LaRue, B., Deane, R., Zlokovic, B.V. 2010. Pericytes control key neurovascular functions and neuronal phenotype in the adult brain and during brain aging. *Neuron* 68(3), 409-27. doi:10.1016/j.neuron.2010.09.043.
- Bennett, S.A., Pappas, B.A., Stevens, W.D., Davidson, C.M., Fortin, T., Chen, J. 2000. Cleavage of amyloid precursor protein elicited by chronic cerebral hypoperfusion. *Neurobiol Aging* 21(2), 207-14.
- Bernbaum, M., Menon, B.K., Fick, G., Smith, E.E., Goyal, M., Frayne, R., Coutts, S.B. 2015. Reduced blood flow in normal white matter predicts development of leukoaraiosis. *J Cereb Blood Flow Metab* 35(10), 1610-5. doi:10.1038/jcbfm.2015.92.
- Beswick, R.A., Dorrance, A.M., Leite, R., Webb, R.C. 2001. NADH/NADPH oxidase and enhanced superoxide production in the mineralocorticoid hypertensive rat. *Hypertension* 38(5), 1107-11.
- Blair, G.W., Doubal, F.N., Thrippleton, M.J., Marshall, I., Wardlaw, J.M. 2016. Magnetic resonance imaging for assessment of cerebrovascular reactivity in cerebral small vessel disease: A systematic review. *J Cereb Blood Flow Metab* 36(5), 833-41. doi:10.1177/0271678X16631756.
- Boehm-Sturm, P., Farr, T.D., Adamczak, J., Jikeli, J.F., Mengler, L., Wiedermann, D., Kallur, T., Kiselev, V., Hoehn, M. 2013. Vascular changes after stroke in the rat: a longitudinal study using optimized magnetic resonance imaging. *Contrast Media Mol Imaging* 8(5), 383-92. doi:10.1002/cmmi.1534.
- Boscia, F., Begum, G., Pignataro, G., Sirabella, R., Cuomo, O., Casamassa, A., Sun, D., Annunziato, L. 2016. Glial Na⁽⁺⁾ -dependent ion transporters in pathophysiological conditions. *Glia* 64(10), 1677-97. doi:10.1002/glia.23030.
- Bosomtwi, A., Jiang, Q., Ding, G.L., Zhang, L., Zhang, Z.G., Lu, M., Ewing, J.R., Chopp, M. 2008. Quantitative evaluation of microvascular density after stroke in rats using MRI. *J Cereb Blood Flow Metab* 28(12), 1978-87. doi:10.1038/jcbfm.2008.85.
- Bridges, L.R., Andoh, J., Lawrence, A.J., Khoong, C.H., Poon, W.W., Esiri, M.M., Markus, H.S., Hainsworth, A.H. 2014. Blood-brain barrier dysfunction and cerebral small vessel disease (arteriolosclerosis) in brains of older people. *J Neuropathol Exp Neurol* 73(11), 1026-33. doi:10.1097/NEN.0000000000000124.
- Brown, G.C. 2007. Mechanisms of inflammatory neurodegeneration: iNOS and NADPH oxidase. *Biochem Soc Trans* 35(Pt 5), 1119-21. doi:10.1042/BST0351119.

- Brown, W.R., Thore, C.R. 2011. Review: cerebral microvascular pathology in ageing and neurodegeneration. *Neuropathol Appl Neurobiol* 37(1), 56-74. doi:10.1111/j.1365-2990.2010.01139.x.
- Busch, H.J., Buschmann, I.R., Mies, G., Bode, C., Hossmann, K.A. 2003. Arteriogenesis in hypoperfused rat brain. *J Cereb Blood Flow Metab* 23(5), 621-8. doi:10.1097/01.WCB.0000057741.00152.E4.
- Cai, H., Li, Z., Davis, M.E., Kanner, W., Harrison, D.G., Dudley, S.C. 2003. Akt-dependent phosphorylation of serine 1179 and mitogen-activated protein kinase kinase/extracellular signal-regulated kinase 1/2 cooperatively mediate activation of the endothelial nitric-oxide synthase by hydrogen peroxide. *Mol Pharmacol* 63(2), 325-31.
- Cai, Z., Hussain, M.D., Yan, L.J. 2014. Microglia, neuroinflammation, and beta-amyloid protein in Alzheimer's disease. *Int J Neurosci* 124(5), 307-21. doi:10.3109/00207454.2013.833510.
- Calabro, R.S., Gervasi, G., Baglieri, A., Furnari, A., Marino, S., Bramanti, P. 2013. Is high oral dose L-arginine intake effective in leukoaraiosis? Preliminary data, study protocol and expert's opinion. *Curr Aging Sci* 6(2), 170-7.
- Calhoun, M.E., Burgermeister, P., Phinney, A.L., Stalder, M., Tolnay, M., Wiederhold, K.H., Abramowski, D., Sturchler-Pierrat, C., Sommer, B., Staufenbiel, M., Jucker, M. 1999. Neuronal overexpression of mutant amyloid precursor protein results in prominent deposition of cerebrovascular amyloid. *Proc Natl Acad Sci U S A* 96(24), 14088-93.
- Carare, R.O., Bernardes-Silva, M., Newman, T.A., Page, A.M., Nicoll, J.A., Perry, V.H., Weller, R.O. 2008. Solutes, but not cells, drain from the brain parenchyma along basement membranes of capillaries and arteries: significance for cerebral amyloid angiopathy and neuroimmunology. *Neuropathol Appl Neurobiol* 34(2), 131-44. doi:10.1111/j.1365-2990.2007.00926.x.
- Carare, R.O., Hawkes, C.A., Jeffrey, M., Kalaria, R.N., Weller, R.O. 2013. Review: cerebral amyloid angiopathy, prion angiopathy, CADASIL and the spectrum of protein elimination failure angiopathies (PEFA) in neurodegenerative disease with a focus on therapy. *Neuropathol Appl Neurobiol* 39(6), 593-611. doi:10.1111/nan.12042.
- Castellani, R.J., Rolston, R.K., Smith, M.A. 2010. Alzheimer disease. *Dis Mon* 56(9), 484-546. doi:10.1016/j.disamonth.2010.06.001.
- Cerbai, F., Lana, D., Nosi, D., Petkova-Kirova, P., Zecchi, S., Brothers, H.M., Wenk, G.L., Giovannini, M.G. 2012. The neuron-astrocyte-microglia triad in normal brain ageing and in a model of neuroinflammation in the rat hippocampus. *PLoS One* 7(9), e45250. doi:10.1371/journal.pone.0045250.
- Chabriat, H., Joutel, A., Dichgans, M., Tournier-Lasserre, E., Boussier, M.G. 2009. Cadasil. *Lancet Neurol* 8(7), 643-53. doi:10.1016/S1474-4422(09)70127-9.

- Challa, V.R., Thore, C.R., Moody, D.M., Anstrom, J.A., Brown, W.R. 2004. Increase of white matter string vessels in Alzheimer's disease. *J Alzheimers Dis* 6(4), 379-83; discussion 443-9.
- Chang, C.Y., Choi, D.K., Lee, D.K., Hong, Y.J., Park, E.J. 2013. Resveratrol confers protection against rotenone-induced neurotoxicity by modulating myeloperoxidase levels in glial cells. *PLoS One* 8(4), e60654. doi:10.1371/journal.pone.0060654.
- Chao, L.L., Buckley, S.T., Kornak, J., Schuff, N., Madison, C., Yaffe, K., Miller, B.L., Kramer, J.H., Weiner, M.W. 2010a. ASL perfusion MRI predicts cognitive decline and conversion from MCI to dementia. *Alzheimer Dis Assoc Disord* 24(1), 19-27. doi:10.1097/WAD.0b013e3181b4f736.
- Chao, L.L., Buckley, S.T., Kornak, J., Schuff, N., Madison, C., Yaffe, K., Miller, B.L., Kramer, J.H., Weiner, M.W. 2010b. ASL perfusion MRI predicts cognitive decline and conversion from MCI to dementia. *Alzheimer Dis Assoc Disord* 24(1), 19-27. doi:10.1097/WAD.0b013e3181b4f736.
- Charidimou, A., Martinez-Ramirez, S., Reijmer, Y.D., Oliveira-Filho, J., Lauer, A., Roongpiboonsopit, D., Frosch, M., Vashkevich, A., Ayres, A., Rosand, J., Gurol, M.E., Greenberg, S.M., Viswanathan, A. 2016. Total Magnetic Resonance Imaging Burden of Small Vessel Disease in Cerebral Amyloid Angiopathy: An Imaging-Pathologic Study of Concept Validation. *JAMA Neurol* 73(8), 994-1001. doi:10.1001/jamaneurol.2016.0832.
- Chen, A., Akinyemi, R.O., Hase, Y., Firbank, M.J., Ndung'u, M.N., Foster, V., Craggs, L.J., Washida, K., Okamoto, Y., Thomas, A.J., Polvikoski, T.M., Allan, L.M., Oakley, A.E., O'Brien, J.T., Horsburgh, K., Ihara, M., Kalaria, R.N. 2016. Frontal white matter hyperintensities, clasmotodendrosis and gliovascular abnormalities in ageing and post-stroke dementia. *Brain* 139(Pt 1), 242-58. doi:10.1093/brain/awv328.
- Chen, B.R., Kozberg, M.G., Bouchard, M.B., Shaik, M.A., Hillman, E.M. 2014. A critical role for the vascular endothelium in functional neurovascular coupling in the brain. *J Am Heart Assoc* 3(3), e000787. doi:10.1161/JAHA.114.000787.
- Chen, J.J., Rosas, H.D., Salat, D.H. 2011a. Age-associated reductions in cerebral blood flow are independent from regional atrophy. *Neuroimage* 55(2), 468-78. doi:10.1016/j.neuroimage.2010.12.032.
- Chen, J.J., Rosas, H.D., Salat, D.H. 2011b. Age-associated reductions in cerebral blood flow are independent from regional atrophy. *Neuroimage* 55(2), 468-78. doi:10.1016/j.neuroimage.2010.12.032.
- Cho, H., Lee, H.Y., Han, M., Choi, J.R., Ahn, S., Lee, T., Chang, Y., Park, J. 2016. Localized Down-regulation of P-glycoprotein by Focused Ultrasound and Microbubbles induced Blood-Brain Barrier Disruption in Rat Brain. *Sci Rep* 6, 31201. doi:10.1038/srep31201.

- Choi, D.H., Lee, K.H., Kim, J.H., Seo, J.H., Kim, H.Y., Shin, C.Y., Han, J.S., Han, S.H., Kim, Y.S., Lee, J. 2014. NADPH oxidase 1, a novel molecular source of ROS in hippocampal neuronal death in vascular dementia. *Antioxid Redox Signal* 21(4), 533-50. doi:10.1089/ars.2012.5129.
- Cipolla MJ. 2009. *The Cerebral Circulation*. San Rafael (CA): Morgan & Claypool Life Sciences. Chapter 5, Control of Cerebral Blood Flow. Retrieved from: <http://www.ncbi.nlm.nih.gov/books/NBK53082/>
- Coltman, R., Spain, A., Tsenkina, Y., Fowler, J.H., Smith, J., Scullion, G., Allerhand, M., Scott, F., Kalaria, R.N., Ihara, M., Daumas, S., Deary, I.J., Wood, E., McCulloch, J., Horsburgh, K. 2011a. Selective white matter pathology induces a specific impairment in spatial working memory. *Neurobiol Aging* 32(12), 2324.e7-12. doi:10.1016/j.neurobiolaging.2010.09.005.
- Coltman, R., Spain, A., Tsenkina, Y., Fowler, J.H., Smith, J., Scullion, G., Allerhand, M., Scott, F., Kalaria, R.N., Ihara, M., Daumas, S., Deary, I.J., Wood, E., McCulloch, J., Horsburgh, K. 2011b. Selective white matter pathology induces a specific impairment in spatial working memory. *Neurobiol Aging* 32(12), 2324.e7-12. doi:10.1016/j.neurobiolaging.2010.09.005.
- Conijn, M.M., Hoogduin, J.M., van der Graaf, Y., Hendrikse, J., Luijten, P.R., Geerlings, M.I. 2012. Microbleeds, lacunar infarcts, white matter lesions and cerebrovascular reactivity -- a 7 T study. *Neuroimage* 59(2), 950-6. doi:10.1016/j.neuroimage.2011.08.059.
- Craige, S.M., Chen, K., Pei, Y., Li, C., Huang, X., Chen, C., Shibata, R., Sato, K., Walsh, K., Keaney, J.F. 2011. NADPH oxidase 4 promotes endothelial angiogenesis through endothelial nitric oxide synthase activation. *Circulation* 124(6), 731-40. doi:10.1161/CIRCULATIONAHA.111.030775.
- Daulatzai, M.A. 2016. Cerebral hypoperfusion and glucose hypometabolism: Key pathophysiological modulators promote neurodegeneration, cognitive impairment, and Alzheimer's disease. *J Neurosci Res*. doi:10.1002/jnr.23777.
- Davalos, D., Ryu, J.K., Merlini, M., Baeten, K.M., Le Moan, N., Petersen, M.A., Deerinck, T.J., Smirnov, D.S., Bedard, C., Hakezaki, H., Gonias Murray, S., Ling, J.B., Lassmann, H., Degen, J.L., Ellisman, M.H., Akassoglou, K. 2012. Fibrinogen-induced perivascular microglial clustering is required for the development of axonal damage in neuroinflammation. *Nat Commun* 3, 1227. doi:10.1038/ncomms2230.
- Davis, J., Xu, F., Deane, R., Romanov, G., Previti, M.L., Zeigler, K., Zlokovic, B.V., Van Nostrand, W.E. 2004. Early-onset and robust cerebral microvascular accumulation of amyloid beta-protein in transgenic mice expressing low levels of a vasculotropic Dutch/Iowa mutant form of amyloid beta-protein precursor. *J Biol Chem* 279(19), 20296-306. doi:10.1074/jbc.M312946200.
- Davis, J., Xu, F., Miao, J., Previti, M.L., Romanov, G., Ziegler, K., Van Nostrand, W.E. 2006. Deficient cerebral clearance of vasculotropic mutant Dutch/Iowa Double A beta in

- human A betaPP transgenic mice. *Neurobiol Aging* 27(7), 946-54. doi:10.1016/j.neurobiolaging.2005.05.031.
- De Ley, G., Nshimyumuremyi, J.B., Leusen, I. 1985. Hemispheric blood flow in the rat after unilateral common carotid occlusion: evolution with time. *Stroke* 16(1), 69-73.
- De Silva, T.M., Faraci, F.M. 2016. Microvascular Dysfunction and Cognitive Impairment. *Cell Mol Neurobiol* 36(2), 241-58. doi:10.1007/s10571-015-0308-1.
- Deane, R., Wu, Z., Sagare, A., Davis, J., Du Yan, S., Hamm, K., Xu, F., Parisi, M., LaRue, B., Hu, H.W., Spijkers, P., Guo, H., Song, X., Lenting, P.J., Van Nostrand, W.E., Zlokovic, B.V. 2004. LRP/amyloid beta-peptide interaction mediates differential brain efflux of Abeta isoforms. *Neuron* 43(3), 333-44. doi:10.1016/j.neuron.2004.07.017.
- den Abeelen, A.S., Lagro, J., van Beek, A.H., Claassen, J.A. 2014. Impaired cerebral autoregulation and vasomotor reactivity in sporadic Alzheimer's disease. *Curr Alzheimer Res* 11(1), 11-7.
- Dickson, M.C., Martin, J.S., Cousins, F.M., Kulkarni, A.B., Karlsson, S., Akhurst, R.J. 1995. Defective haematopoiesis and vasculogenesis in transforming growth factor-beta 1 knock out mice. *Development* 121(6), 1845-54.
- Dierksen, G.A., Skehan, M.E., Khan, M.A., Jeng, J., Nandigam, R.N., Becker, J.A., Kumar, A., Neal, K.L., Betensky, R.A., Frosch, M.P., Rosand, J., Johnson, K.A., Viswanathan, A., Salat, D.H., Greenberg, S.M. 2010a. Spatial relation between microbleeds and amyloid deposits in amyloid angiopathy. *Ann Neurol* 68(4), 545-8. doi:10.1002/ana.22099.
- Dierksen, G.A., Skehan, M.E., Khan, M.A., Jeng, J., Nandigam, R.N., Becker, J.A., Kumar, A., Neal, K.L., Betensky, R.A., Frosch, M.P., Rosand, J., Johnson, K.A., Viswanathan, A., Salat, D.H., Greenberg, S.M. 2010b. Spatial relation between microbleeds and amyloid deposits in amyloid angiopathy. *Ann Neurol* 68(4), 545-8. doi:10.1002/ana.22099.
- Dobre, M.C., Uğurbil, K., Marjanska, M. 2007. Determination of blood longitudinal relaxation time (T1) at high magnetic field strengths. *Magn Reson Imaging* 25(5), 733-5. doi:10.1016/j.mri.2006.10.020.
- Doerfler, A., Engelhorn, T., Heiland, S., Knauth, M., Wanke, I., Forsting, M. 2000. MR contrast agents in acute experimental cerebral ischemia: potential adverse impacts on neurologic outcome and infarction size. *J Magn Reson Imaging* 11(4), 418-24.
- Dong, Y.F., Kataoka, K., Toyama, K., Sueta, D., Koibuchi, N., Yamamoto, E., Yata, K., Tomimoto, H., Ogawa, H., Kim-Mitsuyama, S. 2011. Attenuation of brain damage and cognitive impairment by direct renin inhibition in mice with chronic cerebral hypoperfusion. *Hypertension* 58(4), 635-42. doi:10.1161/HYPERTENSIONAHA.111.173534.

- Dorr, A., Sahota, B., Chinta, L.V., Brown, M.E., Lai, A.Y., Ma, K., Hawkes, C.A., McLaurin, J., Stefanovic, B. 2012. Amyloid- β -dependent compromise of microvascular structure and function in a model of Alzheimer's disease. *Brain* 135(Pt 10), 3039-50. doi:10.1093/brain/aws243.
- Dorr, A., Sled, J.G., Kabani, N. 2007. Three-dimensional cerebral vasculature of the CBA mouse brain: a magnetic resonance imaging and micro computed tomography study. *Neuroimage* 35(4), 1409-23. doi:10.1016/j.neuroimage.2006.12.040.
- Drummond, G.R., Selemidis, S., Griendling, K.K., Sobey, C.G. 2011. Combating oxidative stress in vascular disease: NADPH oxidases as therapeutic targets. *Nat Rev Drug Discov* 10(6), 453-71. doi:10.1038/nrd3403.
- Du, S.Q., Wang, X.R., Xiao, L.Y., Tu, J.F., Zhu, W., He, T., Liu, C.Z. 2016. Molecular Mechanisms of Vascular Dementia: What Can Be Learned from Animal Models of Chronic Cerebral Hypoperfusion? *Mol Neurobiol*. doi:10.1007/s12035-016-9915-1.
- Duan, W., Gui, L., Zhou, Z., Liu, Y., Tian, H., Chen, J.F., Zheng, J. 2009. Adenosine A2A receptor deficiency exacerbates white matter lesions and cognitive deficits induced by chronic cerebral hypoperfusion in mice. *J Neurol Sci* 285(1-2), 39-45. doi:10.1016/j.jns.2009.05.010.
- Dumas, A., Dierksen, G.A., Gurol, M.E., Halpin, A., Martinez-Ramirez, S., Schwab, K., Rosand, J., Viswanathan, A., Salat, D.H., Polimeni, J.R., Greenberg, S.M. 2012a. Functional magnetic resonance imaging detection of vascular reactivity in cerebral amyloid angiopathy. *Ann Neurol* 72(1), 76-81. doi:10.1002/ana.23566.
- Dumas, A., Dierksen, G.A., Gurol, M.E., Halpin, A., Martinez-Ramirez, S., Schwab, K., Rosand, J., Viswanathan, A., Salat, D.H., Polimeni, J.R., Greenberg, S.M. 2012b. Functional magnetic resonance imaging detection of vascular reactivity in cerebral amyloid angiopathy. *Ann Neurol* 72(1), 76-81. doi:10.1002/ana.23566.
- Dushek, S., Schandry, R. 2006. Deficient adjustment of cerebral blood flow to cognitive activity due to chronically low blood pressure. *Biol Psychol* 72(3), 311-7. doi:10.1016/j.biopsycho.2005.12.003.
- Dushek, S., Schandry, R. 2007. Reduced brain perfusion and cognitive performance due to constitutional hypotension. *Clin Auton Res* 17(2), 69-76. doi:10.1007/s10286-006-0379-7.
- Dysken, M.W., Sano, M., Asthana, S., Vertrees, J.E., Pallaki, M., Llorente, M., Love, S., Schellenberg, G.D., McCarten, J.R., Malphurs, J., Prieto, S., Chen, P., Loreck, D.J., Trapp, G., Bakshi, R.S., Mintzer, J.E., Heidebrink, J.L., Vidal-Cardona, A., Arroyo, L.M., Cruz, A.R., Zachariah, S., Kowall, N.W., Chopra, M.P., Craft, S., Thielke, S., Turvey, C.L., Woodman, C., Monnell, K.A., Gordon, K., Tomaska, J., Segal, Y., Peduzzi, P.N., Guarino, P.D. 2014. Effect of vitamin E and memantine on functional decline in Alzheimer disease: the TEAM-AD VA cooperative randomized trial. *JAMA* 311(1), 33-44. doi:10.1001/jama.2013.282834.

- El Tayara, N.I.T., Delatour, B., Volk, A., Dhenain, M. 2010. Detection of vascular alterations by in vivo magnetic resonance angiography and histology in APP/PS1 mouse model of Alzheimer's disease. *MAGMA* 23(1), 53-64. doi:10.1007/s10334-009-0194-y.
- Ellsworth, M.L., Ellis, C.G., Goldman, D., Stephenson, A.H., Dietrich, H.H., Sprague, R.S. 2009. Erythrocytes: oxygen sensors and modulators of vascular tone. *Physiology (Bethesda)* 24, 107-16. doi:10.1152/physiol.00038.2008.
- Engelhardt, B., Carare, R.O., Bechmann, I., Flügel, A., Laman, J.D., Weller, R.O. 2016. Vascular, glial, and lymphatic immune gateways of the central nervous system. *Acta Neuropathol* 132(3), 317-38. doi:10.1007/s00401-016-1606-5.
- Engelhardt, S., Al-Ahmad, A.J., Gassmann, M., Ogunshola, O.O. 2014. Hypoxia selectively disrupts brain microvascular endothelial tight junction complexes through a hypoxia-inducible factor-1 (HIF-1) dependent mechanism. *J Cell Physiol* 229(8), 1096-105. doi:10.1002/jcp.24544.
- Esiri, M.M., Joachim, C., Sloan, C., Christie, S., Agacinski, G., Bridges, L.R., Wilcock, G.K., Smith, A.D. 2014. Cerebral subcortical small vessel disease in subjects with pathologically confirmed Alzheimer disease: a clinicopathologic study in the Oxford Project to Investigate Memory and Ageing (OPTIMA). *Alzheimer Dis Assoc Disord* 28(1), 30-5. doi:10.1097/WAD.0b013e31829b72f1.
- Esposito, L., Raber, J., Kekoni, L., Yan, F., Yu, G.Q., Bien-Ly, N., Puoliväli, J., Scarce-Levie, K., Masliah, E., Mucke, L. 2006. Reduction in mitochondrial superoxide dismutase modulates Alzheimer's disease-like pathology and accelerates the onset of behavioral changes in human amyloid precursor protein transgenic mice. *J Neurosci* 26(19), 5167-79. doi:10.1523/JNEUROSCI.0482-06.2006.
- Faraco, G., Park, L., Zhou, P., Luo, W., Paul, S.M., Anrather, J., Iadecola, C. 2016. Hypertension enhances A β -induced neurovascular dysfunction, promotes β -secretase activity, and leads to amyloidogenic processing of APP. *J Cereb Blood Flow Metab* 36(1), 241-52. doi:10.1038/jcbfm.2015.79.
- Farrall, A.J., Wardlaw, J.M. 2009. Blood-brain barrier: ageing and microvascular disease--systematic review and meta-analysis. *Neurobiol Aging* 30(3), 337-52. doi:10.1016/j.neurobiolaging.2007.07.015.
- Fernando, M.S., Simpson, J.E., Matthews, F., Brayne, C., Lewis, C.E., Barber, R., Kalaria, R.N., Forster, G., Esteves, F., Wharton, S.B., Shaw, P.J., O'Brien, J.T., Ince, P.G., Group, M.C.F.a.A.N.S. 2006. White matter lesions in an unselected cohort of the elderly: molecular pathology suggests origin from chronic hypoperfusion injury. *Stroke* 37(6), 1391-8. doi:10.1161/01.STR.0000221308.94473.14.
- Ferreira, A.P., Rodrigues, F.S., Della-Pace, I.D., Mota, B.C., Oliveira, S.M., Velho Gewehr, C.e.C., Bobinski, F., de Oliveira, C.V., Brum, J.S., Oliveira, M.S., Furian, A.F., de Barros, C.S., Ferreira, J., Santos, A.R., Figuera, M.R., Royes, L.F. 2013. The effect of NADPH-oxidase inhibitor apocynin on cognitive impairment induced by moderate

- lateral fluid percussion injury: role of inflammatory and oxidative brain damage. *Neurochem Int* 63(6), 583-93. doi:10.1016/j.neuint.2013.09.012.
- Firbank, M.J., Wiseman, R.M., Burton, E.J., Saxby, B.K., O'Brien, J.T., Ford, G.A. 2007. Brain atrophy and white matter hyperintensity change in older adults and relationship to blood pressure. Brain atrophy, WMH change and blood pressure. *J Neurol* 254(6), 713-21. doi:10.1007/s00415-006-0238-4.
- Fisher, M., Vasilevko, V., Passos, G.F., Ventura, C., Quiring, D., Cribbs, D.H. 2011. Therapeutic modulation of cerebral microhemorrhage in a mouse model of cerebral amyloid angiopathy. *Stroke* 42(11), 3300-3. doi:10.1161/STROKEAHA.111.626655.
- Fleisher, A.S., Podraza, K.M., Bangen, K.J., Taylor, C., Sherzai, A., Sidhar, K., Liu, T.T., Dale, A.M., Buxton, R.B. 2009. Cerebral perfusion and oxygenation differences in Alzheimer's disease risk. *Neurobiol Aging* 30(11), 1737-48. doi:10.1016/j.neurobiolaging.2008.01.012.
- Frances, A., Sandra, O., Lucy, U. 2016. Vascular cognitive impairment, a cardiovascular complication. *World J Psychiatry* 6(2), 199-207. doi:10.5498/wjp.v6.i2.199.
- Gao, H.M., Zhou, H., Hong, J.S. 2012. NADPH oxidases: novel therapeutic targets for neurodegenerative diseases. *Trends Pharmacol Sci* 33(6), 295-303. doi:10.1016/j.tips.2012.03.008.
- Gao, Y.Z., Zhang, J.J., Liu, H., Wu, G.Y., Xiong, L., Shu, M. 2013. Regional cerebral blood flow and cerebrovascular reactivity in Alzheimer's disease and vascular dementia assessed by arterial spinlabeling magnetic resonance imaging. *Curr Neurovasc Res* 10(1), 49-53.
- Garcia-Alloza, M., Subramanian, M., Thyssen, D., Borrelli, L.A., Fauq, A., Das, P., Golde, T.E., Hyman, B.T., Bacskaï, B.J. 2009. Existing plaques and neuritic abnormalities in APP:PS1 mice are not affected by administration of the gamma-secretase inhibitor LY-411575. *Mol Neurodegener* 4, 19. doi:10.1186/1750-1326-4-19.
- Garcia-Osta, A., Alberini, C.M. 2009. Amyloid beta mediates memory formation. *Learn Mem* 16(4), 267-72. doi:10.1101/lm.1310209.
- Gauberti, M., Montagne, A., Marcos-Contreras, O.A., Le Béhot, A., Maubert, E., Vivien, D. 2013. Ultra-sensitive molecular MRI of vascular cell adhesion molecule-1 reveals a dynamic inflammatory penumbra after strokes. *Stroke* 44(7), 1988-96. doi:10.1161/STROKEAHA.111.000544.
- Gauthier, C.J., Madjar, C., Desjardins-Crépeau, L., Bellec, P., Bherer, L., Hoge, R.D. 2013. Age dependence of hemodynamic response characteristics in human functional magnetic resonance imaging. *Neurobiol Aging* 34(5), 1469-85. doi:10.1016/j.neurobiolaging.2012.11.002.

- Ghosh M, Balbi M, Hellal F, Dichgans M, Lindauer U, Plesnila N. 2015 Pericytes are involved in the pathogenesis of cerebral autosomal dominant arteriopathy with subcortical infarcts and leukoencephalopathy. *Ann Neurol* 78(6):887-900
- Ghosh, A., Kanthasamy, A., Joseph, J., Anantharam, V., Srivastava, P., Dranka, B.P., Kalyanaraman, B., Kanthasamy, A.G. 2012. Anti-inflammatory and neuroprotective effects of an orally active apocynin derivative in pre-clinical models of Parkinson's disease. *J Neuroinflammation* 9, 241. doi:10.1186/1742-2094-9-241.
- Giannoni, P., Arango-Lievano, M., Neves, I.D., Rousset, M.C., Baranger, K., Rivera, S., Jeanneteau, F., Claeysen, S., Marchi, N. 2016. Cerebrovascular pathology during the progression of experimental Alzheimer's disease. *Neurobiol Dis* 88, 107-17. doi:10.1016/j.nbd.2016.01.001.
- Girouard, H., Iadecola, C. 2006. Neurovascular coupling in the normal brain and in hypertension, stroke, and Alzheimer disease. *J Appl Physiol* (1985) 100(1), 328-35. doi:10.1152/japplphysiol.00966.2005.
- Glodzik, L., Randall, C., Rusinek, H., de Leon, M.J. 2013. Cerebrovascular reactivity to carbon dioxide in Alzheimer's disease. *J Alzheimers Dis* 35(3), 427-40. doi:10.3233/JAD-122011.
- Godin, O., Tzourio, C., Maillard, P., Mazoyer, B., Dufouil, C. 2011. Antihypertensive treatment and change in blood pressure are associated with the progression of white matter lesion volumes: the Three-City (3C)-Dijon Magnetic Resonance Imaging Study. *Circulation* 123(3), 266-73. doi:10.1161/CIRCULATIONAHA.110.961052.
- Gordon, G.R., Choi, H.B., Rungta, R.L., Ellis-Davies, G.C., MacVicar, B.A. 2008. Brain metabolism dictates the polarity of astrocyte control over arterioles. *Nature* 456(7223), 745-9. doi:10.1038/nature07525.
- Gordon, G.R., Howarth, C., MacVicar, B.A. 2016. Bidirectional Control of Blood Flow by Astrocytes: A Role for Tissue Oxygen and Other Metabolic Factors. *Adv Exp Med Biol* 903, 209-19. doi:10.1007/978-1-4899-7678-9_15.
- Gorelick, P.B., Scuteri, A., Black, S.E., Decarli, C., Greenberg, S.M., Iadecola, C., Launer, L.J., Laurent, S., Lopez, O.L., Nyenhuis, D., Petersen, R.C., Schneider, J.A., Tzourio, C., Arnett, D.K., Bennett, D.A., Chui, H.C., Higashida, R.T., Lindquist, R., Nilsson, P.M., Roman, G.C., Sellke, F.W., Seshadri, S., American Heart Association Stroke Council, C.o.E.a.P., Council on Cardiovascular Nursing, Council on Cardiovascular Radiology and Intervention, and Council on Cardiovascular Surgery and Anesthesia. 2011. Vascular contributions to cognitive impairment and dementia: a statement for healthcare professionals from the american heart association/american stroke association. *Stroke* 42(9), 2672-713. doi:10.1161/STR.0b013e3182299496.
- Gottesman, R.F., Coresh, J., Catellier, D.J., Sharrett, A.R., Rose, K.M., Coker, L.H., Shibata, D.K., Knopman, D.S., Jack, C.R., Mosley, T.H. 2010. Blood pressure and white-matter

- disease progression in a biethnic cohort: Atherosclerosis Risk in Communities (ARIC) study. *Stroke* 41(1), 3-8. doi:10.1161/STROKEAHA.109.566992.
- Grabowski, T.J., Cho, H.S., Vonsattel, J.P., Rebeck, G.W., Greenberg, S.M. 2001. Novel amyloid precursor protein mutation in an Iowa family with dementia and severe cerebral amyloid angiopathy. *Ann Neurol* 49(6), 697-705.
- Greenan, C., Murphy, L., Yu, L.M., Kehoe, P.G., Coulthard, E., Bath, P., Stewart, R., Jones, R., Corbett, A., Thomas, A., Connelly, P., Arrojo, F., Canning, R., Wallach, S., Henderson, C., McGuinness, B., O'Sullivan, M., Holmes, C., Knapp, M., Ballard, C., Passmore, P., Investigators, A. 2016. A randomised controlled trial of calcium channel blockade (CCB) with Amlodipine For the treatment of subcortical ischaemic vascular dementia (AFFECT): study protocol. *Trials* 17(1), 324. doi:10.1186/s13063-016-1449-3.
- Guo, S., Chen, X. 2015. The human Nox4: gene, structure, physiological function and pathological significance. *J Drug Target* 23(10), 888-96. doi:10.3109/1061186X.2015.1036276.
- Gurol, M.E., Dierksen, G., Betensky, R., Gidicsin, C., Halpin, A., Becker, A., Carmasin, J., Ayres, A., Schwab, K., Viswanathan, A., Salat, D., Rosand, J., Johnson, K.A., Greenberg, S.M. 2012. Predicting sites of new hemorrhage with amyloid imaging in cerebral amyloid angiopathy. *Neurology* 79(4), 320-6. doi:10.1212/WNL.0b013e31826043a9.
- Gurol, M.E., Irizarry, M.C., Smith, E.E., Raju, S., Diaz-Arrastia, R., Bottiglieri, T., Rosand, J., Growdon, J.H., Greenberg, S.M. 2006. Plasma beta-amyloid and white matter lesions in AD, MCI, and cerebral amyloid angiopathy. *Neurology* 66(1), 23-9. doi:10.1212/01.wnl.0000191403.95453.6a.
- Gąsecki, D., Kwarciany, M., Nyka, W., Narkiewicz, K. 2013. Hypertension, brain damage and cognitive decline. *Curr Hypertens Rep* 15(6), 547-58. doi:10.1007/s11906-013-0398-4.
- Hajjar, I., Marmorelis, V., Shin, D.C., Chui, H. 2014. Assessment of cerebrovascular reactivity during resting state breathing and its correlation with cognitive function in hypertension. *Cerebrovasc Dis* 38(1), 10-6. doi:10.1159/000365349.
- Hall, C.N., Reynell, C., Gesslein, B., Hamilton, N.B., Mishra, A., Sutherland, B.A., O'Farrell, F.M., Buchan, A.M., Lauritzen, M., Attwell, D. 2014a. Capillary pericytes regulate cerebral blood flow in health and disease. *Nature* 508(7494), 55-60. doi:10.1038/nature13165.
- Hall, C.N., Reynell, C., Gesslein, B., Hamilton, N.B., Mishra, A., Sutherland, B.A., O'Farrell, F.M., Buchan, A.M., Lauritzen, M., Attwell, D. 2014b. Capillary pericytes regulate cerebral blood flow in health and disease. *Nature* 508(7494), 55-60. doi:10.1038/nature13165.

- Hamel, E. 2006a. Perivascular nerves and the regulation of cerebrovascular tone. *J Appl Physiol* (1985) 100(3), 1059-64. doi:10.1152/japplphysiol.00954.2005.
- Hamel, E. 2006b. Perivascular nerves and the regulation of cerebrovascular tone. *J Appl Physiol* (1985) 100(3), 1059-64. doi:10.1152/japplphysiol.00954.2005.
- Hamel, E. 2015. Cerebral circulation: function and dysfunction in Alzheimer's disease. *J Cardiovasc Pharmacol* 65(4), 317-24. doi:10.1097/FJC.000000000000177.
- Han, B.H., Zhou, M.L., Abousaleh, F., Brendza, R.P., Dietrich, H.H., Koenigsknecht-Talboo, J., Cirrito, J.R., Milner, E., Holtzman, D.M., Zipfel, G.J. 2008a. Cerebrovascular dysfunction in amyloid precursor protein transgenic mice: contribution of soluble and insoluble amyloid-beta peptide, partial restoration via gamma-secretase inhibition. *J Neurosci* 28(50), 13542-50. doi:10.1523/JNEUROSCI.4686-08.2008.
- Han, B.H., Zhou, M.L., Abousaleh, F., Brendza, R.P., Dietrich, H.H., Koenigsknecht-Talboo, J., Cirrito, J.R., Milner, E., Holtzman, D.M., Zipfel, G.J. 2008b. Cerebrovascular dysfunction in amyloid precursor protein transgenic mice: contribution of soluble and insoluble amyloid-beta peptide, partial restoration via gamma-secretase inhibition. *J Neurosci* 28(50), 13542-50. doi:10.1523/JNEUROSCI.4686-08.2008.
- Han, B.H., Zhou, M.L., Johnson, A.W., Singh, I., Liao, F., Vellimana, A.K., Nelson, J.W., Milner, E., Cirrito, J.R., Basak, J., Yoo, M., Dietrich, H.H., Holtzman, D.M., Zipfel, G.J. 2015. Contribution of reactive oxygen species to cerebral amyloid angiopathy, vasomotor dysfunction, and microhemorrhage in aged Tg2576 mice. *Proc Natl Acad Sci U S A* 112(8), E881-90. doi:10.1073/pnas.1414930112.
- Harraz, M.M., Marden, J.J., Zhou, W., Zhang, Y., Williams, A., Sharov, V.S., Nelson, K., Luo, M., Paulson, H., Schöneich, C., Engelhardt, J.F. 2008. SOD1 mutations disrupt redox-sensitive Rac regulation of NADPH oxidase in a familial ALS model. *J Clin Invest* 118(2), 659-70. doi:10.1172/JCI34060.
- Harris, J.J., Jolivet, R., Attwell, D. 2012. Synaptic energy use and supply. *Neuron* 75(5), 762-77. doi:10.1016/j.neuron.2012.08.019.
- Hartman, R.E., Shah, A., Fagan, A.M., Schwetye, K.E., Parsadanian, M., Schulman, R.N., Finn, M.B., Holtzman, D.M. 2006. Pomegranate juice decreases amyloid load and improves behavior in a mouse model of Alzheimer's disease. *Neurobiol Dis* 24(3), 506-15. doi:10.1016/j.nbd.2006.08.006.
- Haseloff, R.F., Dithmer, S., Winkler, L., Wolburg, H., Blasig, I.E. 2015. Transmembrane proteins of the tight junctions at the blood-brain barrier: structural and functional aspects. *Semin Cell Dev Biol* 38, 16-25. doi:10.1016/j.semcdb.2014.11.004.
- Hattori, Y., Enmi, J., Iguchi, S., Saito, S., Yamamoto, Y., Nagatsuka, K., Iida, H., Ihara, M. 2016. Substantial Reduction of Parenchymal Cerebral Blood Flow in Mice with Bilateral Common Carotid Artery Stenosis. *Sci Rep* 6, 32179. doi:10.1038/srep32179.

- Hattori, Y., Enmi, J., Kitamura, A., Yamamoto, Y., Saito, S., Takahashi, Y., Iguchi, S., Tsuji, M., Yamahara, K., Nagatsuka, K., Iida, H., Ihara, M. 2015. A novel mouse model of subcortical infarcts with dementia. *J Neurosci* 35: 3915-28
- Hattori, Y., Kitamura, A., Nagatsuka, K., Ihara, M. 2014. A novel mouse model of ischemic carotid artery disease. *PLoS One* 9(6), e100257. doi:10.1371/journal.pone.0100257.
- Hawkes, C.A., Gatherer, M., Sharp, M.M., Dorr, A., Yuen, H.M., Kalaria, R., Weller, R.O., Carare, R.O. 2013. Regional differences in the morphological and functional effects of aging on cerebral basement membranes and perivascular drainage of amyloid- β from the mouse brain. *Aging Cell* 12(2), 224-36. doi:10.1111/acer.12045.
- Hawkes, C.A., Härtig, W., Kacza, J., Schliebs, R., Weller, R.O., Nicoll, J.A., Carare, R.O. 2011. Perivascular drainage of solutes is impaired in the ageing mouse brain and in the presence of cerebral amyloid angiopathy. *Acta Neuropathol* 121(4), 431-43. doi:10.1007/s00401-011-0801-7.
- Hawkes, C.A., Jayakody, N., Johnston, D.A., Bechmann, I., Carare, R.O. 2014. Failure of perivascular drainage of β -amyloid in cerebral amyloid angiopathy. *Brain Pathol* 24(4), 396-403. doi:10.1111/bpa.12159.
- Heneka, M.T., Carson, M.J., El Khoury, J., Landreth, G.E., Brosse, F., Feinstein, D.L., Jacobs, A.H., Wyss-Coray, T., Vitorica, J., Ransohoff, R.M., Herrup, K., Frautsch, S.A., Finsen, B., Brown, G.C., Verkhratsky, A., Yamanaka, K., Koistinaho, J., Latz, E., Halle, A., Petzold, G.C., Town, T., Morgan, D., Shinohara, M.L., Perry, V.H., Holmes, C., Bazan, N.G., Brooks, D.J., Hunot, S., Joseph, B., Deigendesch, N., Garaschuk, O., Boddeke, E., Dinarello, C.A., Breitner, J.C., Cole, G.M., Golenbock, D.T., Kummer, M.P. 2015. Neuroinflammation in Alzheimer's disease. *Lancet Neurol* 14(4), 388-405. doi:10.1016/S1474-4422(15)70016-5.
- Heumüller, S., Wind, S., Barbosa-Sicard, E., Schmidt, H.H., Busse, R., Schröder, K., Brandes, R.P. 2008. Apocynin is not an inhibitor of vascular NADPH oxidases but an antioxidant. *Hypertension* 51(2), 211-7. doi:10.1161/HYPERTENSIONAHA.107.100214.
- Higuchi M, Ji B, Maeda J, Sahara S, Suhara T. 2016. In vivo imaging of neuroinflammation in Alzheimer's disease. *Clinical and Experimental Neuroimmunology*. 7, 139-144
- Hill, R.A., Tong, L., Yuan, P., Murikinati, S., Gupta, S., Grutzendler, J. 2015a. Regional Blood Flow in the Normal and Ischemic Brain Is Controlled by Arteriolar Smooth Muscle Cell Contractility and Not by Capillary Pericytes. *Neuron* 87(1), 95-110. doi:10.1016/j.neuron.2015.06.001.
- Hill, R.A., Tong, L., Yuan, P., Murikinati, S., Gupta, S., Grutzendler, J. 2015b. Regional Blood Flow in the Normal and Ischemic Brain Is Controlled by Arteriolar Smooth Muscle Cell Contractility and Not by Capillary Pericytes. *Neuron* 87(1), 95-110. doi:10.1016/j.neuron.2015.06.001.

- Hirano, K., Chen, W.S., Chueng, A.L., Dunne, A.A., Seredenina, T., Filippova, A., Ramachandran, S., Bridges, A., Chaudry, L., Pettman, G., Allan, C., Duncan, S., Lee, K.C., Lim, J., Ma, M.T., Ong, A.B., Ye, N.Y., Nasir, S., Mulyanidewi, S., Aw, C.C., Oon, P.P., Liao, S., Li, D., Johns, D.G., Miller, N.D., Davies, C.H., Browne, E.R., Matsuoka, Y., Chen, D.W., Jaquet, V., Rutter, A.R. 2015. Discovery of GSK2795039, a Novel Small Molecule NADPH Oxidase 2 Inhibitor. *Antioxid Redox Signal* 23(5), 358-74. doi:10.1089/ars.2014.6202.
- Holland, C.M., Smith, E.E., Csapo, I., Gurol, M.E., Brylka, D.A., Killiany, R.J., Blacker, D., Albert, M.S., Guttmann, C.R., Greenberg, S.M. 2008. Spatial distribution of white-matter hyperintensities in Alzheimer disease, cerebral amyloid angiopathy, and healthy aging. *Stroke* 39(4), 1127-33. doi:10.1161/STROKEAHA.107.497438.
- Holland, P.R., Searcy, J.L., Salvadores, N., Scullion, G., Chen, G., Lawson, G., Scott, F., Bastin, M.E., Ihara, M., Kalaria, R., Wood, E.R., Smith, C., Wardlaw, J.M., Horsburgh, K. 2015. Gliovascular disruption and cognitive deficits in a mouse model with features of small vessel disease. *J Cereb Blood Flow Metab* 35(6), 1005-14. doi:10.1038/jcbfm.2015.12.
- Hoyte, L.C., Brooks, K.J., Nagel, S., Akhtar, A., Chen, R., Mardiguian, S., McAteer, M.A., Anthony, D.C., Choudhury, R.P., Buchan, A.M., Sibson, N.R. 2010. Molecular magnetic resonance imaging of acute vascular cell adhesion molecule-1 expression in a mouse model of cerebral ischemia. *J Cereb Blood Flow Metab* 30(6), 1178-87. doi:10.1038/jcbfm.2009.287.
- Hsiao, K., Chapman, P., Nilsen, S., Eckman, C., Harigaya, Y., Younkin, S., Yang, F., Cole, G. 1996a. Correlative memory deficits, Abeta elevation, and amyloid plaques in transgenic mice. *Science* 274(5284), 99-102.
- Hsiao, K., Chapman, P., Nilsen, S., Eckman, C., Harigaya, Y., Younkin, S., Yang, F., Cole, G. 1996b. Correlative memory deficits, Abeta elevation, and amyloid plaques in transgenic mice. *Science* 274(5284), 99-102.
- Hudson, L.C., Bragg, D.C., Tompkins, M.B., Meeker, R.B. 2005. Astrocytes and microglia differentially regulate trafficking of lymphocyte subsets across brain endothelial cells. *Brain Res* 1058(1-2), 148-60. doi:10.1016/j.brainres.2005.07.071.
- Hutchison, J.L., Shokri-Kojori, E., Lu, H., Rypma, B. 2013. A BOLD Perspective on Age-Related Neurometabolic-Flow Coupling and Neural Efficiency Changes in Human Visual Cortex. *Front Psychol* 4, 244. doi:10.3389/fpsyg.2013.00244.
- Hutter-Schmid, B., Humpel, C. 2016. Platelet-derived Growth Factor Receptor-beta is Differentially Regulated in Primary Mouse Pericytes and Brain Slices. *Curr Neurovasc Res* 13(2), 127-34.
- Hébert, F., Grand'maison, M., Ho, M.K., Lerch, J.P., Hamel, E., Bedell, B.J. 2013. Cortical atrophy and hypoperfusion in a transgenic mouse model of Alzheimer's disease. *Neurobiol Aging* 34(6), 1644-52. doi:10.1016/j.neurobiolaging.2012.11.022.

- Iadecola, C. 2013. The pathobiology of vascular dementia. *Neuron* 80(4), 844-66. doi:10.1016/j.neuron.2013.10.008.
- Ihara, M., Tomimoto, H., Kinoshita, M., Oh, J., Noda, M., Wakita, H., Akiguchi, I., Shibasaki, H. 2001. Chronic cerebral hypoperfusion induces MMP-2 but not MMP-9 expression in the microglia and vascular endothelium of white matter. *J Cereb Blood Flow Metab* 21(7), 828-34. doi:10.1097/00004647-200107000-00008.
- Iida, H., Ohata, H., Iida, M., Watanabe, Y., Dohi, S. 1998. Isoflurane and sevoflurane induce vasodilation of cerebral vessels via ATP-sensitive K⁺ channel activation. *Anesthesiology* 89(4), 954-60.
- Iliff, J.J., Wang, M., Liao, Y., Plogg, B.A., Peng, W., Gundersen, G.A., Benveniste, H., Vates, G.E., Deane, R., Goldman, S.A., Nagelhus, E.A., Nedergaard, M. 2012. A paravascular pathway facilitates CSF flow through the brain parenchyma and the clearance of interstitial solutes, including amyloid β . *Sci Transl Med* 4(147), 147ra11. doi:10.1126/scitranslmed.3003748.
- Iturria-Medina, Y., Sotero, R.C., Toussaint, P.J., Mateos-Pérez, J.M., Evans, A.C., Initiative, A.s.D.N. 2016. Early role of vascular dysregulation on late-onset Alzheimer's disease based on multifactorial data-driven analysis. *Nat Commun* 7, 11934. doi:10.1038/ncomms11934.
- Iversen, N.K., Malte, H., Baatrup, E., Wang, T. 2012. The normal acid-base status of mice. *Respir Physiol Neurobiol* 180(2-3), 252-7. doi:10.1016/j.resp.2011.11.015.
- Jackman, K.A., Miller, A.A., De Silva, T.M., Crack, P.J., Drummond, G.R., Sobey, C.G. 2009a. Reduction of cerebral infarct volume by apocynin requires pretreatment and is absent in Nox2-deficient mice. *Br J Pharmacol* 156(4), 680-8. doi:10.1111/j.1476-5381.2008.00073.x.
- Jackman, K.A., Miller, A.A., Drummond, G.R., Sobey, C.G. 2009b. Importance of NOX1 for angiotensin II-induced cerebrovascular superoxide production and cortical infarct volume following ischemic stroke. *Brain Res* 1286, 215-20. doi:10.1016/j.brainres.2009.06.056.
- Jacobs, A.H., Tavitian, B., consortium, I. 2012. Noninvasive molecular imaging of neuroinflammation. *J Cereb Blood Flow Metab* 32(7), 1393-415. doi:10.1038/jcbfm.2012.53.
- Jahn, H. 2013. Memory loss in Alzheimer's disease. *Dialogues Clin Neurosci* 15(4), 445-54.
- Jankowsky, J.L., Fadale, D.J., Anderson, J., Xu, G.M., Gonzales, V., Jenkins, N.A., Copeland, N.G., Lee, M.K., Younkin, L.H., Wagner, S.L., Younkin, S.G., Borchelt, D.R. 2004. Mutant presenilins specifically elevate the levels of the 42 residue beta-amyloid peptide in vivo: evidence for augmentation of a 42-specific gamma secretase. *Hum Mol Genet* 13(2), 159-70. doi:10.1093/hmg/ddh019.

- Jennings, J.R., Muldoon, M.F., Ryan, C., Price, J.C., Greer, P., Sutton-Tyrrell, K., van der Veen, F.M., Meltzer, C.C. 2005. Reduced cerebral blood flow response and compensation among patients with untreated hypertension. *Neurology* 64(8), 1358-65. doi:10.1212/01.WNL.0000158283.28251.3C.
- Jensen, J.H., Chandra, R. 2000. MR imaging of microvasculature. *Magn Reson Med* 44(2), 224-30.
- Jespersen, S.N., Østergaard, L. 2012. The roles of cerebral blood flow, capillary transit time heterogeneity, and oxygen tension in brain oxygenation and metabolism. *J Cereb Blood Flow Metab* 32(2), 264-77. doi:10.1038/jcbfm.2011.153.
- Jessen, N.A., Munk, A.S.F., Lundgaard, I., Nedergaard, M. 2015. The Glymphatic System – A Beginner’s Guide. *Neurochem Res* 40(12):2583-2599
- Jiao, S.S., Yao, X.Q., Liu, Y.H., Wang, Q.H., Zeng, F., Lu, J.J., Liu, J., Zhu, C., Shen, L.L., Liu, C.H., Wang, Y.R., Zeng, G.H., Parikh, A., Chen, J., Liang, C.R., Xiang, Y., Bu, X.L., Deng, J., Li, J., Xu, J., Zeng, Y.Q., Xu, X., Xu, H.W., Zhong, J.H., Zhou, H.D., Zhou, X.F., Wang, Y.J. 2015. Edaravone alleviates Alzheimer's disease-type pathologies and cognitive deficits. *Proc Natl Acad Sci U S A* 112(16), 5225-30. doi:10.1073/pnas.1422998112.
- Jiwa, N.S., Garrard, P., Hainsworth, A.H. 2010. Experimental models of vascular dementia and vascular cognitive impairment: a systematic review. *J Neurochem* 115(4), 814-28. doi:10.1111/j.1471-4159.2010.06958.x.
- Johnson, D.K., Schillinger, K.J., Kwait, D.M., Hughes, C.V., McNamara, E.J., Ishmael, F., O'Donnell, R.W., Chang, M.M., Hogg, M.G., Dordick, J.S., Santhanam, L., Ziegler, L.M., Holland, J.A. 2002. Inhibition of NADPH oxidase activation in endothelial cells by ortho-methoxy-substituted catechols. *Endothelium* 9(3), 191-203.
- Johnson, N.A., Jahng, G.H., Weiner, M.W., Miller, B.L., Chui, H.C., Jagust, W.J., Gorno-Tempini, M.L., Schuff, N. 2005. Pattern of cerebral hypoperfusion in Alzheimer disease and mild cognitive impairment measured with arterial spin-labeling MR imaging: initial experience. *Radiology* 234(3), 851-9. doi:10.1148/radiol.2343040197.
- Jokinen, H., Melkas, S., Ylikoski, R., Pohjasvaara, T., Kaste, M., Erkinjuntti, T., Hietanen, M. 2015. Post-stroke cognitive impairment is common even after successful clinical recovery. *Eur J Neurol* 22(9), 1288-94. doi:10.1111/ene.12743.
- Joutel, A., Corpechot, C., Ducros, A., Vahedi, K., Chabriat, H., Mouton, P., Alamowitch, S., Domenga, V., Cécillion, M., Marechal, E., Maciazek, J., Vayssiere, C., Cruaud, C., Cabanis, E.A., Ruchoux, M.M., Weissenbach, J., Bach, J.F., Bousser, M.G., Tournier-Lasserre, E. 1996. Notch3 mutations in CADASIL, a hereditary adult-onset condition causing stroke and dementia. *Nature* 383(6602), 707-10. doi:10.1038/383707a0.
- Joutel, A., Monet-Leprêtre, M., Gosele, C., Baron-Menguy, C., Hammes, A., Schmidt, S., Lemaire-Carrette, B., Domenga, V., Schedl, A., Lacombe, P., Hubner, N. 2010.

- Cerebrovascular dysfunction and microcirculation rarefaction precede white matter lesions in a mouse genetic model of cerebral ischemic small vessel disease. *J Clin Invest* 120(2), 433-45. doi:10.1172/JCI39733.
- Kalaria, R.N. 1997. Cerebrovascular degeneration is related to amyloid-beta protein deposition in Alzheimer's disease. *Ann N Y Acad Sci* 826, 263-71.
- Kalaria, R.N. 2010. Vascular basis for brain degeneration: faltering controls and risk factors for dementia. *Nutr Rev* 68 Suppl 2, S74-87. doi:10.1111/j.1753-4887.2010.00352.x.
- Kalaria, R.N. 2016. Neuropathological diagnosis of vascular cognitive impairment and vascular dementia with implications for Alzheimer's disease. *Acta Neuropathol* 131(5), 659-85. doi:10.1007/s00401-016-1571-z.
- Kalaria, R.N., Cohen, D.L., Greenberg, B.D., Savage, M.J., Bogdanovic, N.E., Winblad, B., Lannfelt, L., Adem, A. 1996. Abundance of the longer A beta 42 in neocortical and cerebrovascular amyloid beta deposits in Swedish familial Alzheimer's disease and Down's syndrome. *Neuroreport* 7(8), 1377-81.
- Kehl, F., Shen, H., Moreno, C., Farber, N.E., Roman, R.J., Kampine, J.P., Hudetz, A.G. 2002. Isoflurane-induced cerebral hyperemia is partially mediated by nitric oxide and epoxyeicosatrienoic acids in mice in vivo. *Anesthesiology* 97(6), 1528-33.
- Kim, J.H., Jang, B.G., Choi, B.Y., Kim, H.S., Sohn, M., Chung, T.N., Choi, H.C., Song, H.K., Suh, S.W. 2013. Post-treatment of an NADPH oxidase inhibitor prevents seizure-induced neuronal death. *Brain Res* 1499, 163-72. doi:10.1016/j.brainres.2013.01.007.
- Kim, J.S., Yun, I., Choi, Y.B., Lee, K.S., Kim, Y.I. 2008. Ramipril protects from free radical induced white matter damage in chronic hypoperfusion in the rat. *J Clin Neurosci* 15(2), 174-8. doi:10.1016/j.jocn.2006.12.003.
- Kim, S.K., Cho, K.O., Kim, S.Y. 2008. White Matter Damage and Hippocampal Neurodegeneration Induced by Permanent Bilateral Occlusion of Common Carotid Artery in the Rat: Comparison between Wistar and Sprague-Dawley Strain. *Korean J Physiol Pharmacol* 12(3), 89-94. doi:10.4196/kjpp.2008.12.3.89.
- Kimbrough, I.F., Robel, S., Roberson, E.D., Sontheimer, H. 2015. Vascular amyloidosis impairs the gliovascular unit in a mouse model of Alzheimer's disease. *Brain* 138(Pt 12), 3716-33. doi:10.1093/brain/awv327.
- Kitaguchi, H., Tomimoto, H., Ihara, M., Shibata, M., Uemura, K., Kalaria, R.N., Kihara, T., Asada-Utsugi, M., Kinoshita, A., Takahashi, R. 2009. Chronic cerebral hypoperfusion accelerates amyloid beta deposition in APPSwInd transgenic mice. *Brain Res* 1294, 202-10. doi:10.1016/j.brainres.2009.07.078.
- Kitamura, A., Fujita, Y., Oishi, N., Kalaria, R. N., Washida, K., Maki, T., Okamoto, Y., Hase, Y., Yamada, M., Takahashi, J., Ito, H., Tomimoto, H., Fukuyama, H., Takahashi, R.,

- Ihara, M. 2012. Selective white matter abnormalities in a novel rat model of vascular dementia. *Neurobiol Aging*. 33: 1012.e25-35
- Kleinschnitz, C., Grund, H., Wingler, K., Armitage, M.E., Jones, E., Mittal, M., Barit, D., Schwarz, T., Geis, C., Kraft, P., Barthel, K., Schuhmann, M.K., Herrmann, A.M., Meuth, S.G., Stoll, G., Meurer, S., Schrewe, A., Becker, L., Gailus-Durner, V., Fuchs, H., Klopstock, T., de Angelis, M.H., Jandeleit-Dahm, K., Shah, A.M., Weissmann, N., Schmidt, H.H. 2010a. Post-stroke inhibition of induced NADPH oxidase type 4 prevents oxidative stress and neurodegeneration. *PLoS Biol* 8(9). doi:10.1371/journal.pbio.1000479.
- Kleinschnitz, C., Grund, H., Wingler, K., Armitage, M.E., Jones, E., Mittal, M., Barit, D., Schwarz, T., Geis, C., Kraft, P., Barthel, K., Schuhmann, M.K., Herrmann, A.M., Meuth, S.G., Stoll, G., Meurer, S., Schrewe, A., Becker, L., Gailus-Durner, V., Fuchs, H., Klopstock, T., de Angelis, M.H., Jandeleit-Dahm, K., Shah, A.M., Weissmann, N., Schmidt, H.H. 2010b. Post-stroke inhibition of induced NADPH oxidase type 4 prevents oxidative stress and neurodegeneration. *PLoS Biol* 8(9). doi:10.1371/journal.pbio.1000479.
- Klen, J., Goričar, K., Janež, A., Dolžan, V. 2015. NLRP3 Inflammasome Polymorphism and Macrovascular Complications in Type 2 Diabetes Patients. *J Diabetes Res* 2015, 616747. doi:10.1155/2015/616747.
- Klohs, J., Baltes, C., Princz-Kranz, F., Ratering, D., Nitsch, R.M., Knuesel, I., Rudin, M. 2012. Contrast-enhanced magnetic resonance microangiography reveals remodeling of the cerebral microvasculature in transgenic ArcA β mice. *J Neurosci* 32(5), 1705-13. doi:10.1523/JNEUROSCI.5626-11.2012.
- Klohs, J., Deistung, A., Ielacqua, G.D., Seuwen, A., Kindler, D., Schweser, F., Vaas, M., Kipar, A., Reichenbach, J.R., Rudin, M. 2015a. Quantitative assessment of microvasculopathy in arcA β mice with USPIO-enhanced gradient echo MRI. *J Cereb Blood Flow Metab*. doi:10.1177/0271678X15621500.
- Klohs, J., Deistung, A., Ielacqua, G.D., Seuwen, A., Kindler, D., Schweser, F., Vaas, M., Kipar, A., Reichenbach, J.R., Rudin, M. 2015b. Quantitative assessment of microvasculopathy in arcA β mice with USPIO-enhanced gradient echo MRI. *J Cereb Blood Flow Metab*. doi:10.1177/0271678X15621500.
- Klohs, J., Deistung, A., Schweser, F., Grandjean, J., Dominietto, M., Waschkes, C., Nitsch, R.M., Knuesel, I., Reichenbach, J.R., Rudin, M. 2011. Detection of cerebral microbleeds with quantitative susceptibility mapping in the ArcAbeta mouse model of cerebral amyloidosis. *J Cereb Blood Flow Metab* 31(12), 2282-92. doi:10.1038/jcbfm.2011.118.
- Kober, F., Duhamel, G., Cozzone, P.J. 2008. Experimental comparison of four FAIR arterial spin labeling techniques for quantification of mouse cerebral blood flow at 4.7 T. *NMR Biomed* 21(8), 781-92. doi:10.1002/nbm.1253.

- Kober, F., Iltis, I., Izquierdo, M., Desrois, M., Ibarrola, D., Cozzone, P.J., Bernard, M. 2004. High-resolution myocardial perfusion mapping in small animals in vivo by spin-labeling gradient-echo imaging. *Magn Reson Med* 51(1), 62-7. doi:10.1002/mrm.10676.
- Koehler, R.C., Gebremedhin, D., Harder, D.R. 2006. Role of astrocytes in cerebrovascular regulation. *J Appl Physiol* (1985) 100(1), 307-17. doi:10.1152/jappphysiol.00938.2005.
- Korani, M.S., Farbood, Y., Sarkaki, A., Fathi Moghaddam, H., Taghi Mansouri, M. 2014. Protective effects of gallic acid against chronic cerebral hypoperfusion-induced cognitive deficit and brain oxidative damage in rats. *Eur J Pharmacol* 733, 62-7. doi:10.1016/j.ejphar.2014.03.044.
- Kress, B.T., Iliff, J.J., Xia, M., Wang, M., Wei, H.S., Zeppenfeld, D., Xie, L., Kang, H., Xu, Q., Liew, J.A., Plog, B.A., Ding, F., Deane, R., Nedergaard, M. 2014. Impairment of paravascular clearance pathways in the aging brain. *Ann Neurol* 76(6), 845-61. doi:10.1002/ana.24271.
- Krishnan, S.M., Sobey, C.G., Latz, E., Mansell, A., Drummond, G.R. 2014. IL-1 β and IL-18: inflammatory markers or mediators of hypertension? *Br J Pharmacol* 171(24), 5589-602. doi:10.1111/bph.12876.
- Krueyer, A., Soplop, N., Strickland, S., Norris, E.H. 2015. Chronic Hypertension Leads to Neurodegeneration in the TgSwDI Mouse Model of Alzheimer's Disease. *Hypertension* 66(1), 175-82. doi:10.1161/HYPERTENSIONAHA.115.05524.
- Kryscio, R.J., Abner, E.L., Schmitt, F.A., Goodman, P.J., Mendiondo, M., Caban-Holt, A., Dennis, B.C., Mathews, M., Klein, E.A., Crowley, J.J., Investigators, S. 2013. A randomized controlled Alzheimer's disease prevention trial's evolution into an exposure trial: the PREADViSE Trial. *J Nutr Health Aging* 17(1), 72-5. doi:10.1007/s12603-012-0083-3.
- Kuroda, J., Ago, T., Nishimura, A., Nakamura, K., Matsuo, R., Wakisaka, Y., Kamouchi, M., Kitazono, T. 2014. Nox4 is a major source of superoxide production in human brain pericytes. *J Vasc Res* 51(6), 429-38. doi:10.1159/000369930.
- Kwon, K.J., Lee, E.J., Kim, M.K., Kim, S.Y., Kim, J.N., Kim, J.O., Kim, H.J., Kim, H.Y., Han, J.S., Shin, C.Y., Han, S.H. 2015. Diabetes augments cognitive dysfunction in chronic cerebral hypoperfusion by increasing neuronal cell death: implication of cilostazol for diabetes mellitus-induced dementia. *Neurobiol Dis* 73, 12-23. doi:10.1016/j.nbd.2014.08.034.
- Landmesser, U., Dikalov, S., Price, S.R., McCann, L., Fukui, T., Holland, S.M., Mitch, W.E., Harrison, D.G. 2003. Oxidation of tetrahydrobiopterin leads to uncoupling of endothelial cell nitric oxide synthase in hypertension. *J Clin Invest* 111(8), 1201-9. doi:10.1172/JCI14172.

- Lannfelt, L., Relkin, N.R., Siemers, E.R. 2014. Amyloid- β -directed immunotherapy for Alzheimer's disease. *J Intern Med* 275(3), 284-95. doi:10.1111/joim.12168.
- Lapi, D., Vagnani, S., Pignataro, G., Esposito, E., Paterni, M., Colantuoni, A. 2012. Protective Effects of Quercetin on Rat Pial Microvascular Changes during Transient Bilateral Common Carotid Artery Occlusion and Reperfusion. *Front Physiol* 3, 32. doi:10.3389/fphys.2012.00032.
- Larsson, J., Goumans, M.J., Sjöstrand, L.J., van Rooijen, M.A., Ward, D., Levéen, P., Xu, X., ten Dijke, P., Mummery, C.L., Karlsson, S. 2001. Abnormal angiogenesis but intact hematopoietic potential in TGF-beta type I receptor-deficient mice. *EMBO J* 20(7), 1663-73. doi:10.1093/emboj/20.7.1663.
- Last, D., Alsop, D.C., Abduljalil, A.M., Marquis, R.P., de Bazelaire, C., Hu, K., Cavallerano, J., Novak, V. 2007. Global and regional effects of type 2 diabetes on brain tissue volumes and cerebral vasoreactivity. *Diabetes Care* 30(5), 1193-9. doi:10.2337/dc06-2052.
- Lee, H.M., Kim, J.J., Kim, H.J., Shong, M., Ku, B.J., Jo, E.K. 2013. Upregulated NLRP3 inflammasome activation in patients with type 2 diabetes. *Diabetes* 62(1), 194-204. doi:10.2337/db12-0420.
- Levy, E., Carman, M.D., Fernandez-Madrid, I.J., Power, M.D., Lieberburg, I., van Duinen, S.G., Bots, G.T., Luyendijk, W., Frangione, B. 1990. Mutation of the Alzheimer's disease amyloid gene in hereditary cerebral hemorrhage, Dutch type. *Science* 248(4959), 1124-6.
- Li, B., Zhang, J., Wang, Z., Chen, S. 2016. Ivabradine Prevents Low Shear Stress Induced Endothelial Inflammation and Oxidative Stress via mTOR/eNOS Pathway. *PLoS One* 11(2), e0149694. doi:10.1371/journal.pone.0149694.
- Li, H., Wang, Y., Feng, D., Liu, Y., Xu, M., Gao, A., Tian, F., Zhang, L., Cui, Y., Wang, Z., Chen, G. 2014. Alterations in the time course of expression of the Nox family in the brain in a rat experimental cerebral ischemia and reperfusion model: effects of melatonin. *J Pineal Res* 57(1), 110-9. doi:10.1111/jpi.12148.
- Li, J., Yang, J.Y., Yao, X.C., Xue, X., Zhang, Q.C., Wang, X.X., Ding, L.L., Wu, C.F. 2013. Oligomeric A β -induced microglial activation is possibly mediated by NADPH oxidase. *Neurochem Res* 38(2), 443-52. doi:10.1007/s11064-012-0939-2.
- Li, J.J., Chen, J.L. 2005. Inflammation may be a bridge connecting hypertension and atherosclerosis. *Med Hypotheses* 64(5), 925-9. doi:10.1016/j.mehy.2004.10.016.
- Li, L., Welser, J.V., Dore-Duffy, P., del Zoppo, G.J., Lamanna, J.C., Milner, R. 2010. In the hypoxic central nervous system, endothelial cell proliferation is followed by astrocyte activation, proliferation, and increased expression of the alpha 6 beta 4 integrin and dystroglycan. *Glia* 58(10), 1157-67. doi:10.1002/glia.20995.

- Lin, A.L., Zheng, W., Halloran, J.J., Burbank, R.R., Hussong, S.A., Hart, M.J., Javors, M., Shih, Y.Y., Muir, E., Solano Fonseca, R., Strong, R., Richardson, A.G., Lechleiter, J.D., Fox, P.T., Galvan, V. 2013. Chronic rapamycin restores brain vascular integrity and function through NO synthase activation and improves memory in symptomatic mice modeling Alzheimer's disease. *J Cereb Blood Flow Metab* 33(9), 1412-21. doi:10.1038/jcbfm.2013.82.
- Lin, C.Y., Chang, C., Cheung, W.M., Lin, M.H., Chen, J.J., Hsu, C.Y., Chen, J.H., Lin, T.N. 2008. Dynamic changes in vascular permeability, cerebral blood volume, vascular density, and size after transient focal cerebral ischemia in rats: evaluation with contrast-enhanced magnetic resonance imaging. *J Cereb Blood Flow Metab* 28(8), 1491-501. doi:10.1038/jcbfm.2008.42.
- Lindner, J.R. 2009. Contrast ultrasound molecular imaging of inflammation in cardiovascular disease. *Cardiovasc Res* 84(2), 182-9. doi:10.1093/cvr/cvp302.
- Linker, R.A., Kroner, A., Horn, T., Gold, R., Mäurer, M., Bendszus, M. 2006. Iron particle-enhanced visualization of inflammatory central nervous system lesions by high resolution: preliminary data in an animal model. *AJNR Am J Neuroradiol* 27(6), 1225-9.
- Liu, H., Zhang, J. 2012. Cerebral hypoperfusion and cognitive impairment: the pathogenic role of vascular oxidative stress. *Int J Neurosci* 122(9), 494-9. doi:10.3109/00207454.2012.686543.
- Liu, Y., Zhu, X., Feinberg, D., Guenther, M., Gregori, J., Weiner, M.W., Schuff, N. 2012. Arterial spin labeling MRI study of age and gender effects on brain perfusion hemodynamics. *Magn Reson Med* 68(3), 912-22. doi:10.1002/mrm.23286.
- Lok, J., Gupta, P., Guo, S., Kim, W.J., Whalen, M.J., van Leyen, K., Lo, E.H. 2007. Cell-cell signaling in the neurovascular unit. *Neurochem Res* 32(12), 2032-45. doi:10.1007/s11064-007-9342-9.
- Lourenço, C.F., Ledo, A., Dias, C., Barbosa, R.M., Laranjinha, J. 2015. Neurovascular and neurometabolic derailment in aging and Alzheimer's disease. *Front Aging Neurosci* 7, 103. doi:10.3389/fnagi.2015.00103.
- Love, S., Miners, J.S. 2016a. Cerebrovascular disease in ageing and Alzheimer's disease. *Acta Neuropathol* 131(5), 645-58. doi:10.1007/s00401-015-1522-0.
- Love, S., Miners, J.S. 2016b. Cerebrovascular disease in ageing and Alzheimer's disease. *Acta Neuropathol* 131(5), 645-58. doi:10.1007/s00401-015-1522-0.
- Lubrano, V., Balzan, S. 2016. Roles of LOX-1 in microvascular dysfunction. *Microvasc Res* 105, 132-40. doi:10.1016/j.mvr.2016.02.006.

- Lucas, M.L., Carraro, C.C., Belló-Klein, A., Kalil, A.N., Aerts, N. 2016. Oxidative stress in carotid arteries of patients submitted to carotid endarterectomy. The role of aging process. *Acta Cir Bras* 31(8), 564-8. doi:10.1590/S0102-865020160080000010.
- Lull, M.E., Levesque, S., Surace, M.J., Block, M.L. 2011. Chronic apocynin treatment attenuates beta amyloid plaque size and microglial number in hAPP(751)(SL) mice. *PLoS One* 6(5), e20153. doi:10.1371/journal.pone.0020153.
- Luo, X.G., Ding, J.Q., Chen, S.D. 2010. Microglia in the aging brain: relevance to neurodegeneration. *Mol Neurodegener* 5, 12. doi:10.1186/1750-1326-5-12.
- Lénárt, N., Brough, D., Dénes, Á. 2016. Inflammasomes link vascular disease with neuroinflammation and brain disorders. *J Cereb Blood Flow Metab.* doi:10.1177/0271678X16662043.
- Maeda, K., Mies, G., Oláh, L., Hossmann, K.A. 2000. Quantitative measurement of local cerebral blood flow in the anesthetized mouse using intraperitoneal [¹⁴C]iodoantipyrine injection and final arterial heart blood sampling. *J Cereb Blood Flow Metab* 20(1), 10-4. doi:10.1097/00004647-200001000-00003.
- Maki, R.A., Tyurin, V.A., Lyon, R.C., Hamilton, R.L., DeKosky, S.T., Kagan, V.E., Reynolds, W.F. 2009. Aberrant expression of myeloperoxidase in astrocytes promotes phospholipid oxidation and memory deficits in a mouse model of Alzheimer disease. *J Biol Chem* 284(5), 3158-69. doi:10.1074/jbc.M807731200.
- Malouf, R., Birks, J. 2004. Donepezil for vascular cognitive impairment. *Cochrane Database Syst Rev* (1), CD004395. doi:10.1002/14651858.CD004395.pub2.
- Mandell, D.M., Han, J.S., Poublanc, J., Crawley, A.P., Kassner, A., Fisher, J.A., Mikulis, D.J. 2008. Selective reduction of blood flow to white matter during hypercapnia corresponds with leukoaraiosis. *Stroke* 39(7), 1993-8. doi:10.1161/STROKEAHA.107.501692.
- Mander, P.K., Jekabsone, A., Brown, G.C. 2006. Microglia proliferation is regulated by hydrogen peroxide from NADPH oxidase. *J Immunol* 176(2), 1046-52.
- Marik, S.A., Olsen, O., Tessier-Lavigne, M., Gilbert, C.D. 2016. Physiological role for amyloid precursor protein in adult experience-dependent plasticity. *Proc Natl Acad Sci U S A* 113(28), 7912-7. doi:10.1073/pnas.1604299113.
- Massaad, C.A., Amin, S.K., Hu, L., Mei, Y., Klann, E., Pautler, R.G. 2010a. Mitochondrial superoxide contributes to blood flow and axonal transport deficits in the Tg2576 mouse model of Alzheimer's disease. *PLoS One* 5(5), e10561. doi:10.1371/journal.pone.0010561.
- Massaad, C.A., Amin, S.K., Hu, L., Mei, Y., Klann, E., Pautler, R.G. 2010b. Mitochondrial superoxide contributes to blood flow and axonal transport deficits in the Tg2576 mouse model of Alzheimer's disease. *PLoS One* 5(5), e10561. doi:10.1371/journal.pone.0010561.

- Mastantuono, T., Battiloro, L., Sabatino, L., Chiurazzi, M., Di Maro, M., Muscariello, E., Colantuoni, A., Lapi, D. 2015. Effects of Citrus Flavonoids Against Microvascular Damage Induced by Hypoperfusion and Reperfusion in Rat Pial Circulation. *Microcirculation* 22(5), 378-90. doi:10.1111/micc.12207.
- Matin, N., Fisher, C., Jackson, W.F., Dorrance, A.M. 2016. Bilateral common carotid artery stenosis in normotensive rats impairs endothelium-dependent dilation of parenchymal arterioles. *Am J Physiol Heart Circ Physiol* 310(10), H1321-9. doi:10.1152/ajpheart.00890.2015.
- Matthews, F.E., Stephan, B.C., Robinson, L., Jagger, C., Barnes, L.E., Arthur, A., Brayne, C., Collaboration, C.F.a.A.S.C. 2016. A two decade dementia incidence comparison from the Cognitive Function and Ageing Studies I and II. *Nat Commun* 7, 11398. doi:10.1038/ncomms11398.
- Mayhan, W.G., Arrick, D.M., Sharpe, G.M., Sun, H. 2008. Age-related alterations in reactivity of cerebral arterioles: role of oxidative stress. *Microcirculation* 15(3), 225-36. doi:10.1080/10739680701641421.
- McCann, S.K., Dusting, G.J., Roulston, C.L. 2014. Nox2 knockout delays infarct progression and increases vascular recovery through angiogenesis in mice following ischaemic stroke with reperfusion. *PLoS One* 9(11), e110602. doi:10.1371/journal.pone.0110602.
- McQueen, J., Reimer, M.M., Holland, P.R., Manso, Y., McLaughlin, M., Fowler, J.H., Horsburgh, K. 2014a. Restoration of oligodendrocyte pools in a mouse model of chronic cerebral hypoperfusion. *PLoS One* 9(2), e87227. doi:10.1371/journal.pone.0087227.
- McQueen, J., Reimer, M.M., Holland, P.R., Manso, Y., McLaughlin, M., Fowler, J.H., Horsburgh, K. 2014b. Restoration of oligodendrocyte pools in a mouse model of chronic cerebral hypoperfusion. *PLoS One* 9(2), e87227. doi:10.1371/journal.pone.0087227.
- Mecocci, P., Polidori, M.C. 2012. Antioxidant clinical trials in mild cognitive impairment and Alzheimer's disease. *Biochim Biophys Acta* 1822(5), 631-8. doi:10.1016/j.bbadis.2011.10.006.
- Meier, I.B., Gu, Y., Guzaman, V.A., Wiegman, A.F., Schupf, N., Manly, J.J., Luchsinger, J.A., Viswanathan, A., Martinez-Ramirez, S., Greenberg, S.M., Mayeux, R., Brickman, A.M. 2014. Lobar microbleeds are associated with a decline in executive functioning in older adults. *Cerebrovasc Dis* 38(5), 377-83. doi:10.1159/000368998.
- Miao, J., Xu, F., Davis, J., Otte-Höller, I., Verbeek, M.M., Van Nostrand, W.E. 2005. Cerebral microvascular amyloid beta protein deposition induces vascular degeneration and neuroinflammation in transgenic mice expressing human vasculotropic mutant amyloid beta precursor protein. *Am J Pathol* 167(2), 505-15.

- Mildner, A., Schmidt, H., Nitsche, M., Merkler, D., Hanisch, U.K., Mack, M., Heikenwalder, M., Brück, W., Priller, J., Prinz, M. 2007. Microglia in the adult brain arise from Ly-6ChiCCR2+ monocytes only under defined host conditions. *Nat Neurosci* 10(12), 1544-53. doi:10.1038/nn2015.
- Minter, M.R., Taylor, J.M., Crack, P.J. 2016. The contribution of neuroinflammation to amyloid toxicity in Alzheimer's disease. *J Neurochem* 136(3), 457-74. doi:10.1111/jnc.13411.
- Mirzaei, N., Tang, S.P., Ashworth, S., Coello, C., Plisson, C., Passchier, J., Selvaraj, V., Tyacke, R.J., Nutt, D.J., Sastre, M. 2016. In vivo imaging of microglial activation by positron emission tomography with [(11)C]PBR28 in the 5XFAD model of Alzheimer's disease. *Glia* 64(6), 993-1006. doi:10.1002/glia.22978.
- Modrick, M.L., Didion, S.P., Sigmund, C.D., Faraci, F.M. 2009. Role of oxidative stress and AT1 receptors in cerebral vascular dysfunction with aging. *Am J Physiol Heart Circ Physiol* 296(6), H1914-9. doi:10.1152/ajpheart.00300.2009.
- Mohtasib, R.S., Lumley, G., Goodwin, J.A., Emsley, H.C., Sluming, V., Parkes, L.M. 2012. Calibrated fMRI during a cognitive Stroop task reveals reduced metabolic response with increasing age. *Neuroimage* 59(2), 1143-51. doi:10.1016/j.neuroimage.2011.07.092.
- Montagne, A., Barnes, S.R., Sweeney, M.D., Halliday, M.R., Sagare, A.P., Zhao, Z., Toga, A.W., Jacobs, R.E., Liu, C.Y., Amezcua, L., Harrington, M.G., Chui, H.C., Law, M., Zlokovic, B.V. 2015. Blood-brain barrier breakdown in the aging human hippocampus. *Neuron* 85(2), 296-302. doi:10.1016/j.neuron.2014.12.032.
- Moorhouse, P., Rockwood, K. 2008. Vascular cognitive impairment: current concepts and clinical developments. *Lancet Neurol* 7(3), 246-55. doi:10.1016/S1474-4422(08)70040-1.
- Morley, J.E., Farr, S.A., Banks, W.A., Johnson, S.N., Yamada, K.A., Xu, L. 2010. A physiological role for amyloid-beta protein: enhancement of learning and memory. *J Alzheimers Dis* 19(2), 441-9. doi:10.3233/JAD-2009-1230.
- Mucke, L., Masliah, E., Yu, G.Q., Mallory, M., Rockenstein, E.M., Tatsuno, G., Hu, K., Kholodenko, D., Johnson-Wood, K., McConlogue, L. 2000. High-level neuronal expression of abeta 1-42 in wild-type human amyloid protein precursor transgenic mice: synaptotoxicity without plaque formation. *J Neurosci* 20(11), 4050-8.
- Murray, I.V., Proza, J.F., Sohrabji, F., Lawler, J.M. 2011. Vascular and metabolic dysfunction in Alzheimer's disease: a review. *Exp Biol Med* (Maywood) 236(7), 772-82. doi:10.1258/ebm.2011.010355.
- Nagata, K., Yamazaki, T., Takano, D., Maeda, T., Fujimaki, Y., Nakase, T., Sato, Y. 2016. Cerebral circulation in aging. *Ageing Res Rev*. doi:10.1016/j.arr.2016.06.001.

- Naik, E., Dixit, V.M. 2011. Mitochondrial reactive oxygen species drive proinflammatory cytokine production. *J Exp Med* 208(3), 417-20. doi:10.1084/jem.20110367.
- Nakaji, K., Ihara, M., Takahashi, C., Itohara, S., Noda, M., Takahashi, R., Tomimoto, H. 2006. Matrix metalloproteinase-2 plays a critical role in the pathogenesis of white matter lesions after chronic cerebral hypoperfusion in rodents. *Stroke* 37(11), 2816-23. doi:10.1161/01.STR.0000244808.17972.55.
- Nation, D.A., Wierenga, C.E., Clark, L.R., Dev, S.I., Stricker, N.H., Jak, A.J., Salmon, D.P., Delano-Wood, L., Bangen, K.J., Rissman, R.A., Liu, T.T., Bondi, M.W. 2013. Cortical and subcortical cerebrovascular resistance index in mild cognitive impairment and Alzheimer's disease. *J Alzheimers Dis* 36(4), 689-98. doi:10.3233/JAD-130086.
- Nediani, C., Borch, E., Giordano, C., Baruzzo, S., Ponziani, V., Sebastiani, M., Nassi, P., Mugelli, A., d'Amati, G., Cerbai, E. 2007. NADPH oxidase-dependent redox signalling in human heart failure: relationship between the left and right ventricle. *J Mol Cell Cardiol* 42(4), 826-34. doi:10.1016/j.yjmcc.2007.01.009
- Neuwelt, A., Sidhu, N., Hu, C.A., Mlady, G., Eberhardt, S.C., Sillerud, L.O. 2015. Iron-based superparamagnetic nanoparticle contrast agents for MRI of infection and inflammation. *AJR Am J Roentgenol* 204(3), W302-13. doi:10.2214/AJR.14.12733.
- Nishimura, A., Ago, T., Kuroda, J., Arimura, K., Tachibana, M., Nakamura, K., Wakisaka, Y., Sadoshima, J., Ihara, K., Kitazono, T. 2016. Detrimental role of pericyte Nox4 in the acute phase of brain ischemia. *J Cereb Blood Flow Metab* 36(6), 1143-54. doi:10.1177/0271678X15606456.
- Nishino, A., Tajima, Y., Takuwa, H., Masamoto, K., Taniguchi, J., Wakizaka, H., Kokuryo, D., Urushihata, T., Aoki, I., Kanno, I., Tomita, Y., Suzuki, N., Ikoma, Y., Ito, H. 2016. Long-term effects of cerebral hypoperfusion on neural density and function using misery perfusion animal model. *Sci Rep* 6, 25072. doi:10.1038/srep25072.
- Nishio, K., Ihara, M., Yamasaki, N., Kalaria, R.N., Maki, T., Fujita, Y., Ito, H., Oishi, N., Fukuyama, H., Miyakawa, T., Takahashi, R., Tomimoto, H. 2010. A mouse model characterizing features of vascular dementia with hippocampal atrophy. *Stroke* 41(6), 1278-84. doi:10.1161/STROKEAHA.110.581686.
- Niwa, K., Kazama, K., Younkin, L., Younkin, S.G., Carlson, G.A., Iadecola, C. 2002a. Cerebrovascular autoregulation is profoundly impaired in mice overexpressing amyloid precursor protein. *Am J Physiol Heart Circ Physiol* 283(1), H315-23. doi:10.1152/ajpheart.00022.2002.
- Niwa, K., Kazama, K., Younkin, S.G., Carlson, G.A., Iadecola, C. 2002b. Alterations in cerebral blood flow and glucose utilization in mice overexpressing the amyloid precursor protein. *Neurobiol Dis* 9(1), 61-8. doi:10.1006/nbdi.2001.0460.
- Novak, V., Last, D., Alsop, D.C., Abduljalil, A.M., Hu, K., Lepicovsky, L., Cavallerano, J., Lipsitz, L.A. 2006. Cerebral blood flow velocity and periventricular white matter

- hyperintensities in type 2 diabetes. *Diabetes Care* 29(7), 1529-34. doi:10.2337/dc06-0261.
- Nöth, U., Meadows, G.E., Kotajima, F., Deichmann, R., Corfield, D.R., Turner, R. 2006. Cerebral vascular response to hypercapnia: determination with perfusion MRI at 1.5 and 3.0 Tesla using a pulsed arterial spin labeling technique. *J Magn Reson Imaging* 24(6), 1229-35. doi:10.1002/jmri.20761.
- O'Brien, J.T. 2006. Vascular cognitive impairment. *Am J Geriatr Psychiatry* 14(9), 724-33. doi:10.1097/01.JGP.0000231780.44684.7e.
- O'Brien, J.T., Thomas, A. 2015. Vascular dementia. *Lancet* 386(10004), 1698-706. doi:10.1016/S0140-6736(15)00463-8.
- O'Leary, T.P., Brown, R.E. 2013. Optimization of apparatus design and behavioral measures for the assessment of visuo-spatial learning and memory of mice on the Barnes maze. *Learn Mem* 20(2), 85-96. doi:10.1101/lm.028076.112.
- Obari D, Ozcelik SO, Girouard H, Hamel E. 2016. Hypertension and the brain as an end-organ target. Chapter 5: Cognitive Dysfunction and Dementia in Animal Models of Hypertension. Retrieved from: <http://www.springer.com/gp/book/9783319256146>
- Okamoto, Y., Yamamoto, T., Kalaria, R.N., Senzaki, H., Maki, T., Hase, Y., Kitamura, A., Washida, K., Yamada, M., Ito, H., Tomimoto, H., Takahashi, R., Ihara, M. 2012a. Cerebral hypoperfusion accelerates cerebral amyloid angiopathy and promotes cortical microinfarcts. *Acta Neuropathol* 123(3), 381-94. doi:10.1007/s00401-011-0925-9.
- Okamoto, Y., Yamamoto, T., Kalaria, R.N., Senzaki, H., Maki, T., Hase, Y., Kitamura, A., Washida, K., Yamada, M., Ito, H., Tomimoto, H., Takahashi, R., Ihara, M. 2012b. Cerebral hypoperfusion accelerates cerebral amyloid angiopathy and promotes cortical microinfarcts. *Acta Neuropathol* 123(3), 381-94. doi:10.1007/s00401-011-0925-9.
- Omi, T., Kumada, M., Kamesaki, T., Okuda, H., Munkhtulga, L., Yanagisawa, Y., Utsumi, N., Gotoh, T., Hata, A., Soma, M., Umemura, S., Ogihara, T., Takahashi, N., Tabara, Y., Shimada, K., Mano, H., Kajii, E., Miki, T., Iwamoto, S. 2006. An intronic variable number of tandem repeat polymorphisms of the cold-induced autoinflammatory syndrome 1 (CIAS1) gene modifies gene expression and is associated with essential hypertension. *Eur J Hum Genet* 14(12), 1295-305. doi:10.1038/sj.ejhg.5201698.
- Otori, T., Katsumata, T., Muramatsu, H., Kashiwagi, F., Katayama, Y., Terashi, A. 2003. Long-term measurement of cerebral blood flow and metabolism in a rat chronic hypoperfusion model. *Clin Exp Pharmacol Physiol* 30(4), 266-72.
- Otsu, Y., Couchman, K., Lyons, D.G., Collot, M., Agarwal, A., Mallet, J.M., Pfrieger, F.W., Bergles, D.E., Charpak, S. 2015. Calcium dynamics in astrocyte processes during neurovascular coupling. *Nat Neurosci* 18(2), 210-8. doi:10.1038/nn.3906.

- Paiardi, S., Rodella, L.F., De Ciuceis, C., Porteri, E., Boari, G.E., Rezzani, R., Rizzardi, N., Platto, C., Tiberio, G.A., Giulini, S.M., Rizzoni, D., Agabiti-Rosei, E. 2009. Immunohistochemical evaluation of microvascular rarefaction in hypertensive humans and in spontaneously hypertensive rats. *Clin Hemorheol Microcirc* 42(4), 259-68. doi:10.3233/CH-2009-1195.
- Pappata, S., Levasseur, M., Gunn, R.N., Myers, R., Crouzel, C., Syrota, A., Jones, T., Kreutzberg, G.W., Banati, R.B. 2000. Thalamic microglial activation in ischemic stroke detected in vivo by PET and [¹¹C]PK1195. *Neurology* 55(7), 1052-4.
- Park, J.H., Seo, S.W., Kim, C., Kim, S.H., Kim, G.H., Kim, S.T., Jeon, S., Lee, J.M., Oh, S.J., Kim, J.S., Choe, Y.S., Lee, K.H., Shin, J.S., Kim, C.H., Noh, Y., Cho, H., Yoon, C.W., Kim, H.J., Ye, B.S., Ewers, M., Weiner, M.W., Lee, J.H., Werring, D.J., Na, D.L. 2014. Effects of cerebrovascular disease and amyloid beta burden on cognition in subjects with subcortical vascular cognitive impairment. *Neurobiol Aging* 35(1), 254-60. doi:10.1016/j.neurobiolaging.2013.06.026.
- Park, L., Anrather, J., Girouard, H., Zhou, P., Iadecola, C. 2007. Nox2-derived reactive oxygen species mediate neurovascular dysregulation in the aging mouse brain. *J Cereb Blood Flow Metab* 27(12), 1908-18. doi:10.1038/sj.jcbfm.9600491.
- Park, L., Anrather, J., Zhou, P., Frys, K., Pitstick, R., Younkin, S., Carlson, G.A., Iadecola, C. 2005a. NADPH-oxidase-derived reactive oxygen species mediate the cerebrovascular dysfunction induced by the amyloid beta peptide. *J Neurosci* 25(7), 1769-77. doi:10.1523/JNEUROSCI.5207-04.2005.
- Park, L., Anrather, J., Zhou, P., Frys, K., Pitstick, R., Younkin, S., Carlson, G.A., Iadecola, C. 2005b. NADPH-oxidase-derived reactive oxygen species mediate the cerebrovascular dysfunction induced by the amyloid beta peptide. *J Neurosci* 25(7), 1769-77. doi:10.1523/JNEUROSCI.5207-04.2005.
- Park, L., Koizumi, K., El Jamal, S., Zhou, P., Previti, M.L., Van Nostrand, W.E., Carlson, G., Iadecola, C. 2014. Age-dependent neurovascular dysfunction and damage in a mouse model of cerebral amyloid angiopathy. *Stroke* 45(6), 1815-21. doi:10.1161/STROKEAHA.114.005179.
- Park, L., Zhou, P., Pitstick, R., Capone, C., Anrather, J., Norris, E.H., Younkin, L., Younkin, S., Carlson, G., McEwen, B.S., Iadecola, C. 2008. Nox2-derived radicals contribute to neurovascular and behavioral dysfunction in mice overexpressing the amyloid precursor protein. *Proc Natl Acad Sci U S A* 105(4), 1347-52. doi:10.1073/pnas.0711568105.
- Patel, A., MacMahon, S., Chalmers, J., Neal, B., Billot, L., Woodward, M., Marre, M., Cooper, M., Glasziou, P., Grobbee, D., Hamet, P., Harrap, S., Heller, S., Liu, L., Mancia, G., Mogensen, C.E., Pan, C., Poulter, N., Rodgers, A., Williams, B., Bompont, S., de Galan, B.E., Joshi, R., Travert, F., Group, A.C. 2008. Intensive blood glucose control and vascular outcomes in patients with type 2 diabetes. *N Engl J Med* 358(24), 2560-72. doi:10.1056/NEJMoa0802987.

- Paxinos G, Franklin KBJ. 2001. *The Mouse Brain in Stereotaxic Coordinates*. 2nd ed. San Diego: Academic Press.
- Pendlebury, S.T., Rothwell, P.M. 2009. Prevalence, incidence, and factors associated with pre-stroke and post-stroke dementia: a systematic review and meta-analysis. *Lancet Neurol* 8(11), 1006-18. doi:10.1016/S1474-4422(09)70236-4.
- Peng, Y., Xu, S., Chen, G., Wang, L., Feng, Y., Wang, X. 2007. 1-3-n-Butylphthalide improves cognitive impairment induced by chronic cerebral hypoperfusion in rats. *J Pharmacol Exp Ther* 321(3), 902-10. doi:10.1124/jpet.106.118760.
- Perassa, L.A., Graton, M.E., Potje, S.R., Troiano, J.A., Lima, M.S., Vale, G.T., Pereira, A.A., Nakamune, A.C., Sumida, D.H., Tirapelli, C.R., Bendhack, L.M., Antoniali, C. 2016. Apocynin reduces blood pressure and restores the proper function of vascular endothelium in SHR. *Vascul Pharmacol*. doi:10.1016/j.vph.2016.06.005.
- Perrotta, M., Lembo, G., Carnevale, D. 2016. Hypertension and Dementia: Epidemiological and Experimental Evidence Revealing a Detrimental Relationship. *Int J Mol Sci* 17(3), 347. doi:10.3390/ijms17030347.
- Phillips, A.A., Chan, F.H., Zheng, M.M., Krassioukov, A.V., Ainslie, P.N. 2016. Neurovascular coupling in humans: Physiology, methodological advances and clinical implications. *J Cereb Blood Flow Metab* 36(4), 647-64. doi:10.1177/0271678X15617954.
- Pimentel-Coelho, P.M., Michaud, J.P., Rivest, S. 2013. Effects of mild chronic cerebral hypoperfusion and early amyloid pathology on spatial learning and the cellular innate immune response in mice. *Neurobiol Aging* 34(3), 679-93. doi:10.1016/j.neurobiolaging.2012.06.025.
- Pober, J.S., Sessa, W.C. 2015. Inflammation and the blood microvascular system. *Cold Spring Harb Perspect Biol* 7(1), a016345. doi:10.1101/cshperspect.a016345.
- Primiani, C.T., Ryan, V.H., Rao, J.S., Cam, M.C., Ahn, K., Modi, H.R., Rapoport, S.I. 2014. Coordinated gene expression of neuroinflammatory and cell signaling markers in dorsolateral prefrontal cortex during human brain development and aging. *PLoS One* 9(10), e110972. doi:10.1371/journal.pone.0110972.
- Promjunyakul, N., Lahna, D., Kaye, J.A., Dodge, H.H., Erten-Lyons, D., Rooney, W.D., Silbert, L.C. 2015. Characterizing the white matter hyperintensity penumbra with cerebral blood flow measures. *Neuroimage Clin* 8, 224-9. doi:10.1016/j.nicl.2015.04.012.
- Qin, W.D., Mi, S.H., Li, C., Wang, G.X., Zhang, J.N., Wang, H., Zhang, F., Ma, Y., Wu, D.W., Zhang, M. 2015. Low shear stress induced HMGB1 translocation and release via PECAM-1/PARP-1 pathway to induce inflammation response. *PLoS One* 10(3), e0120586. doi:10.1371/journal.pone.0120586.

- Qiu, C., von Strauss, E., Bäckman, L., Winblad, B., Fratiglioni, L. 2013. Twenty-year changes in dementia occurrence suggest decreasing incidence in central Stockholm, Sweden. *Neurology* 80(20), 1888-94. doi:10.1212/WNL.0b013e318292a2f9.
- Ransohoff, R.M., Schafer, D., Vincent, A., Blachère, N.E., Bar-Or, A. 2015. Neuroinflammation: Ways in Which the Immune System Affects the Brain. *Neurotherapeutics* 12(4), 896-909. doi:10.1007/s13311-015-0385-3.
- Raz, L., Knoefel, J., Bhaskar, K. 2016. The neuropathology and cerebrovascular mechanisms of dementia. *J Cereb Blood Flow Metab* 36(1), 172-86. doi:10.1038/jcbfm.2015.164.
- Reckelhoff, J.F., Romero, J.C. 2003. Role of oxidative stress in angiotensin-induced hypertension. *Am J Physiol Regul Integr Comp Physiol* 284(4), R893-912. doi:10.1152/ajpregu.00491.2002.
- Reijmer, Y.D., van Veluw, S.J., Greenberg, S.M. 2016. Ischemic brain injury in cerebral amyloid angiopathy. *J Cereb Blood Flow Metab* 36(1), 40-54. doi:10.1038/jcbfm.2015.88.
- Reimer, M.M., McQueen, J., Searcy, L., Scullion, G., Zonta, B., Desmazieres, A., Holland, P.R., Smith, J., Gliddon, C., Wood, E.R., Herzyk, P., Brophy, P.J., McCulloch, J., Horsburgh, K. 2011. Rapid disruption of axon-glial integrity in response to mild cerebral hypoperfusion. *J Neurosci* 31(49), 18185-94. doi:10.1523/JNEUROSCI.4936-11.2011.
- Reuter, B., Venus, A., Heiler, P., Schad, L., Ebert, A., Hennerici, M.G., Grudzenski, S., Fatar, M. 2016. Development of Cerebral Microbleeds in the APP23-Transgenic Mouse Model of Cerebral Amyloid Angiopathy-A 9.4 Tesla MRI Study. *Front Aging Neurosci* 8, 170. doi:10.3389/fnagi.2016.00170.
- Richiardi, J., Monsch, A.U., Haas, T., Barkhof, F., Van de Ville, D., Radü, E.W., Kressig, R.W., Haller, S. 2015. Altered cerebrovascular reactivity velocity in mild cognitive impairment and Alzheimer's disease. *Neurobiol Aging* 36(1), 33-41. doi:10.1016/j.neurobiolaging.2014.07.020.
- Rigau, V., Morin, M., Rousset, M.C., de Bock, F., Lebrun, A., Coubes, P., Picot, M.C., Baldy-Moulinier, M., Bockaert, J., Crespel, A., Lerner-Natoli, M. 2007. Angiogenesis is associated with blood-brain barrier permeability in temporal lobe epilepsy. *Brain* 130(Pt 7), 1942-56. doi:10.1093/brain/awm118.
- Ritter, A., Pillai, J.A. 2015. Treatment of Vascular Cognitive Impairment. *Curr Treat Options Neurol* 17(8), 367. doi:10.1007/s11940-015-0367-0.
- Rochfort, K.D., Collins, L.E., McLoughlin, A., Cummins, P.M. 2015. Shear-dependent attenuation of cellular ROS levels can suppress proinflammatory cytokine injury to human brain microvascular endothelial barrier properties. *J Cereb Blood Flow Metab* 35(10), 1648-56. doi:10.1038/jcbfm.2015.102.

- Rochfort, K.D., Collins, L.E., Murphy, R.P., Cummins, P.M. 2014. Downregulation of blood-brain barrier phenotype by proinflammatory cytokines involves NADPH oxidase-dependent ROS generation: consequences for interendothelial adherens and tight junctions. *PLoS One* 9(7), e101815. doi:10.1371/journal.pone.0101815.
- Rochfort, K.D., Cummins, P.M. 2015. The blood-brain barrier endothelium: a target for pro-inflammatory cytokines. *Biochem Soc Trans* 43(4), 702-6. doi:10.1042/BST20140319.
- Rodgers, S.P., Born, H.A., Das, P., Jankowsky, J.L. 2012. Transgenic APP expression during postnatal development causes persistent locomotor hyperactivity in the adult. *Mol Neurodegener* 7, 28. doi:10.1186/1750-1326-7-28.
- Rodrigo, R., Fernández-Gajardo, R., Gutiérrez, R., Matamala, J.M., Carrasco, R., Miranda-Merchak, A., Feuerhake, W. 2013. Oxidative stress and pathophysiology of ischemic stroke: novel therapeutic opportunities. *CNS Neurol Disord Drug Targets* 12(5), 698-714.
- Roher, A.E., Kuo, Y.M., Esh, C., Knebel, C., Weiss, N., Kalback, W., Luehrs, D.C., Childress, J.L., Beach, T.G., Weller, R.O., Kokjohn, T.A. 2003. Cortical and leptomeningeal cerebrovascular amyloid and white matter pathology in Alzheimer's disease. *Mol Med* 9(3-4), 112-22.
- Rosenberg, G.A. 2009. Inflammation and white matter damage in vascular cognitive impairment. *Stroke* 40(3 Suppl), S20-3. doi:10.1161/STROKEAHA.108.533133.
- Rossi, B., Angiari, S., Zenaro, E., Budui, S.L., Constantin, G. 2011. Vascular inflammation in central nervous system diseases: adhesion receptors controlling leukocyte-endothelial interactions. *J Leukoc Biol* 89(4), 539-56. doi:10.1189/jlb.0710432.
- Rouch, L., Cestac, P., Hanon, O., Cool, C., Helmer, C., Bouhanick, B., Chamontin, B., Dartigues, J.F., Vellas, B., Andrieu, S. 2015. Antihypertensive drugs, prevention of cognitive decline and dementia: a systematic review of observational studies, randomized controlled trials and meta-analyses, with discussion of potential mechanisms. *CNS Drugs* 29(2), 113-30. doi:10.1007/s40263-015-0230-6.
- Ruitenbergh, A., den Heijer, T., Bakker, S.L., van Swieten, J.C., Koudstaal, P.J., Hofman, A., Breteler, M.M. 2005. Cerebral hypoperfusion and clinical onset of dementia: the Rotterdam Study. *Ann Neurol* 57(6), 789-94. doi:10.1002/ana.20493.
- Saggu, R., Schumacher, T., Gerich, F., Rakers, C., Tai, K., Delekate, A., Petzold, G.C. 2016. Astroglial NF- κ B contributes to white matter damage and cognitive impairment in a mouse model of vascular dementia. *Acta Neuropathol Commun* 4(1), 76. doi:10.1186/s40478-016-0350-3.
- Saleh, A., Schroeter, M., Jonkmanns, C., Hartung, H.P., Mödder, U., Jander, S. 2004. In vivo MRI of brain inflammation in human ischaemic stroke. *Brain* 127(Pt 7), 1670-7. doi:10.1093/brain/awh191.

- Salminen, A., Ojala, J., Kauppinen, A., Kaarniranta, K., Suuronen, T. 2009. Inflammation in Alzheimer's disease: amyloid-beta oligomers trigger innate immunity defence via pattern recognition receptors. *Prog Neurobiol* 87(3), 181-94.
- Sam, K., Crawley, A.P., Conklin, J., Poulblanc, J., Sobczyk, O., Mandell, D.M., Venkatraghavan, L., Duffin, J., Fisher, J.A., Black, S.E., Mikulis, D.J. 2016a. Development of White Matter Hyperintensity Is Preceded by Reduced Cerebrovascular Reactivity. *Ann Neurol* 80(2), 277-85. doi:10.1002/ana.24712.
- Sam, K., Crawley, A.P., Conklin, J., Poulblanc, J., Sobczyk, O., Mandell, D.M., Venkatraghavan, L., Duffin, J., Fisher, J.A., Black, S.E., Mikulis, D.J. 2016b. Development of White Matter Hyperintensity is Preceded by Reduced Cerebrovascular Reactivity. *Ann Neurol*. doi:10.1002/ana.24712.
- Sam, K., Crawley, A.P., Poulblanc, J., Conklin, J., Sobczyk, O., Mandell, D.M., Duffin, J., Venkatraghavan, L., Fisher, J.A., Black, S.E., Mikulis, D.J. 2016c. Vascular Dysfunction in Leukoaraiosis. *AJNR Am J Neuroradiol*. doi:10.3174/ajnr.A4888.
- Santhanam, A.V., d'Uscio, L.V., He, T., Das, P., Yonkin, S.G., Katusic, Z.S. 2015. Uncoupling of endothelial nitric oxide synthase in cerebral vasculature of Tg2576 mice. *J Neurochem* 134(6), 1129-38. doi:10.1111/jnc.13205.
- Schiffman, E.L. 2010. Antioxidants in hypertension and cardiovascular disease. *Mol Interv* 10(6), 354-62. doi:10.1124/mi.10.6.4.
- Schley, D., Carare-Nnadi, R., Please, C.P., Perry, V.H., Weller, R.O. 2006. Mechanisms to explain the reverse perivascular transport of solutes out of the brain. *J Theor Biol* 238(4), 962-74. doi:10.1016/j.jtbi.2005.07.005.
- Schneider, J.A., Arvanitakis, Z., Bang, W., Bennett, D.A. 2007. Mixed brain pathologies account for most dementia cases in community-dwelling older persons. *Neurology* 69(24), 2197-204. doi:10.1212/01.wnl.0000271090.28148.24.
- Schneider, J.A., Wilson, R.S., Bienias, J.L., Evans, D.A., Bennett, D.A. 2004. Cerebral infarctions and the likelihood of dementia from Alzheimer disease pathology. *Neurology* 62(7), 1148-55.
- Schuff, N., Matsumoto, S., Kmiecik, J., Studholme, C., Du, A., Ezekiel, F., Miller, B.L., Kramer, J.H., Jagust, W.J., Chui, H.C., Weiner, M.W. 2009a. Cerebral blood flow in ischemic vascular dementia and Alzheimer's disease, measured by arterial spin-labeling magnetic resonance imaging. *Alzheimers Dement* 5(6), 454-62. doi:10.1016/j.jalz.2009.04.1233.
- Schuff, N., Matsumoto, S., Kmiecik, J., Studholme, C., Du, A., Ezekiel, F., Miller, B.L., Kramer, J.H., Jagust, W.J., Chui, H.C., Weiner, M.W. 2009b. Cerebral blood flow in ischemic vascular dementia and Alzheimer's disease, measured by arterial spin-labeling magnetic resonance imaging. *Alzheimers Dement* 5(6), 454-62. doi:10.1016/j.jalz.2009.04.1233.

- Scremin, O.U., Holschneider, D.P., Chen, K., Li, M.G., Shih, J.C. 1999a. Cerebral cortical blood flow maps are reorganized in MAOB-deficient mice. *Brain Res* 824(1), 36-44.
- Scremin, O.U., Holschneider, D.P., Chen, K., Li, M.G., Shih, J.C. 1999b. Cerebral cortical blood flow maps are reorganized in MAOB-deficient mice. *Brain Res* 824(1), 36-44.
- Sengillo, J.D., Winkler, E.A., Walker, C.T., Sullivan, J.S., Johnson, M., Zlokovic, B.V. 2013. Deficiency in mural vascular cells coincides with blood-brain barrier disruption in Alzheimer's disease. *Brain Pathol* 23(3), 303-10. doi:10.1111/bpa.12004.
- Seo, J.H., Miyamoto, N., Hayakawa, K., Pham, L.D., Maki, T., Ayata, C., Kim, K.W., Lo, E.H., Arai, K. 2013. Oligodendrocyte precursors induce early blood-brain barrier opening after white matter injury. *J Clin Invest* 123(2), 782-6. doi:10.1172/JCI65863.
- Serrats, J., Schiltz, J.C., García-Bueno, B., van Rooijen, N., Reyes, T.M., Sawchenko, P.E. 2010. Dual roles for perivascular macrophages in immune-to-brain signaling. *Neuron* 65(1), 94-106. doi:10.1016/j.neuron.2009.11.032.
- Seyfer, P., Pagenstecher, A., Mandic, R., Klose, K.J., Heverhagen, J.T. 2014. Cancer and inflammation: differentiation by USPIO-enhanced MR imaging. *J Magn Reson Imaging* 39(3), 665-72. doi:10.1002/jmri.24200.
- Shi, H., Zheng, K., Su, Z., Su, H., Zhong, M., He, X., Zhou, C., Chen, H., Xiong, Q., Zhang, Y. 2016. MCP-1 mediated activation of microglia promotes white matter lesions and cognitive deficits by chronic cerebral hypoperfusion in mice. *Mol Cell Neurosci*. doi:10.1016/j.mcn.2016.08.003.
- Shi, Y., Thrippleton, M.J., Makin, S.D., Marshall, I., Geerlings, M.I., de Craen, A.J., van Buchem, M.A., Wardlaw, J.M. 2016. Cerebral blood flow in small vessel disease: A systematic review and meta-analysis. *J Cereb Blood Flow Metab*. doi:10.1177/0271678X16662891.
- Shibata, H., Nabika, T., Moriyama, H., Masuda, J., Kobayashi, S. 2004. Correlation of NO metabolites and 8-iso-prostaglandin F2a with periventricular hyperintensity severity. *Arterioscler Thromb Vasc Biol* 24(9), 1659-63. doi:10.1161/01.ATV.0000137415.67349.3c.
- Shibata, M., Ohtani, R., Ihara, M., Tomimoto, H. 2004. White matter lesions and glial activation in a novel mouse model of chronic cerebral hypoperfusion. *Stroke* 35(11), 2598-603. doi:10.1161/01.STR.0000143725.19053.60.
- Shibata, M., Yamasaki, N., Miyakawa, T., Kalaria, R.N., Fujita, Y., Ohtani, R., Ihara, M., Takahashi, R., Tomimoto, H. 2007. Selective impairment of working memory in a mouse model of chronic cerebral hypoperfusion. *Stroke* 38(10), 2826-32. doi:10.1161/STROKEAHA.107.490151.
- Shimizu, H., Ghazizadeh, M., Sato, S., Oguro, T., Kawanami, O. 2009. Interaction between beta-amyloid protein and heparan sulfate proteoglycans from the cerebral capillary

- basement membrane in Alzheimer's disease. *J Clin Neurosci* 16(2), 277-82. doi:10.1016/j.jocn.2008.04.009.
- Sigovan, M., Boussel, L., Sulaiman, A., Sappey-Marinié, D., Alsaïd, H., Desbleds-Mansard, C., Ibarrola, D., Gamondès, D., Corot, C., Lancelot, E., Raynaud, J.S., Vives, V., Laclédère, C., Violas, X., Douek, P.C., Canet-Soulas, E. 2009. Rapid-clearance iron nanoparticles for inflammation imaging of atherosclerotic plaque: initial experience in animal model. *Radiology* 252(2), 401-9. doi:10.1148/radiol.2522081484.
- Skrobot, O.A., Attems, J., Esiri, M., Hortobágyi, T., Ironside, J.W., Kalaria, R.N., King, A., Lammie, G.A., Mann, D., Neal, J., Ben-Shlomo, Y., Kehoe, P.G., Love, S. 2016. Vascular cognitive impairment neuropathology guidelines (VCING): the contribution of cerebrovascular pathology to cognitive impairment. *Brain*. doi:10.1093/brain/aww214.
- Snowdon, D.A., Greiner, L.H., Mortimer, J.A., Riley, K.P., Greiner, P.A., Markesbery, W.R. 1997. Brain infarction and the clinical expression of Alzheimer disease. The Nun Study. *JAMA* 277(10), 813-7.
- Sokunbi, M.O. 2016. BOLD fMRI complexity predicts changes in brain processes, interactions and patterns, in health and disease. *J Neurol Sci* 367, 347-8. doi:10.1016/j.jns.2016.06.040.
- Soria, G., Tudela, R., Márquez-Martín, A., Camón, L., Batalle, D., Muñoz-Moreno, E., Eixarch, E., Puig, J., Pedraza, S., Vila, E., Prats-Galino, A., Planas, A.M. 2013. The ins and outs of the BCCAO model for chronic hypoperfusion: a multimodal and longitudinal MRI approach. *PLoS One* 8(9), e74631. doi:10.1371/journal.pone.0074631.
- Soriano, P. 1994. Abnormal kidney development and hematological disorders in PDGF beta-receptor mutant mice. *Genes Dev* 8(16), 1888-96.
- Sorond, F.A., Hurwitz, S., Salat, D.H., Greve, D.N., Fisher, N.D. 2013. Neurovascular coupling, cerebral white matter integrity, and response to cocoa in older people. *Neurology* 81(10), 904-9. doi:10.1212/WNL.0b013e3182a351aa.
- Soto, I., Graham, L.C., Richter, H.J., Simeone, S.N., Radell, J.E., Grabowska, W., Funkhouser, W.K., Howell, M.C., Howell, G.R. 2015. APOE Stabilization by Exercise Prevents Aging Neurovascular Dysfunction and Complement Induction. *PLoS Biol* 13(10), e1002279. doi:10.1371/journal.pbio.1002279.
- Stasia, M.J., Li, X.J. 2008. Genetics and immunopathology of chronic granulomatous disease. *Semin Immunopathol* 30(3), 209-35. doi:10.1007/s00281-008-0121-8.
- Stefanska, J., Pawliczak, R. 2008. Apocynin: molecular aptitudes. *Mediators Inflamm* 2008, 106507. doi:10.1155/2008/106507.

- Stevenson, S.F., Doubal, F.N., Shuler, K., Wardlaw, J.M. 2010. A systematic review of dynamic cerebral and peripheral endothelial function in lacunar stroke versus controls. *Stroke* 41(6), e434-42. doi:10.1161/STROKEAHA.109.569855.
- Storck, S.E., Meister, S., Nahrath, J., Meißner, J.N., Schubert, N., Di Spiezio, A., Baches, S., Vandenbroucke, R.E., Bouter, Y., Prikulis, I., Korth, C., Weggen, S., Heimann, A., Schwaninger, M., Bayer, T.A., Pietrzik, C.U. 2016. Endothelial LRP1 transports amyloid- β (1-42) across the blood-brain barrier. *J Clin Invest* 126(1), 123-36. doi:10.1172/JCI81108.
- Sudduth, T.L., Weekman, E.M., Brothers, H.M., Braun, K., Wilcock, D.M. 2014. β -amyloid deposition is shifted to the vasculature and memory impairment is exacerbated when hyperhomocysteinemia is induced in APP/PS1 transgenic mice. *Alzheimers Res Ther* 6(3), 32. doi:10.1186/alzrt262.
- Sun, X., He, G., Qing, H., Zhou, W., Dobie, F., Cai, F., Staufenbiel, M., Huang, L.E., Song, W. 2006. Hypoxia facilitates Alzheimer's disease pathogenesis by up-regulating BACE1 gene expression. *Proc Natl Acad Sci U S A* 103(49), 18727-32. doi:10.1073/pnas.0606298103.
- Suridjan, I., Pollock, B.G., Verhoeff, N.P., Voineskos, A.N., Chow, T., Rusjan, P.M., Lobaugh, N.J., Houle, S., Mulsant, B.H., Mizrahi, R. 2015. In-vivo imaging of grey and white matter neuroinflammation in Alzheimer's disease: a positron emission tomography study with a novel radioligand, [18F]-FEPPA. *Mol Psychiatry* 20(12), 1579-87. doi:10.1038/mp.2015.1.
- Tajima, Y., Takuwa, H., Kokuryo, D., Kawaguchi, H., Seki, C., Masamoto, K., Ikoma, Y., Taniguchi, J., Aoki, I., Tomita, Y., Suzuki, N., Kanno, I., Saeki, N., Ito, H. 2014. Changes in cortical microvasculature during misery perfusion measured by two-photon laser scanning microscopy. *J Cereb Blood Flow Metab* 34(8), 1363-72. doi:10.1038/jcbfm.2014.91.
- Tang, T.Y., Howarth, S.P., Miller, S.R., Graves, M.J., Patterson, A.J., U-King-Im, J.M., Li, Z.Y., Walsh, S.R., Brown, A.P., Kirkpatrick, P.J., Warburton, E.A., Hayes, P.D., Varty, K., Boyle, J.R., Gaunt, M.E., Zalewski, A., Gillard, J.H. 2009. The ATHEROMA (Atorvastatin Therapy: Effects on Reduction of Macrophage Activity) Study. Evaluation using ultrasmall superparamagnetic iron oxide-enhanced magnetic resonance imaging in carotid disease. *J Am Coll Cardiol* 53(22), 2039-50. doi:10.1016/j.jacc.2009.03.018.
- Tang, X.N., Cairns, B., Cairns, N., Yenari, M.A. 2008. Apocynin improves outcome in experimental stroke with a narrow dose range. *Neuroscience* 154(2), 556-62. doi:10.1016/j.neuroscience.2008.03.090.
- ten Dam, V.H., van den Heuvel, D.M., de Craen, A.J., Bollen, E.L., Murray, H.M., Westendorp, R.G., Blauw, G.J., van Buchem, M.A. 2007. Decline in total cerebral blood flow is linked with increase in periventricular but not deep white matter hyperintensities. *Radiology* 243(1), 198-203. doi:10.1148/radiol.2431052111.

- Thal, D.R., Ghebremedhin, E., Orantes, M., Wiestler, O.D. 2003. Vascular pathology in Alzheimer disease: correlation of cerebral amyloid angiopathy and arteriosclerosis/lipohyalinosis with cognitive decline. *J Neuropathol Exp Neurol* 62(12), 1287-301.
- Thambisetty, M., Beason-Held, L., An, Y., Kraut, M.A., Resnick, S.M. 2010. APOE epsilon4 genotype and longitudinal changes in cerebral blood flow in normal aging. *Arch Neurol* 67(1), 93-8. doi:10.1001/archneurol.2009.913.
- Thomas, S.R., Stocker, R. 2000. Molecular action of vitamin E in lipoprotein oxidation: implications for atherosclerosis. *Free Radic Biol Med* 28(12), 1795-805.
- Tian, J., Shi, J., Bailey, K., Mann, D.M. 2004. Relationships between arteriosclerosis, cerebral amyloid angiopathy and myelin loss from cerebral cortical white matter in Alzheimer's disease. *Neuropathol Appl Neurobiol* 30(1), 46-56.
- Tolppanen, A.M., Solomon, A., Kulmala, J., Kåreholt, I., Ngandu, T., Rusanen, M., Laatikainen, T., Soininen, H., Kivipelto, M. 2015. Leisure-time physical activity from mid- to late life, body mass index, and risk of dementia. *Alzheimers Dement* 11(4), 434-43.e6. doi:10.1016/j.jalz.2014.01.008.
- Toyama, K., Koibuchi, N., Uekawa, K., Hasegawa, Y., Kataoka, K., Katayama, T., Sueta, D., Ma, M.J., Nakagawa, T., Yasuda, O., Tomimoto, H., Ichijo, H., Ogawa, H., Kim-Mitsuyama, S. 2014. Apoptosis signal-regulating kinase 1 is a novel target molecule for cognitive impairment induced by chronic cerebral hypoperfusion. *Arterioscler Thromb Vasc Biol* 34(3), 616-25. doi:10.1161/ATVBAHA.113.302440.
- Trachootham, D., Lu, W., Ogasawara, M.A., Nilsa, R.D., Huang, P. 2008. Redox regulation of cell survival. *Antioxid Redox Signal* 10(8), 1343-74. doi:10.1089/ars.2007.1957.
- Trivedi, R.A., Mallawarachi, C., U-King-Im, J.M., Graves, M.J., Horsley, J., Goddard, M.J., Brown, A., Wang, L., Kirkpatrick, P.J., Brown, J., Gillard, J.H. 2006. Identifying inflamed carotid plaques using in vivo USPIO-enhanced MR imaging to label plaque macrophages. *Arterioscler Thromb Vasc Biol* 26(7), 1601-6. doi:10.1161/01.ATV.0000222920.59760.df.
- Troen, A.M., Shea-Budgell, M., Shukitt-Hale, B., Smith, D.E., Selhub, J., Rosenberg, I.H. 2008. B-vitamin deficiency causes hyperhomocysteinemia and vascular cognitive impairment in mice. *Proc Natl Acad Sci U S A* 105(34), 12474-9. doi:10.1073/pnas.0805350105.
- Trumbull, K.A., McAllister, D., Gandelman, M.M., Fung, W.Y., Lew, T., Brennan, L., Lopez, N., Morr , J., Kalyanaraman, B., Beckman, J.S. 2012. Diapocynin and apocynin administration fails to significantly extend survival in G93A SOD1 ALS mice. *Neurobiol Dis* 45(1), 137-44. doi:10.1016/j.nbd.2011.07.015.
- Tucsek, Z., Toth, P., Tarantini, S., Sosnowska, D., Gautam, T., Warrington, J.P., Giles, C.B., Wren, J.D., Koller, A., Ballabh, P., Sonntag, W.E., Ungvari, Z., Csiszar, A. 2014. Aging

- exacerbates obesity-induced cerebromicrovascular rarefaction, neurovascular uncoupling, and cognitive decline in mice. *J Gerontol A Biol Sci Med Sci* 69(11), 1339-52. doi:10.1093/gerona/glu080.
- Tullberg, M., Fletcher, E., DeCarli, C., Mungas, D., Reed, B.R., Harvey, D.J., Weiner, M.W., Chui, H.C., Jagust, W.J. 2004. White matter lesions impair frontal lobe function regardless of their location. *Neurology* 63(2), 246-53.
- Turner, R.J., Sharp, F.R. 2016. Implications of MMP9 for Blood Brain Barrier Disruption and Hemorrhagic Transformation Following Ischemic Stroke. *Front Cell Neurosci* 10, 56. doi:10.3389/fncel.2016.00056.
- Ueno, Y., Koike, M., Shimada, Y., Shimura, H., Hira, K., Tanaka, R., Uchiyama, Y., Hattori, N., Urabe, T. 2015. L-carnitine enhances axonal plasticity and improves white-matter lesions after chronic hypoperfusion in rat brain. *J Cereb Blood Flow Metab* 35(3), 382-91. doi:10.1038/jcbfm.2014.210.
- Ueno, Y., Zhang, N., Miyamoto, N., Tanaka, R., Hattori, N., Urabe, T. 2009. Edaravone attenuates white matter lesions through endothelial protection in a rat chronic hypoperfusion model. *Neuroscience* 162(2), 317-27. doi:10.1016/j.neuroscience.2009.04.065.
- Ullrich, R.T., Jikeli, J.F., Diedenhofen, M., Böhm-Sturm, P., Unruh, M., Vollmar, S., Hoehn, M. 2011. In-vivo visualization of tumor microvessel density and response to anti-angiogenic treatment by high resolution MRI in mice. *PLoS One* 6(5), e19592. doi:10.1371/journal.pone.0019592.
- Valenti, R., Del Bene, A., Poggesi, A., Ginestroni, A., Salvadori, E., Pracucci, G., Ciolli, L., Marini, S., Nannucci, S., Pasi, M., Pescini, F., Diciotti, S., Orlandi, G., Cosottini, M., Chiti, A., Mascalchi, M., Bonuccelli, U., Inzitari, D., Pantoni, L., Group, V.-T.S. 2016. Cerebral microbleeds in patients with mild cognitive impairment and small vessel disease: The Vascular Mild Cognitive Impairment (VMCI)-Tuscany study. *J Neurol Sci* 368, 195-202. doi:10.1016/j.jns.2016.07.018.
- Valenzuela, M., Esler, M., Ritchie, K., Brodaty, H. 2012. Antihypertensives for combating dementia? A perspective on candidate molecular mechanisms and population-based prevention. *Transl Psychiatry* 2, e107. doi:10.1038/tp.2012.28.
- Valko, M., Leibfritz, D., Moncol, J., Cronin, M.T., Mazur, M., Telser, J. 2007. Free radicals and antioxidants in normal physiological functions and human disease. *Int J Biochem Cell Biol* 39(1), 44-84. doi:10.1016/j.biocel.2006.07.001.
- Vallet, P., Charnay, Y., Steger, K., Ogier-Denis, E., Kovari, E., Herrmann, F., Michel, J.P., Szanto, I. 2005. Neuronal expression of the NADPH oxidase NOX4, and its regulation in mouse experimental brain ischemia. *Neuroscience* 132(2), 233-8. doi:10.1016/j.neuroscience.2004.12.038.

- van der Veen, P.H., Muller, M., Vincken, K.L., Hendrikse, J., Mali, W.P., van der Graaf, Y., Geerlings, M.I., Group, S.S. 2015. Longitudinal relationship between cerebral small-vessel disease and cerebral blood flow: the second manifestations of arterial disease-magnetic resonance study. *Stroke* 46(5), 1233-8. doi:10.1161/STROKEAHA.114.008030.
- van Veluw, S.J., Biessels, G.J., Bouvy, W.H., Spliet, W.G., Zwanenburg, J.J., Luijten, P.R., Macklin, E.A., Rozemuller, A.J., Gurol, M.E., Greenberg, S.M., Viswanathan, A., Martinez-Ramirez, S. 2016. Cerebral amyloid angiopathy severity is linked to dilation of juxtacortical perivascular spaces. *J Cereb Blood Flow Metab* 36(3), 576-80. doi:10.1177/0271678X15620434.
- Vara, D., Pula, G. 2014. Reactive oxygen species: physiological roles in the regulation of vascular cells. *Curr Mol Med* 14(9), 1103-25.
- Vecil, G.G., Larsen, P.H., Corley, S.M., Herx, L.M., Besson, A., Goodyer, C.G., Yong, V.W. 2000. Interleukin-1 is a key regulator of matrix metalloproteinase-9 expression in human neurons in culture and following mouse brain trauma in vivo. *J Neurosci Res* 61(2), 212-24. doi:10.1002/1097-4547(20000715)61:2<212::AID-JNR12>3.0.CO;2-9.
- Verkhatsky, A., Rodríguez-Arellano, J.J., Parpura, V., Zorec, R. 2016. Astroglial calcium signalling in Alzheimer's disease. *Biochem Biophys Res Commun*. doi:10.1016/j.bbrc.2016.08.088.
- Vetri, F., Xu, H., Paisansathan, C., Pelligrino, D.A. 2012. Impairment of neurovascular coupling in type 1 diabetes mellitus in rats is linked to PKC modulation of BK(Ca) and Kir channels. *Am J Physiol Heart Circ Physiol* 302(6), H1274-84. doi:10.1152/ajpheart.01067.2011.
- Vicenzini, E., Ricciardi, M.C., Altieri, M., Puccinelli, F., Bonaffini, N., Di Piero, V., Lenzi, G.L. 2007a. Cerebrovascular reactivity in degenerative and vascular dementia: a transcranial Doppler study. *Eur Neurol* 58(2), 84-9. doi:10.1159/000103642.
- Vicenzini, E., Ricciardi, M.C., Altieri, M., Puccinelli, F., Bonaffini, N., Di Piero, V., Lenzi, G.L. 2007b. Cerebrovascular reactivity in degenerative and vascular dementia: a transcranial Doppler study. *Eur Neurol* 58(2), 84-9. doi:10.1159/000103642.
- Virdis, A., Bacca, A., Colucci, R., Duranti, E., Fornai, M., Materazzi, G., Ippolito, C., Bernardini, N., Blandizzi, C., Bernini, G., Taddei, S. 2013. Endothelial dysfunction in small arteries of essential hypertensive patients: role of cyclooxygenase-2 in oxidative stress generation. *Hypertension* 62(2), 337-44. doi:10.1161/HYPERTENSIONAHA.111.00995.
- Virdis, A., Colucci, R., Versari, D., Ghisu, N., Fornai, M., Antonioli, L., Duranti, E., Daghini, E., Giannarelli, C., Blandizzi, C., Taddei, S., Del Tacca, M. 2009. Atorvastatin prevents endothelial dysfunction in mesenteric arteries from spontaneously hypertensive rats:

- role of cyclooxygenase 2-derived contracting prostanoids. *Hypertension* 53(6), 1008-16. doi:10.1161/HYPERTENSIONAHA.109.132258.
- Viridis, A., Dell'Agnello, U., Taddei, S. 2014. Impact of inflammation on vascular disease in hypertension. *Maturitas* 78(3), 179-83. doi:10.1016/j.maturitas.2014.04.012.
- Viridis, A., Duranti, E., Colucci, R., Ippolito, C., Tirotta, E., Lorenzini, G., Bernardini, N., Blandizzi, C., Taddei, S. 2015. Ghrelin restores nitric oxide availability in resistance circulation of essential hypertensive patients: role of NAD(P)H oxidase. *Eur Heart J* 36(43), 3023-30. doi:10.1093/eurheartj/ehv365.
- Viticchi, G., Falsetti, L., Vernieri, F., Altamura, C., Bartolini, M., Luzzi, S., Provinciali, L., Silvestrini, M. 2012a. Vascular predictors of cognitive decline in patients with mild cognitive impairment. *Neurobiol Aging* 33(6), 1127.e1-9. doi:10.1016/j.neurobiolaging.2011.11.027.
- Viticchi, G., Falsetti, L., Vernieri, F., Altamura, C., Bartolini, M., Luzzi, S., Provinciali, L., Silvestrini, M. 2012b. Vascular predictors of cognitive decline in patients with mild cognitive impairment. *Neurobiol Aging* 33(6), 1127.e1-9. doi:10.1016/j.neurobiolaging.2011.11.027.
- Walder, C.E., Green, S.P., Darbonne, W.C., Mathias, J., Rae, J., Dinanuer, M.C., Curnutte, J.T., Thomas, G.R. 1997. Ischemic stroke injury is reduced in mice lacking a functional NADPH oxidase. *Stroke* 28(11), 2252-8.
- Wang, F., Guo, X., Shen, X., Kream, R.M., Mantione, K.J., Stefano, G.B. 2014. Vascular dysfunction associated with type 2 diabetes and Alzheimer's disease: a potential etiological linkage. *Med Sci Monit Basic Res* 20, 118-29. doi:10.12659/MSMBR.891278.
- Wang, Y., Jin, S., Sonobe, Y., Cheng, Y., Horiuchi, H., Parajuli, B., Kawanokuchi, J., Mizuno, T., Takeuchi, H., Suzumura, A. 2014. Interleukin-1 β induces blood-brain barrier disruption by downregulating Sonic hedgehog in astrocytes. *PLoS One* 9(10), e110024. doi:10.1371/journal.pone.0110024.
- Wardlaw, J.M. 2010. Blood-brain barrier and cerebral small vessel disease. *J Neurol Sci* 299(1-2), 66-71. doi:10.1016/j.jns.2010.08.042.
- Wardlaw, J.M., Makin, S., Valdes Hernandez, M.C., Armitage, P., Heye, A.K., Chappell, F.M., Munoz-Maniega, S., Sakka, E., Shuler, K., Dennis, M.S., Thruppelton, M.J. 2016. Blood-brain barrier failure as a core mechanism in cerebral small vessel disease and dementia: evidence from a cohort study. *Alzheimer's and Dementia* (article in press)
- Wardlaw, J.M., Smith, C., Dichgans, M. 2013a. Mechanisms of sporadic cerebral small vessel disease: insights from neuroimaging. *Lancet Neurol* 12(5), 483-97. doi:10.1016/S1474-4422(13)70060-7.

- Wardlaw, J.M., Smith, E.E., Biessels, G.J., Cordonnier, C., Fazekas, F., Frayne, R., Lindley, R.I., O'Brien, J.T., Barkhof, F., Benavente, O.R., Black, S.E., Brayne, C., Breteler, M., Chabriat, H., Decarli, C., de Leeuw, F.E., Doubal, F., Duering, M., Fox, N.C., Greenberg, S., Hachinski, V., Kilimann, I., Mok, V., Oostenbrugge, R., Pantoni, L., Speck, O., Stephan, B.C., Teipel, S., Viswanathan, A., Werring, D., Chen, C., Smith, C., van Buchem, M., Norrving, B., Gorelick, P.B., Dichgans, M., v1), S.f.R.V.c.o.n.S. 2013b. Neuroimaging standards for research into small vessel disease and its contribution to ageing and neurodegeneration. *Lancet Neurol* 12(8), 822-38. doi:10.1016/S1474-4422(13)70124-8.
- Washida, K., Ihara, M., Nishio, K., Fujita, Y., Maki, T., Yamada, M., Takahashi, J., Wu, X., Kihara, T., Ito, H., Tomimoto, H., Takahashi, R. 2010. Nonhypotensive dose of telmisartan attenuates cognitive impairment partially due to peroxisome proliferator-activated receptor-gamma activation in mice with chronic cerebral hypoperfusion. *Stroke* 41(8), 1798-806. doi:10.1161/STROKEAHA.110.583948.
- Wei, H.S., Kang, H., Rasheed, I.Y., Zhou, S., Lou, N., Gershteyn, A., McConnell, E.D., Wang, Y., Richardson, K.E., Palmer, A.F., Xu, C., Wan, J., Nedergaard, M. 2016. Erythrocytes Are Oxygen-Sensing Regulators of the Cerebral Microcirculation. *Neuron* 91(4), 851-62. doi:10.1016/j.neuron.2016.07.016.
- Weiss, H.R., Buchweitz, E., Murtha, T.J., Auletta, M. 1982. Quantitative regional determination of morphometric indices of the total and perfused capillary network in the rat brain. *Circ Res* 51(4), 494-503.
- Weissmann, N., Sydykov, A., Kalwa, H., Storch, U., Fuchs, B., Mederos y Schnitzler, M., Brandes, R.P., Grimminger, F., Meissner, M., Freichel, M., Offermanns, S., Veit, F., Pak, O., Krause, K.H., Schermuly, R.T., Brewer, A.C., Schmidt, H.H., Seeger, W., Shah, A.M., Gudermann, T., Ghofrani, H.A., Dietrich, A. 2012. Activation of TRPC6 channels is essential for lung ischaemia-reperfusion induced oedema in mice. *Nat Commun* 3, 649. doi:10.1038/ncomms1660.
- Weller, R.O., Hawkes, C.A., Kalaria, R.N., Werring, D.J., Carare, R.O. 2015. White matter changes in dementia: role of impaired drainage of interstitial fluid. *Brain Pathol* 25(1), 63-78. doi:10.1111/bpa.12218.
- Wellons, J.C., Sheng, H., Laskowitz, D.T., Mackensen, G.B., Pearlstein, R.D., Warner, D.S. 2000. A comparison of strain-related susceptibility in two murine recovery models of global cerebral ischemia. *Brain Res* 868(1), 14-21.
- Werring, D.J., Gregoire, S.M., Cipolotti, L. 2010. Cerebral microbleeds and vascular cognitive impairment. *J Neurol Sci* 299(1-2), 131-5. doi:10.1016/j.jns.2010.08.034.
- Whang, J.S., Kolber, M., Powell, D.K., Libfeld, E. 2015. Diffusion-weighted signal patterns of intracranial haemorrhage. *Clin Radiol* 70(8), 909-16. doi:10.1016/j.crad.2015.04.006.

- Wilcock, D.M., Vitek, M.P., Colton, C.A. 2009. Vascular amyloid alters astrocytic water and potassium channels in mouse models and humans with Alzheimer's disease. *Neuroscience* 159(3), 1055-69. doi:10.1016/j.neuroscience.2009.01.023.
- Wosik, K., Cayrol, R., Dodelet-Devillers, A., Berthelet, F., Bernard, M., Moumdjian, R., Bouthillier, A., Reudelhuber, T.L., Prat, A. 2007. Angiotensin II controls occludin function and is required for blood brain barrier maintenance: relevance to multiple sclerosis. *J Neurosci* 27(34), 9032-42. doi:10.1523/JNEUROSCI.2088-07.2007.
- Wu, C., Honarmand, A.R., Schnell, S., Kuhn, R., Schoeneman, S.E., Ansari, S.A., Carr, J., Markl, M., Shaibani, A. 2016. Age-Related Changes of Normal Cerebral and Cardiac Blood Flow in Children and Adults Aged 7 Months to 61 Years. *J Am Heart Assoc* 5(1). doi:10.1161/JAHA.115.002657.
- Ximenes, V.F., Kanegae, M.P., Rissato, S.R., Galhiane, M.S. 2007. The oxidation of apocynin catalyzed by myeloperoxidase: proposal for NADPH oxidase inhibition. *Arch Biochem Biophys* 457(2), 134-41. doi:10.1016/j.abb.2006.11.010.
- Xu, Y., Zhang, J.J., Xiong, L., Zhang, L., Sun, D., Liu, H. 2010. Green tea polyphenols inhibit cognitive impairment induced by chronic cerebral hypoperfusion via modulating oxidative stress. *J Nutr Biochem* 21(8), 741-8. doi:10.1016/j.jnutbio.2009.05.002.
- Yamada, M., Ihara, M., Okamoto, Y., Maki, T., Washida, K., Kitamura, A., Hase, Y., Ito, H., Takao, K., Miyakawa, T., Kalara, R.N., Tomimoto, H., Takahashi, R. 2011. The influence of chronic cerebral hypoperfusion on cognitive function and amyloid β metabolism in APP overexpressing mice. *PLoS One* 6(1), e16567. doi:10.1371/journal.pone.0016567.
- Yan, W., Zhao, X., Chen, H., Zhong, D., Jin, J., Qin, Q., Zhang, H., Ma, S., Li, G. 2016. β -Dystroglycan cleavage by matrix metalloproteinase-2/-9 disturbs aquaporin-4 polarization and influences brain edema in acute cerebral ischemia. *Neuroscience* 326, 141-57. doi:10.1016/j.neuroscience.2016.03.055.
- Yang, C.M., Hsieh, H.L., Yu, P.H., Lin, C.C., Liu, S.W. 2015. IL-1 β Induces MMP-9-Dependent Brain Astrocytic Migration via Transactivation of PDGF Receptor/NADPH Oxidase 2-Derived Reactive Oxygen Species Signals. *Mol Neurobiol* 52(1), 303-17. doi:10.1007/s12035-014-8838-y.
- Yates, P.A., Villemagne, V.L., Ellis, K.A., Desmond, P.M., Masters, C.L., Rowe, C.C. 2014. Cerebral microbleeds: a review of clinical, genetic, and neuroimaging associations. *Front Neurol* 4, 205. doi:10.3389/fneur.2013.00205.
- Yezhuvath, U.S., Uh, J., Cheng, Y., Martin-Cook, K., Weiner, M., Diaz-Arrastia, R., van Osch, M., Lu, H. 2012. Forebrain-dominant deficit in cerebrovascular reactivity in Alzheimer's disease. *Neurobiol Aging* 33(1), 75-82. doi:10.1016/j.neurobiolaging.2010.02.005.

- Yoshizaki, K., Adachi, K., Kataoka, S., Watanabe, A., Tabira, T., Takahashi, K., Wakita, H. 2008. Chronic cerebral hypoperfusion induced by right unilateral common carotid artery occlusion causes delayed white matter lesions and cognitive impairment in adult mice. *Exp Neurol* 210(2), 585-91. doi:10.1016/j.expneurol.2007.12.005.
- Yousif S, Marie-Claire C, Roux F, Scherrmann JM, Declèves X. Expression of drug transporters at the blood-brain barrier using an optimized isolated rat brain microvessel strategy. *Brain Res* 2007;1134(1):1-11
- Zago, W., Schroeter, S., Guido, T., Khan, K., Seubert, P., Yednock, T., Schenk, D., Gregg, K.M., Games, D., Bard, F., Kinney, G.G. 2013. Vascular alterations in PDAPP mice after anti-A β immunotherapy: Implications for amyloid-related imaging abnormalities. *Alzheimers Dement* 9(5 Suppl), S105-15. doi:10.1016/j.jalz.2012.11.010.
- Zhang, G., Zhao, Z., Gao, L., Deng, J., Wang, B., Xu, D., Liu, B., Qu, Y., Yu, J., Li, J., Gao, G. 2011. Gypenoside attenuates white matter lesions induced by chronic cerebral hypoperfusion in rats. *Pharmacol Biochem Behav* 99(1), 42-51. doi:10.1016/j.pbb.2011.03.019.
- Zhang, X., Huang, X., Fang, C., Li, Q., Cui, J., Sun, J., Li, L. 2016. miR-124 Regulates the Expression of BACE1 in the Hippocampus Under Chronic Cerebral Hypoperfusion. *Mol Neurobiol*. doi:10.1007/s12035-016-9845-y.
- Zhang, Z.G., Zhang, L., Jiang, Q., Zhang, R., Davies, K., Powers, C., Bruggen, N., Chopp, M. 2000. VEGF enhances angiogenesis and promotes blood-brain barrier leakage in the ischemic brain. *J Clin Invest* 106(7), 829-38. doi:10.1172/JCI9369.
- Zhiyou, C., Yong, Y., Shanquan, S., Jun, Z., Liangguo, H., Ling, Y., Jieying, L. 2009. Upregulation of BACE1 and beta-amyloid protein mediated by chronic cerebral hypoperfusion contributes to cognitive impairment and pathogenesis of Alzheimer's disease. *Neurochem Res* 34(7), 1226-35. doi:10.1007/s11064-008-9899-y.
- Zhu, J., Wang, Y., Li, J., Deng, J., Zhou, H. 2014. Intracranial artery stenosis and progression from mild cognitive impairment to Alzheimer disease. *Neurology* 82(10), 842-9. doi:10.1212/WNL.0000000000000185.
- Zlokovic, B.V. 2008. The blood-brain barrier in health and chronic neurodegenerative disorders. *Neuron* 57(2), 178-201. doi:10.1016/j.neuron.2008.01.003.
- Zlokovic, B.V. 2011. Neurovascular pathways to neurodegeneration in Alzheimer's disease and other disorders. *Nat Rev Neurosci* 12(12), 723-38. doi:10.1038/nrn3114.
- Zou, M.H. 2007a. Peroxynitrite and protein tyrosine nitration of prostacyclin synthase. *Prostaglandins Other Lipid Mediat* 82(1-4), 119-27. doi:10.1016/j.prostaglandins.2006.05.005.

- Zou, M.H. 2007b. Peroxynitrite and protein tyrosine nitration of prostacyclin synthase. *Prostaglandins Other Lipid Mediat* 82(1-4), 119-27. doi:10.1016/j.prostaglandins.2006.05.005.
- Zuo, L., Zhou, T., Pannell, B.K., Ziegler, A.C., Best, T.M. 2015. Biological and physiological role of reactive oxygen species--the good, the bad and the ugly. *Acta Physiol (Oxf)* 214(3), 329-48. doi:10.1111/apha.12515.

Chapter 9. Appendices

Appendix

9.1 List of publications

Duncombe J, Lennen RJ, Jansen MA, Marshall I, Wardlaw JM, Horsburgh K. (2016) Ageing causes prominent neurovascular dysfunction associated with loss of astrocytic contacts and gliosis. *Neuropathol Appl Neurobiol*. doi: 10.1111/nan.12375. [Epub ahead of print]

Kitamura A, Sanz Y, **Duncombe J**, Searcy J, Koudelka J, Binnie M, Webster S, Lennen R, Jansen M, Marshall I, Ihara M, Kalaria R, Horsburgh K. (2017) Long-term cilostazol treatment reduces gliovascular damage and memory impairment via endothelial protection in a mouse model of chronic cerebral hypoperfusion. *Scientific Reports* (In Press)

Manso Y, Holland PR, Kitamura A, Searcy L, Marangoni M, Szymkowiak A, **Duncombe J**, Hennessey E, Randall AD, Brown JT, McColl BW, Horsburgh K. (2017) Minocycline reduces microgliosis and improves subcortical white matter function in a model of cerebral vascular disease. *Glia* (In submission)